DESTRESS

Demonstration of soft stimulation treatments
of geothermal reservoirs

# Deliverable 2.2: Key performance indicator analyses based on Monte Carlo simulation

## WP 2: Business case - key performance indicator-based analysis

| | |
|---|---|
| **Lead Beneficiary** | EnBW |
| **Type** | ☑ R - report, document etc. ☐ OTHER - software, technical diagram etc.<br>☐ DEM - demonstrator, pilot etc. ☐ E - ethics<br>☐ DEC - website, patent filing etc. |
| **Status** | ☑ Draft<br>☐ WP manager accepted<br>☐ Project coordinator accepted |
| **Dissemination level** | ☑ PU – Public<br>☐ CO - Confidential: only for members of the consortium |
| **Contributors** | ☐ 1-GFZ ☐ 5-GES ☐ 9-GTL ☐ 13-SNU<br>☑ 2-ENB ☑ 6-TNO ☐ 10-UoS ☐ 14-KIC<br>☑ 3-ESG ☐ 7-ETH ☐ 11-TUD ☐ 15-ECW<br>☑ 4-UoG ☐ 8-GTN ☐ 12-NEX ☐ 16-WES |
| **Creation date** | 06 April 2018 |
| **Last change** | 06 May 2019 |
| **Version** | 61 |
| **Due date** | 30 April 2019 |
| **Submission date** | 02.05.2019 |

DESTRESS

Demonstration of soft stimulation treatments
of geothermal reservoirs

# Key performance indicator analyses based on Monte Carlo simulation

## DESTRESS investment decision support tool for geothermal fields

Figure 1: Wellhead with pipeline for stimulation (© EnBW)


## Authors:

Sören Welter (EnBW), Carl Bormann (EnBW), Christian Bos (TNO), Peter Collings (UoG), Régis Hehn (ésg), Guillaume Ravier (ésg), Elif Kaymakci (EnBW), Dorothee Siefert (EnBW), Dr. Thomas Kölbel (EnBW), Aaron Förderer (EnBW), Robin Seyfarth (EnBW), Jonas Greve (EnBW)



## Publication Date

May 6, 2019

# Table of Contents

Table of Contents ..... I

**List of figures** ..... IV

List of tables ..... VI

Nomenclature ..... VII

Abstract XI

1 Introduction ..... 1

1.1 Deliverable 2.2 in the context of DESTRESS ..... 1
1.2 Investment decisions supported by simulation model ..... 2

1.2.1 Decision analysis process ..... 2
1.2.2 Types of decisions ..... 3
1.2.3 Project maturity ..... 4
1.2.4 What do managers need to make good decisions? ..... 4
1.2.5 Purpose of the DESTRESS tool ..... 5
1.2.6 Tool design ..... 5

2 Methodological background for a techno-economic evaluation including uncertainty ..... 9

2.1 Decision analysis as methodological approach for comparing options ..... 9
2.2 Uncertainty within techno-economic evaluations – continuous and discretised representation of uncertainty ..... 10
2.3 Risk analysis process conducted within the DESTRESS project ..... 13

2.3.1 Definition of scope and objectives ..... 14
2.3.2 Identification of risk factors ..... 15
2.3.3 Prioritization of risk factors ..... 15
2.3.4 Quantification of risk factors ..... 16

3 IGEM – Integrated geothermal energy model ..... 19

3.1 Technical model ..... 21

3.1.1 Reservoir model ..... 21
3.1.2 Thermal water circuit (TWC) ..... 30
3.1.3 Energy utilization model ..... 35

3.2 Economic model ..... 50

3.2.1 Module costing approach ..... 51
3.2.2 Cost engineering approaches for the technical sub-models ..... 51
3.2.3 Adaption of the model to different European markets ..... 63

4 Framing the problem ..... 64

4.1 Framing the problem – clarification of the term ..... 64
4.2 KPIs and time-series investigated ..... 64

4.3 Investigated risk-factors ..... 65
4.3.1 Risk-factors for the investigated stimulation measures ..... 65
4.3.2 Deduction of Probability density functions ..... 67
4.3.3 Risk mitigation measures and their effect on PDFs ..... 69

5 Evaluation of decision alternatives based on KPI ..... 71

5.1 Soultz-sous-Forêts ..... 72
5.1.1 Presentation of site ..... 72
5.1.2 Results of techno-economic modelling ..... 74

5.2 Mezöberény ..... 77
5.2.1 Presentation of site ..... 77
5.2.2 Results of techno-economic modelling ..... 79

5.3 Upper Rhine Graben ..... 82
5.3.1 Presentation of site ..... 82
5.3.2 Results of techno-economic modelling ..... 83

6 Summary and conclusions ..... 88

Literature ..... 91

A. Decision gate review process ..... 106

A.1. DECISION GATE REVIEW # 1: Approval of Project Initiation ..... 106

A.2. DECISION GATE REVIEW # 2: Approval of Concept Short List ..... 107

A.3. DECISION GATE REVIEW # 3: Project Concept Selection and Definition ..... 108

A.4. DECISION GATE REVIEW # 4: Approval to issue PDO / PIO[6] ..... 109

A.5. DECISION GATE REVIEW # 5: Approval to Start Execution ..... 110

A.6. DECISION GATE REVIEW # 6: Approval to Start Operation ..... 110

A.7. DECISION GATE REVIEW # 7: Post Implementation Assessment ..... 111

B. Quantification of risk factors in soft stimulation activities Calculation of interest rates including taxes ..... 112

B.1. Introduction ..... 112

B.2. Risk evaluation ..... 113

B.2.1. Public acceptance ..... 113

B.2.2. Fluid-rock and fluid-fluid interactions ..... 116

B.2.3. Political instability ..... 119

B.2.4. Lost in hole ..... 119

B.2.5. Blowout ..... 120

B.2.6. Induced Seismicity ..... 121

B.2.7. Lack of information ..... 124

B.2.8. Unwanted subsurface hydraulic connections ..... 125

C. Literature review - effect of stimulation ..... 128

D. Program flow charts ..... 134

D.1. Overall model ..... 134

D.2. Power plant ..... 135

D.3. Wellbore ..... 136

E. Calculation of overall heat transfer coefficient ..... 137

# List of figures

FIGURE 1: WELLHEAD WITH PIPELINE FOR STIMULATION ..... II
FIGURE 2: DESTRESS OVERALL GOALS FOR THE DEMONSTRATION OF STIMULATION ACTIVITIES ..... 1
FIGURE 3: "THE MODELLING CUBE" ..... 8
FIGURE 4: STEPS IN THE DECISION ANALYSIS (DA) PROCESS, INCLUDING DETAILED SUB-PROCESSES ..... 10
FIGURE 5: UNCERTAINTY ON THE REALIZATION OF A PARAMETER IN TECHNO-ECONOMIC MODELLING ..... 11
FIGURE 6: DECISION TREE ON THE EXAMPLE OF A "DRILL/NO-DRILL" DECISION ..... 12
FIGURE 7: TAXONOMY ON THE INTEGRATION OF UNCERTAINTY INTO INVESTMENT DECISIONS ..... 13
FIGURE 8: QUANTITATIVE RISK ASSESSMENT PROCESS ..... 14
FIGURE 9: PROJECT SCHEDULE ADAPTED TO A CHEMICAL STIMULATION OF GEOTHERMAL SYSTEMS ..... 15
FIGURE 10: PRIORITIZATION PROCESS WITH THE EXAMPLE OF A TEMPERATURE GRADIENT ..... 16
FIGURE 11: IDENTIFICATION OF A CONTINUOUS PROBABILITY DISTRIBUTION BASED ON DISCRETISED SCENARIOS ..... 18
FIGURE 12: MODEL OVERVIEW ON THE INTEGRATED GEOTHERMAL ENERGY MODEL ..... 20
FIGURE 13: RELATIVE IMPROVEMENT THROUGH STIMULATION ..... 25
FIGURE 14: RELATIVE IMPROVEMENT THROUGH HYDRAULIC STIMULATION .....FEHLER! TEXTMARKE NICHT DEFINIERT.
FIGURE 15: RELATIVE IMPROVEMENT THROUGH CHEMICAL STIMULATION ..... 26
FIGURE 16: STIMULATIONS WITH PUBLISHED PI ..... 26
FIGURE 17: STIMULATIONS WITH PUBLISHED II ..... 27
FIGURE 18: DESCRIPTION OF THE DATA ON THE EFFECT OF STIMULATION WITH A CONTINUOUS DISTRIBUTION ..... 28
FIGURE 19: SCHEMATIC STRUCTURE OF PRODUCTION AND INJECTION WELLBORE ..... 31
FIGURE 20: SCHEMATIC DEPICTION OF ORC WITH CHP ..... 36
FIGURE 21: COMPARISON BETWEEN PURE WORKING MEDIUM AND ZEOTROPIC WORKING MEDIUM MIXTURE IN AN ORC ..... 37
FIGURE 22: PROGRAM FLOW CHART OVERALL MODEL WITH ROUTINE NAMES ..... 38
FIGURE 23: SCHEMATIC DEPICTION OF EVAPORATOR IN ORC-MODEL ..... 39
FIGURE 24: HEAT INTEGRATION FOR THERMAL WATER AND WORKING MEDIUM IN EVAPORATOR ..... 40
FIGURE 25: DIVISION INTO SUBSECTIONS OF EVAPORATOR FOR PRE-HEATING ..... 43
FIGURE 26: SCHEMATIC DEPICTION CONDENSER IN ORC-MODEL ..... 45
FIGURE 27: SCHEMATIC DEPICTION RECUPERATOR IN ORC-MODEL ..... 45
FIGURE 28: MODELLED COMPONENT COSTS OF SOULTZ-SOUS-FORÊTS ..... 53
FIGURE 29: EXAMPLE FOR A HALF NORMAL DISTRIBUTION WITH $\mu = 0$ AND $\sigma = 10$ ..... 68
FIGURE 30: HEAT AND POWER PROVISION IN THE HEAT-CONTROLLED OPERATION MODE ..... 71
FIGURE 31: POWER PLANT MODELLING: LCOE OVER PRESSURE AFTER FEED-PUMP ..... 74
FIGURE 32: POWER PLANT MODELLING: LCOE OVER TEMPERATURE AFTER OVERHEATING ..... 75

FIGURE 33: POWER PLANT MODELLING: LCOE OVER OVERHEATING ..... 75
FIGURE 34: POWER PLANT MODELLING: LCOE OVER OVERHEATING ..... 76
FIGURE 35: POWER PLANT MODELLING: LCOE OVER THERMAL WATER OUTLET TEMPERATURE ..... 76
FIGURE 36: EFFECT OF A CHANGING PERMEABILITY ON THE LCOE ..... 77
FIGURE 37: EFFECT OF PERMEABILITY ON PRODUCTION PUMP POWER DEMAND AND LCOE ..... 77
FIGURE 38: TEMPERATURE LOSS IN THE WELLBORE AT MEZÖBERÉNY SITE ..... 79
FIGURE 39: COMPARISON OF BASELOAD AND HEAT-CONTROLLED ENERGY PROVISION FOR THE MEZÖBERÉNY CASE .. 80
FIGURE 40: EFFECT OF STIMULATION FOR THE MEZÖBERÉNY SITE ..... 80
FIGURE 41: EFFECT OF INCREASED FLOW RATE ON TECHNO-ECONOMIC PERFORMANCE ..... 81
FIGURE 42: STIMULATION COSTS INCLUDING RISK ASSOCIATED COSTS ..... 82
FIGURE 43: EFFECT OF RISK MITIGATION MEASURES ON THE TECHNO-ECONOMIC PERFORMANCE ..... 82
FIGURE 44: COMPARISON OF PURE ELECTRICITY PROVISION AND CHP BASED ON IRR, NPV AND LCOE ..... 84
FIGURE 45: NET ELECTRICAL POWER FOR POWER PLANT CONFIGURATIONS SELECTED ON THEIR IRR ..... 86
FIGURE 46: COMPARISON OF LCOH OF-LARGE-SCALE HEAT PROVISION TECHNOLOGIES ..... 87
FIGURE 47: OCCURRENCES OF THREATS TO GROUNDWATER VERSUS THE ACCEPTANCE LEVEL TOWARDS HYDRAULIC FRACTURING ..... 114
FIGURE 48: MEDIAN HOUSEHOLD INCOME VERSUS THE ACCEPTANCE LEVEL TOWARDS HYDRAULIC FRACTURING..... 114
FIGURE 49: DENSITY OF HYDRAULICALLY FRACTURED WELLS VERSUS THE ACCEPTANCE LEVEL. ..... 115
FIGURE 50: INFLUENCE OF TEMPERATURE ON THE PERMEABILITY REDUCTION BY FINES MIGRATION..... 116
FIGURE 51: DEPTH DEPENDENCE OF THE MAXIMUM EXPECTED MAGNITUDE DERIVED FROM 1000 MODEL REALIZATIONS ..... 122
FIGURE 52: ACCELERATION RECORD FOR A TYPICAL STRONG TECTONIC EARTHQUAKE, WITH THE PGA INDICATED (THE DUTCH STATE SUPERVISION OF MINES (SSM), 2015). ..... 123
FIGURE 53: SOCIETAL-RISK F-N CURVE FOR THE CENTRAL AREA OF THE GRONINGEN GAS FIELD. FOR REFERENCE, THE F-N CURVE FOR DUTCH FLOODING RISK IS ALSO SHOWN ..... 124
FIGURE 54: LITERATURE REVIEW ON EFFECT OF STIMULATION ..... 128
FIGURE 55: LITERATURE REVIEW ON EFFECT OF STIMULATION ..... 129
FIGURE 56: LITERATURE REVIEW ON EFFECT OF STIMULATION ..... 130
FIGURE 57: LITERATURE REVIEW ON EFFECT OF STIMULATION ..... 131
FIGURE 58: LITERATURE REVIEW ON EFFECT OF STIMULATION ..... 132
FIGURE 59: LITERATURE REVIEW ON EFFECT OF STIMULATION ..... 133
FIGURE 60: PROGRAM FLOW CHART OVERALL MODEL ..... 134
FIGURE 61: PROGRAM FLOW CHART POWER PLANT MODEL ..... 135
FIGURE 62: PROGRAM FLOW CHART WELLBORE MODEL ..... 136

# List of tables


TABLE 1 MAIN PROCESSES GOVERNING THE EVOLUTION OF A SUBSURFACE ASSET ALONG ITS LIFE-CYCLE ..... 2

TABLE 2: OVERVIEW OF NEAR WELL RESERVOIR PROCESSES AFFECTING PRODUCTIVITY AND INJECTIVITY OF A GEOTHERMAL WELL IN A FRACTURED POROUS CARBONATE RESERVOIR ..... 30

TABLE 3: PARAMETERS FOR CALCULATING HEAT EXCHANGER SURFACES ..... 42

TABLE 4: COMPARISON ORC-MODEL WITH SOULTZ-SOUS-FORÊTS ..... 46

TABLE 5: SALINITY OF THERMAL WATER AT DESTRESS-LOCATIONS, ..... 47

TABLE 6: OVERVIEW MONTE-CARLO-PARAMETERS POWER PLANT ..... 49

TABLE 7: OVERVIEW OF THE POWER PLANT COSTS ..... 52

TABLE 8: COEFFICIENTS FOR MODULE COST CALCULATION OF THE ORC ..... 54

TABLE 9: OVERVIEW OF THE COSTS OF THE THERMAL WATER CYCLE ..... 57

TABLE 10: COEFFICIENTS FOR MODULE COST CALCULATION OF THE THERMAL WATER CIRCUIT ..... 59

TABLE 11: OVERVIEW OF RESERVOIR COSTS ..... 59

TABLE 12: RISK FACTORS IN SOFT STIMULATION MEASURES ..... 66

TABLE 13: PARAMETERS FOR THE INTEGRATION OF RISK FACTORS IN TECHNO-ECONOMIC MODELLING ..... 67

TABLE 14: RISK MITIGATION MEASURES ..... 70

TABLE 15: INPUT PARAMETER SOULTZ-SOUS-FORÊTS SITE ..... 73

TABLE 16: INPUT PARAMETER MEZÖBERÉNY SITE ..... 78

TABLE 17: INPUT PARAMETER UPPER RHINE GRABEN SITE ..... 83

TABLE 18: DECISION GATE REVIEW # 1: APPROVAL OF PROJECT INITIATION ..... 106

TABLE 19: DECISION GATE REVIEW # 2: APPROVAL OF CONCEPT SHORT LIST ..... 107

TABLE 20: DECISION GATE REVIEW # 3: PROJECT CONCEPT SELECTION AND DEFINITION ..... 108

TABLE 21: DECISION GATE REVIEW # 4: APPROVAL TO ISSUE PDO / PIO1 ..... 109

TABLE 22: DECISION GATE REVIEW # 5: APPROVAL TO START EXECUTION ..... 110

TABLE 23: DECISION GATE REVIEW # 6: APPROVAL TO START OPERATION ..... 110

TABLE 24: DECISION GATE REVIEW # 7: POST IMPLEMENTATION ASSESSMENT ..... 111

TABLE 25: LOCATION CHARACTERISTICS AND THEIR INFLUENCE ON THE PUBLIC ACCEPTANCE OF GEOTHERMAL PROJECTS AND SOFT STIMULATION ..... 115

TABLE 26: CRITICAL IONIC STRENGTHS FOR FINES MIGRATION. ..... 117

# Nomenclature

## Abbreviation

| Symbol | Explanation | Unit |
|---|---|---|
| $CaCl_2$ | Calcium chloride | - |
| CEPCI | Chemical engineering plant cost index | - |
| CHP | Combined heat and power | - |
| EGEC | European geothermal energy council | - |
| ESP | Electrical submersible pump | - |
| EU28 | European Union (members 2018) | - |
| EUR | Euro | - |
| EV | Evaporator | - |
| E&P | Oil and gas industry | - |
| FBHP | Flowing bottom hole pressure | bar |
| FBHT | Flowing bottom hole temperature | K; °C |
| FTHP | Flowing tubing head pressure | bar |
| FTHT | Flowing tubing head temperature | K; °C |
| $H_2O$ | Water | - |
| HDR | Hot-Dry-Rock approach | - |
| IGEM | Integrated geothermal energy model | - |
| IRR | Internal rate of return | - |
| KCl | Calcium chloride | - |
| KPI | Key performance indicator | - |
| LCOE | Levelized Costs of energy | - |
| LCOH | Levelized cost of heat | - |
| LMH | Low – medium – high | - |
| LSP | Line shaft pump | - |
| MC | Monte-Carlo | - |
| MCT | Module costing technique | - |
| MD | Measured depth | - |
| NaCl | Sodium chloride | - |
| NPV | Net present value | - |
| OECD | Organisation for Economic Co-Operation and Development | - |
| OH | Overheating | - |
| ORC | Organic Rankine Cycle | - |
| PBT | Pay-back time | - |
| PDF | Probability distribution function | - |
| PH | Preheating | - |
| PLI | Price level indices | - |
| PV | Photovoltaics | - |
| SHE | Shell and tube heat exchangers | - |
| TDS | Total dissolved solids | - |

| | | |
|---|---|---|
| TVD | True vertical depth | - |
| TW | Thermal water | - |
| TW | Thermal water | - |
| TWC | Thermal water circuit | - |
| USD | US-Dollar | - |
| UW | Underground withdrawal | - |

### Greek formula symbols

| Symbol | Explanation | Unit |
|---|---|---|
| $\tau_V$ | Full load hours | h |
| $\alpha$ | Heat transfer coefficient | $W/(m^2 * K)$ |
| $\beta$ | Thermal coefficient of expansion | $1/K$ |
| $\delta$ | Boundary layer thickness | m |
| $\eta$ | Dynamic viscosity | $kg/m * s$ |
| $\kappa$ | Power- and areal parameter | kW; m² |
| $\lambda$ | Thermal conductivity | $W/m * K$ |
| $\mu$ | Mean value distribution | EUR; m² |
| $\rho$ | Density | $-kg/m^2$ |
| $\varsigma$ | Pressure loss coefficient | - |
| $\sigma$ | Standard deviation | EUR; m² |

### Indices

| Abbreviation | Explanation | Unit |
|---|---|---|
| a | Apparent / outside | - |
| WM | Working medium | - |
| out | Output value | - |
| BM | Bare module | - |
| Well / wellbore | Production- / Injection well | - |
| Bypass | CHP in parallel connection | - |
| in | Input value | - |
| el | Electrical | - |
| geo | Rock, soil, formation | - |
| hyd | Hydraulic | - |
| hydro | Hydrostatic | - |
| i | Sumindex; inside | - |
| I to IV | State points with heat exchanger | - |
| is | Isentrop | - |
| Cond | Condensator | - |
| crit | Critical | - |
| PP | Power plant | - |

| | | |
|---|---|---|
| lam | Laminar | - |
| Pump | Feed-; Production-; Injection-pump | - |
| rand | Random value | - |
| Rec | Recuperator | - |
| BF | Back-flow | - |
| turb | Turbulent | - |
| TW | Thermal water | - |
| Loss | Energy- / Temperature loss | - |
| at-rest | steady state | - |
| 1 to 10 | State points in the working medium cycle | - |
| 2009 | Year 2009 | - |
| 2013 | Year 2013 | - |
| 2016 | Year 2016 | - |

### Indicator

| Abbreviation | Explanation | Unit |
|---|---|---|
| Nu | Nusselt number | - |
| Pr | Prandtl-Zahl | - |
| Re | Reynolds-Zahl | - |

### Latin formula symbols

| Abbreviation | Explanation | Unit |
|---|---|---|
| $\dot{V}$ | Volume flow | $m^3/s$ |
| $\dot{m}$ | Mass flow | $kg/s$ |
| $\bar{x}$ | Mean value population | EUR; m² |
| A | Area | m² |
| a | Thermal conductivity | $m^2/s$ |
| C | Costs | EUR |
| $c_p$ | Specific heat capacity | $J/kg * K$ |
| d | Diameter | m |
| E | Earnings | EUR |
| $F_m$ | Material factor | - |
| $F_p$ | Pressure factor | - |
| H | Water level | - |
| h | Enthalpy | $J/kg$ |
| $h_M$ | Thicknessaquifer | m |
| $I_0$ | Investment costs | EUR |
| K | Permeability | m² |
| k | Heat transition coefficient | $W/m^2 * K$ |
| l | Length | m |

| | | |
|---|---|---|
| M | Molar mass | $^{kg}/_{mol}$ |
| n | Quantity | - |
| p | Pressure | Pa |
| $p_t$ | Mean pipe distance | m |
| R | Radial distance between wells (at bottom hole) | m |
| r | Radius | m |
| S | Storage coefficient | - |
| s | Drilling distance (measured depth) | m |
| $S_x$ | Standard deviation population | EUR; m² |
| T | Temperature | K; °C |
| u | Speed | $^{m}/_{s}$ |
| v | Specific volume | $^{m^3}/_{kg}; ^{m^3}/_{mol}$ |
| w | Mass fraction | $^{kg}/_{kg}$ |
| X | Steam content | - |
| x | Substance share | - |
| Z | Interest on construction period | EUR |
| z | Vertical depth (true vertical depth) | m |
| $Z_c$ | Confidence level | - |

# Abstract

The EU H2020 project DESTRESS shall demonstrate the application of stimulation techniques in different plays. The overall goal is an improvement of hydraulic reservoir parameters with minimal impact on environment and residents. Besides the applied research the investigation of risk factors as well as the economic effect of soft stimulation is a part of the DESTRESS project. The report at hand combines the topics uncertainty/risk factors and economic evaluation. The integration of uncertainty in general and uncertainty of risk factors in particular, is a further development step in the techno-economic evaluation of geothermal power.

The integration of uncertainty into techno-economic modelling is not completely new in industries looking for underground resources. One of the synergies coming from oil and gas business is the approach of decision analysis that integrates techno-economic evaluation with uncertainty into decision making. Decision analysis is presented in detail in this report. The approach shall improve the quality of decisions in project development and operation and thereby enhance the success of geothermal projects. The uncertainty caused by risk factors is a major topic of this report. The quantification of risk factors presented in this study, enables the integration of uncertainty into techno-economic modelling. Identification and quantification of risk factors are important elements of risk management. For project developers/operators the risk mitigation, as part of risk management, is even more interesting. Therefore, mitigation measures and the evaluation of mitigation measures are also analyzed. The main subject of the study at hand is a techno-economic model of geothermal heat and power plants which is developed to determine the impact of technical and economic risk factors on levelized cost of heat and electricity. To investigate those correlations, the Monte Carlo method is used. Altogether the model consists of three main parts: the reservoir, the thermal fluid cycle and the heat or power plant, respectively. The power plant is implemented as an Organic Rankine Cycle. Pure power or heat generation as well as combined heat and power in parallel and serial setup are considered. Furthermore, both continuous operation and heat-driven operation dependent on a predefined heat load are considered. The model is explained in detail and applied to the three selected demonstration sites. The aim is to demonstrate the “integrated geothermal energy model” (IGEM) and evaluate soft stimulation measures including uncertainty caused by risk factors. On the example of the Soultz-sous-Forêts site, the possibilities and first results of power plant optimization with the Monte-Carlo approach are demonstrated. In addition, the technical effects of the implemented risk factors are shown. The implemented risk factors also affect model parameters on an economic level. These effects are demonstrated on the example of the heat plant in Mezöberény (Hungary). The Mezöberény site is also used to show the enhancement of hydraulic parameters through a stimulation and their effect on selected key performance indicators (KPI). The report is concluded with a comparison of pure electricity provision and combined heat and power (CHP) on the example of a fictitious site in the Upper Rhine Graben (Germany). Based on the frame conditions of this site, a comparison is drawn between geothermal heat supply and other renewable and conventional energy sources capable of large-scale heat provision.

# 1 Introduction

## 1.1 Deliverable 2.2 in the context of DESTRESS

The DESTRESS project has the overall goal to investigate, improve and demonstrate the application of the Enhanced geothermal system (EGS) approach. EGS allow the usage of geothermal reservoirs that can't be exploited under the naturally given techno-economic frame conditions. Low hydraulic conductivities prevent an enormous potential of renewable energy to be used. Therefore, EGS measures aim to improve the productivity of a geothermal reservoir by increasing the hydraulic conductivity of the reservoir. DESTRESS puts forward the idea of soft stimulation. Soft stimulation is a collective term for geothermal reservoir stimulation techniques that aim to increase reservoir performance while minimizing environmental impacts including the risk posed by induced seismicity. Soft stimulation includes techniques such as cyclic/fatigue stimulation multi-stage stimulation, chemical stimulation and thermal stimulation.

The developments achieved in DESTRESS shall be demonstrated considering the site-specific geological requirements. Thereby three overall goals shall be followed:

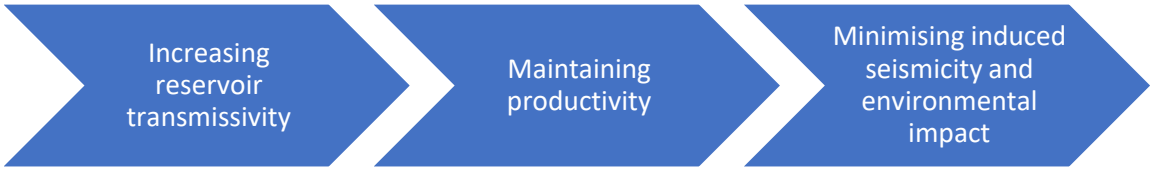


Figure 2: DESTRESS overall goals for the demonstration of stimulation activities

The demonstration of the DESTRESS concept is applied at a variety of different sites representing the majority of reservoir properties as they can be found in Europe. Thereby the soft stimulation approach is in the focus of any demonstration activities, meaning a minimization of environmental hazards. This also includes a comprehensive and progressive risk management together with a detailed investigation of the caused environmental footprint.

The soft stimulation concepts applied in DESTRESS are the developments based on the experiences in previous projects, synergies from other fields, mainly the oil and gas sector, but also the scientific progress reached in fields like i.e. fluid-rock interactions. The better understanding of fluid-rock interaction enables a more accurate determination of the stress field which leads to an improved analysis of induced seismicity.

Within work package 2 of the DESTRESS project the impact of soft stimulation on the techno-economic performance including public acceptance of a geothermal project has to be analysed. Common cost accounting in business case calculations are insufficient to reflect the characteristics of geothermal energy production, because the key technical data can vary widely and are often poorly characterized in early project phases. To deal with this aspect, experiences from the oil and gas industry E&P industries are applied by developing and using a Monte Carlo (MC) based cost calculation model. The necessary probability distributions and cost data are taken from the results of task 2.1 and 2.2, and from the assessment of the latest geothermal power production technologies, especially the most recent optimizations of Organic Rankine Cycles. The completed model is validated using the existing data from geothermal power plants in operation. Further effort is spent on the adaption of the MC based cost calculation model on regional markets. For the evaluation of geothermal projects, the common accounting key performance indicators (KPI) such as internal rate of return (IRR), net present value (NPV) and levelized cost of energy (LCOE) will be used. The LCOE methodology opens the possibility of a techno-economic comparison with other technologies in the field of energy provision. However, whereas most other renewables are incapable of directly providing heat, geothermal is

particularly suited to district heating or combined heat and power (CHP) application. To demonstrate the economic and environmental benefits of heat and CHP provision these usage pathways of geothermal energy are also mapped in the model. Another major aim of the MC based cost calculation model is the detailed analysis of technical and non-technical risk factors.

## 1.2 Investment decisions supported by simulation model

This section 1.2 discusses how simulation models support the investment decision-making process by computing state variables of possible futures[1]. The processes discussed are generic and apply equally to geothermal fields that may have to be developed using alternative well stimulation techniques. Investment decision-making is however a complex process, especially in case of large uncertainties about the productive system (such as when dealing with the poorly sampled subsurface, early in its asset life-cycle) and about the commercial aspects to be expected. These generic processes are described here, as they constitute important boundary conditions on how models should be designed and used.

### 1.2.1 Decision analysis process

The technical / economic model to be delivered as part of the DESTRESS project aims at computing a series of well-founded time-series of state variables and Key Performance Indicators (KPIs), to compare, on a consistent basis, alternative investment options for developing a geothermal field. The absolute value of the model's output and the comparative difference between alternative development options should help decision-makers to further mature a project until Final Investment Decision (FID). The targeted technical / economic model has a role in the Decision Analysis process's, steps 2, 3 and 4 (see Table 1 below).

The Decision Analysis (DA) process is the main building block of a company's project maturation (Decision Gate / DG process) and asset life-cycle processes. The DA process feeds into the DG process, which on its turn drives the physical and economic evolution of a subsurface asset. The objective of the DG process is to *phase* the capital commitment from project initiation to FID, and only commit a next DG-phase's capital when sufficient clarity has been obtained to proceed. The headlines of these three processes are described in Table 1 below. Note that different companies may have their individual variants on these processes. Depending on the project maturity (decision gate) and the asset's life-cycle phase, different data will be available, and different types of decisions to be analysed will be pertinent. Also, different tools, whether qualitative or (semi-) quantitative, will be appropriate.

Table 1 Main processes governing the evolution of a subsurface asset along its life-cycle

| **Decision Analysis process**<br>Feeding each Decision Gate | **Decision Gate process**<br>Maturing a project to FID and start of operation | **Asset life-cycle process**<br>Evolving along an asset's phases |
|---|---|---|
| **Step 1** – *Framing the problem*: defining project alternatives, decision hierarchy, discussing value drivers and risk drivers, main uncertainties, which KPIs to use as decision criteria | **Decision Gate 1** - *Approval of Project Initiation*: validate basis to pursue the business opportunity; initiate the project | **Phase 1** – *Exploration*: discovering a subsurface resource that is established to be economical |
| **Step 2** – *Set-up quantitative models*: agree which model / model functionality to use, including uncertainty | **Decision Gate 2** - *Approval of Concept Short List*: confirm that resolution of uncertainties supports | **Phase 2** – *Appraisal*: obtaining additional information on the discovered subsurface resource in |

[1] Note that a common definition of a '*decision*' is: *an irrevocable allocation of scarce resources*. Decision-makers make these allocations.

| **Decision Analysis process**<br>Feeding each Decision Gate | **Decision Gate process**<br>Maturing a project to FID and start of operation | **Asset life-cycle process**<br>Evolving along an asset's phases |
|---|---|---|
| quantification method (fitness-for-purpose of model detail) | continuation of definition and move to Concept selection. | order to optimize its development plan |
| **Step 3** – *Generate range of outcomes*: deterministic ranges or probabilistic histograms of KPIs | **Decision Gate 3** - *Project Concept Selection and Definition*: confirm approval of the Concept Selection | **Phase 3** – *Development:* developing the appraised resource by drilling wells and installing surface facilities |
| **Step 4** – *Perform sensitivity analysis*: establish which uncertain input parameters have most impact on risk and value | **Decision Gate 4** - *Approval to issue PDO / PIO*: Project considered sound and ready to execute, prior to and conditional on PDO / PIO approval. | **Phase 4** – *Operation*, i.e. production, including incremental development |
| **Step 5** – *Apply decision criteria*: describe process and recommend optimal solution / way forward; communication | **Decision Gate 5** - *Approval to Start Execution (Final Investment Decision / FID)*: confirm that conditions as at DG Review # 4 are still valid. | **Phase 5** – *Decommissioning / abandonment* |
| **Step 6** – *Assess decision quality:* a look-back analysis of the DA process. Assess whether the decision process had sufficient quality in terms of: appropriate frame, meaningful reliable information, creative alternatives, clear values and trade-offs, logically correct reasoning, fostering learning and working towards "best practices", commitment to action. | **Decision Gate 6** - *Approval to Start Operation:* To confirm ready to start operation and hand over of Operatorship | |
| | **Decision Gate 7** - *Post Implementation Assessment*: assess to what degree the objectives of the development project have been fulfilled. To provide experience feedback for future projects. | |

The targeted DESTRESS geothermal project evaluation tool is aimed primarily at assessing situations where uncertainties are large and, therefore, precision of the predicted physical processes cannot be obtained. The tool should be applicable and useful primarily in case of sparse information on the geothermal reservoir and rather contrasting development options (thereby targeting the 'concept selection' of DG 3). Therefore, the tool aims essentially at a geothermal asset that is relatively immature, i.e. early in its life-cycle phase (say, phases 1-3 in Table 1 above), and early in its project maturation (say, decision gates 1-3 in Table 1 above, until concept selection).

### 1.2.2 Types of decisions

With the targeted DESTRESS tool decision in an early project phase can be answered. Typically, these decisions pertain to a relatively immature geothermal asset, i.e. early in its life-cycle and project maturation phase (say, DG 1-3). In the following examples for these decisions are given:

- Explore yes/no a mapped, but undrilled prospect.
- Appraise yes/no a mapped, drilled resource; and if so, establish the number and sequence of appraisal wells. Understand the value of new information by translating alternative information outcomes into alternative reservoir development plans.

    - Note: the targeted DESTRESS tool will *not* model spatial heterogeneity of the reservoir. Hence, the tool will not help in optimizing the location of a new well. However, the effect of spatial heterogeneity in terms of reinjected cold-water breakthrough into the production well can be modelled in the DESTRESS tool, i.e. if a 3D reservoir simulation study has been done.
- Concept selection for developing the appraised resource; understanding the economic feasibility of the geothermal resource. This includes, for example:
    - Number, sequence, spacing/pattern and timing of development wells to be drilled
        - Producers
        - Injectors
        - Number of well clusters
    - Well design: depth, diameters, completions, vertical lift
    - Types and frequency of well stimulation jobs to be done
        - Soft stimulation vs. conventional stimulation + associated costs.
        - Impact on skin factor remediation + impact on post stimulation job skin build-up.
    - Decision on type of energy utilized
        - Heat plant (HP)
        - Combined heat and power plant (CHP)
        - Power plant (PP)
    - Technical configuration of surface facilities to be installed:
        - Pressure condenser outlet
        - Pressure feed pump outlet
        - Temperature superheater outlet
        - Recuperated energy

### 1.2.3 Project maturity

As discussed in section 1.2.1 and in Table 1 above, a project's maturity evolves along the so-called Decision Gates (DGs). It is important to understand how project evaluation tools, such as the targeted DESTRESS tool, can help maturing a project along these Decision Gates. After having reached the next Decision Gate, a formal Decision Gate Review (DGR) is held, during which the project's maturation is tested. In case the DGR has fulfilled the requirements of management, then in principle the management allocates a new budget to work towards the next DGR, and so on.

In Appendix A, Table 18 - Table 24, a possible breakdown into phased decisions related to a project's maturity ('Decision Gates') is given (Jonkman, Bos, Breunese, Morgan, & Spencer, 2000). It is considered that this process is a possible analogue for analysing geothermal asset development cases. For the case studies envisaged by the DESTRESS tool, the requirements of DGR #1, #2 and/or #3 are likely to be applied, at least to some extent. Note however that this DG process pertains to capital-intensive, complex projects that are subject to significant uncertainties. For less costly, less complex and less uncertain projects, a much simpler process could be adopted.

### 1.2.4 What do managers need to make good decisions?

First, let us discuss what managers need to make adequate decisions. Many conferences have been held around this theme. A consensus seems to be:

- They need to know if the team evaluated a range of different alternatives that have been framed because of their pre-supposed relevance.
- For each alternative they need to understand:
    - The value (including the option value) and its top drivers;

    - The risk and its top drivers;
    - What combination of outcomes would cause them to change their choice.
- They need to be convinced that the calculated uncertainty range reasonably captures the range of possible outcomes.
- They need to have confidence that their decision is robust under a range of possible assumptions.
- They want to know that all projects / alternatives have been evaluated on a consistent basis, and that the evaluation tool is based on sound principles. Also, they would like to know how the evaluation tool has performed in the past and which potential pitfalls the tool may have.

In conclusion, the DESTRESS tool takes a central place in the Decision Analysis (DA) process. The DESTRESS tool should be designed such that it can reasonably well capture the impact that a decision will have on the asset's future (technical and economic) performance.

### 1.2.5 Purpose of the DESTRESS tool

The purpose of the DESTRESS tool is to feed the Decision Analysis (DA) process and thereby support the project maturation / Decision Gate process (see also Table 1 on page 2). In the tables of section 1.2.3 above, where the Decision Gate Review requirements are discussed, there is in principle a role for quantitative tools to address many of the indicated questions. As discussed in the last paragraph of section 1.2.1, the application range of the tools is aimed mainly at decision support for early Decision Gates and early in an asset's life-cycle, i.e. when there is a relative data paucity. The targeted DESTRESS tool is not aimed at detailed computations of physical processes in the three spatial dimensions with important spatial heterogeneities, nor at detailed time-steps. The latter computations would be pertinent in case of availability of more detailed data and in case of more detailed decisions such as locating a next well to be drilled, or the detailed design of a production facility (i.e. in case of a decision gate beyond 'concept selection').

To provide support to the indicated type of decisions, the targeted DESTRESS tool processes physical, technical, economic and planning data into deterministic and probabilistic time-series of heat production, electricity production and cash flows, and into (histograms of) KPIs, which can be used as decision criteria. Examples of KPIs are: NPV, IRR, LCOE, maximum exposure, $GWh_{th}$ and $GWh_e$ sales, Unit Technical Cost, $CO_2$ emissions to the atmosphere avoided, etc. (see also section 4.2 on page 64). Moreover, the tool will help performing a sensitivity analysis to obtain insight into which parameters contribute most to the uncertainty in a KPI.

### 1.2.6 Tool design

#### 1.2.6.1 Principal design concepts

The tool design is based on the following main concepts:

- The tool uses analytical equations only. These are fast to solve and therefore allow more comprehensive uncertainty and holistic analysis. Iterative calculations within a time-step are avoided as much as possible.
- Spatial heterogeneity cannot be modelled in detail. The reservoir is represented in a zero-dimensional point. For each well reservoir-averaged physical property is used. Similarly, state variables are assumed to be constant within a modelling time-step.
- Per time-step, the system's state variables are computed in the physical variables domain and converted into the time domain using the planning assumptions (i.e. timing of a new well, of a workover). The time-step used in the model is 1 year. Per time-step, stabilised conditions are presumed.

- Producers and injectors differ in terms of their hydraulic properties i.e. their skin factor, II, or PI.
- Modelling of physics:
  - Reservoir initial static situation: “Heat in Place”.
  - Reservoir dynamics: Material balance in case of semi-steady-state inflow. No material balance modelling in case of steady-state inflow (i.e. in case of geothermal doublet). No conductive heat flow in the reservoir during the asset’s productive life. All heat flow is convective flow related to the production / injection of water by the wells.
  - Reservoir dynamics: Decline of produced water temperature in production wells, i.e. after the breakthrough of the (cold) injected water. This is represented by a simple analytical function, which can be derived from a separate 3D thermal reservoir simulation study.
  - Reservoir/well dynamics: (semi-)steady-state radial well inflow equation, both for producers and injectors. The drainage area per well is assumed to be the area of the reservoir divided by the number of wells.
  - Skin factor: given a build-up rate, the skin (for producers, and for injectors) is computed per time-step. Following a well stimulation job, the skin factor is re-set at its given starting value
  - Intra-well dynamics: Vertical Flow Performance (VFP), computing $\Delta p$ and $\Delta T$ between bottom hole and tubing head as a function of the production rate, well/tubing geometry, and absolute value of pressure (p) & temperature (T) at the upstream end. Calculation of flowing tubing heat temperature (FTHT) & flowing tubing head pressure (FTHP) and flowing bottom hole temperature (FBHT) & flowing bottom hole pressure (FBHP) of the re-injected thermal water.
  - Heat exchange / thermodynamics in surface facilities. Enthalpy and entropy calculations to transfer energy to a binary cycle, evaporate the working medium of the binary cycle and convert steam into electricity. Calculation of h, s, p and T for a defined number of state points.

- Planning variables:
  - Timing of geophysical / geological survey CAPEX, drilling expenditures, (facility) CAPEX, well workovers, stimulation jobs, etc.
  - Timing of first production
  - Build-up time to plateau production
  - Automatic stopping criteria: (1) Following onset of production decline (i.e. $MWh_{th}$/yr and $MWh_e$/yr sales), the field is shut-in when Net Cash Flow has been <0 for more than *n* consecutive years; or (2) the field is shut-in when FBHT of production well < minimum required FBHT.
  - After the field is permanently closed-in, an automatic mandatory observation / monitoring period is started with the associated monitoring OPEX. At the end of this period, the field is decommissioned / abandoned, with the associated abandonment CAPEX.

- Modelling of economics:
  - For tax purposes, the project / geothermal asset is assumed to be stand-alone / ring-fenced, i.e. the tool does not consolidate the asset being studied into a corporate portfolio of assets.
  - Discounted Cash Flow analysis (DCF), with a fixed discount rate in time.
  - Fiscal regimes of specific countries are included through an adaption of the interest rate. A method is presented by (Konstantin, 2013) for the determination of interest rates including taxes. The calculation rules together with exemplary results can be found in chapter B of the annex.
    Depreciation is not included into the calculations. This would demand for a detailed profit and loss account. Cost engineering with the methodological approach used in the Integrated geothermal model (IGEM) (see chapter 3) shows a range of accuracy. The used

approach is classified by (Lemmens, 2015) as category 3 according to (AACE, 2016). Which means an accuracy range of – 20 % to + 30 %. Given the uncertainty in the input parameters and following the „fitness for purpose" approach stated by (Bos, 2005) together with the recommendation for project evaluation by (Konstantin, Praxisbuch Energiewirtschaft – Energieumwandlung, -transport und -beschaffung im liberalisierten Markt, 2013), an in deep profit and loss account seems over ambitious under the given circumstances.

- Various types of government stimulation / subsidies (capex, per MWh sold, etc.).
  - Premium tariff for electricity

- Uncertainty modelling:
  - The tool is based on the concept of Monte Carlo sampling of those input variables to which the user has assigned a pdf (probability density function).
  - The tool will *not* model multiple discrete uncertainty scenarios as in a scenario-tree (with chance nodes and discrete scenario branches, each having a finite probability, with all branch probabilities adding up to 100%).
  - The input pdfs can be correlated stochastically. In case of conflicting correlations, the correlation matrix is solved, and the stochastic correlations are re-set.
  - Decisions, continuous uncertainties and deterministic assumptions are clearly distinguished.
  - The tool computes histograms of KPIs, and probabilistic time-series of state variables (i.e. $p_{90}$-$p_{50}$-$p_{10}$ forecasts[2]).
  - The tool allows multi-variate sensitivity analysis by computing sorted tornado diagrams according to standard measures such as *contribution to variance* and *rank correlation*. Correlations between input variables and output KPIs, and between output KPIs / output KPIs are also computed.

#### 1.2.6.2 "Fitness for purpose"

Although tools are often designed to be *generic* to be able to address a wide range of cases, any tool will nevertheless invite a debate on its "*fitness for purpose*" to address the given research question. This debate can be quite complex and can go much in-depth. The essential question is always: Which tool functionality is required to allow decision-makers to be confident about the conclusions of the DA (Decision Analysis) process to a given well-formulated research question? In other words, they would like to understand whether improved tool functionality would change the conclusions of the DA process. Such a sensitivity analysis to understand whether the DA conclusions would change if another tool or another fundamental functionality were selected is however seldom done. The tool's fitness-for-purpose for a given research question therefore demands some *a priori* judgement of the required level of detail (i.e. physical/technical process descriptions, economics, planning aspects, HSE impact, spatial and temporal resolution, etc.). Another question sometimes is whether the tool is primarily aimed at *comparing* decision alternatives, thereby focusing on the *differences* in KPIs, or whether the tool is also supposed to provide *absolute* values that are correct.

An *a priori* judgement of the tool's required functionality to address typical geothermal project evaluations that pertain to the Life-cycle phases 1-2/3, and to Decision Gates 1-3 (see Table 1 on page 2), is given in the beginning of this section. More detailed tool design concepts (modelling principles) are, in our opinion, normally unnecessary for a sound comparison of project alternatives that are subject to large uncertainties. The precise level of detail within the various concepts mentioned above

[2] Note that a $p_{xx}$ (i.e. $p_{50}$) forecast is not the forecast obtained by assigning the $p_{50}$ values to the uncertain input variables and then running the tool deterministically. Rather, the $p_{50}$ forecast is the result of running all stochastic realizations completely, and then computing per time-step the statistics. The concatenation *in time* of all $p_{50}$ values is then defined as the $p_{50}$ forecast.

is however still to be established. But on headlines we believe our main design concepts to be adequate for addressing research questions that include *holistic modelling* (full technical chain and economics) and *comprehensive uncertainty modelling* (Monte Carlo sampling etc.).

Trading-off model precision (i.e. no detailed physics modelling but rather approximate physics modelling, no detailed spatial heterogeneity modelling, no small time-step modelling) to the benefit of more uncertainty and holistic modelling[3] is considered justified for life-cycle phases 1-2/3, and Decision Gates 1-3. See also Figure 3 below:

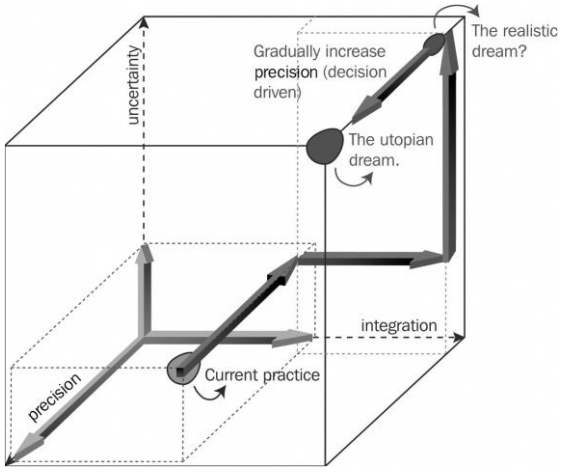


Figure 3: "The modelling cube" (Bos, 2005)

Rather than using high-precision models from the onset of a study, it is recommended to reduce model precision (whilst preserving the "essence" of the physics in terms of fit-for-decision-making-purpose), and opt for maximum integration & uncertainty modelling, thereby moving closer to the ideal corner.

[3] Reference is made here to two well-known quotes, i.e. 1) George Box (1976): "*All models are wrong, but some are useful*" (Journal of the American Statistical Association), and 2) Carveth Read (1920): "*It is better to be vaguely right than exactly wrong*" (in his book 'Logic: Deductive and Inductive'). Paradigms like these are at the basis of the DESTRESS tool.

# 2 Methodological background for a techno-economic evaluation including uncertainty

As discussed in chapter 1.2 the techno-economic evaluation of a project, also called investment decisions, is a generic approach that can be found in basically every business discipline. Therefore, a general introduction in financial mathematics and the standard processes of investment decisions is out of the scope of this report. Here it shall be referred to the widely available literature. For the DESTRESS project uncertainty, also but not only caused by risk factors, plays a major role within the techno-economic evaluation. As mentioned in chapter 1.2 decision analysis gives the structure for this approach. Besides the rather theoretical structure practical questions like the identification of risk factors and the integration of uncertainty into techno-economic evaluations shall be discussed within this chapter.

## 2.1 Decision analysis as methodological approach for comparing options

Decision Analysis (DA) and Decision Quality (DQ) have become standard organizational concepts for complex decision-making problems under uncertainty[4]. Since the DESTRESS project aims at "industry ownership", which calls for a practical decision-making approach, and as decision-making relies on much more than collecting data, setting up a case and running models, it is deemed appropriate to put the DESTRESS WP2 activities in such wider context.

DA comprises the following steps[5]:

- Clear articulation of the decision to be made
- Framing
- Recognition of a decision hierarchy
- Development of alternatives
- Identification of uncertainties
- Valuation, including probabilistic analysis
- Sensitivity analysis
- Interpretation and communication
- Assessment of decision quality (DQ)

Establishing *Decision Quality* is the last step in the *Decision Analysis* process. It essentially is a look-back on the decision process to assess whether it had sufficient quality. Criteria are:

- Appropriate frame
- Meaningful, reliable information
- Creative alternatives
- Clear values and trade-offs
- Logically correct reasoning
- Fostering corporate learning and working towards "best practices"
- Commitment to action

The DA process can be depicted as follows:

[4] See i.e. http://www.decisionprofessionals.com/library/DecisionPedia
[5] See i.e. (HOWARD & ABBAS, 2016)

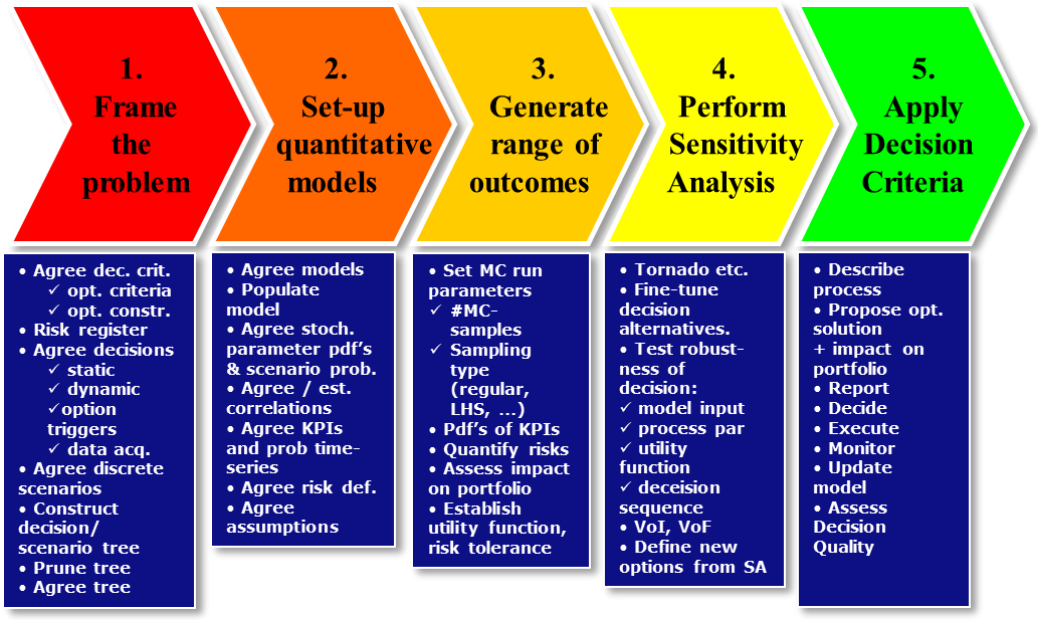


Figure 4: Steps in the Decision Analysis (DA) process, including detailed sub-processes

Each main DA step comprises several sub-processes where the decision / uncertainty space must be defined and assumptions on process parameters must be made. The targeted DESTRESS tool is essentially aimed at supporting the quantitative DA-steps 2, 3 and 4, where the quantitative calculations are prepared or performed. As DESTRESS focuses on soft stimulation, the tool should be able to compare conventional vs. soft-stimulation techniques of geothermal wells, when developing and producing the geothermal asset. This comparison should be framed in DA-step 1.

## 2.2 Uncertainty within techno-economic evaluations – continuous and discretised representation of uncertainty

Uncertainty on the realization of a parameter (at a defined point in time as well as over a time-series) causes an infinite number of possible scenarios. A first experiment of mind would be to think about a defined number of scenarios. But as there is an endless number of scenarios, this task is ambitious as long as the parameter in question is not framed by either technical (i.e. limited number of balls in a lottery), conceptual or any other kind of frame condition (Gleißner, 2015) (Coopersmith, Dean, McVean, & Storaune, 2010/2011). For the sake of techno-economic modelling Figure 5a presents the described mind-set.

Techno-economic modelling as it is done during the DESTRESS-project has the goal to support investment decisions. Thereby, techno-economic models are also subject to the effect of uncertainty as described above. To be able to integrate uncertainty into investment decisions the so-called scenario technique is often used. There, in most cases, three scenarios are chosen to describe the uncertainty of parameters as follows (Gleißner, 2015):

- Best case: The most favourable realistic possibility of realization
- Worst case: The most pessimistic realistic scenario
- Base case: The most probable scenario

Often investment decisions are built only on information on the actual value of the investigated parameter/parameters, while there is no statement on the probability of occurrence/frequency of realization of the discretized scenarios. If this information can be given either through empirical data or expert elicitation the value of information can be increased. Figure 5b pictures the situation when

besides the value for a certain scenario also the probability of occurrence is known. The description of a discretized scenario through a set of values and their probability of occurrence is already a binominal probability distribution function.

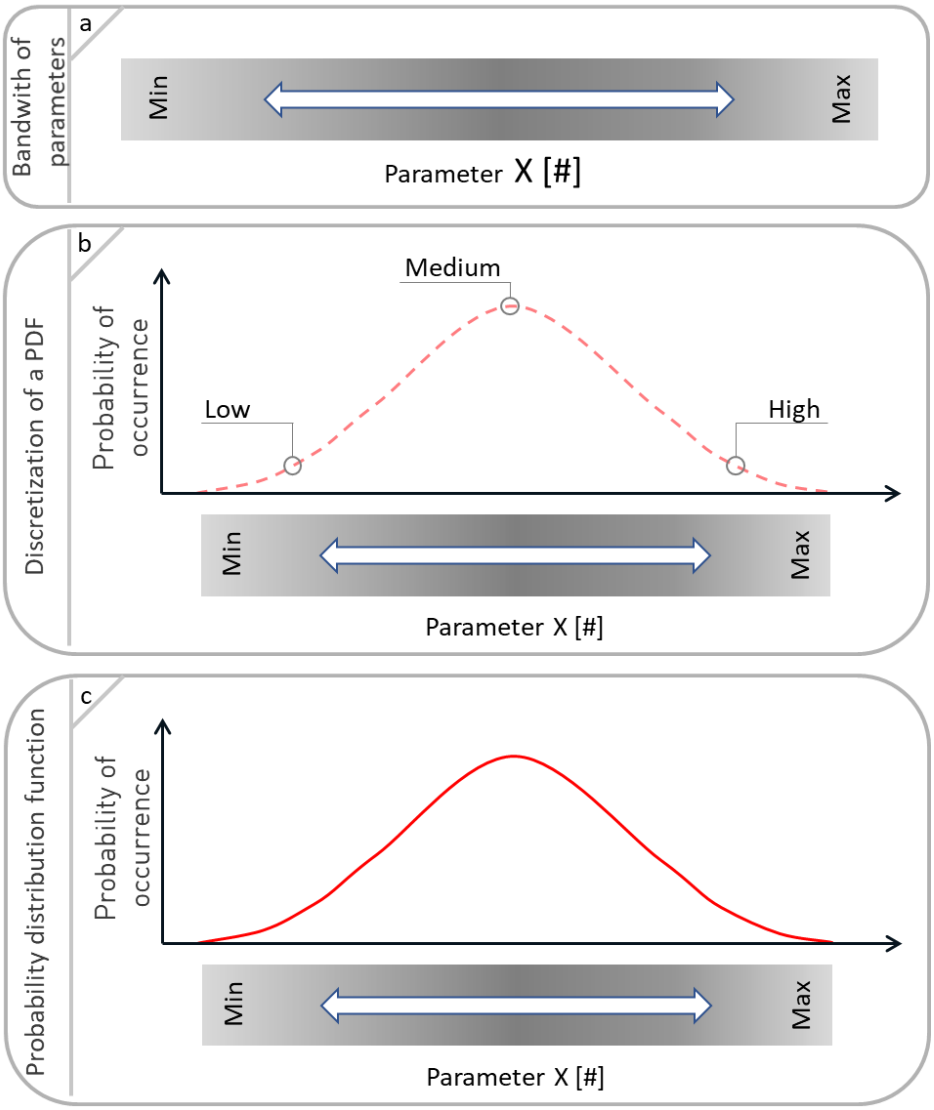


Figure 5: Uncertainty on the realization of a parameter in techno-economic modelling

Faced with the enormous number of possible realizations it is challenging to decide on a discretized unbiased scenario, pointed out by (Gleißner, 2015). Through a continuous probability distribution function as shown in Figure 5c, this problem can be solved. Standardized mathematical descriptions of probability distribution can be found in literature on statistics. As shown in Figure 5c often a normal distribution describes the reality quite well.

While the scenario technique without information on probabilities can be handled with simple spreadsheets, binominal probability distribution functions (PDF) or continuous PDF (Figure 5b and Figure 5c) already need a Monte-Carlo-Simulation. The additional gain of information for decision making and the possibility of doing sensitivity analysis emphasized by (Gleißner, 2015) (Coopersmith, Dean, McVean, & Storaune, 2010/2011) to identify the most important input parameters for a certain key performance indicator (KPI). On the other hands side, more information with the goal of increasing modelling precision, can also weaken the decision-making process. The fit for purpose approach is postulated by (Bos, 2005). He points out, that models are for insight into the complex relationships

that govern the technical and economic feasibility of an (investment) project. Thereby, more information is not a goal of modelling: insight is the goal. More information is not necessarily useful. Probabilistic models, using binominal or continuous PDFs, are generally more insightful and less biased than deterministic models, as used with the scenario technique. This is especially true, when uncertainties are relatively large. This enhanced insight may improve the quality of a decision (see chapter 1.2.1 and 2.1). Probabilistic models require however more skills and time to run and analyse.

Within probabilistic simulations discretized and continuous PDF are not opposite concepts but can be combined in decision trees. Figure 6 shows an example for a decision tree. Through following a branch at each chance node, a discretized scenario is pictured. The scenario chance given for each branch shows the binominal probability distribution. At the end nodes (leaves) continuous distributions can be integrated. The whole decision tree is calculated in a Monte-Carlo-Simulation to get a value for the desired KPI for each scenario (see also (Coopersmith, Dean, McVean, & Storaune, 2010/2011))

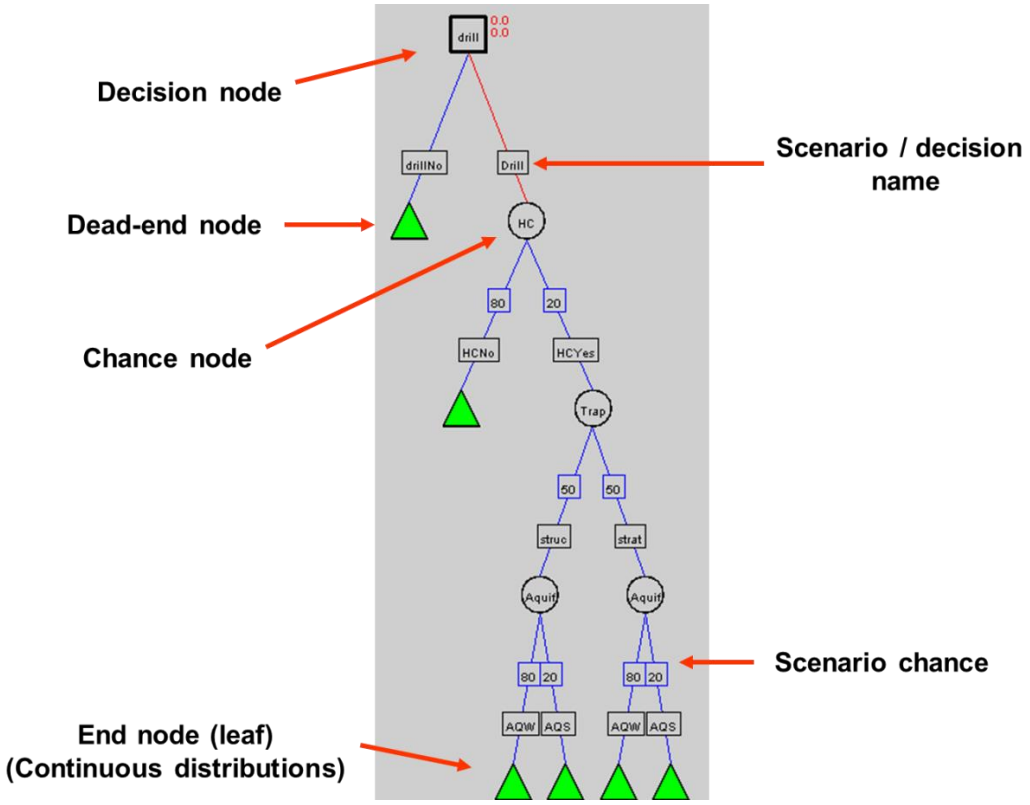


Figure 6: Decision tree on the example of a “drill/no-drill” decision (Bos, 2017)

All uncertainties that are deemed to be significant for the model’s output KPI histograms and probabilistic time-series should be modelled as uncertainties. In the end, all decisions to be evaluated should obviously receive the full range of possible outcomes with their probabilities. In practice, however, many companies take a short-cut and only model a few uncertainties discretely, or approximate continuous uncertainties by a few values only (i.e. low-medium-high – LMH). The level of integration of uncertainty can range from the above mentioned LMH-approach to a Real-Option-Valuation. Thereby not only endogenous but also exogenous uncertainties can be included. A taxonomy is presented by (Bos, 2017) that tries to structure the different levels of the integration of uncertainty into techno-economic modelling.

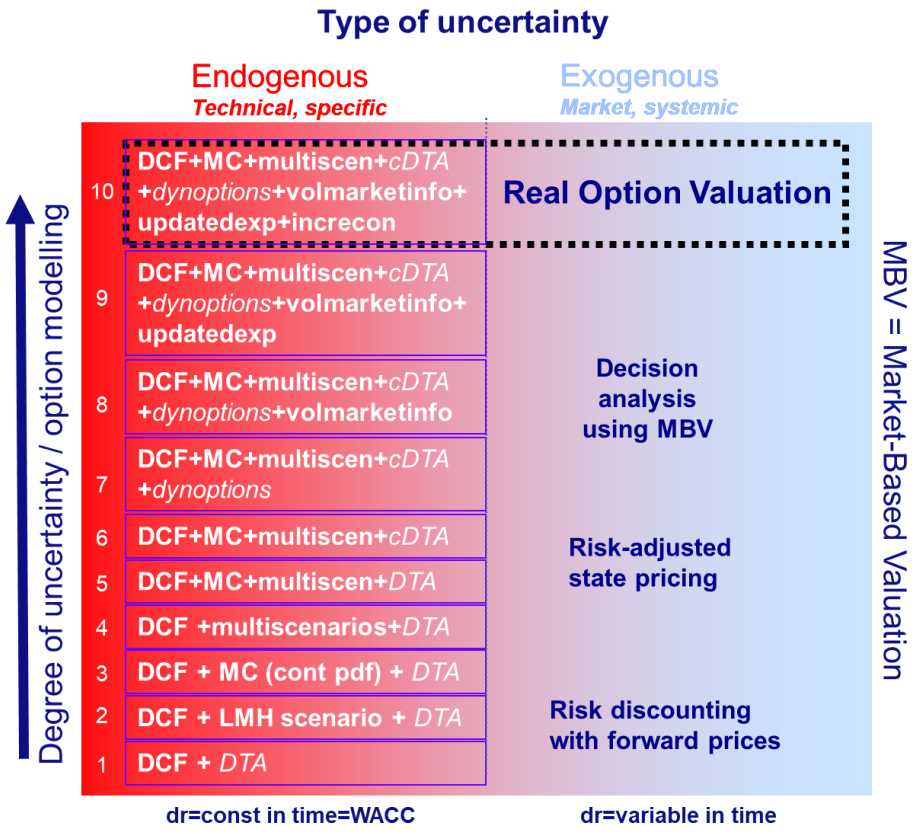


Figure 7: Taxonomy on the integration of uncertainty into investment decisions (Bos, 2017); DR = Discount rate; DCF = Discount of cash flow; DTA = Decision tree analysis; LMH = Low-Medium-High scenarios; multiscen = multiple discrete scenarios; cDTA = Condition decision tree analysis; dynoptions = dynamic options – decisions taken after acquiring new information in the future; MC = Monte-Carlo-Simulation; cont pdf = Continuous probability distribution functions; volmarketinfo = volatile market information (i.e. oil price over time); updatedexp = Updated expectation – new simulations after following a certain path in reality; increcom = incremental economics

## 2.3 Risk analysis process conducted within the DESTRESS project

The identification and quantification of risk factors was published in (Reith, Hehn, Mergner , & Kölbel, 2017) but shall be summarized in the following as it is the basis for the modelling of risk factors within WP2. As pointed out by (Macmillan, 2000) multiple definitions for risk can be found in the literature. For this report, risk shall be defined as “Probability of an undesired impact multiplied by the magnitude of that undesired impact” (Bos & Wilschut, 2011). Following this definition, risk factors are “Model input parameter that have a high potential impact on risk” (Bos & Wilschut, 2011).

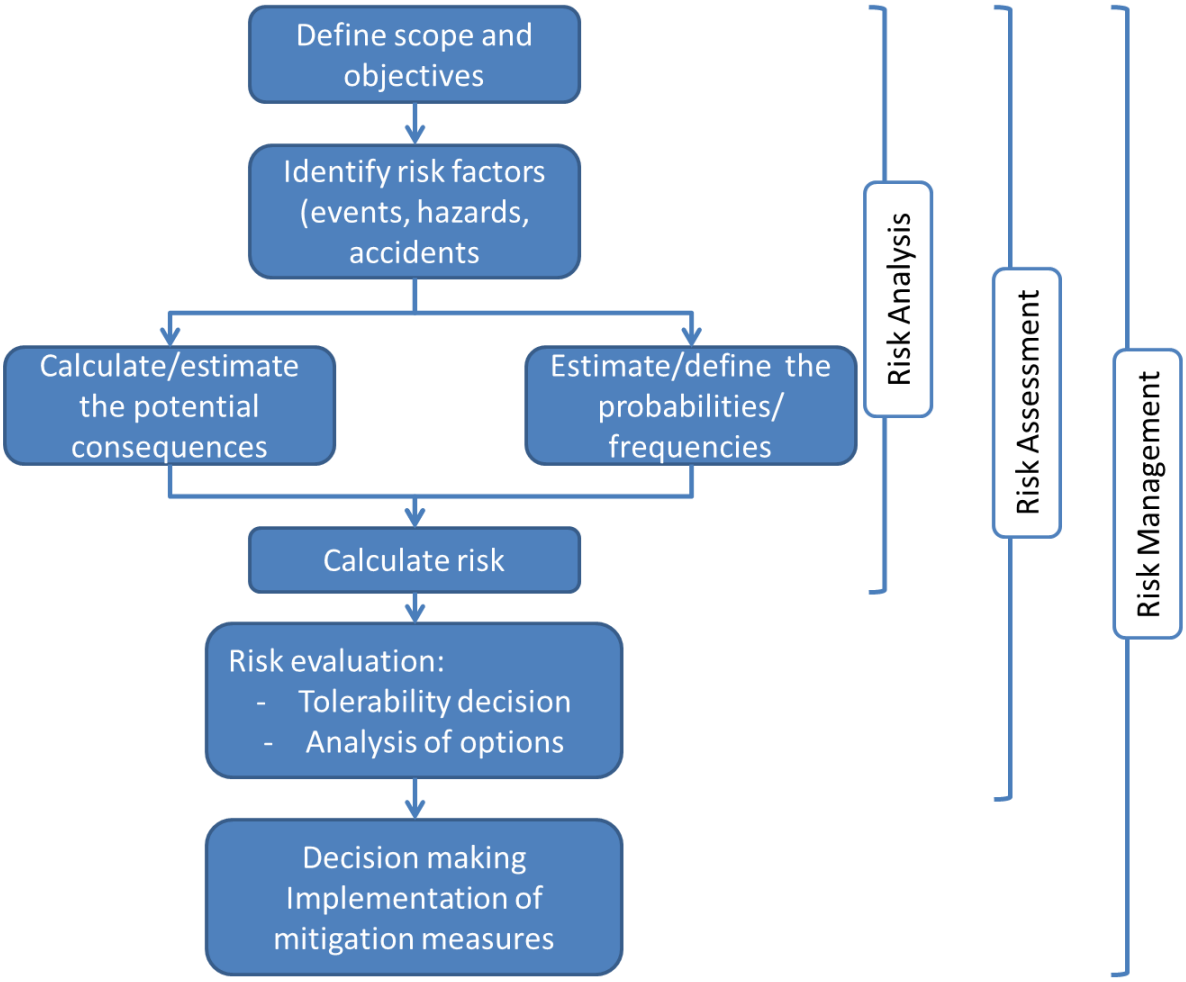


Figure 8: Quantitative risk assessment process (Abrahamsson, 2002) (Reith, Hehn, Mergner , & Kölbel, 2017)

Risk factors can have a generic character like accidents or delays, they can be linked to certain operations like the handling of hazardous goods during a chemical stimulation but can also be site specific like the effect of local geology on operations. The focus of this report is the evaluation of soft stimulation measures in general, therefore site-specific effects shall not be included in the investigations. For the identification and quantification of risk factors the so-called quantitative risk assessment process, presented in deliverable 2.1, is used. Figure 8 gives a short overview of the quantitative risk assessment process first published by (Abrahamsson, 2002) and adapted by (Reith, Hehn, Mergner , & Kölbel, 2017). As a first step, the "Definition of scope and objectives" must be conducted (see chapter 2.3.1). Afterwards, the identification of risk factors can take place (see chapter 2.3.2). To limit the quantification effort, an additional step is introduced. Between the identification and the quantification of risk factors, a prioritization is performed which is explained in chapter 2.3.3. Chapter 2.3.4 then finally gives a short overview on the quantification of risk factors.

### 2.3.1 Definition of scope and objectives

The DESTRESS project focuses on the demonstration of soft stimulation activities. The goal is to enhance hydraulic properties of existing sites with a minimum environmental impact. Therefore, the risk analysis takes the same focus and investigates only the uncertainties caused by risk factors directly associated with the stimulation measures.

### 2.3.2 Identification of risk factors

A structured approach is presented by (Reith, Hehn, Mergner , & Kölbel, 2017) based on expert elicitation that is designed to ease the identification of risk factors. The expert elicitation is done in a group discussion with a project schedule as a basis. In Figure 2 the project schedule for the risk identification at the Mezöberény project in Hungary (chemical stimulation) is presented. The questions listed within each project phase shall serve as a starting point for the identification process.

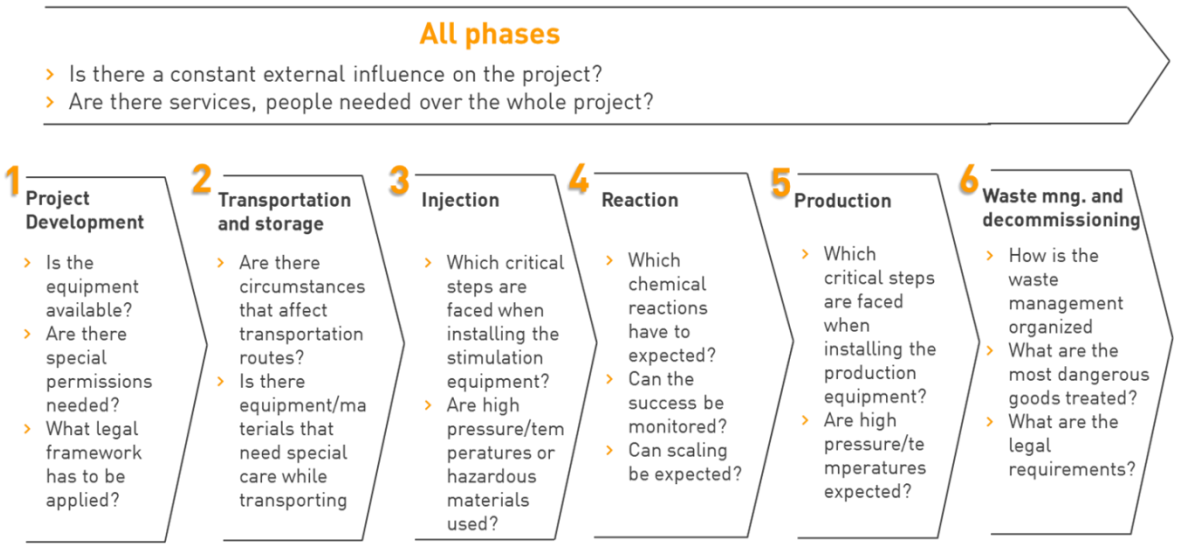


Figure 9: Project schedule adapted to a chemical stimulation of geothermal systems

The outcome of an expert elicitation as it is described above would be a “risk inventory”. A database of risk factors associated with the investigated operation/project that states at least name, description of cause and description of effect for each identified risk factor.

### 2.3.3 Prioritization of risk factors

For the prioritization of risk factors contradictions to existing literature can be found. For example, in (Bos & Wilschut, 2011) the ranking/prioritization is done by a sensitivity analysis on modelling results. In DESTRESS the prioritization of risk factors is already done before the techno-economic modelling and the results (prioritized list of risk factors) are implemented into the techno-economic model. This allows a preliminary overview on the most important risk factors without modelling effort. And for the following modelling steps, the reduced number of risk factors limits the effort needed to implement risk factors into the techno-economic model. Nevertheless, a prioritization before modelling is methodological weaker and resilient.

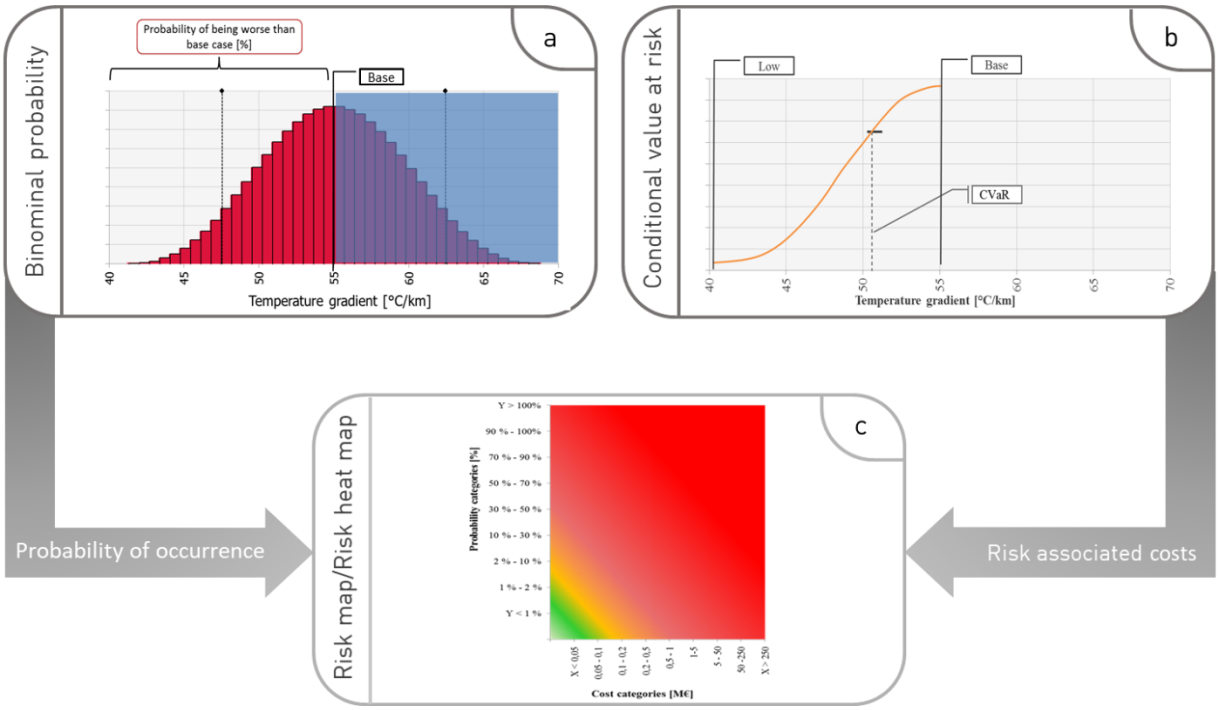


Figure 10: Prioritization process with the example of a temperature gradient

Figure 10 gives an overview on the prioritization process also published in (Reith, Hehn, Mergner , & Kölbel, 2017). The ranking of the risk factors is done by a methodology called “risk heat map” shown in Figure 10c. Within the risk map, the probability of occurrence (POO) is drawn over Risk associated costs (RAC). Risk factors with high probability and high risk associated costs are prioritized. For the use of risk heat maps a single value for risk associated costs and probability of occurrence is needed. But risk factors are uncertain and thereby connected to a continuous PDF. This fact makes it difficult to derive a single value for risk associated costs and probability of occurrence.

A solution is the definition of key performance indicators (KPI) that can map the whole range of the PDF associated with a risk factor. For the definition of these KPI in a first step, discretized scenarios must be defined along the PDF (see chapter 2.2). As can be seen in Figure 7a and Figure 7b a “base case” and a “low case” is needed. The “base case” represents the most likely outcome, while the “low case” describes a less likely but realistic negative outcome. Through the definition of these two scenarios a binominal PDF is created.

The first KPI is a single value for the probability of occurrence. It is estimated by giving the probability of having a realization worse than the base case (see Figure 10a). the second KPI gives the risk associated costs. They are derived by assuming a normal distribution between the low and the base case. For this PDF the conditional value at risk (CVaR) can be calculated. To be able to get the CVaR, risk associated costs for the base and the low case must be estimated beforehand. Through this approach it is possible to use the risk map as a tool for prioritization, through aggregating the information associated with a continuous PDF.

### 2.3.4 Quantification of risk factors

The quantification of risk factors or uncertainty in general is best done with empirical data or an analytical correlation. As described in (Reith, Hehn, Mergner , & Kölbel, 2017) such data is only rarely available. This claim was challenged for the risk factors prioritized in (Reith, Hehn, Mergner , & Kölbel, 2017). Chapter B presents an in deep literature review on the quantifiability of the prioritized risk

factors. The focus is on the quantification of their likelihood and on their impact (technical or economic) on power plant development/operation.

The literature review found that geothermal reservoir stimulation is a relatively uncharted technology and little empirical data exists that could be used to build stochastic models. The factors that influence the prioritized risk factors are often inherently uncertain and very dependent on the locality, culture or physical-geological conditions. A “true” quantitative, stochastic assessment of the risks therefore proved to be not feasible. The main factors that influence the single risk factors are sorted out from the literature presented in chapter B.2.1-B.2.8. Additionally, recommendations for the mitigation are given.

A semi-quantitative assessment regarding the risk factor as well as quantifiable parameters are given where possible. For example, the issue of public acceptance can be estimated beforehand by several parameters specific to the location. As another example, “formation damage by fluid-fluid and fluid-rock interactions” can also be estimated. But these estimations are limited because of the special boundary conditions that apply to geothermal reservoirs. In contradiction, other factors, such as political instability or tool loss, are subject to great uncertainties and attempts to quantify these are not productive.

Based on the results presented in chapter B (Annex), a semi quantitative method had to be used to describe the PDF of the investigated risk factors. As shown in chapter 2.2 (see also Figure 5) the uncertainty of a parameter can be described by a continuous PDF. If the continuous PDF is not known or because of simplicity it shall not be used, a PDF can be discretised. Ideally the discretization would be done on empirical data. If there is no empirical data, expert elicitation has proven to be a reliable source of information (Bos & Wilschut, 2011). To simplify the process for the participating experts a limited number of discretised scenarios must be defined. In practice the so called Low-Medium-High-approach (LMH) is widely used. By using the discretised scenarios as supporting points, a probability distribution (i.e. normal distribution, Weibull-distribution …) can be selected that describes the discretised scenarios best. Figure 11 shows this approach as an example of a temperature gradient. Three discretized scenarios consisting of a dataset of probability and effect [°C/km] form the basis for the selection of a continuous PDF, in that case a normal distribution is seen. This simplified approach can be used if time, data availability or scarcity of resources limit the possibilities for the identification of an appropriate continuous PDF.

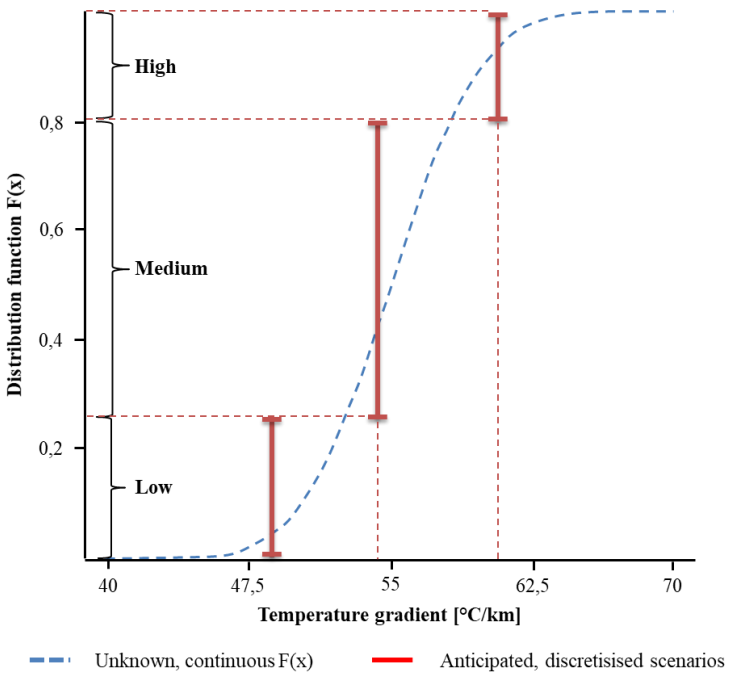


Figure 11: Identification of a continuous probability distribution based on discretised scenarios

While the probability of occurrence is expressed in the same way for each risk factor, the effect of a risk factor can vary widely. The effect of risk factors must be described in a way, that it can be used as model input parameters. Units that are not used in the techno-economic model are not appropriate to describe a risk factor. Therefore, the effect of risk factors must be translated into technical parameters, economic parameters or time. Risk associated costs, changes in technical parameters or delays in the project schedule have proven to be appropriate. Thereby correlations must be respected, i.e. while drilling several wells delays must be shifted from well to well.

# 3 IGEM – Integrated geothermal energy model

The IGEM in its current development status is based on the techno-economic model used in (Welter, Technisch-ökonomische Analyse der Energiegewinnung aus Tiefengeothermie in Deutschland, 2018) and has been further developed by the DESTRESS-partners University of Glasgow (UoG), Netherlands organization for applied scientific research (TNO) and Energie Baden-Württemberg (EnBW). In the following a brief introduction shall be given. For further information, please refer to (Welter, Technisch-ökonomische Analyse der Energiegewinnung aus Tiefengeothermie in Deutschland, 2018).

The IGEM consists of several sub models that are merged through a model backbone. One of the central development approaches of the IGEM is the usage of Monte-Carlo-Simulations. The “Monte Carlo Method” is a powerful tool to solve problems, where analytical approaches fail or can only be implemented with considerable effort. It is used in diverse scientific disciplines for quantitative analysis. Basis for this is many similar random experiments. The goal is the analysis of the system behaviour in the random experiments. From the results obtained conclusions on the real system behaviour can be drawn (Dunn & Shultis, 2011) (Bundesverband Geothermie, 2018). Is the method used in a simulation, the term Monte Carlo simulation that is used by (Dunn & Shultis, 2011). Monte-Carlo-Simulations are often used to integrate uncertainty into models. Within work package 2 of the DESTRESS project, a clear focus is put on the integration of uncertainty into techno-economic modelling. The uncertainty comes from parameters as well as from risk factors. In addition, the report at hand also documents new approaches in power plant modelling. While (Welter, Technisch-ökonomische Analyse der Energiegewinnung aus Tiefengeothermie in Deutschland, 2018) used a heuristic optimization for the identification of an optimal power plant design, UoG and EnBW integrated the Monte-Carlo-approach into the optimization of power plant designs. The heuristic optimization used in (Welter, Technisch-ökonomische Analyse der Energiegewinnung aus Tiefengeothermie in Deutschland, 2018) limited the solution space by changing only one parameter in a defined step size. The power plant modelling presented in this report manipulates five central parameters at different state points of the power plant. Thereby, the solution space is enlarged, and the optimal solution can be better approximated. IGEM is using the Monte-Carlo approach on two different topics that are statistically independent. The integration of uncertainty, mainly caused by risk factors, as well as the simulation and optimization of power plants designs. While both fields are methodologically integrated in the main model, they are technically separated in the actual code to limit the computational effort. The power plant modelling is outsourced from the main model. Based on a set of deterministic, technical input parameters, the Monte-Carlo-Simulation for the power plant is done before running the main model. The results (multiple deterministic power plant designs) are stored in a database and can accessed by the main model through a function defined by a parameter set.

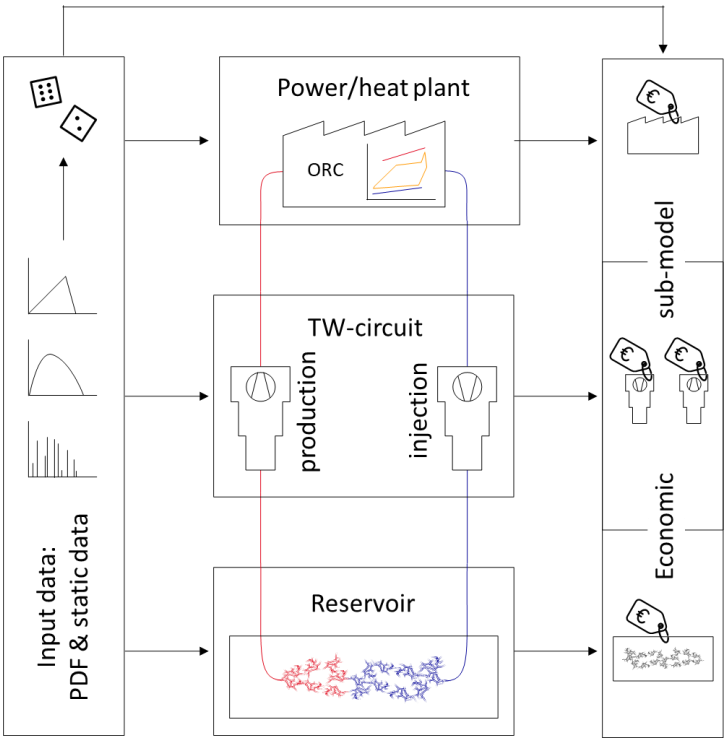


Figure 12: Model overview on the integrated geothermal energy model

Figure 12 gives an overview of the "Integrated geothermal energy model". The model is organized in five different parts. As a starting point the input data set is fed into the model. This includes uncertain parameters i.e. risk factors, which are described with a PDF. In the centre of Figure 12 the technical models are pictured. Between the single models only data on the physical state of the thermal water is exchanged. Starting from the reservoir model a closed loop is simulated. This includes:

- Drawdown in the production reservoir
- Temperature and pressure reduction in the production wellbore
- Energy utilization in the power/heat plant
- Pressure and temperature changes in the injection well
- Up arching in the injection reservoir
- Pressure coupling with production reservoir.

All technical models feed data into the economic model, where different cost engineering approaches are used to calculate costs, earnings and the different KPI. Uncertainty mainly caused by risk factors also plays an important role in the economic evaluation. Risk factors are often integrated into the model by using risk associated costs that put a burden on the economic results. The technical as well as the economic models use yearly time steps. Thereby the model is static on a short time step but dynamic over the whole observation period. Maintenance costs, a decrease of reservoir temperature or any other time dependent changes show their effect in specified/calculated time steps (=years). According to the rules of financial mathematics', all costs are discounted/compounded to the base year, which is the year with the first delivery of energy to customers.

The technical models are described in detail in chapter 3.1. Starting with the reservoir model in chapter 3.1.1, the model describing the thermal water circuit in chapter 3.1.2 and the energy utilization in chapter 3.1.3. Within the economic model in chapter 3.2 first the evaluated key performance indicators are introduced, followed by the methodological approach of cost engineering in chapter 3.2,

the used cost functions in 3.2.2 and the adaptions to different European markets in chapter 3.2.3. A flow chart of the programming of the overall model can be found in chapter D.1 of the annex.

## 3.1 Technical model

In the following the three technical models will be described in detail. Each technical model manipulates the physical conditions of the thermal water. The single models are connected through the transfer of data on the physical status of the thermal water. The whole technical model is designed as a closed loop system. All thermal water produced from the reservoir is also injected back.

### 3.1.1 Reservoir model

The following chapter introduces the reservoir model. Besides an introduction of basic analytical equations, the general frame conditions of the model are presented, and the input data are explained. Additionally, the effect of stimulation is quantified and the possibility of time dependent changes in injectivity are evaluated.

#### 3.1.1.1 Basic analytical equations used

The reservoir model is based on two main principles, i.e. 1) the material balance equation, and 2) the stabilised radial well inflow equation for vertical wells completed on a porous and permeable reservoir. The material balance represents the reservoir as a single tank (zero-dimensional, i.e. a point in space) in which a uniform pressure exists. The evolution of the average reservoir pressure in time is a function of the net volume ('material') withdrawn from the reservoir (i.e. the volume produced minus the volume injected), and of the compressibility of the fluid and of the rock. Hydraulic communication to remote volumes, away from the main reservoir, may also influence the pressure in the reservoir.

The basic well inflow equation describes how a vertical well, completed with full penetration of a horizontal reservoir layer, produces fluids as a function of a pressure difference applied between the reservoir and the bottom of the well. The flow rate is a function of variables such as reservoir permeability, skin factor, fluid viscosity, drainage area diameter and well diameter. The basic solution for the inflow is based on the radial diffusivity differential equation for a homogeneous porous reservoir, on the assumptions of a vertical line-source (i.e. a vertical well), and of fluids with a small and constant compressibility. Two situations are distinguished:

1. *Steady-state flow* from the reservoir into the production well and from the injection well into the reservoir: this means that as much volume is withdrawn from the reservoir as injected (net underground withdrawal = 0). The pressure gradient between injectors and producers, and the absolute level of the reservoir pressure remains constant in time. As the net underground withdrawal is zero (i.e. the reservoir pressure does not change in time), the material balance equation is superfluous. Only the stabilised steady-state well inflow equation is used.
2. *Semi-steady-state flow* from the reservoir into the production well: this means that the net underground withdrawal (UW) is unequal to zero, and the reservoir pressure decreases if UW > 0. Normally, this is for instance achieved in case of no (re-)injection of the produced water. In this situation, both the material balance equation and the stabilised semi-steady-state well inflow equation are used to describe the reservoir/well performance.

The pertinent analytical equations can be found in the reservoir engineering literature e.g. (Krusemann & de Ridder, 2000).

#### 3.1.1.2 Modelling choices made

*1. Wells of each category (injection/production) are identical:* no differentiation is made between wells of the same category. The reservoir is assumed to be homogenous, and skin factors, FBHPs are

assumed to be identical in all production/injection wells. Nevertheless, injection and production reservoirs can be described by different hydraulic and geological parameters. Skin factors and FBHPs in injection wells can be different.

*2. Pressure vs. rate-constrained*: The reservoir produces rate-constrained (i.e. a flow rate is given to the simulation model) until a pressure-constraint, i.e. a maximum drawdown/build-up in a well, is violated. The pressure constraint then takes over and the flow rate is re-calculated. The flow rate is given, together with the maximum pressure constraint. If the rate, given the minimum FBHP or the FTHP, does not violate the pressure constraint, then the given rate applies. Else, the pressure constraint applies.

*3. Reservoir flow regimes (Darcy vs. fracture-dominated flow)*: two approaches are enabled, i.e.

i. The flow rate is calculated from the fundamental equations and reservoir properties (Darcy flow from reservoir into well or vice versa, (semi-)steady-state radial inflow equation)
ii. The flow rate or the PI / II is user-defined. A well's rate, or PI and II, are input, rather than calculated from the fundamental properties. For example, in tight crystalline rock Darcy primary porosity flow will not apply, and only fracture flow may be possible. Although analytical equations exist to compute fracture flow from basic reservoir properties, they are not enabled in the DESTRESS tool (estimating the required fundamental properties would imply that poorly verifiable assumptions must be made).

Approach i. is applied when the flow is matrix-dominated, and the fundamental reservoir properties can be estimated, while approach ii. can be used when the flow is fracture-dominated and/or when the fundamental reservoir properties are difficult to estimate or when the user prefers to impose a given rate, rather than calculating it from the fundamental properties.

*4. Representation of stimulation effects*
For wells, a dynamic skin build-up rate can be specified to model the gradual decline in well productivity / injectivity due to fines migration or geochemical precipitation, resulting in the wellbore or wellbore vicinity being clogged. If positive (i.e. $\Delta$skin > 0/yr), a well's rate will gradually decline in time. However, this decline can often be remedied by 'stimulating' the wells. A user defined stimulation job frequency (number of years in between two stimulation jobs for a producer and injector, respectively) can be defined. All wells will receive this treatment accordingly and yield the $\Delta$skin or $\Delta$ II/PI. This again results in an increase in production or injection rate, given the drawdown specified. The workover OPEX is automatically accrued to the cashflow. See therefore also chapter 3.1.1.6

In line with the above two approaches, the effect of stimulation can be modelled either by specifying a post-stimulation change in the skin factor (in case of primary / Darcy porosity), or by specifying a change in the PI or II (i.e. in case of tight crystalline rock). Since all wells are assumed to be identical, this stimulation effect applies equally to all wells of the same category (injection/production).

Currently, the DESTRESS tool enables a skin factor that can change in time ($\Delta$skin to be specified in 1/yr). A more meaningful variation could however be that the skin factor evolves with i.e. the cumulative production or injection per well. Given a time-step's production, the skin-factor can then be calculated in the time-domain. However, establishing a parametric, empirical relationship to describe the evolution of a well's skin factor to our knowledge has not yet been done.

*5. Representation of reservoir performance degradation*
The overall average reservoir performance can deteriorate due to injecting cooled water, which may

trigger geochemical precipitation of minerals in the pores or joints/fractures. This effect is described in detail in chapter 3.1.1.6. Due to simulation complexity and availability of data, the approaches documented in the literature weren't implemented in the DESTRESS model.

*6. Representation of temperature depletion in production well*
The analytical DESTRESS tool can model temperature depletion in the production well by specifying a breakthrough time for the total field, when the cooled injection water reaches the production wells. This assumption is valid, since all production wells are assumed to be identical. If the breakthrough time is below the user defined operating life of the power plant, the production rate can be adapted. An analytical approach is presented by (Schulz & Jobmann, 1989) for the calculation of the breakthrough time.

#### 3.1.1.3 Populating the model with site data

The model is in principle generic, i.e. it applies in principle to a wide range of reservoir characteristics. But in any case, it cannot substitute a software specifically designed for reservoir analysis. The user however has to accept the modelling simplifications made, and judge for herself/himself to which extent these simplifications may negatively affect the validity of the outcomes (see also section 1.2.6 in this report, paragraph on "Fitness-for-purpose", where the trade-off between precision/holistic/uncertainty modelling is discussed). Averaging detailed well data and spatially averaging this data between the different wells to obtain one average value that is representative for the injection/production reservoir, is however not trivial. It is beyond the scope of this report to present some of the available methods, and reference is made to the pertinent textbooks.

Populating the tool to run a case means that all the required input data are specified. This can mean that so-called 'scalar input variables' (deterministic data i.e. reservoir temperature) or time-series data have to be filled in ('vector data'). Preparing the data for all decision alternatives is normally rather time-consuming. Not only should detailed data (i.e. well logs, representative information on skin evolution, etc.) be upscaled and averaged, but they should also be made internally consistent (i.e. CAPEX and OPEX) and be consistent between alternative decisions. This requires a great deal of expertise and judgement. The input data will come from a multitude of sources, and quality control is paramount to avoid 'rubbish in, rubbish out'.

Note that both in the scalar and time-series input data, a more detailed representation of the conventional vs. soft stimulation activities and effects may have to be enabled in the DESTRESS tool. In the current version, a stimulation job is defined in terms of its frequency (1/yr, for injectors and producers, respectively), duration (days, this reduces the field's 'uptime'), its cost (OPEX) and its effect in terms of $\Delta$skin (or $\Delta$PI, $\Delta$II). Then the skin build-up rate ($\Delta$skin/yr) for injectors and producers, respectively, is applied to compute a well's declining productivity / injectivity.

#### 3.1.1.4 Verification of reservoir model

All models should in principle be 'verified' to gain confidence in their predictive capabilities. For several reasons, however, model verification is not trivial. To name a few:

Indeed, an important complication for verifying a model are the uncertainties in the system properties, combined with a range of alternative development and operational options ('controllable') that are typically modified relative to the assumptions made at time of forecasting, during the forecast horizon. The question of what is to be verified, and how is to be clarified: the input data and/or the model's parametric relationships? Should the input data be 'inverted' / estimated from the observed reservoir performance (pressures, rates, etc.)? And if the model does not have the spatial and time resolution that one would wish with hindsight, should this resolution be improved? Is the modelling environment

then still adequate? Moreover, the long-time-horizons complicate the issue. For example, if the asset is immature and there is a relative data paucity, should one 'verify' the initial model based on the newly acquired data? Or is this just hindsight that is not useful at time of making the forecast? In practice, one continuously updates the model and renders it in line with the historical observations. Moreover, models tend to become much more detailed (i.e. individual wells will be history-matched, rather than only the total reservoir performance).

In practice, all models are initialized and then are forward looking, based on diligently selected numerical values for the input variables. Analytical models describe, up to some extent, the pertinent physics and consider the planning and economic variables to derive plausible time-series and KPIs. Analytical models are used to compute complex chains / interactions and uncertainties. The parametric relationships of the model are often accepted when making a choice for a model (presuming the model to be '*fit-for-purpose*'), and the model is then initialized to match the starting conditions. For example, initializing cumulative production / injection and current reservoir pressure may require updating the hydraulically connected reservoir volume. Observed FTHPs and well rates may require updating the wells' PIs an IIs (or permeability, skin factor, etc.).

Another way to 'verify' the model is to study the model's *partial derivatives* when doing sensitivity analysis / Monte Carlo analysis. Studying the many ∂y/∂x, for example a ∂KPI/∂(input variable) such as $\partial(\text{cum volume injected})_{t=t1}$ / ∂(permeability), will help understanding whether the model is consistent with the underlying theories. When doing multi-variate analysis, however, the partial derivatives are not explicitly calculated, but the statistical trend and sign of the sensitivity (i.e. contribution to variance) should match the underlying theory.

To a large extent, the user of the tool is responsible for specifying input data that are consistent. For example, when supplying a breakthrough volume and trend for the temperature decline in a well, then the user should ascertain that this volume/trend is consistent with the number of wells, injector/producer ratio and drainage area supplied to the same input deck.

#### 3.1.1.5 Effect of stimulation

Reservoir stimulation is common practice to enhance the productivity and injectivity of low permeability geothermal reservoirs (Zimmermann, Blöcher, & Huenges, 2012). To improve the probability of an economic success, tailored stimulation techniques are used. Especially in Enhanced Geothermal Systems the poor hydraulic connection between production well and injection well is a common problem (Portier, Vuataz, Nami, Sanjuan, & Gérard, 2009) The different stimulation techniques can roughly be divided into mechanical and chemical stimulation, whereby combinations of both as acid fracturing are common practice. The main goal of mechanical stimulation is to fracture the reservoir by inducing artificial stress within the formation. The hydraulic stimulation plays an important role particularly within the mechanical stimulation. Hydraulic fracturing usually refers to failure of the rock. The shearing effect should occur when the fluid injection is below fracturing pressure but above the pressure in an existing fissure. This injection decreases the effective stress and thus puts the medium closer to the shear failure envelope. Alternatively, the injection can promote a shear displacement along already existing fracture planes (Chabora, et al., 2012). Chemical stimulation aims to improve fluid flow by removing restricting mineral phases, predominately by acidizing (Portier, Vuataz, Nami, Sanjuan, & Gérard, 2009). Besides adaption to given geological conditions, hydrofluoric acid (HF) and hydrogen chloride acid (HCl) or mixtures of them ("mud acid") are the standard acids for chemical stimulations. HCl dissolves carboniferous rocks as limestone or dolomite, whereas HF is used for clay minerals and silica. To enhance conductive paths along fracture planes, acidizing of fractures is mostly accompanied by a pressure build-up for allowing the compound to penetrate deeper into the reservoir (Portier, Vuataz, Nami, Sanjuan, & Gérard, 2009). Acidizing of an existing fracture should

focus on maintaining the treating fluid inside that fracture. Chemical stimulation is further used to remove mineral precipitations occurred during the geothermal energy production.

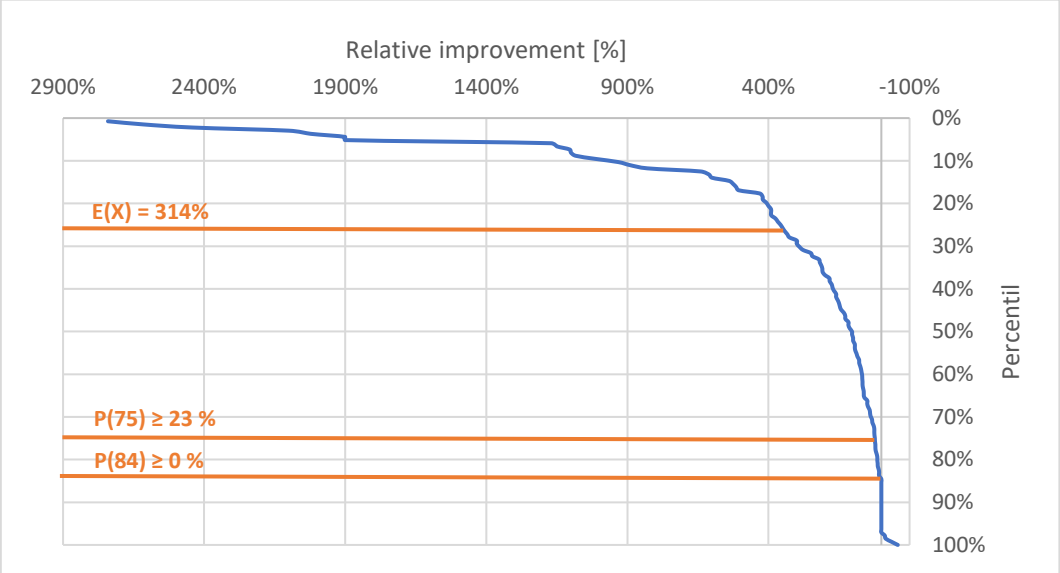


Figure 13: Relative improvement through stimulation [6]

To evaluate the effect of stimulation measures, a literature review on published data for stimulation activities is conducted. In total, data on 136 geothermal stimulation jobs conducted since 1970 in 15 countries is acquired (see Appendix C). Figure 13 shows the relative improvement achieved by the different stimulation jobs, including chemical, hydraulic and thermal stimulation techniques. The relative improvement shows a wide range depending on technical and geological issues. The expected value of improvement of the considered jobs is 314 %. 84 % of all cases show an improvement, whereby 75 % show an improvement larger than 23 %.

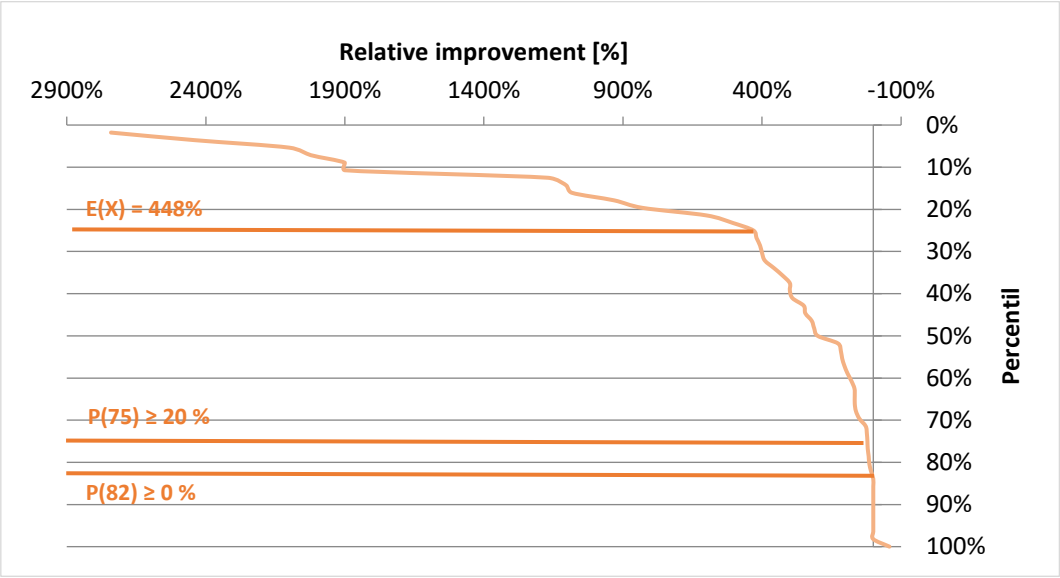


Figure 14: Relative improvement through hydraulic stimulation [6]

[6] Relative improvement – z = (x-y)/y; Improvement of a value X relative to its initial value

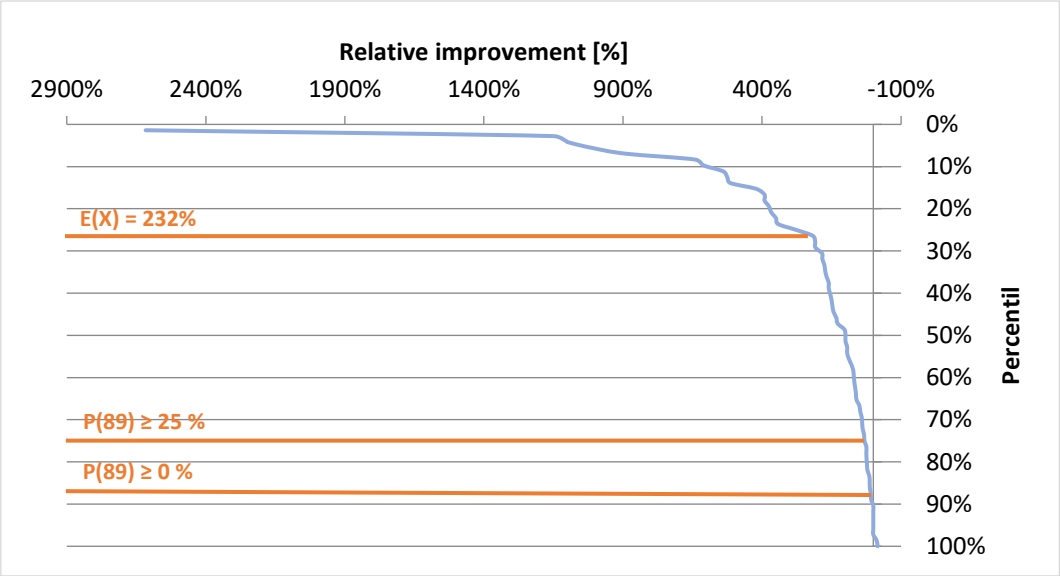


Figure 15: Relative improvement through chemical stimulation [6]

Figure 15 illustrate the relative improvement achieved by the hydraulic and chemical stimulation jobs, respectively. Although the success of both stimulation measures depends on different frame conditions, Figure 15 and Figure 16 confirm that, when applied correctly, both stimulation measures show similar success rates. The expectation value of improvement of the considered jobs is 448 % for hydraulic stimulations and 232 % for chemical stimulations. 75 % of all hydraulic stimulations show an improvement of at least 20%, while only 18 % of all hydraulic stimulations show no or a negative effect. For chemical stimulations 75 % of all measures show an improvement higher than 25 % and 89 % have an improvement higher than 0.

Focusing on the simulation data with available PI-data (see Figure 16), 93 % of all published stimulation jobs improved the productivity index. In Figure 16, it is also noticeable that the highest improvements are derived by hydraulic stimulation.

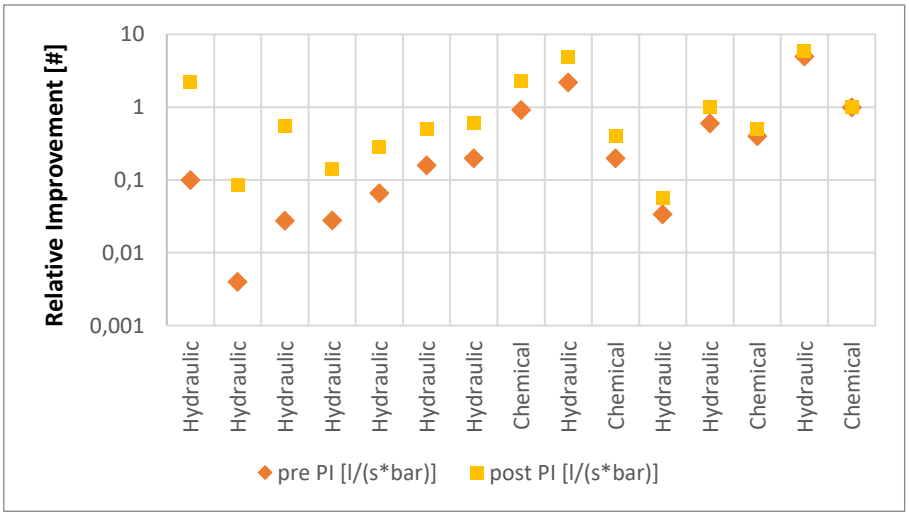


Figure 16: Stimulations with published PI [6]

Regarding the simulation with available II-data (see Figure 17), 88 % of published stimulation jobs improved the injectivity index. It is also implied that the highest improvements are derived by chemical stimulation. This might be due to the distribution of the stimulation type. Here the majority are

chemical stimulation jobs. The improvement gained by hydraulic stimulation seams to range widely without a certain trend.

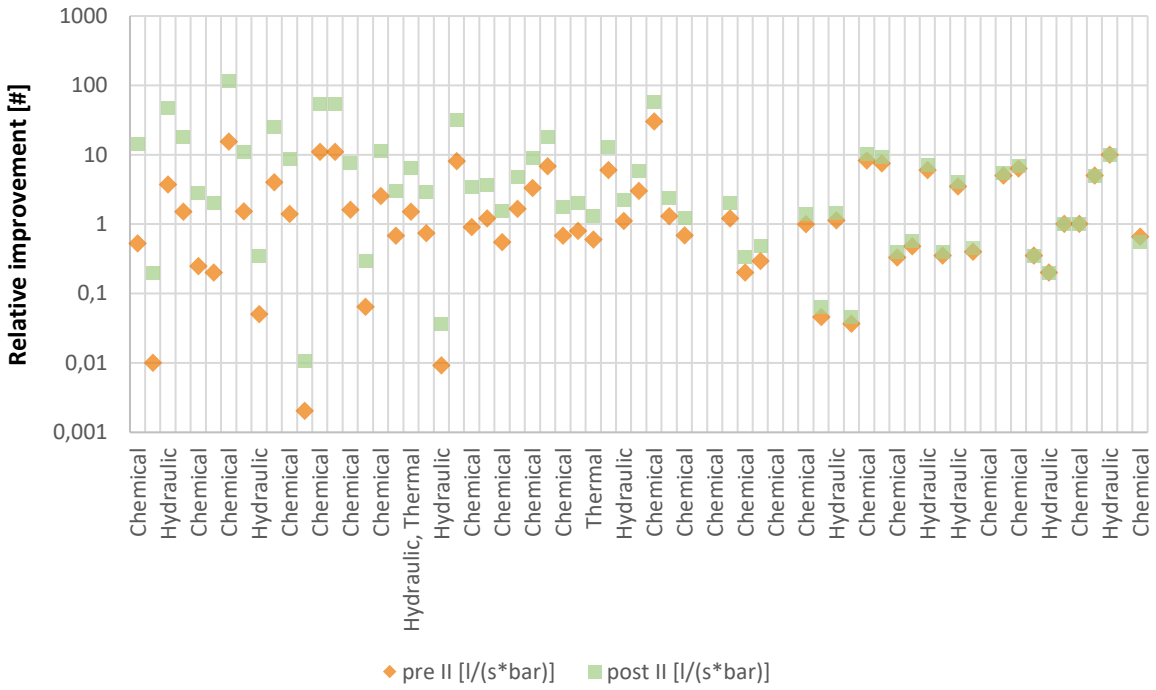


Figure 17: Stimulations with published II 6

Based on the data presented above, an existing continuous probability distribution is identified that describes the data well and can be implemented into the IGEM. A best fit was possible with an “Inverse Gaussian” distribution as can be seen in Figure 18. On the left-hand side of Figure 18 one can see the fit for chemical stimulations and on the right-hand side for hydraulic stimulations. In both cases the Inverse Gaussian distribution shows good accordance with 5 %- and the 95 %-percentile. Furthermore, the standard deviation also shows good accordance. The Inverse Gaussian distribution has an infinite maximum. Therefore, the maximum result a random pick from the distribution is limited to the maximum values identified in the literature research. For thermal stimulations only one data point is published. An improvement of 117% documented by (Baujard C. , et al., 2017) through a thermal stimulation at the geothermal power plant in Rittershofen (France). Faced with the scarcity of data, one fixed value for the effect of thermal stimulation is implemented into the IGEM.

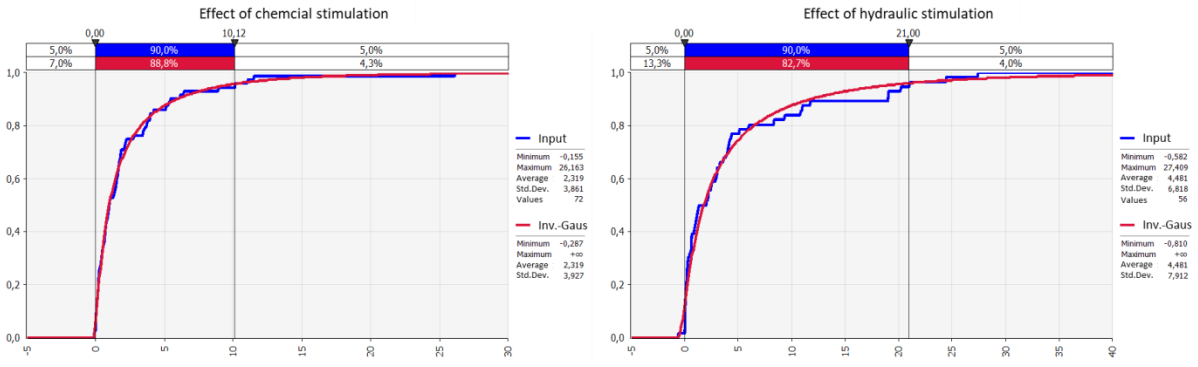


Figure 18: Description of the data on the effect of stimulation with a continuous distribution

The presented data will be used in the IGEM to describe the uncertainty related to the effect of stimulation measures. This approach has been critically reflected. On the one hand side the generalization of the effect of a stimulation is deceptive. Local geological, geophysical and geochemical frame conditions have a major influence on the success of a stimulation. On the other hands side, from a statistical point of view, case specific details become less important with a growing number of cases that form the basis for a PDF. An argumentation based on statistics could be questioned by challenging the data source. Have unsuccessful projects been published? Is the quantification method for the effect of stimulation in the different references comparable? Answers to these questions can only be given on a qualitative basis. The database used is the result of an in-deep literature review. Nevertheless, completeness can't be guaranteed. For the quality of published data, the authors of this study have a strong faith in the work of the scientific community. A different approach would have been to simulate the effect of stimulation for each investigated site based on geological, geophysical and geochemical data. Having the "fit for purpose approach" on techno-economic modelling (Bos, 2005) in mind and knowing on the complexity of such simulations (Hoffmann, 2019) (Zimemrmann, 2019) (Guinot, 2019) (Genter, 2019), it is decided not to include simulations of that extent into the IGEM. Evaluating pros and cons, the suggested approach for mapping the effect of stimulation in the techno-economic modelling of the DESTRESS project fulfills the scientific approach and can map the desired effect very well.

#### 3.1.1.6 Change of II/PI over time

The change of II/PI over time can have a decisive influence on the reservoir performance and hence the energy produced from a geothermal field. So, the precise knowledge of geological and geochemical conditions forms an essential prerequisite for a successful geothermal operation. Injection experiments demonstrate that mineralogical properties of the wellbore strongly influence the behaviour of injectivity perturbations. Thus, for the further investigations, a simplified categorization of the three formation lithologies is proposed (clastic/crystalline/carbonatic).

##### 3.1.1.7.1 Clastic reservoirs

Field experience and core percolation tests show that II/PI impairment over time are prevalent associated with matrix-type clastic reservoirs as a consequence of one and more damaging factors (Ungemach, 2003), whereas the followings are major problems:

i. **fine particle migration/settling processes and relative pore throat bridging, pore retention/bridging and formation plugging**

The predominate damage from internal/external fines migration or geochemical precipitation results in the clogging of the wellbore or wellbore vicinity and consequently modifies the skin-factor of the impaired formation. If positive, the injectivity index will gradually decline in time. Thus, a model to predict the decline in injectivity that properly accounts for both the build-up of clogging and infiltration of particles is desirable. In this concern the knowledge of the particle/pore/fissure size distribution, injected solids concentration, permeability of the formation and fluid velocity is of utmost importance to determine whether internal or external filter cakes are formed. Models are conducted (Egberts, Heedderik, van der Meer, & Vernoux, 1995; Shutong, 1997; Eric van Oort, 1993) with the goal of calculating II/PI decline using the aforementioned parameters. To enable these simulations in the DESTRESS techno-economic, a lack of the preceding parameters within the frame of DESTRESS consequently leads to an enormous uncertainty and thus is not recommended to implement.

**ii. Fluid incompatibilities and subsequent supersaturation/precipitation of solid particles and clay swelling**

Physical-chemical conditions, particularly the flow velocity and salinity of the reinjected brine determine the damage associated with clay swelling and clay particle stability. Hence the dispersion of colloidal clay particles is clearly related to fresh water, it seems less important in geothermal reinjection, as the latter generally involves saline brines. Empirically, a higher salinity correlates with higher flow rates that can be achieved before the particles migrate and the reduction in permeability is less pronounced (Ochi & Vernoux, 1996), which is why this group of PI/II-changes is not considered within the DESTRESS techno-economic modelling.

#### 3.1.1.7.2 Crystalline reservoirs

In tight crystalline reservoirs (i.e. Upper Rhine valley, Central Europe), primary porosity flow will not contribute to the overall flow and only natural or induced secondary fracture flow may be possible (i.e. fractured wells). Freshly opened fractures after stimulation treatments can face hydrothermal transformation at their exposed surfaces. Through the contact of feldspars with geothermal brine, a transformation into clay minerals and their subsequent swelling can occur. Additional mineral transformation reactions are mentioned by (Schmidt R. , Bucher, Drüppel, Mundhenk, & Stober, 2017a; Schmidt, Bucher, & Stober, Reactivity of geothermal reservoir rocks under temperature conditions found in the Upper Rhine Graben (Germany), 2017b) and attributed to aperture changes. Further the heat-depleted brine may trigger adverse thermochemical reactions and the consequent formation of scaling caused by pressure induced $CO_2$ degassing (Ungemach & Roque, 1988; Vetter, Kandarpa, Stattom, & Veith, 1987) and has a major impact on the permeability of the overall system.

#### 3.1.1.7.3 Carbonate dominated reservoirs

Regarding the reinjection in carbonate rocks minor injectivity disturbances occur in terms of scaling or clogging. Opposed, the reinjection of heat-depleted geothermal brines into carbonates after thermal usage positively affects the injectivity due to an enhanced solution index as a function of temperature difference or pressure increase of the reinjected brine (Rükhaak, et al., 2015). Examples from the Molasse Basin (Megies & Wassermann, 2014) indicate cavitation and associated micro-seismicity after years of operation. Similar effects are well documented in $CO_2$ sequestration in carbonate reservoirs (Izgec, Demiral, Bertin, & Akin, 2006). Here a distinctive feature is that either a permeability improvement or permeability reduction can be obtained as shown in Table 2. An injectivity improvement is noticed as highly non-uniform dissolution patterns which forms additional pathways

in the shape of channels. Thus, an enhancement in injectivity, or at least in varying degrees a constant injection rate owing to an offset of possible scale can be expected.

Table 2: Overview of near well reservoir processes affecting productivity and injectivity of a geothermal well in a fractured porous carbonate reservoir (injectivity index II = injection rate/bottom hole pressure increase) (Megies & Wassermann, 2014).

| | PROCESS | POSSIBLE EFFECT ON INJECTIVITY |
|---|---|---|
| **1** | Carbonate transport by near well dissolution in cold water and far well precipitation | Long term II increase |
| **2** | Variation of fracture aperture at well inflow by pressure variation | Short term II improvement |
| **3** | Increase of fracture aperture by rock cooling | Short term II improvement |
| **4** | Decrease of hydraulic conductivity around the injection well by increase of reservoir fluid viscosity caused by cooling | Short term II reduction |
| **5** | Transition from laminar to turbulent flow regime near the well at high flow rates | Short term II reduction |

Regarding the DESTRESS techno-economic simulation tool a lithology unbiased consideration appears to be mistaken, since it is documented by several authors that mineralogical attributes of varying reservoir-types have a lithology-related impact on the injectivity impairment. Due to lacking information, an implementation of the proposed simulations is not valuable and thus a model for II changes over time not feasible. Attempting to enable this function in the DESTRESS tool requires further knowledge of mineral reaction rates and preceding processes to quantify these. Thus, within the current situation of DESTRESS it is dissuaded to implement this contemplation due to high uncertainties.

### 3.1.2 Thermal water circuit (TWC)

The term "thermal water circuit" summarizes all parts of the geothermal system, that are necessary for the connection of the geothermal reservoir to the surface power plant. According to (Hoth, Seibt, Kellner, & Huenges, 1997) a thermal water cycle for the use of geothermal fluids consists of production wells, connecting lines, pressure retaining devices, filters, slop pits, heat exchangers and injection wells. In addition, production and injection pump can also be part of the thermal water circuit if they're installed. The following section 3.1.2.1 describes the structure of the technical model of the thermal water circuit. This model is validated in section 3.1.1.4.

#### 3.1.2.1 Technical model for the thermal water circuit

The model of the thermal water circuit connects the power plant and the reservoir model. Based on given temperature and pressure values of the thermal water in the reservoir, pressure and temperature at the power plant entrance are determined. Likewise, from the corresponding values at the power plant output, the pressure and temperature values that the geothermal fluid has upon re-entry into the reservoir are determined. In the following, the calculation of the thermal water pressure and the thermal water temperature within the thermal water cycle is explained. Only production and injection wells including pumps and heat exchangers are considered. Connecting lines, pressure retaining devices, overhead filters and sloping pits are neglected.

To determine the pressure and temperature of the thermal water in the well, knowledge of the well geometry is necessary as the diameter and angle of the well influence pressure losses and heat

exchange with the environment. In addition, temperature calculations require information about the temperatures in the soil surrounding the hole. Both the geometry of the hole and the temperatures in the subsurface are specified by the user for the simulation. Figure 19a shows schematically a vertical and a deflected hole.

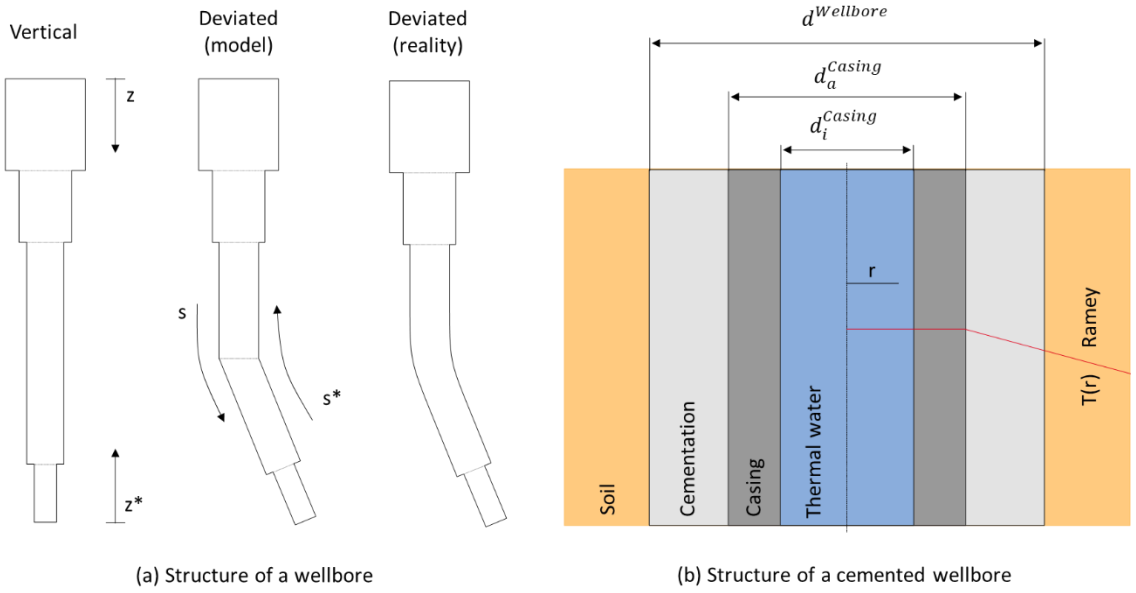


(a) Structure of a wellbore (b) Structure of a cemented wellbore

Figure 19: Schematic structure of production and injection wellbore

Geothermal wells- are constructed telescopically. The deviation is approximated as a kink at the kick-off point. In fact, the deviation angle is steadily built up starting at the kick-off point, so that, as shown schematically in Figure 19, there is a bend rather than a kink. Typically, build-up rates of less than 1.5 ° (Ngugi, 2002) to 4.5 ° (Legarth, 2003) are reached per 10 m. In Figure 19a, z means the vertical depth (true vertical depth, TVD) and s describes the measured depth (measured depth, MD) which is the drilled distance. In vertical wells TVD and MD are identical. The calculation of pressure and temperature of the thermal water in the well is done in sections. Within each section, the diameters, the wellbore, the angle of the well and the geothermal temperature gradient are constant. Figure 19b shows a schematic representation of a section of a cemented wellbore. In the borehole with a diameter $d^{wellbore}$, the thermal water flows in the casing with the inside diameter $d_i^{casing}$ and the outer diameter $d_a^{casing}$. The space between soil and casing is filled with cement. In the injection well, pressure and temperature of the thermal water at the surface are known, coming from the power plant model. By means of section-by-section calculation of temperature and pressure changes based on these known values, pressure and temperature can be determined at the lowest point of the wellbore, i.e. at the reservoir inlet. Conversely, in the production well, the pressure and temperature of the thermal water at the lowest point of the well are known as initial values of the reservoir model. Accordingly, pressure and temperature within the wellbore can be determined analogously to the procedure for the injection well, the sections being run through from bottom to top. Figure 62 shows a flow chart for the wellbore model.

In order to determine the course of the thermal water pressure and temperature in the borehole, as shown in Figure 62, the at-rest water level ($H_{TW}^{at-rest}$) is first calculated on the basis of the given parameters. This is determined by the prevailing reservoir pressure and the density of thermal water, which is assumed to be constant across the well (see Equation (1)). According to (Francke, 2014), this approximation is permissible for the calculation of the at-rest water level.

$$H_{TW}^{at-rest} = \frac{p_{reservoir}}{\rho_{TW} * g} \quad (1)$$

For the position of the pump it is assumed that it is installed 50m below the water level (Welter, Technisch-ökonomische Analyse der Energiegewinnung aus Tiefengeothermie in Deutschland, 2018). It is necessary to know the pump position to assign the pressure and temperature increase caused by the pump to the correct wellbore section. Subsequently, the pressure and temperature calculations for the wellbore sections are made which will be explained in more detail below.

### Pressure calculation

The thermal water pressure at the outlet of each wellbore section ($p_{TW,out}$) is derived from the pressure at the inlet of the respective section ($p_{TW,in}$), the change in hydrostatic pressure ($\Delta p_{hydro}$), the pressure losses due to friction ($\Delta p_{loss}$) and, if applicable, the pressure increase by the pump ($\Delta p_{pump}$) according to the equation (2).

$$p_{TW,out} = p_{TW,in} + \Delta p_{hydro} + \Delta p_{loss} + \Delta p_{pump} \quad (2)$$

The change in hydraulic pressure is coupled to the change in position z of the fluid in the wellbore as shown in equation (3).

$$\Delta p_{hydro} = \rho_{TW} * g * \Delta z \quad (3)$$

It is important to pay attention to the sign of z: If the sections in the production well are calculated from the reservoir towards the top ground level, the sign is negative. In the case of the injection well, i.e. for a passage through the sections from top ground level towards the reservoir, the sign is correspondingly positive. The thermal water density $\rho_{TW}$ is assumed to be constant in sections, i.e. it varies over the length of the hole.

The pressure losses due to friction in the individual sections are calculated using expression (4) (Oertel & Reviol, 2015) (Schlagermann, 2014).

$$\Delta p_{loss} = \frac{1}{2} * \rho_{TW} * u_{TW}^2 * |\Delta s| * \left( \frac{\lambda}{d_i^{casing}} + \zeta \right) \quad (4)$$

$|\Delta s|$ describes the length of the pipe section as the absolute value of the difference of the measured depth. When calculating the pressure loss, the speed of the thermal water $u_{TW}$ is calculated in sections based on the inner diameter of the piping. In addition, the density of the thermal water is assumed to be constant over all sections. This simplification is reasonable because the density of the geothermal fluid varies by less than 10 % in the typical pressure and temperature range of geothermal wells (see (Welter, Technisch-ökonomische Analyse der Energiegewinnung aus Tiefengeothermie in Deutschland, 2018)) and the pressure change $\Delta p_{loss}$ is small in relation to $\Delta p_{hydro}$. For the determination of the pipe friction coefficient $\lambda$ and the drag coefficient $\zeta$ a distinction must be made between laminar and turbulent pipe flow and between hydraulically smooth and hydraulically rough pipes.

In the deepest section of the well, the geothermal fluid usually enters and leaves the well through a filter (Welter, Technisch-ökonomische Analyse der Energiegewinnung aus Tiefengeothermie in Deutschland, 2018). This is considered in this section of the hole similar to the procedure of (Fischer, 2010). A constant inflow over the filter section is assumed (Fischer, 2010). As a result, the flow velocity in the filter increases linearly and the pressure loss ($\Delta p_{loss}^{filter}$) is given by equation (5).

$$\Delta p_{loss}^{filter} = \frac{1}{6} * \rho_{TW} * u_{TW}^2 * \lambda * \frac{|\Delta s|}{d_i^{casing}} \quad (5)$$

In this case, $u_{TW}$ describes the velocity of the thermal water which sets itself at the nominal mass flow in the wellbore. In the present model, it is assumed that the filter section occupies the entire user-defined deepest wellbore section.

### Temperature calculation

The temperature of the thermal water at the outlet of each section of the well shall be determined on the basis of the inlet temperature ($T_{TW,in}$) and the temperature difference as a result of the heat transfer ($\Delta T_{HE}$) to the ground and, if applicable, the temperature difference $\Delta T_{pump}$ generated by the pump, as specified in equation (11). The latter is only included in the section in which the pump is installed.

$$T_{TW,out} = T_{TW,in} + \Delta T_{HE} + \Delta T_{pump} \quad (6)$$

In the following it is explained how the temperature differences are calculated from equation (6).

For the determination of $\Delta T_{HE}$, the approach presented by (Ramey, 1962) for determining the temperature profile of a fluid injected into a borehole is evaluated section by section. The expression used is shown in equation (7).

$$\Delta T_{TW} = T_{TW,in} - \frac{dT_{geo}}{ds} * \Delta s - T_{geo}(z = z_{out}) + \frac{dT_{geo}}{ds} * F(t) - \left[T_{TW,in} + \frac{dT_{geo}}{ds} - T_{geo}(z = z_{out})\right] * e^{\frac{-\Delta s}{F(t)}} \quad (7)$$

$\Delta T_{TW}$ stands for the change of the thermal water temperature over a section depending on the measured depth (MD) s and the observation time t. The latter is the time elapsed between the start of production of geothermal fluids and the observation time of the stationary state depicted in the simulation. In (Ramey, 1962), a value of 30 days is set for the observation period. $T_{geo}$ describes the temperature in the rock surrounding the borehole. The gradient of this temperature in z-direction is assumed to be constant in sections in this paper. $z_{out}$ symbolizes the depth at which the outlet of the respective section lies. $F(t)$ is a time function according to context (8).

$$F(t) = \frac{\dot{m}_{TW} * c_{p,TW} * \left[\lambda_{geo} + 0{,}5 * d_i^{casing} * k * f(t)\right]}{\pi * d_i^{casing} * \lambda_{geo}} \quad (8)$$

Here $d_i^{casing}$ describes the inner diameter of the casing in the borehole as shown in Figure 19. $\lambda_{geo}$ stands for the thermal conductivity of the rock and k for the heat transfer coefficient from the thermal water into the rock. $f(t)$ describes a dimensionless time function of the heat transfer in the ground. The quantities k and $f(t)$ are of decisive importance for the sufficiently precise approximation of the real conditions. Particularly the determination of the heat transfer coefficient k is difficult in many applications. For the application to geothermal energy wells, however, the thermal resistance within the borehole can be neglect (Ramey, 1962). This simplification corresponds to the assumption that the temperature in thermal water and piping is the same in the stationary state. Furthermore, the cementation is neglected and its thermal conductivity with that of the surrounding rock. The associated idealized temperature profile is shown in Figure 19. Under this assumption equation (8) is simplified to expression (9).

$$F(t) = \frac{\dot{m}_{TW} * c_{p,TW} * f(t)}{2 * \pi * \lambda_{geo}} \quad (9)$$

The specific heat capacity of the thermal water $c_{p,TW}$ is calculated at the inlet of each section as described in Section 2.3 and assumed to be constant over the section (Francke, 2014). For the still unknown time function f(t) (Ramey, 1962) uses the equation for transient heat conduction of a line source in an infinite radial system (equation (10)).

$$f(t) = -ln\left(\frac{d_a^{casing}}{4*\sqrt{a_{geo}*t}}\right) - 0{,}29 + \frac{\left(d_a^{casing}\right)^2}{4*a_{geo}*t} \quad (10)$$

Using expression (7), the thermal water temperature at each outlet can be determined for each section of the injection well. Equation (7) can be applied in the same form to the production well if the measured depth (MD) s is substituted by the measured distance from reservoir s* (see Figure 19a). (Haagort, 2004) describes the (Ramey, 1962) approach as "excellent approximation after a short transient period during which the temperature is overestimated". (Ramey, 1962) gives a duration of about 7 days after which this period ends. (Beckers K. J., 2016) also uses the (Ramey, 1962) approach, which proves its continuing relevance. In addition to the heat transfer between thermal water and soil, equation (6) considers the temperature increase caused by the pump ($\Delta T_{\mathrm{pump}}$) possibly installed in the completed borehole. According to (Francke, 2014), the increase in temperature due to the pump results from equation (11).

$$\Delta T_{pump} = \Delta T_{compression} + \Delta T_{loss} \quad (11)$$

$\Delta T_{\mathrm{compression}}$ stands for temperature increase by isentropic compression and $\Delta T_{loss}$ for temperature increase by dissipation in pump and motor. Expression 3.30 describes the respective calculation rule for the temperature increase by compression (Francke, 2014).

$$\Delta T_{compression} = \frac{\beta_{TW}*T_{TW}}{\rho_{TW}*c_{p,TW}} * \Delta p_{pump} \quad (12)$$

$\beta_{TW}$ symbolizes the thermal expansion coefficient of the thermal water and $\Delta p_{pump}$ the increase in pressure by the pump. Both the specific heat capacity $c_{p,TW}$ and the $\rho_{TW}$ of the thermal water are calculated at the inlet of each section according to the approaches presented in (Francke, 2014) and assumed to be constant over the section (Francke, 2014). For the determination of the temperature increase by friction losses, a distinction is made between submersible pump (ESP, equation (13)) and line shaft pump (LSP, equation (14)). With ESP, the engine is in the wellbore and is surrounded by thermal water. Heat losses from the engine are therefore transferred to the geothermal fluid. (Francke, 2014) The engine of the LSP, on the other hand, is located on the surface of the earth and the resulting heat is not transferred to the thermal water or only to a negligible extent.

$$\Delta T_{loss}^{ESP} = \frac{\Delta p_{pump}*(1-\eta_{is}*\eta_{mot})}{\rho_{TW}*c_{p,TW}*\eta_{is}*\eta_{mot}} \quad (13)$$

$$\Delta T_{loss}^{LSP} = \frac{\Delta p_{pump}*(1-\eta_{is})}{\rho_{TW}*c_{p,TW}*\eta_{is}} \quad (14)$$

Here $\eta_{is}$ stands for the isentropic efficiency and $\eta_{mot}$ for the motor efficiency of the pump. The temperature difference calculated in this way is considered in the wellbore section in which the pump is installed. Like the specific heat capacity $c_{p,TW}$, the density of the thermal water $\rho_{TW}$ is calculated as described in (Francke, 2014).

After determining the pressure and temperature curve in the wellbore, the pressure difference to be provided by the pump is calculated. A distinction must be made between production wells (equation (15)) and injection wells (equation (16)).

$$\Delta p_{pump}^{prod} = p_{TW,in}^{power\ plant} - p_{TW,out}^{wellbore} \quad (15)$$

$$\Delta p_{pump}^{inj} = p_{reservoir} - p_{TW,out}^{wellbore} \quad (16)$$

In the case of production wellbore, the pressure difference in the $\Delta p_{pump}^{prod}$ is measured as the difference between the pressure at the power plant inlet $p_{TW,in}^{power\ plant}$ and the outlet pressure from the production borehole $p_{TW,out}^{wellbore}$. $p_{TW,out}^{wellbore}$ is determined according to program sequence presented in Figure 62. For the injection well, the pressure difference in the pump $\Delta p_{pump}^{inj}$ is calculated from the reservoir pressure $p_{reservoir}$ and the calculated outlet pressure from the injection well without pump $p_{TW,out}^{wellbore}$. If the pressure differences determined are negative, no production or injection pump must be used.

Finally, the pressure curve is corrected by the impact of the pump pressure in the respective section and the electrical pump power is calculated. Expression (17) describes the relationship between the pressure difference in the pump and its electrical power.

$$P_{pump} = \frac{\dot{m}_{TW} * \Delta p_{pump}}{\rho_{TW} * \eta_{is}} \quad (17)$$

The density of the thermal water is approximated to the density of the thermal water at the respective borehole entrance. In the case of the production well, the borehole inlet is at the lowest point of the borehole, while in the case of the injection well it is at the earth's surface.

#### 3.1.2.2 Verification of TWC model

A validation of the model of the thermal water cycle against the Soultz-sous-Forêts site is proving to be difficult because extensive simplifications have been made to the real conditions. In Soultz-sous-Forêts, a total of three boreholes are used for the production and injection of thermal water recently. The present model considers only duplicates, i.e. systems with an injection well and a production well. Furthermore, it is assumed that geothermal fluid exclusively enters the wellbore in a well-defined range at the lowest part of the borehole. This is also not the case in Soultz-sous-Forêts. Decisive for a successful modelling of the site with the help of the available model is first and foremost a sufficient correspondence between the real and modelled thermal water temperature at the power plant entrance at a given mass flow. Not less important is a correspondence between the real and modelled pump power of production and injection pumps. The modelled temperature losses in the production well at the Soultz-sous-Forêts site are less than 20 K. According to information of the operator of the Soultz-sous-Forêts geothermal power plant, the modelled temperature loss is sufficiently close to the measurable temperature losses (Hehn, 2018). The power demand of the production pump during operation is overestimated by less than 10 % compared to real operating data (Hehn, 2018). The deviation can be explained through the simplifications in the reservoir model. It is nevertheless, far below the uncertainties surrounding the cost estimates. (AACE, 2016).

### 3.1.3 Energy utilization model

As described at the beginning of this chapter, the power plant model is divided into the technical part for determining all relevant system sizes and the economic part for calculating the costs incurred. In the following, the technical sub-model is first described, considering all possible uses of geothermal energy. Pure power generation, pure heat supply and combined heat and power generation in parallel or series connection are conceivable. Subsequently, the validation of the power plant model is presented.

### 3.1.3.1 Technical description of the energy utilization model

Within the scope of the present work, a single-stage Organic-Rankine-Cycle (ORC) plant is modelled. Besides the ORC power-plant concept there is also the Kalina concept, named after its inventor, which could be used for low temperature electricity provision. Although the Kalina-Cycle shows advantages in very low temperatures over the ORC concept, it has never been able to prevail in the market. Today there are only a few Kalina power plants in operation. As Kalina cycles don't play a role in the international market, they are not investigated within this study.

In addition to the pure provision of electricity, the simultaneous provision of electricity and heat (CHP - combined heat and power) are studied. For CHP, three circuit variants are being investigated. Heat extraction can be connected in parallel or in series, or a combination of both (Eyerer, et al., 2017). The wiring diagram of the system is shown in Figure 20.

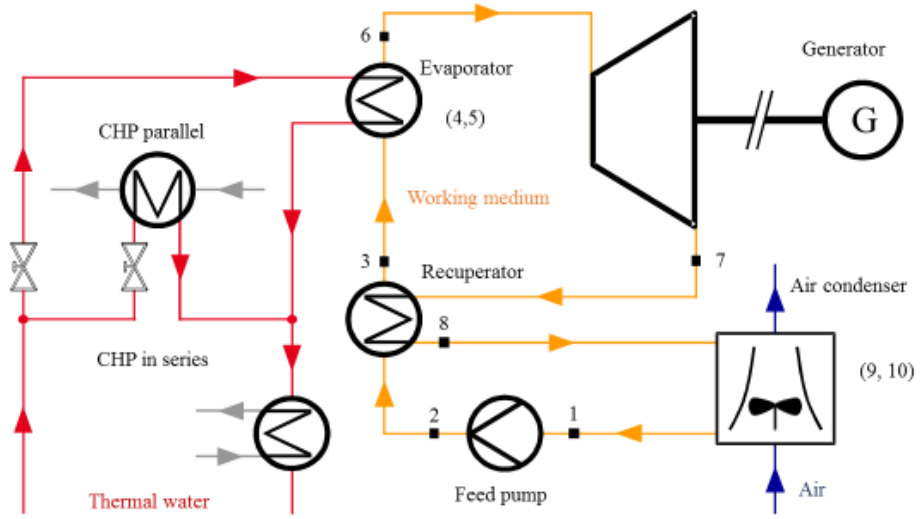


Figure 20: Schematic depiction of ORC with CHP

The central element of the power plant is the clockwise working medium circuit, consisting of the components of working medium pump, optional recuperator, evaporator, turbine, generator and air condenser. Other condenser types are not considered. Furthermore, a heat exchanger (HE) in parallel and series connection is provided for the decoupling of heat if the other design of the power plant permits. CHP in series connection can be provided if the temperature of the thermal water after the evaporator is above the specified minimum injection temperature. Heat extraction in parallel is possible if the minimum temperature difference in the evaporator is maintained, even if only part of the available thermal water flow is routed through it. The necessary condition for this is that the thermal water temperature at the power plant outlet without bypass is above the minimum injection temperature. The determination of the maximum possible bypass mass flow is described in more detail in the section on the evaporator. The state changes of the working medium between the state points entered in Figure 20 are determined within the "BasicCycle.m" working medium circuit routine, as explained in the corresponding section. These are described as key points below:

- $1 \rightarrow 2$: Pressure increase in feed pump
- $2 \rightarrow 3$: Heat supply in recuperator
- $3 \rightarrow 4$: Pre-heating to boiling point in evaporator
- $4 \rightarrow 5$: Complete evaporation in evaporator
- $5 \rightarrow 6$: Overheating in evaporator
- $6 \rightarrow 7$: Decompression in turbine

- 7 → 8: Heat removal in recuperator
- 8 → 9: Pre-cooling to dew point in condenser
- 9 → 10: Complete condensation in condenser
- 10 → 1: Undercooling in condenser (not considered in this work)

The state points in the working medium cycle are visualized for illustration in Figure 21 for a pure working medium such as isobutane Figure 21a and an azeotropic working medium mixture Figure 21b in a qualitative temperature entropy diagram.

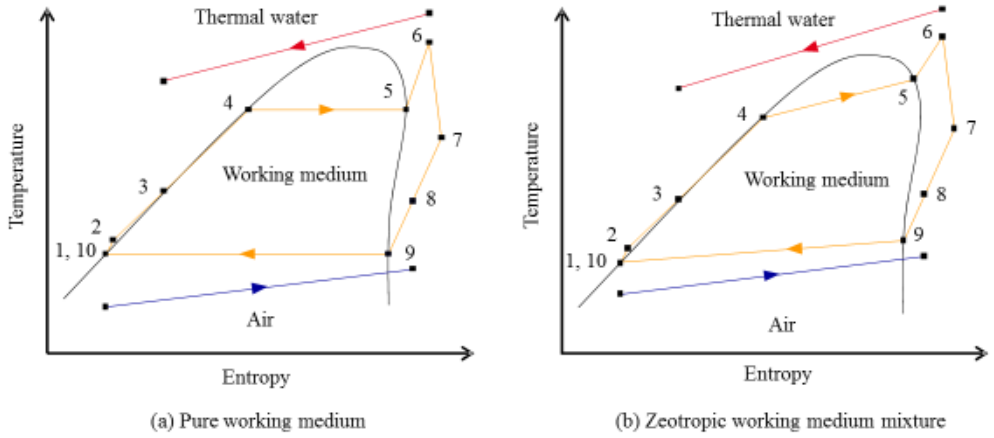


Figure 21: Comparison between pure working medium and zeotropic working medium mixture in an ORC (Welter, Technisch-ökonomische Analyse der Energiegewinnung aus Tiefengeothermie in Deutschland, 2018)

Pure working mediums evaporate and condense almost isothermally. Mixtures of working mediums, on the other hand, exhibit sliding temperatures during evaporation and condensation due to the different evaporation and condensation temperatures of the individual components. In this context, zeotropic mixtures of working mediums exhibit a temperature glide at each composition (Welter, Technisch-ökonomische Analyse der Energiegewinnung aus Tiefengeothermie in Deutschland, 2018). Mixtures of working mediums, which do not exhibit temperature glide at a certain composition (azeotropic mixtures), are not considered in this study. The use of mixtures of working mediums can have an advantageous effect on the efficiency of the power plant, since the temperature profiles of working mediums and thermal water or air can be adjusted to each other as a result of temperature sliding during evaporation and condensation. Thus, the exergy losses in the cycle can be reduced and the efficiency increased accordingly (Welter, Technisch-ökonomische Analyse der Energiegewinnung aus Tiefengeothermie in Deutschland, 2018) (Heberle, 2013). The power plant shown in Figure 20 is implemented in Matlab. A simplified programming flow chart can be found in Figure 22 and in Figure 61 in the Annex. Matlab is used for this purpose. The first step is done in the EnergyConversionShell.m. There site-specific data such as flow rate, temperature, pressure and salinity of the geothermal fluid are read in. Furthermore, the parameters to be varied within the Monte-Carlo simulation and their upper and lower limits are defined. A defined number of Monte Carlo iterations are then run through to simulate a large number of different power plant designs. The power plant model used here is a single-stage ORC plant and consists of individual Matlab routines called upon within the "EnergyConversion.m" program. The input and output variables of the heat exchanger models of evaporator, recuperator and condenser are illustrated in Figure 23 to Figure 27. In the following, the different sub models of the ORC presented in more details.

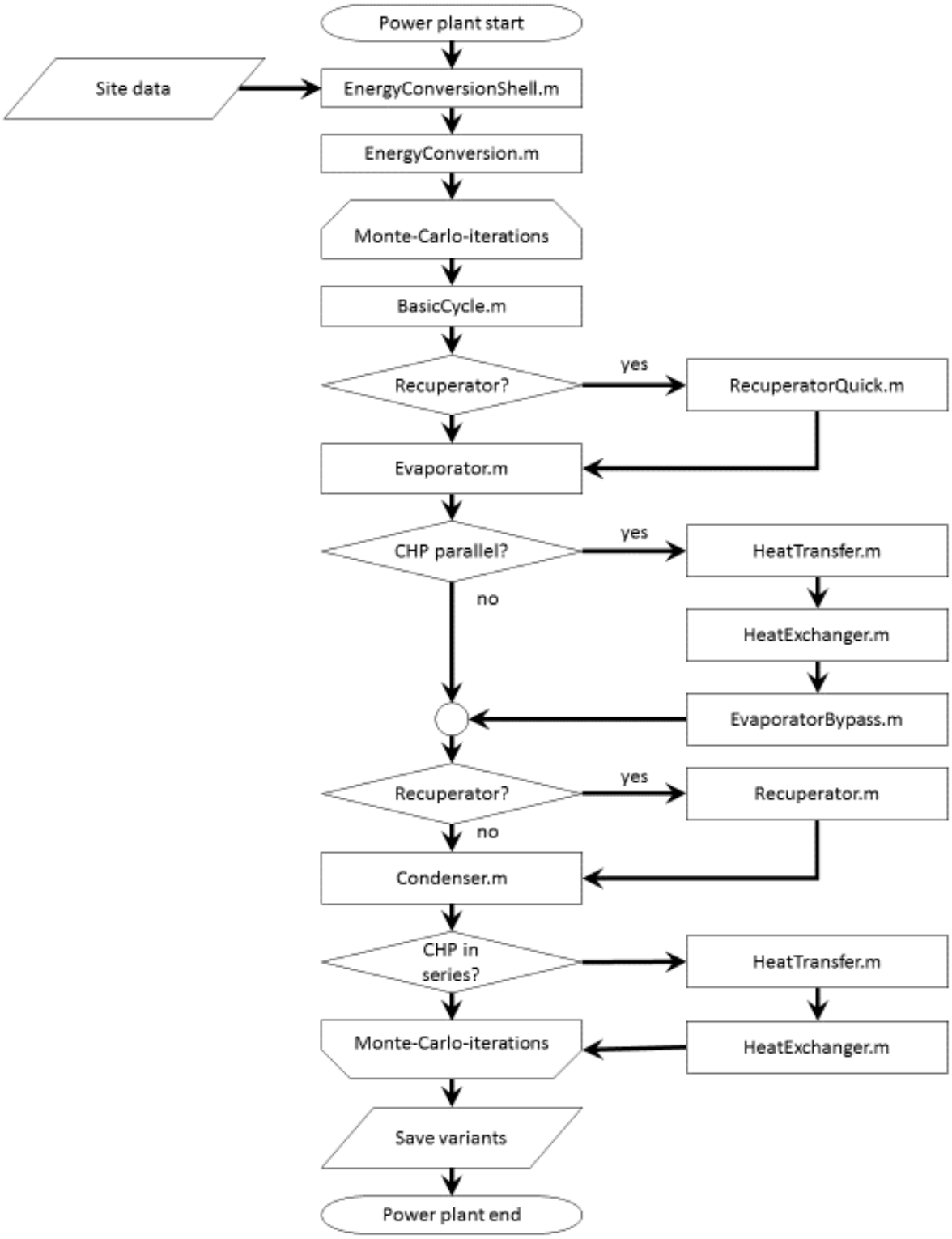


Figure 22: Program flow chart overall model with routine names

### Working medium cycle (BasicCycle.m):

The working medium cycle is mapped with its own Matlab routine and is evaluated based on the process parameters from Table 6, which were sampled during the Monte-Carlo simulation. Thereby temperatures, enthalpies and entropies of the work medium for the ten defined state points shown in Figure 20 are determined using the NIST database according to (Lemmon, Huber, & McLinden, NIST Standard Reference Database 23: Reference Fluid Thermodynamic and Transport Properties REFPROP, Version 9.1, 2013). The selected pressures and pressure losses in the system determine the pressure

at the respective point of state before and after the feed pump. In all heat exchangers, as in (Chacartegui, Sanchez, Munoz, & Sanchez, 2009), a pressure drop of 2% is assumed. Within the same routine, feed pump and turbine are modelled with a firmly defined isentropic efficiency of 80%, respectively 85% and as a value of motor and generator an efficiency of 96% is assumed (Schlagermann, 2014). The generator also has a gearbox, the efficiency of which is approximated to be 98% (Welter, Technisch-ökonomische Analyse der Energiegewinnung aus Tiefengeothermie in Deutschland, 2018).

Whether and to what extent a recuperator is installed in the system is randomly varied in the Monte-Carlo simulation (see chapter 3.1.3.3). If the decision is made in favour of a recuperator, the working medium cycle, initially evaluated without such a recuperator, is modified using the "RecuperatorQuick.m" routine. As a result, state points 3 and 8 change according to the recuperated heat. During the modification, the preservation of the minimum temperature difference is considered for the determination of the maximum recuperated heat. The procedure is based on (Kemp, 2007), as explained in the following section on the evaporator.

The heat exchangers are considered in more detail to calculate the required heat exchanger area. The evaporator, condenser, recuperator and the heat exchanger or exchangers for heat extraction at CHP are simplified and modelled as shell-and-tube heat exchangers (SHE), which are operated in counter-current mode. Compared to plate heat exchangers, these are to be preferred particularly for geothermal fluids with high salinity due to their better suitability for high pressures and easier cleaning (Schlagermann, 2014). In the following, the individual heat exchangers and the correlations used to determine their area are explained. The terms hot and cold do not represent certain temperature levels but define the heat-emitting fluid (hot) and heat-absorbing fluid (cold).

### Evaporator (Evaporator.m):

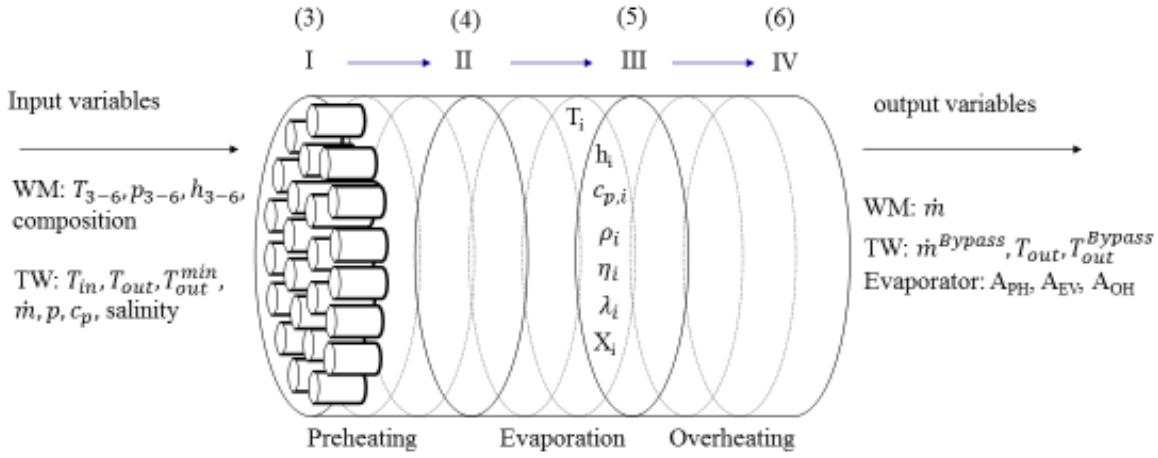


Figure 23: Schematic depiction of evaporator in ORC-model

In the evaporator, the working medium flow corresponds to the cold flow, i.e. it absorbs heat. The sketch of the SHE shows the input variables for the Matlab routine. Pressure, temperature and enthalpy of the working medium at the state points of the ORC are required, as well as the working medium composition and properties of the thermal water at the power plant entrance. Furthermore, the minimum permissible temperature of the thermal water after the evaporator must be known, which is defined by the lower limit of the Monte Carlo parameter $T_{TW}$ in Table 6. In addition, Figure 23 shows the output variables of the routine. These are the heat transfer surfaces for preheating ($A_{PH}$), evaporation ($A_{EV}$) and overheating ($A_{OH}$) and the working medium mass flow. Another output is the

maximum thermal water mass flow required for combined heat and power generation in parallel connection (bypass) in the present design of the ORC, which can be routed past the evaporator. The last output value represents the temperature of the thermal water after the evaporator for both cases with and without heat extraction in parallel.

Working medium and bypass mass flow can be determined by using the temperature profiles of thermal water and working medium. This is done based on the methodology of pinch analysis (Kemp, 2007), so that the defined minimum temperature difference $\Delta T^{min}$ between hot and cold current is maintained. Figure 24 illustrates the procedure used for this purpose.

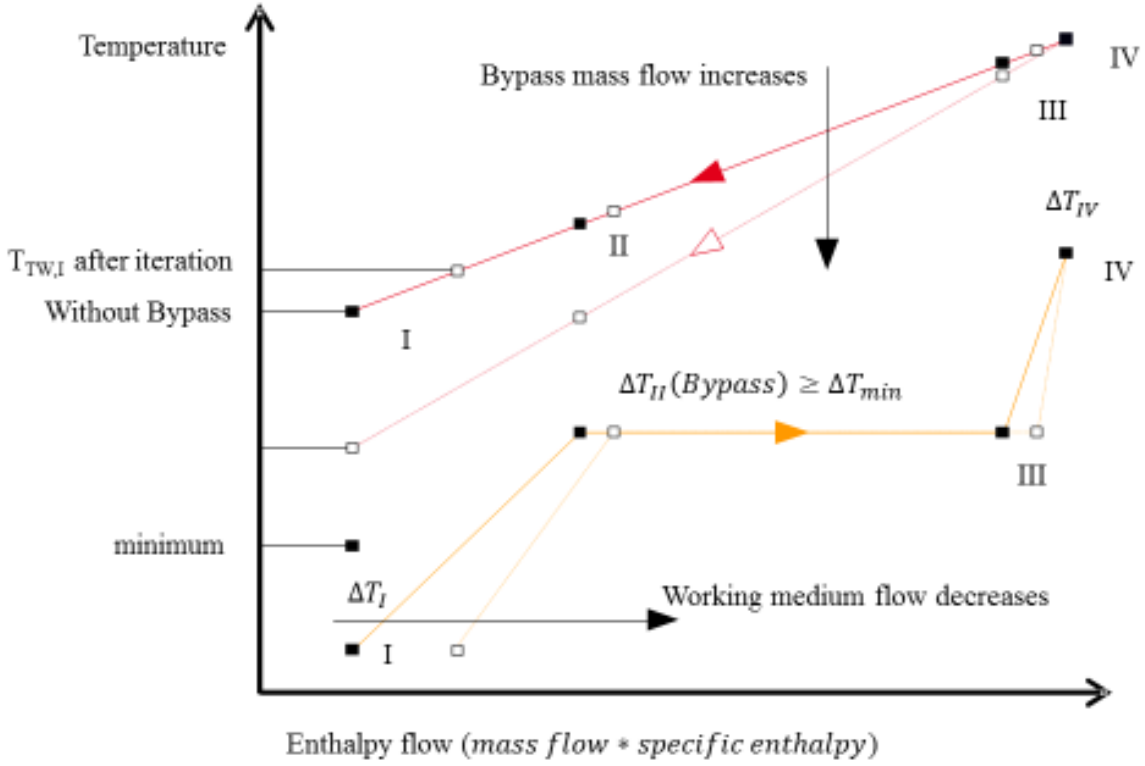


Figure 24: Heat integration for thermal water and working medium in evaporator

For all calculations, the specific heat capacity of the thermal water $c_{p,TW}$ is assumed to be constant over the considered temperature and pressure range. The admissibility of this simplification is demonstrated in (Welter, Technisch-ökonomische Analyse der Energiegewinnung aus Tiefengeothermie in Deutschland, 2018). Figure 24 shows the temperatures over the enthalpy flow of the cold (here yellow) and hot streams (here red). The slope of the curves depends on the reciprocal value of the product of mass flow and specific heat capacity. In the evaporation range of the working medium, however, the curve is horizontal, since no temperature change occurs during the evaporation of a pure working medium. This type of diagram is typical for the graphical solution of heat integration problems. The aim of the investigation is to determine the working medium mass flow, the maximum recoupable bypass mass flow and the outlet temperature of the thermal water at the maximum bypass mass flow rate while maintaining the minimum temperature difference $\Delta T^{min}$ at each point in the evaporator. The different status points of the thermal water (TW) and working medium within the evaporator are shown in Figure 24 with the Roman numbers I to IV. The temperatures of the working medium at these points are input data of the evaporator routine and thus known. The same applies to the specific enthalpies of the working medium and the properties of the thermal water at the entrance. The exact shape of the working medium curve can therefore only be influenced by the working medium

mass flow and the outlet temperature of the thermal water ($T_{TW,I}$). First, it is assumed that the entire available thermal water mass flow is led through the evaporator and that the entire extractable heat is transferred to the working medium flow. This allows to determine the maximum working medium mass flow with equation (18).

$$\dot{m}_{WM} = \frac{\dot{m}_{TW} * (T_{TW,IV} - T_{TW,I}) * c_{p,TW}}{h_{WM,IV} - h_{WM,I}} \quad (18)$$

In this equation, $\dot{m}$ stands for the mass flow, $T$ for the temperature, $c_p$ for the heat capacity, and $h$ for the enthalpy. The WM and TW indices stand for work fluid and thermal water. The enthalpy $h_{WM,I}$ is the enthalpy of the working medium at the temperature at state point I ($T_{TW,I}$). Figure 24 displays this constellation with curves with filled squares, which represent the state points. For the verification of the assumption, it must now be checked, whether the minimum temperature difference between hot and cold current at each point of the heat exchanger is maintained. If this condition is fulfilled for points I, II and IV, the temperature difference is also sufficient at all intermediate points via $\Delta T_{min}$. At point IV, the compliance with the minimum temperature difference is guaranteed by choosing adequate definition of the boundary values for the Monte Carlo parameters $T_6$ and $p_2$. For shoulder point II, the thermal water temperature is derived with equation (19), under the assumption of maximum working medium mass flow.

$$T_{TW,II} = T_{TW,IV} - \frac{\dot{m}_{WM}^{max} * (h_{WM,IV} - h_{WM,II})}{\dot{m}_{TW} * c_{p,TW}} \quad (19)$$

Based on the results of equation (19), it is examined whether at point II the minimum temperature difference is maintained. If this is not the case, the working medium mass flow rate in equation (19) is reduced iteratively until the minimum temperature difference is surpassed at point II. In Figure 24, the temperature $T_{TW,II}$, on the thermal water curve, migrates to the right assuming a higher value than before the iteration. The outlet temperature of the thermal water behaves in the same way when an iteration must be carried out. The adjusted outlet temperatures of the thermal water and the temperature of the thermal water at point II are displayed as unfilled squares on the thermal water curve in Figure 24.

The procedure for determining the maximum bypass mass flow in accordance to Figure 24 is described under the assumption, that no iteration of the working medium mass flow is necessary. In this case, the solid yellow curve, with filled squares for identification of the state points, represents the temperature profile of the working medium.

First, it is assumed that the thermal water can be cooled down to the predefined minimum outlet temperature ($T_{TW,I}^{min}$). This temperature enters the system in Figure 24 at the lowest position of the ordinate. It is an input variable of the evaporator model and thus known. With the mentioned assumption, the minimum necessary thermal water mass flow through the heat exchanger can be calculated and with the available mass flow of the geothermal fluid, results in the maximum bypass mass flow according to equation (20):

$$\dot{m}_{Bypass}^{max} = \dot{m}_{TW} - \dot{m}_{TW}^{min} = \dot{m}_{TW} - \frac{\dot{m}_{WM,IV} * (h_{WM,IV} - h_{WM,II})}{c_{p,TW} * (T_{TW,IV} - T_{TW,I}^{min})} \quad (20)$$

Now, the temperature difference between working medium and thermal water at point II is calculated. To check, whether the minimum temperature difference is maintained, Equation (21) is used.

$$T_{TW,II} = T_{TW,IV} - \frac{\dot{m}_{WM} * (h_{WM,IV} - h_{WM,II})}{\dot{m}_{TW}^{min} * c_{p,TW}} \quad (21)$$

The temperature of the thermal water is modified, if the minimum temperature difference should not be met at this point. That results in the following equation:

$$T_{TW,II} = T_{AM,II} + \Delta T^{min} \quad (22)$$

In this case, the maximum bypass mass flow is calculated with the modified temperature $T_{TW,II}$ and equation (20):

$$\dot{m}_{Bypass} = \dot{m}_{TW} - \dot{m}_{TW}^{min} = \dot{m}_{TW} * \frac{\dot{m}_{WM}*(h_{WM,IV}-h_{WM,II})}{c_{p,TW}*(T_{TW,IV}-T_{TW,II})} \quad (23)$$

The achievable bypass mass flow in this case is lower than the one calculated with equation (20). Afterwards, the temperature of the thermal water after the evaporator is determined assuming that the bypass mass flow is actually being led around the evaporator:

$$T_{TW,I} = T_{TW,IV} - \frac{\dot{m}_{WM}*(h_{WM,IV}-h_{WM,I})}{\dot{m}_{TW}*c_{p,TW}} \quad (24)$$

In case the heat extraction is realized in parallel, the temperature profile of the thermal water assumes the shape of the pale red line in Figure 24.

Depending on the shape of the temperature profiles of thermal water and working medium, the minimum temperature difference can also be undercut at point I, even though it is maintained at point II. In this case, the procedure described above for point II must be repeated for point I and thus the shape of the temperature profiles adapted. The heat exchanger surface areas can be determined based on the completely determined temperature profiles. Since the thermal water mass flow through the evaporator is included in the calculations presented in chapter Calculation of overall heat transfer coefficientE (equation (65)), two design variants of the evaporator are taken into account. A first variant without bypass is realized by “Evaporator.m” and a second variant with maximum bypass mass flow by “EvaporatorBypass.m”. The surface area calculation is carried out for both options and the values are output from the routine. To determine the areas, various geometry parameters and other variables must be defined, which are listed in Table 3 together with the corresponding parameters for all other heat exchangers.

Table 3: Parameters for calculating heat exchanger surfaces a: (Towler & Sinnott, 2013), b: (Wolf & Kirchner, 2013), c: (Heberle & Brüggemann, Thermo-economic analysis of zeotropic mixtures and pure working fluids in organic rankine cycles for waste heat recovery, 2016)

| | | **Evaporator** | **Condensator** | **Recuperator** |
|---|---|---|---|---|
| **Pipes** | Outer diameter[a] $d_a$ | 50mm | 25mm | 25mm |
| | Wall thickness[a] | 2,8mm | 2,1mm | 2,1mm |
| | Positioning | Aligning | Aligning | aligning |
| | Average spacing[a] | 1,25*$d_a$ | 1,25*$d_a$ | 1,25*$d_a$ |
| | Heat conductivity[b] | 20W/mK | 20W/mK | 20W/mK |
| | Fins width[c] | - | 0,3m | - |
| | Fins height[c] | - | 3mm | - |
| | Fins spacing[c] | - | 2mm | - |
| | Fluid | TW | AM | AM |
| **Jacket** | Clearance[a] | 0,1m | 0,1m | 0,1m |
| | Fluid | WM | air | WM |
| **Fluids** | Max. velocity gas[b] | 20m/s | 30m/s | 20m/s |

| | | | |
|---|---|---|---|
| Max. velocity liq.[b] | 1,5m/s | 1,5m/s | 1,5m/s |
| Number passages | 1 | 1 | 1 |

The parameters are either taken from literature or selected based on the values found in literature. Thermal water is highly corrosive and thereby tends to contaminate the heat exchangers. Therefore, it flows inside the evaporator pipes. The outer diameter and wall thickness of these pipes are selected to be larger than in the other heat exchangers (Towler & Sinnott, 2013). In general, in this model the fluid, which causes more pollution, is passed through the pipes. If no distinction can be made on the basis of this criterion, the hotter fluid is assigned to the pipes (Towler & Sinnott, 2013) (Wolf & Kirchner, 2013).

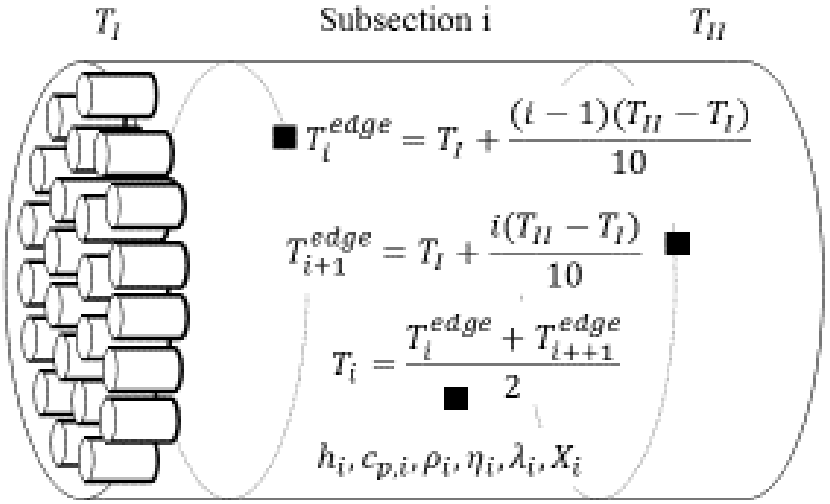


Figure 25: Division into subsections of evaporator for pre-heating

All heat exchangers in this model share the same subdivision of each section into ten sub-sections. For example, the evaporator section, in which the preheating of the working medium takes place, is divided into ten equidistant, individual sections based on the temperature. This subdivision for the evaporator is indicated in Figure 23. In the actual evaporation part of the heat exchanger, the subdivision into sub-sections is carried out based on the vapour content. Where superheating takes place, the evaporator is subdivided into ten sub-sections based on temperature. The sub-sections and edges are numbered from left to right from 1 to 10 and 11, respectively, in relation to Figure 23, so that, for example, an edge value with index 1 represents the left edge of the sub-section with index 1. The boundary value with index 2 forms the right margin of subsection 1 and at the same time the left margin of subsection 2 and so on. Figure 25 shows this division as an example of a subdivision based on temperature. To determine the fluid properties at the edges, it is assumed that pressure losses only occur after a main section in the heat exchanger (e.g. at the transition from preheating to evaporation). Thus, the pressure values at the edge of each section are constant within a main section. The NIST database (Lemmon, Huber, & McLinden, NIST Standard Reference Database 23: Reference Fluid Thermodynamic and Transport Properties REFPROP, Version 9.1, 2013) is then used to calculate physical properties for the corresponding working medium. The specific enthalpy $h$, the specific heat capacity $c_p$, the density $\rho$, the kinematic viscosity $\eta$, the thermal conductivity $\lambda$ and the vapour content $X$ or the temperature $T$ for the edges of all subsections are determined. The boundary values of the material properties obtained in this way and the temperatures or vapour contents are arithmetically averaged to approximate the respective values within each subsection. Within each subsection, the fluid properties are assumed to be constant, but vary from one to another. With the help of the described procedure all prerequisites for the calculation of the heat exchanger areas of each individual

section are given within the evaporator routine. The calculation procedure is described below and is based on the approach presented in (Heberle & Brüggemann, 2016) and (Welter, Technisch-ökonomische Analyse der Energiegewinnung aus Tiefengeothermie in Deutschland, 2018). The heat exchanger area of each individual section (i) can be calculated using equation (25).

$$A_i = \frac{\dot{m}_{WM} * (h_{WM,i+1}^{edge} - h_{WM,i}^{edge})}{k_i * \Delta T_i^{ln}} \quad (25)$$

The working medium mass flow $\dot{m}_{WM}$ is known from the calculations above. The specific enthalpies $h_{WM,i+1}^{edge}$ and $h_{WM,i}^{edge}$ are the left and right boundary values of the subsection and thus taken from the NIST database according to (Lemmon, Huber, & McLinden, NIST Standard Reference Database 23: Reference Fluid Thermodynamic and Transport Properties REFPROP, Version 9.1, 2013). $k_i$ stands for the overall heat transfer coefficient of the subsection. With equation (26), the logarithmic temperature difference $\Delta T_i^{ln}$ between hot and cold current for each range from the temperatures of the working medium and thermal water are calculated at the edges of the subsections.

$$\Delta T_i^{ln} = \frac{\Delta T_{i+1}^{edge} - \Delta T_i^{edge}}{ln\left(\frac{\Delta T_{i+1}^{edge}}{\Delta T_i^{edge}}\right)} \quad (26)$$

With

$\Delta T_{i+1}^{edge} = \left|T_{TW,i+1} - T_{WM,i+1}\right|$, and $\Delta T_i^{edge} = \left|T_{TW,i} - T_{WM,i}\right|$.

To calculate the heat exchanger area, equation (25) with the heat transfer coefficient $k_i$ is used. The procedure for determining the thermal transmittance is explained in the section E of the appendix. That way, all areas of the individual sub-sections can be determined. The total area is calculated by adding the individual results and is then determined by the Evaporator routine broken down into the main areas preheating (PH), evaporation (EV) and overheating (OH).

### Condenser (Condenser.m):

To determine the condenser surface areas, considerations must be made to maintain the minimum temperature difference, similar to the evaporator. Since the working medium mass flow is already known from the evaporator routine, the procedure is simplified. In principle, the heat transfer from the working medium flow to the air flow in the condenser is also considered based on the Pinch method (Kemp, 2007) and is therefore not explained in detail here. The different states of the air in the condenser are determined using the NIST database (Lemmon, Huber, & McLinden, NIST Standard Reference Database 23: Reference Fluid Thermodynamic and Transport Properties REFPROP, Version 9.1, 2013). Equations of state according to (Lemmon, Jacobsen, Penoncello, & Friend, 2000) are used to describe the fluid air. Information on the viscosity and thermal conductivity of air is provided by (Lemmon & Jacobsen, 2004). It is defined that the cooling air shall not heat up by more than 10K. The result of these considerations for the condenser are the output variables air mass flow and outlet temperature of the air. Furthermore, the condenser surface areas and the fan power are determined. The latter is calculated according to equation (27).

$$P_{Fan} = \frac{\dot{m}_{Air} * \Delta p_{Fan}}{\rho_{Air} * \eta_{Fan}} \quad (27)$$

To calculate the fan power, 100 Pa is assumed for the pressure increase $\Delta p_{Fan}$ by the fan and 70% for the total fan efficiency $\eta_{Fan}$. The values were derived from manufacturer data (Systemair, 2018) and a valid EU directive (EU, 2009). Furthermore, the density of the air is approximated with the value at ambient pressure and inlet temperature. An energy balance around the condenser results in the air

mass flow $\dot{m}_{Air}$, which is necessary for cooling the working medium. Figure 26 shows a schematic diagram of the condenser.

Input variables of the condenser routine are the temperatures, pressures and enthalpies at state points 8 to 10, the mass flow and the composition of the working medium. In addition, the inlet temperature and pressure of the air flowing through the condenser jacket, as well as the minimum temperature difference. The determination of the heat exchanger surfaces in the sections of the heat exchanger is like the calculation steps for the evaporator. The difference is that in the condenser the working medium flows in the tubes and air flows through the jacket, while in the evaporator there is thermal water in the tubes and working medium in the jacket. In addition, fins on the outside of the tubes are considered to improve heat transfer. The two main areas of pre-cooling and condensation of the condenser are divided into 10 sub-areas, analogous to the evaporator. All equations for calculating the overall heat transfer coefficient are described in chapter E of the annex. The total area of the condenser is calculated by adding the individual areas for precooling and condensation.

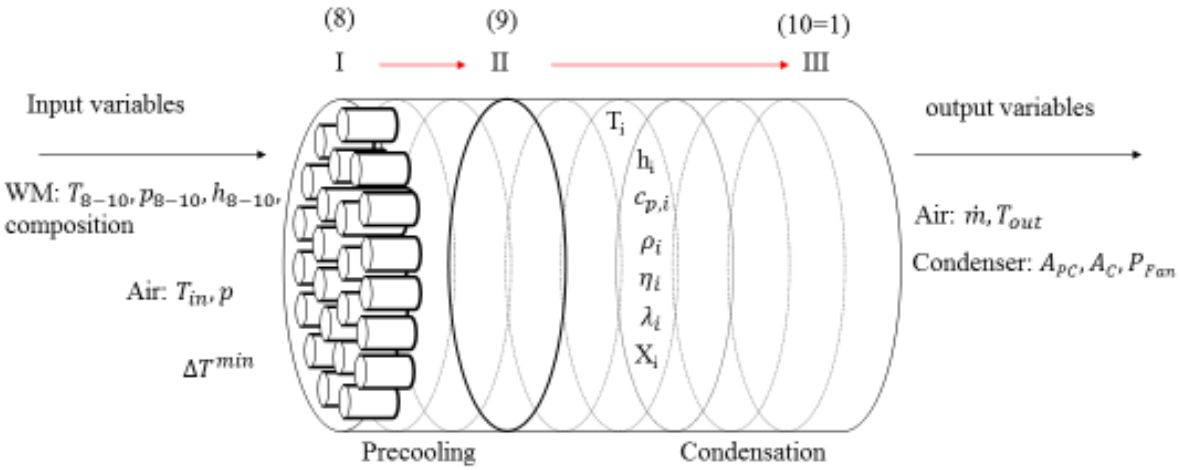


Figure 26: Schematic depiction condenser in ORC-model

### Recuperator (Recuperator.m):

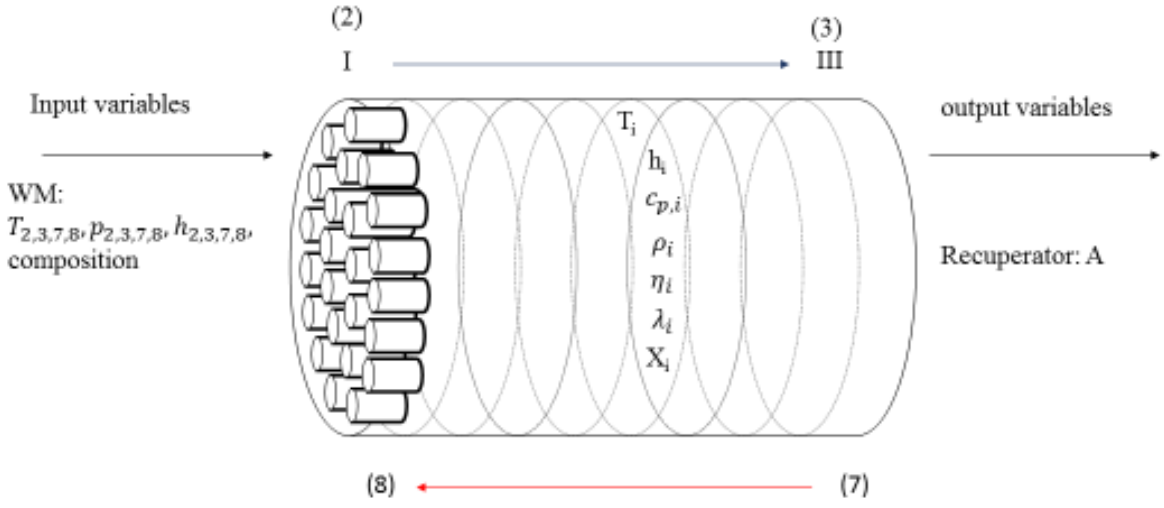


Figure 27: Schematic depiction recuperator in ORC-model

The recuperator is schematically shown in Figure 27. In the recuperator routine, the heat exchanger area is determined from the temperatures, pressures and enthalpies at state points 2, 3, 7 and 8, as well as the composition of the working medium. For the calculation of the evaporator, based on the

"pinch method" (Kemp, 2007) (see page 40), the recuperator state points are already examined. So, the temperature profiles of hot and cold flow can be calculated like the approach shown in Figure 24. This ensures, that the minimum temperature difference is maintained. All in all, the recuperator model is a simplified version of the evaporator or condenser model. But the number of tubes in the recuperator must be calculated according to equation (64), to maintain the maximum fluid velocities given in Table 3. This is mandatory before calculating the heat exchanger area analogously to Equations (25) and (65). In the recuperator, the hot working medium stream flows inside the pipes, the cold one inside the jacket.

#### Heat Exchanger CHP (HeatExchanger.m):

The heat exchangers, which are used for heat extraction and pure heat supply, correspond in principle to the preheating section of the evaporator. The hot thermal water flows in the pipes, in accordance with the design instructions of (Towler & Sinnott, 2013), the cold water of the heating network flows in the jacket. The correlations used to calculate the area thus remain the same as for preheating, only the material properties of the working medium are substituted for those of water. Calculations to maintain the minimum temperature difference according to (Kemp, 2007) are necessary, as explained in detail in the corresponding passage on the evaporator. Similar to the recuperator, this takes place in HeatTransfer.m before the heat exchanger routine (see flow chart Figure 22). Constant temperatures of 70°C and 45°C are assumed for the outgoing flow and return flow in the heat network, respectively. If these temperatures cannot be achieved without falling below the minimum temperature difference, the additional amount of heat required is also determined, but must be provided by a boiler. As no steam-operated heating networks are considered, no phase change of a heat transfer fluid occurs.

The application case of pure heat supply is regarded as a special case of the system, in which simply no working medium circuit is implemented. Only the Matlab routines "HeatTransfer.m" and "HeatExchanger.m" shown in Figure 22 are required. In this case, the distinction between parallel and series connection for heat extraction also becomes obsolete. Only one heat exchanger is then considered for transfer to the heat network. Pure power generation is also regarded as a special case of the power plant diagram shown in Figure 20, in which heat is not decoupled either in parallel or in series. The Matlab routines "HeatTransfer.m" and "HeatExchanger.m" are therefore neglected in this case.

### 3.1.3.2 Verification of the power plant model

Data from the Soultz-sous-Forêts site are used to validate the technical power plant model. Table 4 shows the comparison between the modelled state points, heat transfer areas, capacities and mass flows of the ORC, and the available power plant data from Soultz-sous-Forêts.

Table 4: Comparison ORC-model with Soultz-sous-Forêts a: input parameter at validation, b: from energy balance of recuperator (Seibel, 2018)

| **State point** | **1** | **2** | **3** | **4** | **6** | **7** | **8** | **10** |
|---|---|---|---|---|---|---|---|---|
| $T_{model}$ [°C] | 24,9 | 26,7 | 38,3 | 118,8 | 120[a] | 47,8 | 32,2 | 24,9 |
| $T_{Soultz}$ [°C] | 24,2 | 26,5 | 38,1 | 111,2 | 118,4 | 50,8[b] | 34,0 | 24,2 |
| $p_{model}$ [bar] | 3,5[a] | 28,9[a] | 28,4 | 27,8 | 27,2 | 3,7 | 3,6 | 3,5 |
| $P_{Soultz}$ [°C] | 3,5 | 28,9 | 28,2 | 26,6 | 26,4 | - | 3,6 | 3,5 |
| $h_{model}$ [kJ/kg] | 2588 | 264,6 | 293,0 | 531,5 | 696,1 | 629,1 | 600,7 | 258,8 |

| $h_{Soultz}$ [kJ/kg] | 257,0 | 264,1 | 292,5 | 502,3 | 696,3 | 632,3[b] | 603,9 | 257,0 |
|---|---|---|---|---|---|---|---|---|
| **HE-surface area** | $A_{PH}$ | $A_{evap}$ | $A_{cond}$ | $A_{recup}$ | | | | |
| Model | 401m$^2$ | 148m$^2$ | 6485m$^2$ | 93m$^2$ | | | | |
| Soultz | 338m$^2$ | 168m$^2$ | - | - | | | | |
| **Power** | $P_{Pumpe}$ | $P_{turbine}$ | $P_{Generator}$ | $P_{Fan}$ | | | | |
| Model | 167kW | 1874kW | 1761kW | 112kW | | | | |
| Soultz | ≈150kW | 1810kW[c] | 1725kW | 120kW | | | | |
| **Mass flow** | $\dot{m}_{WM}$ | $\dot{m}_{air}$ | | | | | | |
| Model | 27,9kg/s | 970kg/s | | | | | | |
| Soultz | 28,3kg/s | 1040kg/s | | | | | | |

Isobutane is chosen as the working medium for modelling as in the real power plant. The NIST database (Lemmon & Jacobsen, 2004) is used to determine the substance properties. All information about the different working medium states is derived from the equations of state for isobutane according to (Bäcker & Wagner, 2006). Viscosity and thermal conductivity are determined using expressions valid for isobutane according to (Vogel, Küchenmeister, & Bich, 2000) and (Perkins, 2002). The temperature, pressure and enthalpy values shown are rounded to one decimal place. All pressures are given as absolute pressures, i.e. the sum of ambient pressure and overpressure in the plant. To carry out the validation, the pressure levels before and after the feed pump (points 1 and 2) are firmly defined in the model according to the present comparative values. For the validation of the model against Soultz-sous Forêts data, no combined heat and power generation is considered, since only electricity generation takes place there. The state points 5 and 9 are not considered because there are no comparative values for them. At state point 7, temperature and enthalpy in the real power plant can be estimated from an energy balance around the recuperator. The thermal water temperature at the power plant entrance is 160°C and about 70°C at the exit. The mass flow of the geothermal fluid corresponds to 33.3 kg/s and its pressure is between 2200 and 2250 kPa (Seibel, 2018) (Turbodem, 2015). The salinity of the thermal water is considered according to Table 5.

Table 5: Salinity of thermal water at DESTRESS-locations, a: (Sanjuan, et al., 2016); b: (Kft., Geo-Log, 2012) c: (Welter, Technisch-ökonomische Analyse der Energiegewinnung aus Tiefengeothermie in Deutschland, 2018), TDS: total dissolved solids

| Location | Na [g/ l] | K [g/l] | Ca [g/l] | Cl [g/l] | TDS [g/l] |
|---|---|---|---|---|---|
| **Soultz-sous-Forêts**[a] | 28,1 | 3,2 | 7,2 | 58,6 | 99,0 |
| **Mezöberény**[b] | 1,9 | ≈0 | ≈0 | 0,3 | 6,6 |
| **Oberrheingraben**[c] | 38,2 | 3,3 | 7,8 | 78,0 | 127,3 |

In general, the temperature, pressure and enthalpy values show good agreement between the model and the comparative data: The percentage differences between model and real data are less than 5% everywhere and are significantly lower in most places.

Regarding temperatures, the maximum deviation is almost 2% at state point 4 related to values in the unit Kelvin. This difference is due to the modelling of the evaporator. Simplified, it is assumed that

state point 4 lies exactly on the boiling line of the working medium. In fact, the working medium leaves the preheater with a lower temperature and is heated in the evaporator up to the boiling line. A larger preheater area and correspondingly smaller evaporator area in the model can therefore be expected compared to the power plant data. In fact, this behaviour can be observed when comparing the heat exchanger surfaces in Table 4. The temperatures at points 1 and 10 of the model are larger than the power plant data. In the presented model, sub cooling in the condenser is neglected as mentioned above. Therefore, the working medium is just condensed out at points 1 and 10 in the model, while in fact it is slightly undercooled. Accordingly, the deviation observed there appears plausible and, with an enthalpy increase of about 1%, represents a negligible influence on the model results.

The pressure values of the model deviate by up to 5% from the state points of the power plant in Soultz-sous-Forêts, because the pressure losses in evaporator, condenser and recuperator are estimated to be 2% (Welter, Technisch-ökonomische Analyse der Energiegewinnung aus Tiefengeothermie in Deutschland, 2018). The deviations result mainly from the neglect of the pressure losses in the recuperator. They are tolerable due to the low influence of the pressure on the specific enthalpy of the working medium compared to the temperature. The differences in the enthalpy values correspond approximately to those of the temperature values and are therefore justified and acceptable.

For the heat transfer surfaces in Table 4, the maximum deviation is approximately 17 %, with data available only for the preheating and evaporation sections of the evaporator. One reason for the deviation has already been discussed above. Another factor is the geometry parameters selected, such as the pipe diameter, which have a strong influence on the determined area. Therefore, greater uncertainties are to be expected for the heat exchanger surfaces than for the state points. By changing the choice of geometry parameters, these could be adapted to the existing conditions in Soultz-sous-Forêts but would not gain increased significance for other locations. Furthermore, there is no usable data available on the geometry parameters of the heat exchangers used, because ORC plants for geothermal applications are usually handed over turnkey by the supplier. Therefore, the differences are acceptable. Good agreement between model and real power plant is achieved with less than 7% difference for the determined performances of turbine, generator and fan of the air-cooling tower. For the feed pump, the deviation of almost 19% is significantly greater, but the comparative value of the real power plant is also subject to uncertainties (Seibel, 2018). The mass flows of working medium and cooling air in the model and in reality, correspond sufficiently well with a deviation of less than 10%.

All in all, the real conditions at the Soultz-sous-Forêts power plant site are precisely mapped by the model. Larger deviations only appear for the determined heat exchanger surface areas of preheater and evaporator, whereby a large part of the deviation results from the idealized separation between the two heat exchangers in the model and the selected geometry parameters.

In addition to validation data from the DESTRESS site Soultz-sous-Forêts, comparative data are available from a simulation model validated against real operating data of the geothermal power plant Oberhaching (Eyerer, 2018), which is operated by Erdwärme Grünwald GmbH. In general, there are good similarities with deviations of less than 10 %. Even the few available real operating data from the same location (Eyerer, et al., 2017) can be mapped well with the power plant model described in section 3.1.3.1. Particularly, the achievable power plant output at given thermal water parameters corresponds sufficiently precisely to the real data.

#### 3.1.3.3 Monte-Carlo-approach for power-plant optimization

A large number of technical parameters must be defined for the design of the individual components and their interaction in the ORC. Among other things, the pressure levels before and after the feed

pump, the maximum overheating, the size of the recuperator, the composition of the working medium and the injection temperature of the thermal water must be defined. These parameters result in overriding properties of the ORC, such as pump and turbine performance, working medium mass flow and heat transfer surfaces. Almost all process parameters of the ORC have not only technical but also economic consequences, i.e. they influence not only the performance of the system but also its price. Therefore, the selection of an ORC system that is technically and economically optimal is a complex task and the exact numerical solution requires a great deal of effort. This problem is addressed in the present study with the help of the Monte Carlo method. The Monte Carlo method is a powerful tool for solving problems where analytical approaches fail or can only be implemented with considerable effort. It is used for quantitative analysis in various scientific disciplines. The basis for this is a large number of similar random experiments. The aim is the analysis of the system behavior in random experiments. From the results obtained, conclusions can be drawn about the real system behavior. (Dunn & Shultis, 2011). If the method is used in a simulation, the term Monte Carlo simulation is used (Dunn & Shultis, 2011).

To implement this approach, the pressure levels at state points 1 and 2, the temperature at state point 6, the recuperated internal energy between state points 7 and 8 and the outlet temperature of the thermal water from the evaporator are defined as degrees of freedom in the present model. These are varied randomly and independently of each other, so that any plant design with all resulting variables is created. Table 6 provides an overview of the different degrees of freedom of the Monte Carlo approach with their upper and lower limits. All parameters are equally distributed within the assigned upper and lower limits.

Table 6: Overview Monte-Carlo-parameters power plant

| **Parameter** | **Upper limit** | **Lower limit** |
|---|---|---|
| $p_1$ | $0{,}5p_2$ | $p(X = 0, T_{air,in})$ |
| $p_1$ | If $T_{TW,in} - \Delta T^{min} < T_{crit} - \Delta T^{min}$ $p(X = 1, T = T_{TW,in} - \Delta T^{min})$ Else $p(X = 1, T = T_{crit} - \Delta T^{min})$ | $1{,}5p_1$ |
| $T_6$ | $T_{TW,in} - \Delta T^{min}$ | $T(X = 1, p_2 * \zeta_{evap} * \zeta_{cond})$ |
| $\Delta h_{7,8}$ | Pinch-analysis | $0kJ/kg$ |
| $T_{TW,out}$ | $T_{TW,in} - 50K$ | $55°C$ |

Altogether, the generation of many different concrete design options replaces a numerical optimization of the ORC. If enough different possibilities are considered, a design, which is sufficiently close to the actual optimal solution, can be assumed. An exact determination of the necessary number of iterations to determine the optimal power plant design with regard to the electricity generation costs is not possible. Methods such as those described by (Driels & Shin, 2004) refer to the determination of the number of iterations necessary for the mean value of the results of a Monte Carlo simulation to be sufficiently close to the mean value of the same Monte Carlo simulation with an infinite number of repetitions. In the present case, however, no expected value for the electricity production costs is sought, but rather the technically and economically optimal power plant design. Therefore, the number of power plant designs evaluated in the overall model is limited upwards by the following considerations: The Monte-Carlo method is used for power plant designs in order to save iterations and thus computing time compared to a heuristic optimization as in (Welter, Technisch-ökonomische Analyse der Energiegewinnung aus Tiefengeothermie in Deutschland, 2018). In addition

to the application for the DESTRESS research project, the model is also intended for estimating electricity production costs in early phases of project development in the corporate environment and must therefore deliver results in a limited time. For this reason, the number of evaluated power plant designs is limited to 1000 per site.

## 3.2 Economic model

Figure 12 shows a schematic representation of the overall model for the technical-economic evaluation of a geothermal energy utilisation plant, considering uncertainties and risk factors, as set out in the present study.

The technical part of the model, which is divided into power plant, thermal water circuit (TW circuit) and reservoir, is shown in the middle. The thermal water parameters are passed on the interfaces between the individual technical models, so that the flow of geothermal fluid from the reservoir through the production well into the power plant and subsequently through the injection well back into the reservoir is mapped in the model. Within the technical sub-models, all system properties required for economic evaluation are determined and passed on to the corresponding economic sub-models. These can be found in the right part of Figure 12. In the power plant model, for example, the heat exchanger surfaces and component power are relevant for cost estimation. Within the economic sub-models, the investment and operating costs of the power plant, thermal water cycle and reservoir are determined. With the help of these costs and the technical properties of the system, the "Levelized costs of electricity" (LCOE) are calculated and used for the technical-economic evaluation of the overall system. Additionally, other KPI well known from financial mathematics are calculated within the techno-economic model (see chapter 4.2). The LCOE are calculated according to context (28). The calculation of the net electricity production costs enables an economic comparison of different types of electricity generation. (IEA; NEA; OECD, 2015)

$$LCOE_{net} = \frac{I_0 + Z + \sum_t^{tmax} (1+i)^{-t} * (C_{Operation} - R)}{\sum_t^{tmax} (1+i)^{-t} * \tau v * P_{el,net}} \quad (28)$$

$I_0$ stands for the investment costs and $Z$ for the interest during the construction period. Due to the time lag between the start of the construction and the commissioning of the power plant, the investment costs are incurred before the start of the period under consideration ($t_{max}$). They are referenced to the beginning of the period under consideration by means of the construction period interest rate $Z$. The calculatory interest rate $i$ of 7%, including income taxes, is estimated using the method of (Konstantin, 2017). For a detailed description of this procedure, please see (Welter, Technisch-ökonomische Analyse der Energiegewinnung aus Tiefengeothermie in Deutschland, 2018). $C_{Operation}$ describes the operating costs in relation to an operating year. $R$ stands for heat revenue from cogeneration. Furthermore, $v$ symbolizes the annual full load hours for power generation at the power plant and $P_{el,net}$ its net electrical output, meaning the power fed into the grid minus its own consumption. The cost items in equation (31) consist of the costs of the three components of the overall system. Revenues only accrue in the power plant part:

$$I_0 = I_0^{Powerplant} + I_0^{TWcircuit} + I_0^{Reservoir} \quad (29)$$

$$Z = Z^{Powerplant} + Z^{TWcircuit} + Z^{Reservoir} \quad (30)$$

$$C_{Operation} = C_{Operation}^{Powerplant} + C_{Operation}^{TWcircuit} + C_{Operation}^{Reservoir} \quad (31)$$

$$R = R_{Powerplant} \quad (32)$$

The basis for the calculation cost items for each technical sub-model is explained in Section 3.2.2.1 for the power plant, in section 3.2.2.2 for the thermal water cycle and in Section 3.2.2.1 for the reservoir. The calculated annual costs and revenues are modified over the period under consideration with the aid of nationally resolved producer price indices (EUROSTAT, 2018a) or consumer price indices (EUROSTAT, 2018b) in order to consider price increases over the period under consideration.

Particularly for systems with fixed electricity remuneration, it may be more economical to purchase the electricity required for pumps and other consumers instead of producing it yourself. Therefore, in addition to the net LCOE, the gross LCOE are also calculated according to equation (33).

$$LCOE_{gross} = \frac{I_0 + Z + \sum_t^{tmax}(1+i)^{-t} * (C_{Operation} + C_{Electricity} - R)}{\sum_t^{tmax}(1+i)^{-t} * \tau v * P_{el,gross}} \quad (33)$$

For this purpose, the costs for the purchased electricity ($C_{Electricity}$) are considered in the electricity meter and all costs are referred to the gross electrical output $P_{el,gross}$.

For pure heat generation, the "Levelized costs of heat" (LCOH) are calculated instead of LCOE. As in the case of gross electricity generation cost, electricity must be purchased for the consumers (pumps and condenser fans) in the case of pure heat generation. Since no own demand for heat of the power plant is considered, the distinction between net and gross LCOH is omitted.

$$LCOH = \frac{I_0 + Z + \sum_t^{tmax}(1+i)^{-t} * (C_{Operation} + C_{Electricity} - R)}{\sum_t^{tmax}(1+i)^{-t} * \tau v * \dot{Q}} \quad (34)$$

$V$ stands here for the full load hours regarding the heat generation of the power plant.

### 3.2.1 Module costing approach

The investment costs are calculated using the module costing technique (MCT), which was originally developed for estimating the costs of chemical plants (Turton, Bailie, Whiting, Shaeiwitz, & Bhattacharyya, 2013). The method is also widely used for energy plants, such as ORC plants in (Welter, Technisch-ökonomische Analyse der Energiegewinnung aus Tiefengeothermie in Deutschland, 2018), (Schlagermann, 2014), (Astolfi, 2014), (Collings, Yu, & Wang, 2016 ), (Wang, Li, Li, & Wu, 2015) and (Toffolo, Lazzaretto, Manente, & Paci, 2014). According to (AACE, 2016), such estimates differ from real costs by about -20% to +30%. The methodology is explained in Section 3.2.2.1 page 53 following (Toffolo, Lazzaretto, Manente, & Paci, 2014) and (Turton, Bailie, Whiting, Shaeiwitz, & Bhattacharyya, 2013).

### 3.2.2 Cost engineering approaches for the technical sub-models

In the following the different cost engineering approaches for the single sub-models are explained. As far as possible, the above explained module costing approach is used. If no data from literature was available or could not be deducted from existing plants, other approaches had to be found. Besides the main technical models "Power/heat plant", "Thermal water circuit" and "Reservoir" a special focus is put on the approaches for stimulation costs and the line shaft pump, as these correlations didn't receive much attention in techno-economic modelling for geothermal energy systems, yet.

#### 3.2.2.1 Power/Heat plant

In this section, the various cost items relating to the power plant and the method of calculating the investment costs for ORC and CHP are presented together with the assumptions made. Since a power plant that is thermodynamically optimally tailored to the geothermal energy source is not necessarily the most economical solution for the power plant operator, it is essential to consider the technology and economy of the power plant together. For example, the integration of a recuperator for heat

transfer from the hot working fluid before the condenser to the cold working fluid before the preheater is always advantageous from a purely thermodynamic point of view. In practice, however, the price of the recuperator is an important decision factor. If the heat recoverable by the recuperator is more expensive than the promotion of geothermal energy, no investment decision is made in favour of a recuperator. Table 7 provides an overview of all cost items relating to the power plant, including categorization according to equations (28) to (32). The individual cost items are described in the following with the associated cost functions.

Table 7: Overview of the power plant costs (MK: IDC=Interest during construction; STHE=shell-and-tube heat exchanger)

| | Cost item | Category | Cost function | $t_z$ (IDC) | Operating lifetime |
|---|---|---|---|---|---|
| **I** | Property | $I_0$ | $f(location)$ | 3.5 years | $t_{Operation}$ |
| **II** | ORC | $I_0$ | | 0.5 years | |
| a | Turbine and generator | | $f(power)$ | | 25 years |
| b | Feed pump | | $f(power)$ | | 10 years |
| c | STHE (preheating, evaporation) | | $f(area)$ | | 10 years |
| d | Air condenser | | $f(area)$ | | 25 years |
| e | Fan | | $f(power)$ | | 25 years |
| **III** | CHP | $I_0$ | | 0.5 years | |
| a | STHE | | $f(area)$ | | 10 years |
| b | Boiler | | $f(power)$ | | 25 years |
| **IV** | Preliminary planning | $I_0$ | | 5 years | $t_{Operation}$ |
| a | Project management | | $0.06 * (C_I + C_{II} + C_{III})$ | | |
| b | Approval | | 50,000 EUR | | |
| c | Energy concept | | 100,000 EUR | | |
| **V** | Technical planning | $I_0$ | $0.015 * (C_{II} + C_{III})$ | 2 years | $t_{Operation}$ |
| **VI** | Assembly insurance | $I_0$ | $0.002 * (C_{II} + C_{III})$ | 2 years | $t_{Operation}$ |
| **VII** | Maintenance | $C_{Operation}$ | $0.03 * (C_{II} + C_{III})$ | - | - |
| **VIII** | Staff | $C_{Operation}$ | $130{,}000\ to\ 180{,}000\ EUR$ | - | - |
| **IX** | Insurance | $C_{Operation}$ | $0.006 * (C_{II} + C_{III})$ | - | - |
| **X** | Other | $C_{Operation}$ | $0.01 * (C_{II} + C_{III})$ | - | - |
| XI | Heat revenue | $R$ | $f(location)$ | - | - |

For all investment costs, in addition to the costs themselves, the approximate time of completion $t_z$ is also shown in Table 7, which is necessary for the calculation of the accrued interest $Z$ for the construction period. The interest during construction (IDC) from equation (30) is determined with relation (35) (Konstantin, Praxisbuch Energiewirtschaft, 2017).

$$Z = I_0 * [(1+i)^{t_z} - 1] \quad (35)$$

In contrast to the electricity production costs for $i$, the real imputed interest rate without income taxes is used, which amounts to 4.15% in the present study (Welter, Technisch-ökonomische Analyse der Energiegewinnung aus Tiefengeothermie in Deutschland, 2018). The IDC describes the costs arising from the fact that certain investments are made before the start of plant operation. During this period, the money could have been invested differently and would have yielded interest. This loss of interest forms the IDC and thus an additional cost item. Furthermore, the operational lifetime is shown in Table 7. If the operational lifetime of a component ends before the operating time $t_{operation}$ is reached, the module in question must be replaced and the allocated investment costs are incurred again.

In order to validate the economic part of the power plant model, confidential data on the investment costs of the ORC power plant at Soultz-sous-Forêts (see chapter 3.1.3.2) are used (EnBW, 2015). The present model underestimates the actual costs incurred by less than 10% and thus lies within the expected uncertainty interval of -20% to +30% according to (AACE, 2016). Figure 28 shows the component costs modelled as shares of the total price.

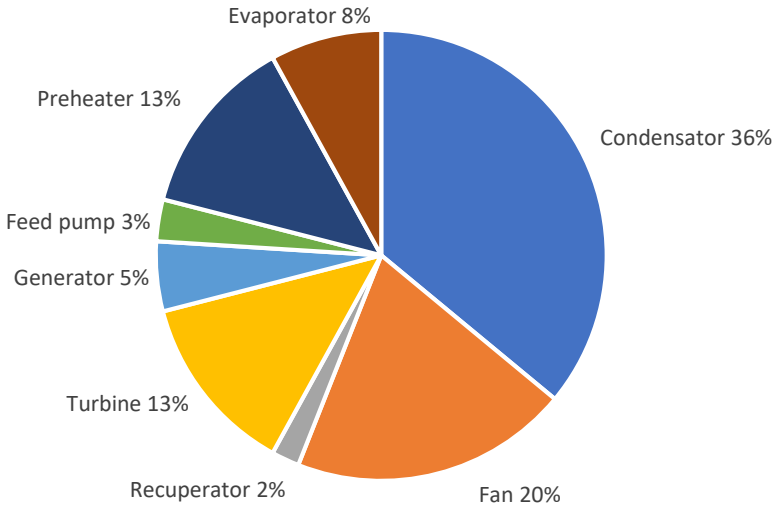


Figure 28: Modelled component costs of Soultz-sous-Forêts

The power plant-related costs can be divided into investment and operating costs or revenues, as shown in Table 7. The cost functions and assumptions assigned to the respective cost positions are explained below. First, the module costing approach according to the methodology of (Turton, Bailie, Whiting, Shaeiwitz, & Bhattacharyya, 2013) is presented, which is used to determine the investment costs of the ORC.

### Module cost calculation according to (Turton, Bailie, Whiting, Shaeiwitz, & Bhattacharyya, 2013):

The investment costs $I_0$ of the ORC are approximated by using the methodology according to (Turton, Bailie, Whiting, Shaeiwitz, & Bhattacharyya, 2013). All direct and indirect costs are referred to the costs of the individual modules for "basic conditions". "Basic conditions" describe the use of a component

made of standard material (usually steel) and at a working pressure equal to the ambient pressure. The cost functions have the form:

$$log_{10}(C_P^0) = K_1 + K_2\, log_{10}(\kappa) + K_3(log_{10}(\kappa))^2 \quad (36)$$

Here, $\kappa$ is the power or area parameter of the individual module and $K_1$, $K_2$ and $K_3$ are component-specific constants. Deviations from the basic conditions are considered by the factors $F_p$ and $F_M$, which depend on the system pressure or construction material. The pressure factor is determined according to equation (37).

$$log_{10}(F_p) = C_1 + C_2\, log_{10}(p) + C_3(log_{10}(p))^2 \quad (37)$$

$C_1$, $C_2$ and $C_3$ are module-specific constants, too. The component costs ("bare module cost") result from relationship (38).

$$C_{BM} = C_p^0 * F_{BM} = C_p^0 * \left(B_1 + B_2 * F_p * F_m\right) \quad (38)$$

$B_1$ and $B_2$ are component-specific weighting factors for the pressure and material factors. $F_{BM}$ is the total correction factor to determine the module costs.

### Investment costs $I_0$:

For the feed pump, preheater, evaporator, condenser, condenser fan and generator, cost functions of the form described above are used. For the turbine, however, an expression by (Astolfi, 2014) is used for a two-stage turbine where 18% of its total mechanical power is generated by the second stage. In this context, the term stage refers to the number of rings of the rotor blades and associated guide vanes of a turbine. A two-stage turbine thus has two rotors and two guide vanes each. In this study, the turbine is also considered simplified as a two-stage turbine of the same design. In practice, turbines used in ORC can also have more than two or only one stage (Astolfi, 2014).

$$C_{BM} = K_1 \kappa^{n1} + K_2 * 2^{n_2} \quad (39)$$

$K_1$, $K_2$, $n_1$ and $n_2$ are obtained by (Astolfi, 2014) by the regression of the curve to known design data of various turbines. $\kappa$ is the power of the turbine. Please consult (Astolfi, 2014) for more detailed information. According to (Astolfi, 2014), the costs of the recuperator are also determined not with the help of the MCT but with an exponential expression that is derived from the manufacturer's data:

$$C_{BM}^{Rec} = 450000 * \left(\frac{\kappa}{1000}\right)^{0,7} \quad (40)$$

For the recuperator $\kappa$ corresponds to the recuperator area in $\mathrm{m}^2$.

For the remaining components, module-specific constants modified from (Turton, Bailie, Whiting, Shaeiwitz, & Bhattacharyya, 2013) are used in the present work ( (Astolfi, 2014); (Wang, Li, Li, & Wu, 2015)). Table 1 provides an overview of the coefficients used for the ORC. The coefficients for all other components whose costs are determined with the help of the MCT are listed in Table 10.

Table 8: Coefficients for module cost calculation of the ORC (Sources: (a): (Astolfi, 2014); (b) (Wang, Li, Li, & Wu, 2015); (c) centrifugal pump, steel; (d) steel casing, steel pipes; (e) steel pipes)

| | Pump (a) | Preheater (a) | Evaporator (a) | Condenser (a) | Fan (b) | Turbine (a) |
|---|---|---|---|---|---|---|
| $K_1$ | 3.985 | 5.105 | 5.105 | 4.151 | 3.176 | 240,000 |
| $K_2$ | 0.000294 | -0.374 | -0.374 | 0.234 | -0.137 | 61,750 |
| $K_3$ | 0.143 | 0.190 | 0.190 | 0.0497 | 0.341 | |

| | | | | | | |
|---|---|---|---|---|---|---|
| $\boldsymbol{n_1}$ | | | | | | 0.99 |
| $\boldsymbol{n_2}$ | | | | | | 1.06 |
| $\boldsymbol{\kappa}$ | $P[\mathrm{kW}]$ | $A[\mathrm{m}^2]$ | $A[\mathrm{m}^2]$ | $A[\mathrm{m}^2]$ | $\dot{m}_{Air}\left[\frac{\mathrm{kg}}{\mathrm{s}}\right]$ | $P[\mathrm{kW}]$ |
| $\boldsymbol{C_1}$ | -3.870 | -3.351 | -3.351 | | | |
| $\boldsymbol{C_2}$ | 2.953 | 1.915 | 1.915 | | | |
| $\boldsymbol{C_3}$ | -0.762 | -0.281 | -0.281 | | | |
| $\boldsymbol{B_1}$ | 1.89 | 1.63 | 1.63 | 0.96 | | |
| $\boldsymbol{B_2}$ | 1.35 | 1.66 | 1.66 | 1.21 | | |
| $\boldsymbol{F_m}$ | 1.5 (c) | 1 (d) | 1 (d) | 1 (e) | | |
| $\boldsymbol{F_{BM}}$ | | | | | 1 | |

For the components of the cogeneration or pure heat extraction, an impact factor according to equation (42) is considered. The preheaters and evaporators are considered separately in the cost estimation, since the heat exchangers in practice can often also be realized as two components. Thus, unwanted economies of scale are avoided through joint consideration.

The costs of the heat exchangers for the decoupling of heat are calculated analogously to the approach for preheater and evaporator. To cover the heat requirement, which is not covered by the geothermal system, a peak-load boiler is used. Its costs are calculated according to equation (41). (Turton, Bailie, Whiting, Shaeiwitz, & Bhattacharyya, 2013).

$$C_{BM}^{Boiler} = C_p^0 * F_{BM} * F_p * F_T \text{ with } F_{BM} = 2 \text{ and } F_T = 1 \quad (41)$$

The pressure factor $F_p$ is formed for the boiler using the coefficients $C_1$ = -0.01633, $C_2$ = 0.056875 and $C_3$ = -0.00876 as described in equation (37). $C_p^0$ is calculated with the constants $K_1$ = 2.0829, $K_2$ = 0.9074 and $K_3$ = -0.0243 used in equation (36). (Turton, Bailie, Whiting, Shaeiwitz, & Bhattacharyya, 2013)

The benchmark for the cost functions of (Astolfi, 2014) is US dollars in 2013 ($\mathrm{USD}_{2013}$). Therefore, the calculated costs are converted, using the chemical engineering plant cost index (CEPCI) as proposed by (Turton, Bailie, Whiting, Shaeiwitz, & Bhattacharyya, 2013) to the base year 2016, which is selected in this paper. The same applies to the cost function for the condenser fan according to (Wang, Li, Li, & Wu, 2015) with reference year 2009 and for the cost correlation of the boiler according to (Turton, Bailie, Whiting, Shaeiwitz, & Bhattacharyya, 2013) with the reference year 2001. The calculated costs are then expressed in $\mathrm{USD}_{2016}$, converted into euros at the exchange rate given in (BMF, 2016), so that the following amounts can be reported as Unit $\mathrm{EUR}_{2016}$.

According to (Turton, Bailie, Whiting, Shaeiwitz, & Bhattacharyya, 2013), in order to deduce the total costs for the integration of the components from the pure component costs, a surcharge of 18% for uncertainty, planning and handling is taken into account for small to medium-sized changes to an existing plant (Welter, Technisch-ökonomische Analyse der Energiegewinnung aus Tiefengeothermie in Deutschland, 2018). This mark-up factor is used for replacement investments at the end of the service life of a component. In the case of a completely new construction, a further 50% of the component costs are added (Turton, Bailie, Whiting, Shaeiwitz, & Bhattacharyya, 2013), so that the total costs of the Plant can be estimated as the sum of the module costs modified with the total mark-up factor, using equation (42).

$$C_{PP,ges} = 1{,}68 * \sum_i C_{BM,i} \quad (42)$$

As the ORC plant in the present model is taken over by the supplier on a turnkey basis in analogy to projects already realised, the exact costs for uncertainty, planning, handling, land development and periphery for the power plant are unknown (Welter, Technisch-ökonomische Analyse der Energiegewinnung aus Tiefengeothermie in Deutschland, 2018) and are taken into account for the preliminary estimate of the purchase price as shown above.

The investment costs for the property of the power plant (point I in Table 7) are calculated according to the empirical equation (43), which is derived from the findings of (Welter, Technisch-ökonomische Analyse der Energiegewinnung aus Tiefengeothermie in Deutschland, 2018) and (Schlagermann, 2014).

$$C_{Property} = \left[-3 * 10^{-5}\left(P_{el} + \frac{\dot{Q}_{max}}{20}\right)^2 + 2{,}4 * \left(P_{el} + \frac{\dot{Q}_{max}}{20}\right) - 90\right] * C_{Surface} * \frac{PLI}{PLI_{ref}} \qquad (43)$$

The electrical and thermal power of the power plant is to be entered in kilowatts. Depending on the location, the price is modified with the corresponding price level indices (PLI) for commercial buildings (EUROSTAT, 2018a). PLIs for land prices are not available. Overall, land costs can only be approximated with great uncertainty due to the strong local price volatility.

Point IV of Table 7 describes the costs for the preliminary planning of the geothermal plant. The power plant related costs for the project management in the planning phase are considered with 6% of the sum of costs I, II and III. A flat rate of EUR 50,000 respectively EUR 100,000 is assumed for approval and energy concept.

Under cost item V, the technical planning is estimated at 1.5% of costs II and III. Under cost item VI, the assembly insurance is estimated at about 0.2% of the same costs.

### Operating costs $\boldsymbol{C_{Operation}}$ and revenues $\boldsymbol{R}$:

The operating costs $\boldsymbol{C_{Operation}}$ operation from Table 7, in contrast to the investment costs, are incurred continuously during operation and are reported as annual costs. They are thus influenced by price increases on the one hand and by interest rate effects on the other. The latter are considered according to equation (28) using the present value factor $(1 + i)^t$. Price increases are included using the arithmetic mean of consumer price indices between 2010 and 2017 (EUROSTAT, 2018a). The average value is derived from country-specific data depending on the location of the installation under study.

According to (Welter, Technisch-ökonomische Analyse der Energiegewinnung aus Tiefengeothermie in Deutschland, 2018), the operating costs of the geothermal power plant are divided into the following items: insurance costs against electronic and machine breakdowns accounting for 0.6% of the investment costs, maintenance and repair costs amounting to 3% of the investment costs, and costs for other operating resources accounting for 1% of the investment costs. Business interruption insurance accounts for 0.6% of the annual income. In addition, personnel costs are allocated to the power plant at a flat rate of EUR 130,000 per year for plants with a thermal output of less than 30 MW. The thermal capacity refers to the thermal energy extracted from the thermal water stream. Personnel costs of around EUR 180,000 are assumed for larger plants. These estimates are based on the values used in (Welter, Technisch-ökonomische Analyse der Energiegewinnung aus Tiefengeothermie in Deutschland, 2018).

Cogeneration of heat and power generates both electricity and heat. The latter is considered in the schematic of electricity production costs according to equations (28) and (32) respectively. The heat

revenues $R$ result from the amount of heat decoupled over one year multiplied by the heat-related full load hours of the power plant.

#### 3.2.2.2 Thermal water circuit

The module costing method (Turton, Bailie, Whiting, Shaeiwitz, & Bhattacharyya, 2013) (see page 54) is not used to calculate the price of the components of the thermal water circuit, due to the lack of suitable correlations. Instead, correlations according to (Welter, Technisch-ökonomische Analyse der Energiegewinnung aus Tiefengeothermie in Deutschland, 2018) and (Schlagermann, 2014) are used to determine the various cost items. Table 9 provides an overview of the investment and operating costs related to the thermal water circuit. The individual calculation regulations are explained in more detail in the following. In particular, the investment or replacement costs for the pumps (cost item II) represent a considerable cost factor due to the short service life of only about one year in the case of ESP or about four years in the case of LSP (Schröder & Schneider, 2014) compared with, for example, the ORC components.

Table 9: Overview of the costs of the thermal water cycle (MK: IDC=interest during construction; ESP=electrical submersible pump; LSP=line shaft pump)

| | Cost item | Category | Cost function | $t_z$ (IDC) | Operating lifetime |
|---|---|---|---|---|---|
| **I** | Property | $I_0$ | $f(location)$ | 3.5 years | $t_{Operation}$ |
| **II** | Pumps | $I_0$ | | 1 years | ESP: 1 year<br>LSP: 4 years |
| a | Production pump | | $f(power)$ | | |
| b | Riser pipe | | $f(length)$ | | |
| c | Power cable | | $f(length)$ | | |
| d | Pump installation | | $f(z_{Pump})$ | | |
| e | Injection pump | | $f(power)$ | | |
| **III** | Filter / pressure vessel | $I_0$ | $f(volume)$ | 1.5 years | $t_{Operation}$ |
| **IV** | Preliminary planning | $I_0$ | | 5 years | $t_{Operation}$ |
| a | Project management | | $0.06 * (C_I + C_{III} + C_{IV})$ | | |
| b | Approval | | 100,000 EUR | | $t_{Operation}$ |
| **V** | Technical planning | $I_0$ | $0.015 * (C_{III} + C_{IV})$ | 2 years | $t_{Operation}$ |
| **VI** | Insurance | $I_0$ | | 3.5 years | $t_{Operation}$ |
| a | Drilling risk | | $0.035 * (C_{III} + C_{IV})$ | | |
| b | Lost-in-hole | | 280,000 EUR | | |
| c | Liability | | 100,000 EUR | | |
| **VII** | Maintenance | $C_{Operation}$ | $0.03 * (C_{II} + C_{III})$ | - | - |
| **VIII** | Insurance | $C_{Operation}$ | $0.006 * (C_{II} + C_{III})$ | - | - |
| IX | Other | $C_{Operation}$ | $0.01 * (C_{II} + C_{III})$ | - | - |

The costs of the thermal water circuit are divided into investment and operating costs. The associated cost functions and assumptions are discussed in the following section.

### Investment costs $I_0$:

Cost item I is the cost of the property from which the wells to exploit the reservoir will be drilled. These are calculated in relation to (44).

$$C_{property} = n_{Drillsites} * A_{Drillsite} * C_{Area} * \frac{PLI}{PLI_{ref}} \quad (44)$$

For the number of drilling sites $n_{Drillsites}$, the value 2 is assumed as a lump sum in this study, since only doublets are considered. The area required per drilling site $A_{Drillsite}$ is estimated at 6,000 $\mathrm{m}^2$. Furthermore, an average value of 60 $\frac{\mathrm{EUR}}{\mathrm{m}^2}$ is used for the property price $C_{Area}$ (Seitz, 2015). Depending on the location, the price is modified with the corresponding price level indices (PLI) for commercial buildings as in the cost function of the land for the power plant (EUROSTAT, 2018c).

According to (Schlagermann, 2014), the costs for the ESP production pump under point II of Table 9 are determined in kilowatts depending on its hydraulic power $P_{\mathrm{hyd}}$ with the aid of empirical correlation (45).

$$C_{Productionpump} = 14{,}000 * P_{hyd}^{0{,}68} \text{ with } P_{hyd} = \dot{V} * \Delta p \quad (45)$$

The hydraulic power is calculated as the product of the volume flow and the pressure difference of the fluid conveyed.

In addition, there are the costs for the riser pipe, the pipe section between the earth's surface and the pump. These result from the product of the installation depth of the pump $z_{Pump}$ (50 m below the static water level) and the length-specific costs of about 80 $\frac{\mathrm{EUR}}{\mathrm{m}}$ (Schlagermann, 2014). Furthermore, the costs for the power cable of an ESP are considered if such a cable is used:

$$C_{Powercable} = z_{Pump} * (80 + 0.02 * P_{Hyd}) \quad (46)$$

The cost of installing the pump is shown in Equation (47).

$$C_{Pumpinstallation} = 10{,}000 + 5{,}000 * \left(4 + \frac{z_{Pump}}{250}\right) \quad (47)$$

With the help of the MCT according to (Turton, Bailie, Whiting, Shaeiwitz, & Bhattacharyya, 2013), the investment costs of the injection pump are determined under cost item II. Table 10 shows the coefficients used. However, in the first step the component costs $C_{BM}$ are estimated according to equation (48).

$$C_{BM}^{Injectionpump} = 1{,}500 * \kappa^{0.48} \quad (48)$$

The filters respectively the pressure vessels are listed under cost item III. A total of four of these are used. Their price is estimated with the help of the MCT according to (Turton, Bailie, Whiting, Shaeiwitz, & Bhattacharyya, 2013). The coefficients used are listed in Table 10. The pressure factor for the filters respectively for the pressure vessels is calculated using equation (49) (Turton, Bailie, Whiting, Shaeiwitz, & Bhattacharyya, 2013).

$$F_p = \left(\frac{(p+1)*d}{2*[850-0.6*(p+1)]} + 0.00315\right) * \frac{1}{0.0063} \quad (49)$$

Where d stands for the diameter and p for the pressure of the components. Their volume is estimated using the continuity equation and the assumption of a flow velocity of 0.15 $\frac{\mathrm{m}}{\mathrm{s}}$. The volume of the components is then calculated from the pressure of the components.

Table 10: Coefficients for module cost calculation of the thermal water circuit ((a) (Turton, Bailie, Whiting, Shaeiwitz, & Bhattacharyya, 2013); $\mathrm{USD}_{2001}$)

| | Injection pump (a) | Pressure vessel (a) |
|---|---|---|
| $K_1$ | | 3.4974 |
| $K_2$ | | 0.4485 |
| $K_3$ | | 0.1074 |
| $\kappa$ | $P$ [kW] | $V$ [$\mathrm{m}^3$] |
| $C_1$ | 0.3935 | |
| $C_2$ | 0.3957 | |
| $C_3$ | -0.00226 | |
| $B_1$ | 2.25 | 2.25 |
| $B_2$ | 1.82 | 1.82 |
| $F_m$ | 1.77 (c) | 1.77 |

Either all other investment costs under points IV to VI are approximated with lump sums or with lump sums depending on the investment costs I, II and III (see Table 9).

Operating costs $C_{Operation}$:

In relation to the thermal water circuit, the costs for maintenance, insurance and other operating costs are considered as operating costs. All cost items are calculated pro rata to the investment costs. The costs for maintenance amount to 3% of the cost items II and III from Table 9. 0.6% of the same investment costs are due for insurance and a further percentage for other operating costs (see Table 9).

### 3.2.2.3 Reservoir

All costs associated with the reservoir are listed in Table 11. As with the other sub-models, the various cost items in the reservoir are broken down into investment and operating costs. In the following, the individual cost items with the associated estimates respectively cost functions from Table 11 are explained. The costs are estimated on the basis of (Welter, Technisch-ökonomische Analyse der Energiegewinnung aus Tiefengeothermie in Deutschland, 2018) and (Schlagermann, 2014), whose cost information is largely derived from expert knowledge in the geothermal sector.

Table 11: Overview of reservoir costs (MK: IDC=interest during construction)

| | **Cost item** | **Category** | **Cost function** | $t_Z$ **(IDC)** | **Operating lifetime** |
|---|---|---|---|---|---|
| **I** | Exploration | $I_0$ | | 4 years | $t_{Operation}$ |
| **a** | Purchase / analysis of existing data | | 180,000 EUR | | |
| **b** | 3D seismics | | 25,000 $\frac{\mathrm{EUR}}{\mathrm{km}^2}$ | | |
| **II** | Exploitation | $I_0$ | | 2 years | $t_{Operation}$ |
| **a** | Drilling costs | | $f(power)$ | | |
| **b** | Exploitation drilling site | | 250,000 EUR | | |
| **c** | Setup drilling place | | 250,000 EUR | | |

| | | | | | |
|---|---|---|---|---|---|
| **d** | Moving drilling equipment | | 60,000 EUR | | |
| **e** | Recultivation drilling site | | 50,000 EUR | | |
| **f** | Stimulation | | 1,100,000 EUR | | |
| **g** | Borehole measurements | | 65 $\frac{\text{EUR}}{\text{m}}$ | | |
| **h** | Circulation test | | 350,000 EUR | | |
| **i** | Production test | | 150,000 EUR | | |
| **III** | Project management | | $0.06 * (C_I + C_{II})$ | | |
| **IV** | Technical planning | $I_0$ | $0.015 * (C_{IIa} + C_{IIe})$ | 2.5 years | $t_{Operation}$ |
| **V** | Seismic monitoring | $I_0$ | 150,000 EUR | 3.5 years | $t_{Operation}$ |
| **VI** | Public relations work | $I_0$ | 100,000 EUR (until start of operation annually) | 4 years | $t_{Operation}$ |
| **VII** | Seismic monitoring | $C_{Operation}$ | 40,000 EUR | - | - |
| **VIII** | Maintenance | $C_{Operation}$ | $0.005 * (C_{IIa} + C_V)$ | - | - |
| **IX** | Liability insurance | $C_{Operation}$ | 90,000 EUR | - | - |
| X | Public relations work | $C_{Operation}$ | 40,000 EUR | - | - |

### Investment costs $I_0$:

Most of the investment costs related to the reservoir are estimated using lump sum costs or as shares of other cost items ( (Schlagermann, 2014); (Welter, Technisch-ökonomische Analyse der Energiegewinnung aus Tiefengeothermie in Deutschland, 2018)). The costs for the exploration of the reservoir (point I) are composed of a lump sum of 180,000 EUR and the costs for the construction of a 3D seismic survey of about 25,000 $\frac{\text{EUR}}{\text{m}^2}$. According to (Welter, Technisch-ökonomische Analyse der Energiegewinnung aus Tiefengeothermie in Deutschland, 2018), the seismic area to be covered in square kilometres is approximated with the help of the (50) context.

$$A_{Seismic} = \left(z_{Drilling}^{max} + 4 + \Delta x\right) * (\Delta x + 4) \quad (50)$$

$\Delta x$ symbolizes the distance between the production and injection wells. This distance is estimated with the distance at the deepest point of the borehole, the depth of which is determined by $z_{Drilling}^{max}$.

Under cost item II, which covers the costs for the exploitation of the reservoir, mainly lump sum estimates according to (Welter, Technisch-ökonomische Analyse der Energiegewinnung aus Tiefengeothermie in Deutschland, 2018) are used. Only the measurements of the borehole (cost item $\text{II}_\text{g}$) are related to the length of the two boreholes and are given as 65 $\frac{\text{EUR}}{\text{m}}$ . In addition, the drilling costs, which constitute a decisive cost item, are estimated in more detail. Equation (51) describes the cost correlation used.

$$C_{Drilling} = 1.1 * 10^6 * exp(5 * 10^{-4} * s) \quad (51)$$

Where $s$ stands for the drilled section (MD). For illustration, please refer to Figure 19.

Project management (point III) and technical planning (point IV) are estimated at 6% of cost items I and II and 1.5% of cost items IIa and IIe respectively. Seismic monitoring under cost item V requires investment costs of approximately EUR 150,000. For public relations work, supporting public acceptance of the geothermal project, annual expenditure of EUR 100,000 is to be expected from 4 years before the start of production.

#### Operating costs $C_{Operation}$:

In addition to investment costs, operating costs are incurred for the seismic monitoring of the reservoir. These costs are estimated at around EUR 40,000 (Point VII in Table 11). Furthermore, the boreholes and all equipment must be kept operational. Therefore, the maintenance costs are about 0.5% of the sum of the investment costs IIa and V per year. The costs of a liability insurance are about 90,000 EUR per year. Eventually, the public relations work must be continued during operation. For this purpose, approximately EUR 40,000 per year are required. ( (Welter, Technisch-ökonomische Analyse der Energiegewinnung aus Tiefengeothermie in Deutschland, 2018); (Schlagermann, 2014))

### 3.2.2.4 Costs of soft stimulation measures

Cost functions as presented in chapter 3.2 are normally based on data given by finalized projects. In a retro perspective, often through regression analysis, functions/approaches are developed that can give the historical data points. For the DESTRESS project (Reith, Hehn, Mergner , & Kölbel, 2017) presented cost functions based on the experience of projects in France. Since until the submission date of this report, no soft stimulations measures were conducted in the DESTRESS project, the already presented cost functions must be used.

### 3.2.2.5 Costs of Line shaft pumps

#### Available LSP technology on the market

A downhole geothermal Line Shaft Pump is a vertical centrifugal pump driven by a motor installed on surface through a shaft. Lineshaft vertical pumps were first developed in the early 1900s for pumping shallow water wells mainly for agriculture in Western United States. The very first application of downhole geothermal LSPs was at the world's first binary power plant in East Mesa, California in the late 1970s. Unfortunately, these units were nothing more than simple water well pumps and had failed after a month of operation. Thus, the design of the downhole geothermal LSP has evolved over the years with greater resistance to wear, deeper settings, higher temperatures and greater pump life.

The wide use of LSP in water wells became possible after the development and adaption of an oil lubrication system for LSP. Currently, there are about 190 downhole geothermal LSP in operation in California, Nevada, Utah and Idaho, and very few pumps in the rest of the world (Germany, France, Japan and Mexico). All these pumps are designed by FROST CONSULTING/ITT GOULDS with oil lubricated bronze bearing (Frost, 2010).

In the 1980s the geothermal utilization in Iceland increased with a focus on district heating application with medium enthalpy geothermal resources. Icelandic engineers (FLOWAYS) therefore have developed an alternative to the oil lubricated bronze bearing, based on water lubricated Teflon bearing. By using water, this technology has a lower impact on the environment compared to oil lubrication. Bowl assembly is based on FLOWAYS design, operating at higher speed than ITT GOULDS design. Currently, there is about 100 Downhole geothermal LSP in operation in Iceland and some in other countries. Unfortunately, Icelandic Downhole LSPs are limited to 300 m setting depth, whereas ITT DOULD pumps can be operated up to 735 m depth.

In central European conditions i.e. the Upper Rhine Graben, most downhole production pumps are installed at a depth below 300 m, therefore ITT GOULDS LSP is the only LSP available on the market for such operating conditions. The first oil lubricated downhole geothermal LSP in Europe was put in operation in 2007 in Landau, followed in 2012 by Insheim and in 2016 by Rittershoffen and Soultz-sous-Forêts. Some experiences with Icelandic LSP were carried out at Soultz-sous-Forêts from 2008 to 2012 but with a very limited success (Ravier, Graf, & Villadangos, Operating a lineshaft production pump in a small pump chamber under highly aggressive geothermal fluid conditions: results from the Soultz EGS site, 2015).

### CAPEX

Capital expenditure related to LSP of the geothermal heat plant at Rittershoffen was investigated in detail by ES-Géothermie. CAPEX in euros for such pump installed in Europe was estimated in following formula (52) using the rule of six-tenths. In this formula, CAPEX includes strainer, pump, lubstring, production column, discharge wellhead, wellhead thermal compensator, surface pump supporting, electrical motor, frequency driver, lubrication system and connection, installation preparation, installation at depth and start-up.

$$CAPEX(z, P_{hydro}) = 470000 + 700 \times z + 225000 \times (\frac{P_{hydro}}{450})^{0.67} \quad (52)$$

Where z is the setting depth in meters and $P_{hydro}$ the hydraulic power of the pump in kW.

### OPEX

Electrical consumption is the main operating cost position. After nearly 3 years of operation, overall efficiency of the LSP installed at Rittershoffen, including the electrical motor and surface cables, can be calculated to 70%. Other operating costs are related to oil bearing consumption and maintenance of surface equipment. Annual oil consumption for the lubrication of the bearings is about 40 barrels per year in 2018. The oil injected is dispersed into the cased wellbore, floats on top of the water level and is recovered every four months during a half day of shut down. The oil for lubrication represents an operational expenditure of nearly 16 k€ per year including oil recycling. During geothermal plant shut down every 4 months, motor and lineshaft must be uncoupled and coupled during start-up procedure. Therefore, crane and maintenance operations are required, representing about 6 k€ per shut down over 1 day. The surface mechanical seal must be replaced every two years, which costs about 6 k€ for the spare part. Bearings of the electrical motor also must be replaced every 5 years during a long shut down period. The costs of such an operation sum up to nearly 15 k€. Based on this data, annual OPEX of downhole geothermal LSP can be estimated with formula (53).

$$OPEX(T_{operating}, P_{elec}, P_{hydro}) = \frac{P_{hydro}}{0.7} \times P_{elec} \times T_{operating} + 28000€$$

Where z is the setting depth in meters and $P_{hydro}$ the hydraulic power of the pump in kW.

### Assumptions on operational life in comparison to ESP

Oil lubricated downhole production line shaft pumps have a typical operational life time of 10 to 15 years in a non-hostile environment. Under the conditions faced in central Europe i.e. the Upper Rhine Graben, a minimum service life of 4 years can be achieved, like in Landau (Frost, Case History of the Lineshaft Downhole Geothermal Pump in Ladau, 2013). As a comparison an electrical submersible pump (ESP) was tested at Soultz-sous-Forêts in 2008 and failed after 10 months of operation. ESP manufacturers never published data on the service life of their products under harsh conditions as faced in the Upper Rhine Graben. In contrast, the service life of ESP in the Bavarian area, with lower downhole temperatures of about 140°C, increases to 2-3 years. Based on the experience of different

operators in that area, this seems to be the highest lifetime. According to literature data this is also an average for the Hoteline 550 ESP of Schlumberger (Lobianco & Wardani, 2010).

### 3.2.3 Adaption of the model to different European markets

The adaption of the financial mathematics calculation to the different European countries is done on three levels.

The calculated annual costs and revenues are modified over the period under review using nationally resolved producer price indices (EUROSTAT, 2018a) or consumer price indices (EUROSTAT, 2018b) in order to take price increases into account over the period under review.

Comparative European price level indices (PLI) for the industrial category “machinery and equipment” (EUROSTAT, 2018c) are used to adjust the calculated investment/operation costs to different European markets. The cost functions refer to the European average of the European Union in its current composition (EU28), to which 100% is assigned as an index. For the individual European markets, the respective costs are calculated by multiplying them by the corresponding PLI determined through the choice of the country.

Furthermore, for the calculation of reference heat prices a gas boiler is used. Heat supply with boilers generates fuel costs which are considered by the site-specific gas price for industrial customers (EUROSTAT, 2018d).

# 4 Framing the problem

## 4.1 Framing the problem – clarification of the term

'*Framing the problem*' is the first step in the *Decision & Risk Analysis* business process that companies apply when defining a new project or investment opportunity (see Figure 4 on page 10). '*Framing*' consists of articulating the nature of the opportunity and how to analyse its technical and economic feasibility. It starts by the company's Decision Board's (management team's) recognizing the situation and approving the proposal of further analysing and maturing the opportunity. To this end, they will have to approve spending manpower resources to study the opportunity and report back to management. In principle, resources will only be committed for completing the work until the next step or '*Decision Gate'*, at which time a new decision can be made to pursue the opportunity and commit additional resources.

Typically, the first decision gate (DG1) following the approval of project initiation (DG0) is to approve the '*frame*' of the analysis, i.e. which decision alternatives to compare, which uncertainties to consider, and how to set up the subsequent detailed decision-analytical process. Issues such as which decision criteria to use, which strategic considerations to consider (i.e. alignment with the company portfolio of projects), the decision timeline and decision hierarchy are also reviewed and agreed. Moreover, the analytical tools to be used will have to be agreed, including how to do the final sensitivity analysis, how to re-define the frame following the sensitivity analysis in order to analyse any risk mitigation measures and/or options that can capture the upside value of the project, how to compare the quantified performance predictions associated with the various decision alternatives, and how to include non-quantitative issues such as social acceptance, political risk, etc.

For a first sensitivity analysis of which decision alternatives are to be included in the frame, a qualitative ranking of the alternatives is often made. For example, alternatives 1 - n are scored qualitatively in terms of relative expected benefit (on short-term production / cash, on longer-term performance such as cashflow, NPV and IRR, on HSE, etc.) by assigning i.e. indicative scores (--, -, 0, +, ++, etc.) for the expected impact of an alternative on the given KPI. Also, the risks per decision alternative are to be qualified in this way. This may result in deleting certain alternatives as they score too low compared to their competing alternatives.

After having discussed the main decision alternatives and uncertainties, the framing-step may be formalized in a decision/scenario tree, which will form the basis for further quantitative computations.

## 4.2 KPIs and time-series investigated

For the techno-economic investigation the used key performance indicators (KPI) play an important role. Decision makers usually use multiple KPI for the evaluation of a decision alternatives. The IGEM can provide every technical or economical detail of the simulation starting from the heat exchanging area of the preheater over the temperature loss in the boreholes down to the labour costs during operation. The pure amount of information would overwhelm decision makers, so that the output KPIs are reduced to KPIs often used in energy industry. The used KPIs can roughly be structured in technical, economic and techno-economic KPIs. Below, the main KPI that are used to describe a decision alternative are listed. For further information on the single KPI, please revere to the model description in chapter 3 or the relevant literature on project evaluation.

- Levelized costs of energy (LCOE)
- Internal rate of return (IRR)
- Net present Value (NPV)

- Payback-Time (PBT)
- Net electrical power $P_{el,net}$
- Gross electrical power $P_{el,gross}$
- Thermal power $P_{th}$
- Investment costs

All KPI are calculated dynamically. The term dynamic is often simplified to a consideration of the inflation. But dynamic means the discounting of a series of payment. Whether the calculations are done real (without inflation) or nominal (with inflation) depends on the investigated time frame (Can the inflation rate be predicted over long times?) and the techno-economic evaluation rules valid for the organization investigating a project (Konstantin, 2013). The investigated time frame of an evaluation must be defined individually. One could either orientate oneself on legal/political, technical or economic frame conditions. In the past years, the development of renewable energies in Europe was largely supported by legal/political support systems. The easiest of them is a fixed feed-in-tariff that is guaranteed over a defined time frame. The support system in France currently guarantees a feed-in-tariff for 15 years, while the German system supports renewable energies over 20 years. While in France the feed-in-tariff is defined individually per power plant (225 €/MWh for Soultz) in Germany there is a general feed-in-tariff of 252 €/MWh (Ravier, 2019) (Bundesministerium für Justiz und Verfassungsschutz, 2018). From a techno-economic point of view the period under review is based on the useful life of cost-intensive components of the overall geothermal power plant system. (Hondo, 2005), (Frick, Kaltschmitt, & Schröder, 2010) and (Schlagermann, 2014) have unanimously chosen a period of 30 years. (Hondo, 2005) bases its choice on experience from existing power plants. (Frick, Kaltschmitt, & Schröder, 2010) see the power plant as a limiting factor, whereas (Schlagermann, 2014) uses the progressive wear of liners and casings in the borehole as a reference point. In accordance with (Welter, Technisch-ökonomische Analyse der Energiegewinnung aus Tiefengeothermie in Deutschland, 2018) and to ensure comparability with other investigations a period of observation of 30 years is chosen.

## 4.3 Investigated risk-factors

### 4.3.1 Risk-factors for the investigated stimulation measures

The definition of what a ‘risk-factor’ is, should be agreed upon first. The point is that in a complex system many variables interact, and that it is often the precise combination of these variables that determines the effect in terms of system performance. Therefore, a simple partial derivative approach around some deterministic base case does not suffice. Two approaches for defining a risk-factor can be distinguished, i.e.

1) An *a priori*, qualitative approach (pre-modelling), and
2) An *a posteriori*, quantitative approach (post-modelling).

For the former approach, a ‘risk-factor’ may be defined as an uncertain model input variable (i.e. a non-controllable) of which it is believed *a priori* (i.e. before quantitative modelling) that the most adverse value of its presumed range will result in driving a given base-case KPI, in a univariate sensitivity analysis, towards or beyond a given acceptance norm. Because of complex relationships and interactions between uncertain multi-variables that *a priori* (i.e. without a quantitative model) cannot be comprehended in-depth, this rather simplified but pragmatic, qualitative definition is proposed here. The qualitative risk-factors thus identified can be subsequently nominated for more in-depth, quantitative analysis. These risk-factors should be discussed and ranked qualitatively when ‘framing the problem’ (see Decision Analysis step 1, Figure 4 on page 10).

When however, using a fully probabilistic quantitative model (approach 2), let us assume that a 'risk-factor' is an uncertain model input variable, which in the *multivariate* sensitivity analysis has a 'contribution to variance' of a given KPI that is large enough to drive, *on its own*, the mean-value of this KPI beyond a given acceptance norm. For example, if the NPV acceptance norm is zero, the square-root of the 'contribution to variance' (i.e. the standard deviation) of the NPV from the reservoir permeability is 6, and the mean-NPV is 5, then the reservoir permeability is a risk-factor. Therefore, when referring to a risk-factor one should specify the following information: 1) the KPI to which it pertains; 2) the acceptance norm of this KPI. And ideally, one should also specify the definition of a risk-factor. This could be denoted, for example, as follows for the two approaches, respectively:

- *Risk-factor: reservoir permeability (mean NPV<0); method: a priori qualitative univariate SA*
- *Risk-factor: reservoir permeability (mean NPV<0); method: a posteriori quantitative multivariate SA, contribution to variance*

The study at hand follows the a priori, qualitative approach. DESTRESS considers itself as applied research. Therefore, the techno-economic model further developed in DESTRESS targets project developers. It is assumed that this target group has only limited amount resources available for modelling. Following the qualitative approaches developed and presented in (Reith, Hehn, Mergner , & Kölbel, 2017), the risk factors presented in Table 12 were implemented in the IGEM and will be evaluated in chapter 5. The integration of additional risk factors is possible with limited effort.

Table 12: Risk factors in soft stimulation measures (Reith, Hehn, Mergner , & Kölbel, 2017)

| # | Risk factor | Description of cause | Description of effect |
|---|---|---|---|
| 1 | Public Acceptance | Citizen groups or NGO's being against the project<br>→ impact of accidents occurred in other Project sites | Loosing permission, strong delay, loss of bankability (after planning before drilling) |
| 2 | Lack of information | Lack of information in engineering<br>→extra data needed for planning the stimulation,<br>→from the point of view of authorities | More/additional measuring effort<br>→redesign based on the new information, |
| 3 | Induced seismicity (with time delay after injection) | High pressure within formation triggers seismicity | Losing public acceptance, surface damage, losing permission depending on the regulations, Project shut down |
| 4 | Change in legislations | Accident occurred in another Project, additional extensive seismic monitoring and precautions etc. needed | Loosing permission, strong delay, not receiving permission |
| 5 | Induced seismicity exceeding threshold | High pressure within formation triggers seismicity | Losing public acceptance, surface damage, losing permission depending on the regulations, Project shut down |
| 6 | Loss of effectivity | Injection pressure damages casing cement, poor cement job | Not getting permeability increase expected, loss of project because it is economically not viable anymore |

| | | | |
|---|---|---|---|
| 7 | Fluid-rock interactions | Interactions including reactions with proppants, wrong selection of acids (concentrations of acids), inhibitors, proppants | Clogging of well, reduction of permeability, loss of project |
| 8 | Fluid-fluid interactions (thermal brine and chemicals) | Interactions including reactions with proppants, wrong selection of acids (concentrations of acids), inhibitors, proppants, microbiological processes, oxygen entrance | Clogging of well, reduction of permeability, corrosion, $H_2S$ and other gasses production |
| 9 | Political Instability | Change in the government on all levels of politics that could affect the project | Loosing permission or get extra official requirements |
| 10 | Lost in hole (measuring tool) | Problems in additional logging with loss of tool, purely related to soft stimulation and the additional data needed | Workover or fishing needed, Losing the well, delay |

### 4.3.2 Deduction of Probability density functions

The stimulation of the reservoir is an integral component of the development of the geothermal reservoirs, if the quality of its hydraulic properties is not sufficient for economic operation. At the same time the stimulation is associated with high costs, not always successful and can have an impact on the environment. A goal of the DESTRESS project is therefore the quantitative analysis of risks arising from the stimulation of reservoirs at various European geothermal sites (Reith, Siefert, Mergner, Kölbel , & Münch, 2018). In this study, the ten most important risk factors identified by (Reith, Hehn, Mergner , & Kölbel, 2017) are therefore implemented. Table 13 provides an overview of the risk factors considered. It describes the model parameters influenced in each case as well as the effect in the negative scenario estimated by expert interviews, published in (Reith, Hehn, Mergner , & Kölbel, 2017), and the probability of occurrence of this negative scenario. The following two assumptions are made for all risk factors (6 to 8 in Table 13) that affect the permeability of the reservoir: First, the individual changes in permeability add up to a total change. And secondly, the individual deviations and the cumulative change of the permeability is such that the reservoir permeability decreases maximum an order of magnitude based on its initial value.

Table 13: Parameters for the integration of risk factors in techno-economic modelling

| | **Risk factor** | **Influenced Parameter** | **Effect** | **Probability** | **σ** |
|---|---|---|---|---|---|
| 1 | Public Acceptance | Investment<br>Public Acceptance (XIf) | 660’000 € | 8,2% | 380’000 € |
| 2 | Lack of information | Investment<br>Exploration (II) | 260’000 € | 6,4% | 140’000 € |
| 3 | Induced seismicity (with time delay after injection) | Investment<br>Public Acceptance (XIf) | 1’400’000 € | 1,6% | 600’000 € |
| 4 | Change in legislations | Investment<br>Planning (III) | 2’300’000 € | 2,0% | 1’000’000 € |
| 5 | Induced seismicity exceeding threshold | Investment<br>Public Acceptance (XIf) | 1’000’000 € | 1,6% | 420’000 € |

| | | | | | |
|---|---|---|---|---|---|
| 6 | Loss of effectivity | Permeability Reservoir | Decrease to 10% | 2,0% | Depends on location |
| 7 | Fluid-rock interactions | Permeability Reservoir | Decrease to 10% | 1,7% | Depends on location |
| 8 | Fluid-fluid interactions (thermal brine and chemicals) | Permeability Reservoir | Decrease to 10% | 1,7% | Depends on location |
| 9 | Political Instability | Investment Planning (III) | 2'300'000 € | 1,2% | 930'000 € |
| 10 | Lost in hole (measuring tool) | Investment Reservoir (V) | 2'300'000 € | 1,3% | 940'000 € |

All risk factors are entered the model using a half-normal distribution with a mean value of 0 and are varied independently of each other. This is shown schematically as a probability density function and cumulative probability function in Figure 29.

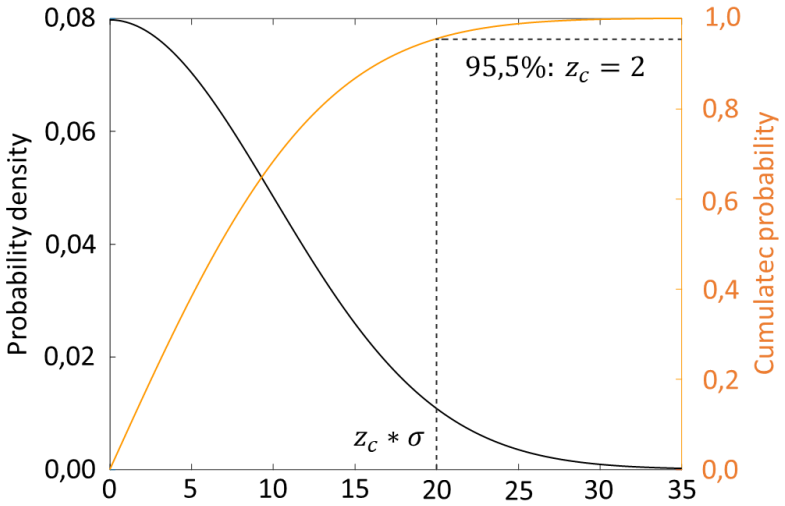


Figure 29: Example for a half normal distribution with $\mu = 0$ and $\sigma = 10$

By means of effect and probability of occurrence the standard deviation of the semi-normal distribution can be estimated through the sigma level. The procedure is illustrated in the following with an example pictured in Figure 29. The probability of occurrence given by (Reith, Hehn, Mergner , & Kölbel, 2017) is translated as the probability that the effect of each risk factor will be at least equal to or greater than the effect given in Table 13. Assuming the effect of a risk factor on a model parameter would have a probability of occurrence of 4.5% and would trigger an unspecified effect with a value of 20 in this negative scenario. In addition, the probability density is semi-normally distributed with an unknown standard deviation. In relation to the cumulative probability, the probability of occurrence means that the effect on the associated model parameter does not exceed the specified value of 20 in 95.5% of all cases and mathematically corresponds to a confidence interval. To any half-normal distribution, a confidence interval can be allocated, i.e. each probability of occurrence can be assigned with a value for $z_c$. In the example shown in Figure 29 $z_c$ equals 2. As the limit of the confidence interval is still known, which here is corresponds to the known threshold value of the effect (20), the standard deviation can be determined according to equation (54) (Schiefer & Schiefer, 2018; Driels & Shin, 2004).

$$\sigma = \frac{Effect}{z_c} \tag{54}$$

Using the known half-normal distributions of the effect of the different risk factors to the corresponding model parameters listed in Table 13 the Monte Carlo simulation of the overall model can be conducted. As for the power plant model, the question of the necessary number of iterations, also needs to be answered for the simulation of the effect of risk factors. Here again, the methodology according to (Driels & Shin, 2004) is used to estimate the number of iterations. According to the methodology, for a Monte Carlo simulation with predefined number of iterations (test run), the standard deviation $s_x$ and the mean value x of the results is determined. In the present study the LCOE are the KPI of interest. The LCOE are calculated including model parameters (see Table 13) influenced by the risk factors listed in Table 12. For a specified relative error E, which must not be exceeded, and an associated confidence interval with confidence level $z_c$ the number of necessary iterations can be determined according to (Driels & Shin, 2004) with (55).

$$n = \left(\frac{z_c * S_x}{E * \bar{x}}\right)^2 \tag{55}$$

For a permitted error of 5% and a confidence interval of 95% the result of equation (55) read as follows: N iterations are required to determine the real mean value of the distribution with 5% accuracy in 95% of the cases. The methodology according to (Driels & Shin, 2004) assumes a normally distributed population. In the half-normal distribution, the one-sided confidence intervals and levels correspond to the two-sided confidence intervals and levels of the normal distribution. The methodology can thus be adopted completely. However, the consideration of several different power plant variants in the overall model results in different values for the required number of iterations depending on of the power plant design under consideration. Especially for power plant variants with net electricity production costs that exceed the minimum value via the power plant variants, high values for the number of necessary iterations will have to be used. As an example, the number of Monte Carlo iterations for the simulation of the risk factors for the Soultz-sous-Forêts site (pure power generation) is estimated with a maximum permitted error of 0.5% and a confidence interval of 99.7% (Zc value 3). With a test population of 1000 power plant designs and 150 risk factor iterations, the maximum number of iterations is 139.

### 4.3.3 Risk mitigation measures and their effect on PDFs

The risk assessment process presented in chapter 2.3 (starting from page 13) serves the identification, prioritization and evaluation of risk factors. Within a holistic risk management approach presented in Figure 8 the risk assessment can be enriched with risk mitigation measures to become a risk management scheme. By managing/mitigating the identified risk factors the realization of risk factors can be prevented or at least the probability of occurrence reduced. Table 14 presents risk mitigation for the Top-10 risk factors presented in (Reith, Hehn, Mergner , & Kölbel, 2017). The single risk mitigation measures are structured in categories called “technical”, “planning” and “organizational”. Thereby it shall be highlighted, that risk mitigation can take place on several levels. Through professional equipment, detailed planning and organizational structures that meet industry standard, the uncertainty caused by risk factors can considerably be reduced. The costs for risk mitigation measures are very project specific and strongly depend on market developments. Therefore, it was only possible to give rough figures for risk mitigation measures. In Table 14 for each risk factor, the cost for its risk mitigation measures are listed. Political risk can’t be mitigated through dedicated measures, as the observance of laws and policies is a mandatory pre-condition for a successful project realization. The risk factor “loss in hole” can be mitigated through taking an insurance. This is already modelled in the IGEM, so that there are no extra costs listed in Table 14.

Table 14: Risk mitigation measures

| # | Risk | Risk mitigation measures | | | Costs for risk mitigation |
|---|---|---|---|---|---|
| | | Technical | Planning | Organisational | |
| 1 | Public Acceptance | Radial well stimulation instead of fracking, more green acids | | Continuous communication (before/after); Ask for participation of people (financial models), Special tax to the local community; Benefits for the local community; Approach single contacts instead of the whole community | 50 k€ |
| 2 | Lack of information | Run measurements | Second party opinion | Stay in close contact with authorities | 1'000 €/m + 10 k€ |
| 3 | Induced seismicity (with time delay after injection) | Gamma ray logs for determining faults near wellbore, tracer tests (push pull test) | Staying away from stress zones stepwise reduction of pressure | Advance traffic light systems, | 1'000 €/m + 50 k€ |
| 4 | Change in legislations | | Insurance for legal costs | | - |
| 5 | Induced seismicity exceeding threshold | Gamma ray logs for determining faults near wellbore; Tracer tests (push pull test) | Staying away from stress zones; Stepwise reduction of pressure | Traffic light systems with threshold | 1'000 €/m + 100 k€ |
| 6 | Loss of effectivity | Cement log prior to stimulation | Chosing appropriate cementing | | 1'000 €/m + 50 k€ |
| 7 | Fluid-rock interactions | Core analysis; Chemical characterization of the fluids; In-situ conditions measurements; X-ray measurements; Inhibitors; Volumes and concentrations of different acids; Precisely inject acids to the targeted zone | Chemical modelling; Analysis considering casing within testing and modelling | Involve chemical companies earlier; Collaboration with other project partners/companies that did stimulation in the same region | 50 k€ |
| 8 | Fluid-fluid interactions (thermal brine and chemicals) | Core analysis; Chemical characterization of the fluids; In-situ conditions measurements; Inhibitors; Volumes and concentrations of different acids; Biocide | Chemical modelling; Analysis considering casing within testing and modelling; Keep spare equipment | Involve chemical companies earlier; Collaboration with other project partners/companies that did stimulation in the same region | 50 k€ |
| 9 | Political Instability | | Insurance for legal costs | | - |
| 10 | Loss in hole (measuring tool) | Work over and fishing | Check certificates of equipment & training personnel | Loss in hole insurance; Look for track record of companies | 140k€/well |

# 5 Evaluation of decision alternatives based on KPI

In this chapter the previously presented model for the techno-economic simulation of deep geothermal energy provision is applied to selected demonstration sites of the DESTRESS project. At the French site Soultz-sous-Forêts pure power generation is investigated. At the geothermal power plant of Mezöberény(Hungary), due to the relatively low reservoir temperature of approximately 100 °C, only pure heat production is considered. Additionally, a fictive location in the German part of the Upper Rhine Graben is investigated. As no other DESTRESS demonstration site plans or operatres a CHP unit, the CHP solutions implemented in the model will be presented at this case study.

For all variants with the exception of pure power generation, two different operating cases are evaluated. First, a stationary operation of the power plant is evaluated over the entire period of observation. In this case only maintenance and repair work is taken into account as down time, which leads to about 8000 annual full load hours. To calculate the economic KPIs, it is assumed that the total heat generated from CHP will be supplied to a customer. Second, a heat-controlled operation of the power plant is considered. A defined heat requirement is covered as much as possible by the geothermal plant. The heat demand is specified in the form of an annual duration curve, which is formed according to the methodology of Sochinsky (Blesl, et al., 2009). Figure 30 shows an example of the annual duration line for a maximum heat demand of 18 $MW_{th}$ and how this demand is covered by a geothermal system. For simplification reasons, it is assumed that there is an annual heat demand whose maximum heat output corresponds exactly to the maximum heat which can be extracted from the geothermal fluid. The maximum amount of heat is transferred when the geothermal fluid is cooled down to the minimum injection temperature and used exclusively for heat generation. This operation mode does not apply to pure power generation.

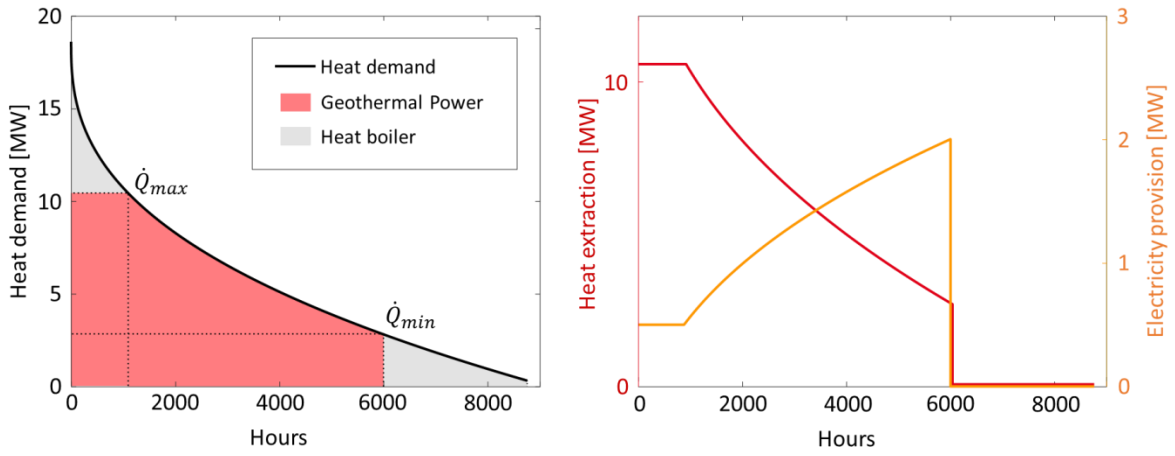


Figure 30: Heat and power provision in the heat-controlled operation mode

In heat-controlled operation at CHP plants, a shift of the thermal water mass flow between heat extraction and power plant is possible, as shown in Figure 30. It is assumed that the ORC power plant can be operated up to a minimum partial load of 25% without changing the individual state points. Under these conditions, the thermal water mass flow used by the power plant is directly proportional to the working fluid mass. If the working fluid mass flow is reduced to 25% of the nominal mass flow, the required thermal water mass flow is also reduced to 25% of the thermal water mass flow in nominal operation. The thermal water not used by the power plant is available for heat extraction in partial load operation. Thereby, not only the rated thermal nominal output of the power plant but also a range of thermal outputs is available to cover the heat demand profile. The nominal mass flows

result from the power plant design. When designing the power plant and CHP components, the described mass flow shift is considered. The heat demand that cannot be covered by the mass flow shift is provided by a boiler. The investment costs for the boiler are calculated using the methodology of (Turton, Bailie, Whiting, Shaeiwitz, & Bhattacharyya, 2013) (see chapter 3.2). When heat is provided by the boiler, fuel cost are incurred, which is considered with the help of the local specific gas price for industrial customers (EUROSTAT, 2018). On the basis of these assumptions, the electrical energy produced can be determined from the heat demand covered (Figure 30 - left). This is proportional to the thermal water flow available for the electricity production and results in the heat production shown in Figure 30 (right).

As can be seen from Figure 30 (right), there are different values for full load hours in terms of heat and electricity production. The model therefore distinguishes between heat and electricity related full load hours. In both cases, the maximum power output is used as the full load, so that the full load hours result according to the equation (56).

$$T_V = \int_0^{8760} \dot{Q}\ dt\ \cdot \frac{1}{\dot{Q}_{max}}\ bwz. \quad T_V = \int_0^{8760} P\ dt\ \cdot \frac{1}{P_{max}} \tag{56}$$

An overview of all site-dependent model parameters can be found in Table 15, Table 16 and Table 17. The required number of Monte Carlo iterations was determined using the methodology described by (Driels & Shin, 2004) (see page 49). For the case studies of the sites Soultz-sous-Forêts and Upper Rhine Graben, 150 Monte Carlo iterations must be used, while for the Mezöberény site 250 iterations are needed. On the example of the case studies below, different functionalities of the IGEM will be presented together with the deduction of general results on soft stimulation and power plant modelling.

## 5.1 Soultz-sous-Forêts

### 5.1.1 Presentation of site

The Soultz-sous-Forêts geothermal project started in 1987 and is the cradle of the European research on harvesting geothermal energy in granitic and fractured systems. All over all five wells were drilled for research purposes at the site. Besides stimulation techniques, corrosion, scaling, power plant technique but also questions concerning the operation of a geothermal power plants were investigated by a group of international researchers. After almost 30 years of research, the geothermal site is exploiting the fractured basement at 5 km depth, under commercial conditions. Between 2015 and 2016 the binary plant on surface was completely renovated. Since June 2016 a new ORC-power plant with isobutane as working medium is operated under commercial conditions. The gross power of the plant is 1.7 $MW_{el}$. The geothermal loop is composed of one production well GPK-2 and two reinjection wells GPK-3 and GPK-4. After the electricity production the geothermal brine is fully reinjected at around 70°C. The volume of reinjected brine is shared between the two injection wells, one third in GPK-4 and two third in GPK-3 without using reinjection pumps (Mouchot, Ravier, Seibel, & Pratiwi, 2019). All three wells are 5km deep and are cased to roughly 4.5 km in the granitic section. Below that depth, the reservoir is made of crystalline basement and underwent various kinds of hydraulic and chemical stimulations together with several periods of long-term circulations (Cuenot & Genter, 2015) (Schill, Genter, Cuenot, & Kohl, 2017). Although GPK-2 is an artesian well, the production of geothermal brine is enhanced by a line shaft pump to around 30 l/s. Although the reservoir temperature is slightly above 200 °C the geothermal brine is produced with a temperature of 150°C (Baujard C. , et al., 2018) (Schill, Genter, Cuenot, & Kohl, 2017). Since commissioning the power plant, between June and August 2016, the overall system showed outstanding availabilities. The total plant availability developed from 90% in 2017 to 95.9% in 2018. In 2017 routine operational maintenance measures were performed as well as an acid cleaning of

the LSP hydraulics, which caused the lower availability compared to 2018. The availability of the ORC plant without the thermal water circuit was even higher with 99,8 % for both 2017 and 2018. The net efficiency of the ORC plant was 11.5 % in 2017. In that year the gross electrical production was nearly 9,7 GWh and the total electrical consumption, including ORC auxiliaries and production pump, was around 3,7 GWh, resulting in an overall net electrical production for the whole plant of 5,9 GWh. These figures varied only slightly for 2018. The gross electricity production was 9,6 GWh together with the consumption of the auxiliaries of 3,9 GWh, the overall net electrical production reached 5,7 GWh (Mouchot, Ravier, Seibel, & Pratiwi, 2019).

Table 15: Input parameter Soultz-sous-Forêts site

| | Parameter | Value/setting | Reference |
|---|---|---|---|
| **Reservoir / Thermal water circuit** | $p_{Reservoir}^{Production}$ | 50,0 MPa | (Scheiber J. , 2018) |
| | $p_{Reservoir}^{Injection}$ | 50,0 MPa | (Scheiber J. , 2018) |
| | $T_{Reservoir}^{Production}$ | 201 °C | (Schill, Genter, Cuenot, & Kohl, 2017) |
| | $T_{Reservoir}^{Injection}$ | 201 °C | (Schill, Genter, Cuenot, & Kohl, 2017) |
| | $h_{Thickness}^{Production}$ | 1000 m | (Scheiber J. , 2018) |
| | $h_{Thickness}^{Injection}$ | 1000 m | (Scheiber J. , 2018) |
| | $K^{Production}$ | 4*10$^{-14}$ m² | (Held, et al., 2014) |
| | $K^{Injection}$ | 2*10$^{-14}$ m² | (Held, et al., 2014) |
| | $S$ | 7,8*10$^{-5}$ | (Guth, 2011) |
| | $\lambda_{geo}$ | 1,58 $W\ /\ mK$ | (Eppelbaum, Kutasov, & Pilchin, 2014) |
| | $a_{geo}$ | 10,28*10$^{-7}$ $m^2\ /\ s$ | (Eppelbaum, Kutasov, & Pilchin, 2014) |
| | $z_{Production}$ | 5000 m | (Mouchot, et al., 2018) |
| | $z_{Injection}$ | 5000 m | (Mouchot, et al., 2018) |
| | Type well | Deviated | (Brandt, 2013) |
| | Type pump | LSP | (Seibel, 2018) |
| | R | 700 m | (Mouchot, et al., 2018) |
| **Power plant** | $\dot{m}_{TW}$ | 33,3 $kg\ /\ s$ | (Seibel, 2018) |
| | $\Delta T^{min}$ | 5 K | Assumption |
| | $T_{air,in}$ | 15 °C | Assumption |
| | Working medium | Isobutane | (Seibel, 2018) |
| | $p_{TW,in}^{Heat\ plant}$ | 2,2 MPa | (Seibel, 2018) |
| **CHP** | $T_{Flow}$ | 70 °C | (Averfalk & Werner, 2017) |
| | $T_{Back\ flow}$ | 45 °C | (Averfalk & Werner, 2017) |
| | $p_{network}$ | 8 bar | Assumption |

For the modelling of the Soultz-sous-Forêts geothermal power plant, the input data presented in Table 15 is used. Although input data for the simulation is chosen on latest available information, the economic key figures are not expected to match the real operational data for two major reasons. The high temperature loss between reservoir and wellhead is caused by a thermal interaction between the production and the injection well. This site-specific effect is not reflected in the IGEM. Economically the commercial operation only must refund the costs of the new over-ground installations and the operational costs. The existing boreholes were financed in concluded research activities. In contrast to the reality, the costs for simulation planning and under-ground facilities are

included in the simulation. Nevertheless, general conclusions can be drawn from the simulation results.

### 5.1.2 Results of techno-economic modelling

The DESTRESS project is mainly focussed on soft stimulation with topics like risk management concerning stimulation, public acceptance of stimulation, technical design of soft stimulation measures … but also techno-economic evaluation of soft stimulation in work package 2. The focus on soft stimulation is also kept in work package 2. But work package 2 is also supposed to investigate power plant technologies. On the example of the Soultz-sous-Forêts power plant, general tendencies in power plant modelling shall be investigated. The IGEM offers the same functionalities but also substantial enhancements to the model presented in (Welter, 2018). Therefore, it can be used for future investigations with a focus on the energy transformation in a heat, power or combined heat and power plant.

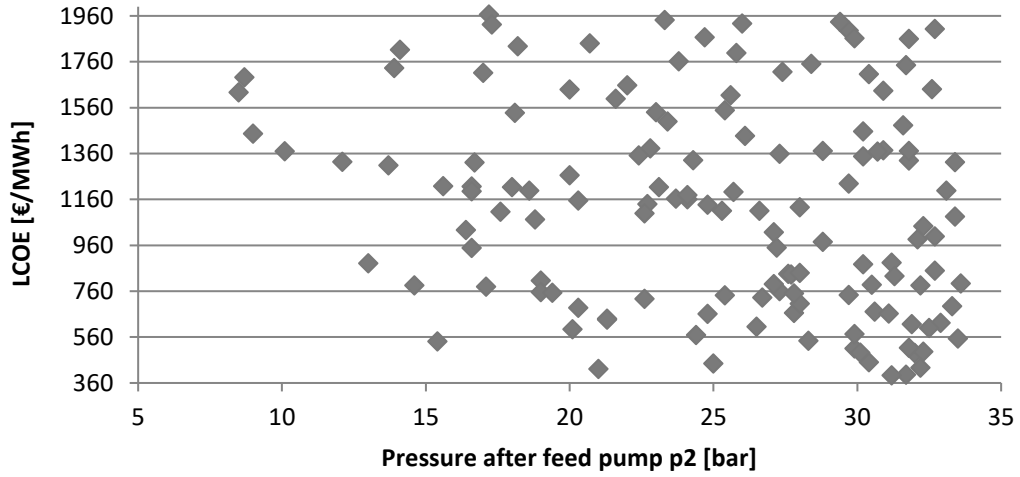


Figure 31: Power plant modelling: LCOE over pressure after feed-pump (Pure electricity; LSP; $\dot{m} = 33\ kg/s$; 150 Monte-Carlo iterations; 1000 power plant configurations; working medium isobutene; chemical stimulation; including risk factors; without risk mitigation measures)

The Monte-Carlo simulation approach in power plant modelling is one of the major development steps between (Welter, 2018) and the IGEM presented in this report. The investigation of sensitivities in power plant modelling opens new possibilities for the optimization of geothermal electricity provision. Figure 31 above illustrates the connection between pressure after the feed-pump and the LCOE. The pressure after feed-pump is one of the parameters manipulated by the Monte-Carlo simulation. The results presented in Figure 31 clearly point out, that the operation of the power plant on a high-pressure level has a positive impact on LCOE.

Such a clear connection between the temperature of the working medium after overheating and the LCOE can't be drawn, as Figure 32 shows. Two local optima could be assumed at 130 °C and 150 °C. But there are also data-points with considerably higher and lower temperatures, that show low LCOE. A similar picture is drawn when investigating the absolute overheating in Figure 33. Over a wide temperature range of around 60 K low LCOE values are reached. These results suggest, that overheating has no direct impact on LCOE and therefore doesn't have to be investigated in further detail.

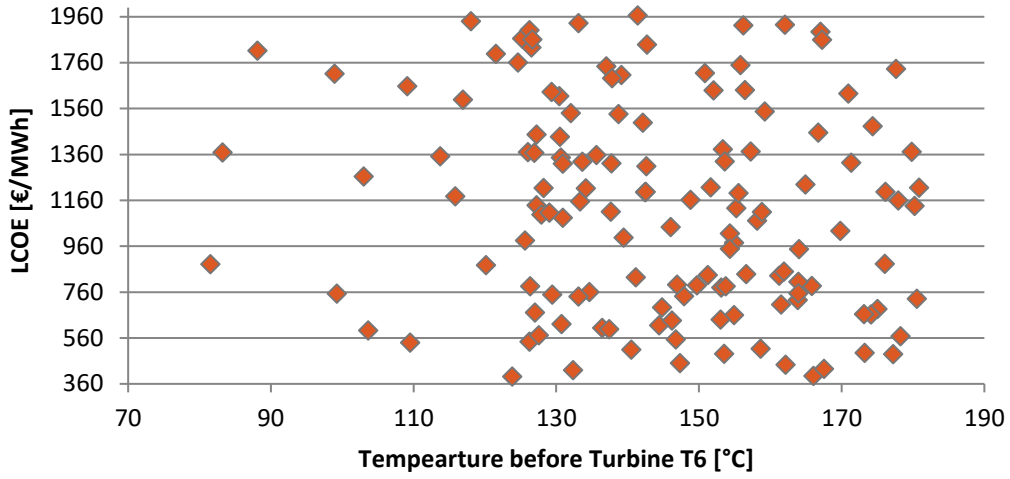


Figure 32: Power plant modelling: LCOE over temperature after overheating (Pure electricity; LSP; $\dot{m} = 33\ kg/s$; 150 Monte-Carlo iterations; 1000 power plant configurations; working medium isobutene; chemical stimulation; including risk factors; without risk mitigation measures)

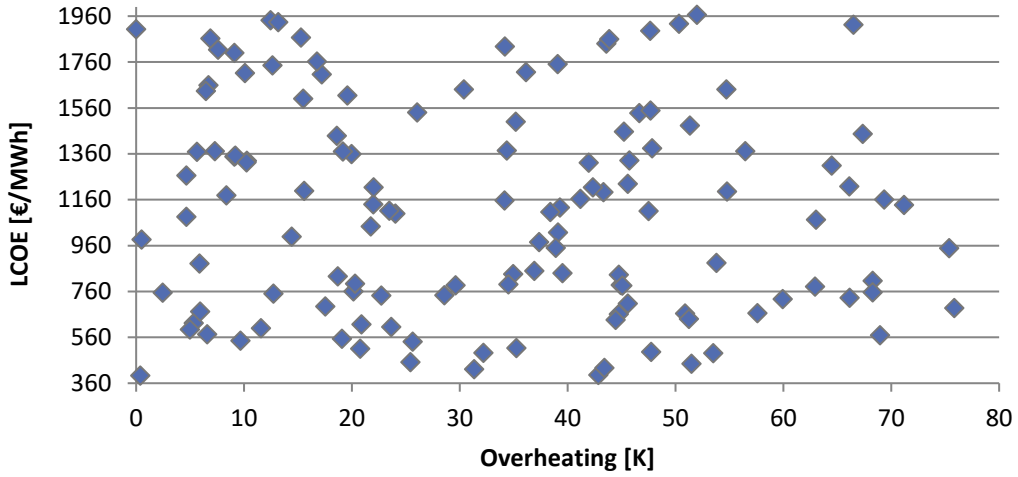


Figure 33: Power plant modelling: LCOE over overheating (Pure electricity; LSP; $\dot{m} = 33\ kg/s$; 150 Monte-Carlo iterations; 1000 power plant configurations; working medium isobutene; chemical stimulation; including risk factors; without risk mitigation measures)

While the influence of overheating on LCOE isn't clear, the connection between thermal water outlet temperature and net power of the overall power plant, including all auxiliaries e.g. production pump, is obvious. Figure 34 clearly shows an increase in the net power with a decrease of the thermal water outlet temperature. But, chapter 5.3.2 presents the simulation results in Figure 45, which suggest that there is no clear correlation between techno-economic KPIs and the overall net power of the power plant. In contrast to the overall net power, for the thermal water outlet temperature a correlation between LCOE is documented in Figure 35. Although, the correlation is weak, a minimization of the LCOE with a decrease of the thermal water outlet temperature is apparent.

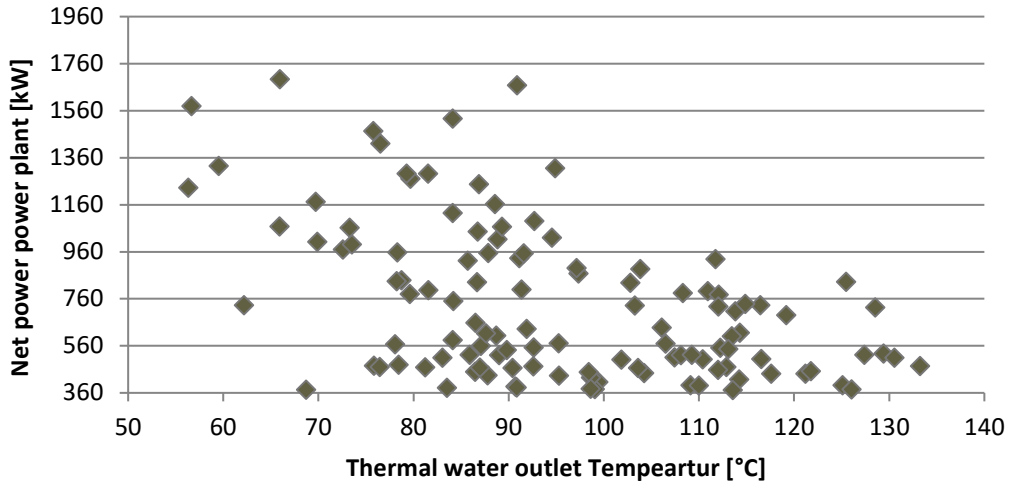


Figure 34: Power plant modelling: LCOE over overheating (Pure electricity; LSP; $\dot{m} = 33\ kg/s$; 150 Monte-Carlo iterations; 1000 power plant configurations; working medium isobutene; chemical stimulation; including risk factors; without risk mitigation measures)

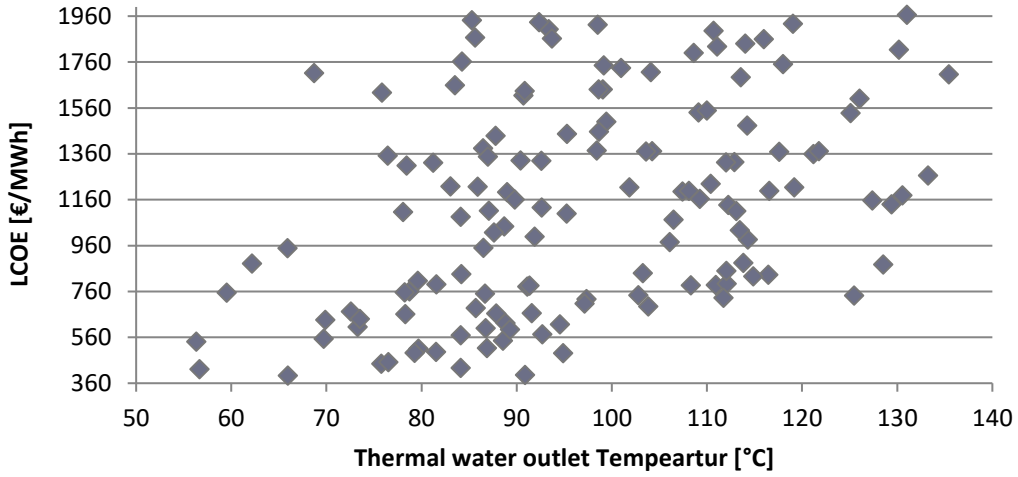


Figure 35: Power plant modelling: LCOE over thermal water outlet temperature (Pure electricity; LSP; $\dot{m} = 33\ kg/s$; 150 Monte-Carlo iterations; 1000 power plant configurations; working medium isobutene; chemical stimulation; including risk factors; without risk mitigation measures)

The risk factors presented in chapter 4.3.1 have an effect either on technical or economic model parameters. Effects of risk factors on economic model parameters are investigated in detail in chapter 5.2.2. In the following, the technical effects of the modelled risk factors shall be investigated. As presented in chapter 4.3.1 risk factors 6, 7 and 8 have an influence on the permeability of the reservoir surrounding the production/injection wellbore. Figure 36 shows for the power plant configuration number 9, the influence of the changing permeability at the production well (left) and the injection well (right) on the LCOE. The cumulated effect of all risk factors is limited to a minimum permeability of 10 % of the initial permeability stated in Table 15. Neither at the injection well nor at the production well, a change of the permeability has an obvious effect on the LCOE. This could be explained by a superimposition of the economic effect of risk factors over the technical effect.

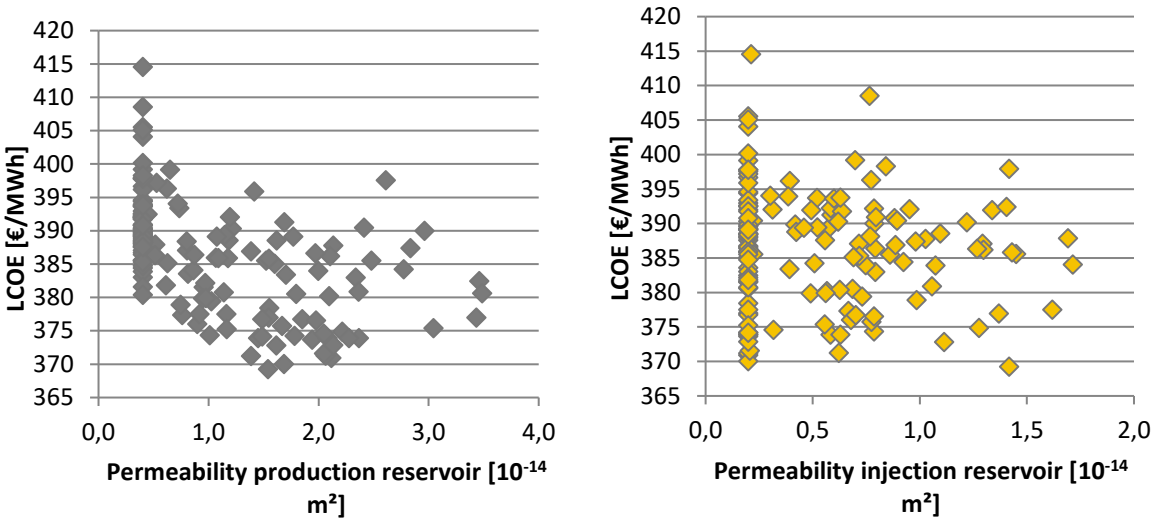


Figure 36: Effect of a changing permeability on the LCOE (Pure electricity; LSP; $\dot{m} = 33\ kg/s$; 150 Monte-Carlo iterations; power plant configuration 9; working medium isobutene; chemical stimulation; including risk factors; without risk mitigation measures)

A direct correlation can be drawn between the permeability and the electrical power demand of the production pump. By changing the permeability, the inflow into the well and thereby the dynamic water level changes. The dynamic water level determines the pump entrance pressure and thereby the pressure difference that must be supplied by the production pump. This correlation is visible Figure 37 (left). Although this connection is very clear, no explicit correlation between the power demand of the production pump and the LCOE can be drawn. Figure 37 (right) only shows a boundary for the maximum power demand, that correlates with the limitations on permeability change around the production and injection well.

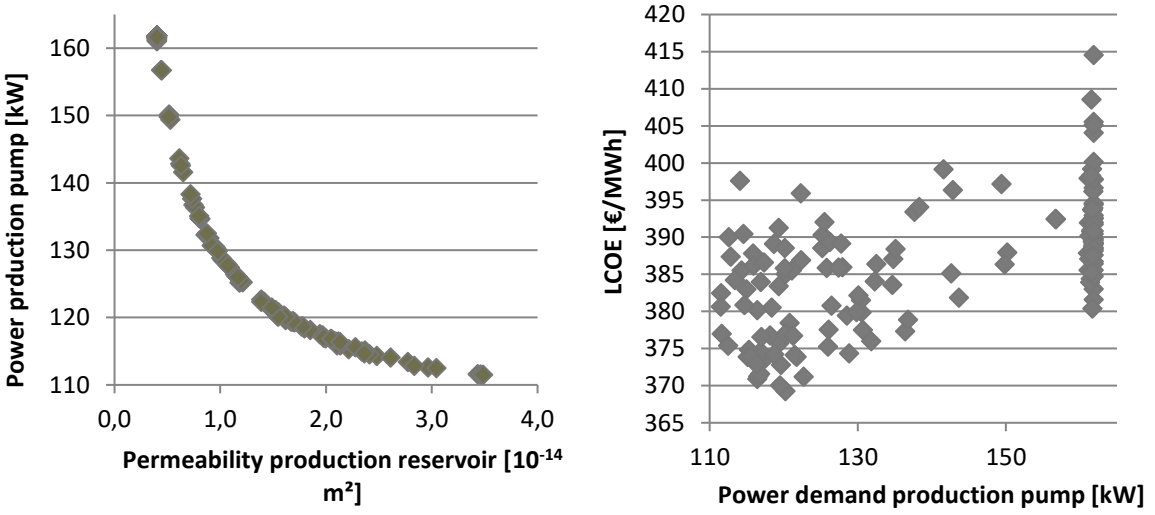


Figure 37: Effect of permeability on production pump power demand and LCOE (Pure electricity; LSP; $\dot{m} = 33\ kg/s$; 150 Monte-Carlo iterations; power plant configuration 9; working medium isobutene; chemical stimulation; including risk factors; without risk mitigation measures)

## 5.2 Mezöberény

### 5.2.1 Presentation of site

The Mezöberény geothermal site can be found in the Pannonian basin (encircled by the Carpathian Mountains). Its origins can be tracked to the Early-Middle Miocene. Through a rolling back

subduction, the basement was pulled off the basin. Thereby the thickness of the crust was reduced, which is today 22-26 km thick. This brings the hot asthenosphere closer to the surface and creates a heat anomaly. A mean heat flow density of 90-100 mW/m$^2$, and an average geothermal gradient of 45°C/km was published by (Royden, Horvath, & Buchfiel, 1982) for the Pannonian basin. After an isostatic descent of the thinned crust the basin that was formed was filled up by Pannonian sediment sequences. These sediments are mostly composed by clastic rocks of different grain size.

According to (Horváth, et al., 2015), the Lower Pannonian sediments are mostly impermeable while the upper Pannonian formations contain vast porous, permeable sand and sandstone beds. These sandstone layers are only between 1-30 m thick and show only a little horizontal extension. Whereas the sand lenses form a hydraulically unified system with an area of 40.000 km² and an average thickness of 200-300 m. The reservoir has an average permeability of 500-1500 mD with a bulk porosity of 20-30 %. While generally a uniform hydrostatic pressure distribution can be expected, local changes through recharge and discharge have to be expected (Tóth A. , 2012) (Dövényi, Horváth, Liebe , Gálfi, & Erki, 1983). Another potential layer for geothermal use is made up of carstified Mesozoic rocks. Around 20 % of all geothermal wells in Hungary are producing from this geothermal reservoir.

The use of geothermal resources has a long tradition in Hungary. The Pannonian Basin has already been used in Roman times. Since 1925 there is a balneological use followed by an agricultural use. The use of geothermal water without reinjection led to a decrease of the water level. For the former artesian wells production pumps must be used, today. Consequently, the reinjection of used geothermal water has become mandatory. The injection into sandstone reservoirs as a counter measure is only recently done (Tóth A. N., 2016) (Szanyi, et al., 2010).

Between 2011 and 2012 the Mezöberény geothermal site was constructed. The goal was to power a geothermal heating system with geothermal water from the Békés Basin. The Production well was planned to exploit the higher upper Pannonian Sandstones of the Zagyva Formation, due to a poor sandstone formation with low productivity the production well was deepened to the Ujfalu-Formation. The injection well was deepened to inject into the same reservoir. When the system was finished in August 2012 one production well (B-115) with a depth of 2003 m, and one reinjection well (K-116) with a depth of 2001 m were put into service. But after a short operation time the injectivity dropped dramatically and the operation was stopped due to injectivity problems. A chemical and mechanical cleaning was performed in 2017, which had the goal to remove the clogging of the downhole filters. But since then no long-term operation has taken place (Siklósi, 2017). Table 16 summarizes the modelling input parameters of the Mezöberény power plant.

Table 16: Input parameter Mezöberény site

| | Parameter | Value/setting | Reference |
|---|---|---|---|
| **Reservoir / Thermal water circuit** | $p_{Reservoir}^{Production}$ | 19,0 MPa | (Geo-Log Kft., 2012) |
| | $p_{Reservoir}^{Injection}$ | 17,1 MPa | (Geo-Log Kft., 2012) |
| | $T_{Reservoir}^{Production}$ | 80 °C | (Geo-Log Kft., 2012) |
| | $T_{Reservoir}^{Injection}$ | 100 °C | Calculated according to temperature gradient |
| | $h_{Thickness}^{Production}$ | 400 m | Assumption |
| | $h_{Thickness}^{Injection}$ | 400 m | Assumption |
| | $K^{Production}$ | 9,5*10$^{-14}$ m² | (Geo-Log Kft., 2012) |
| | $K^{Injection}$ | 5,0*10$^{-14}$ m² | (Geo-Log Kft., 2012) |

| | | | |
|---|---|---|---|
| | $S$ | 7,8*10$^{-5}$ | (Geothermia Expressz Kft., 2016) |
| | $\lambda_{geo}$ | 1,58 $W\ /\ mK$ | (Eppelbaum, Kutasov, & Pilchin, 2014) |
| | $a_{geo}$ | 10,28*10$^{-7}$ $m^2\ /\ s$ | Assumption |
| | $z_{Production}$ | 5000 m | (Geo-Log Kft., 2012) |
| | $z_{Injection}$ | 5000 m | (Geo-Log Kft., 2012) |
| | Type well | Vertical | (Geothermia Expressz Kft., 2016) |
| | Type pump | ESP | Assumption |
| | R | 1400 m | (Geothermia Expressz Kft., 2016) |
| **Heat plant** | $\dot{m}_{TW}$ | 4,8 $kg\ /\ s$ | (Welter, Brehme, Nowak, Kaymakci, & Kölbel, 2019) |
| | $p_{TW,in}^{Heat\ plant}$ | 2,2 MPa | Assumption |
| | $T_{Flow}$ | 70 °C | (Averfalk & Werner, 2017) |
| | $T_{Back\ flow}$ | 45 °C | (Averfalk & Werner, 2017) |
| | $p_{network}$ | 8 bar | Assumption |

### 5.2.2 Results of techno-economic modelling

The production well of the geothermal site at "Mezöberény" exploit the reservoir at a depth of roughly 2000 m where geothermal water with a temperature of 100 °C can be found. This temperature level qualifies the site for geothermal heat provision. Compared to the average geothermal heat gradient of 3 K/100m, Mezöberény offers favourable conditions for geothermal heat provision with a heat gradient of 5 K/100m. Unfortunately, the site suffers from poor hydraulic frame conditions. (Welter, Brehme, Nowak, Kaymakci, & Kölbel, 2019) give a mass flow rate of 4,8 kg/s. The low flow rate leads to a considerable heat loss along the wellbore (see chapter 3.1.2), which additionally negatively affects the techno-economic evaluation of the geothermal site. In the simulated case, the heat plant inlet temperature of the geothermal water is 23 % below the reservoir temperature. Data from operational sites, shows an average temperature loss of 5 - 10 % (Welter, 2018).

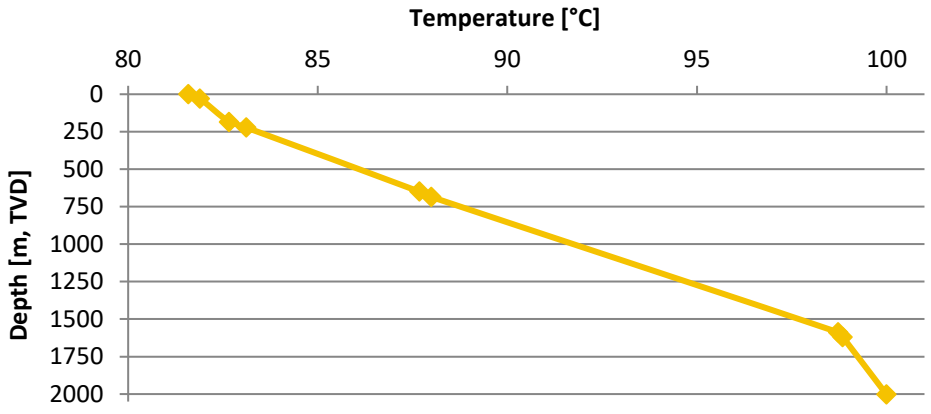


Figure 38: Temperature loss in the wellbore at Mezöberény site (Basecase; pure heat provision; baseload; ESP; $\dot{m} = 4{,}8\ kg/s$; no stimulation; no risk factors)

Besides the technical frame conditions, the techno-economic evaluation also depends on the demand for the provided energy. In contrast to electricity, heat can't be transported economically over long distances. Therefore, it must be distributed locally. The IGEM integrates the customer structure through the evaluation of two demand structures. The derivation of the baseload load

operation and the heat-controlled operation can be found starting from page 71. Figure 39 compares the two simulated cases. Through following the demand curve, the heat-controlled case only has 3'840 full-load hours, while the baseload case operates 8'001 h, only stopping for maintenance. This leads to a relative reduction of produced heat by 108% in the heat-controlled case. Additional gas costs and the effect of discounting (see equation (34)) lead to 67 % lower LCOH, compared to a baseload operation.

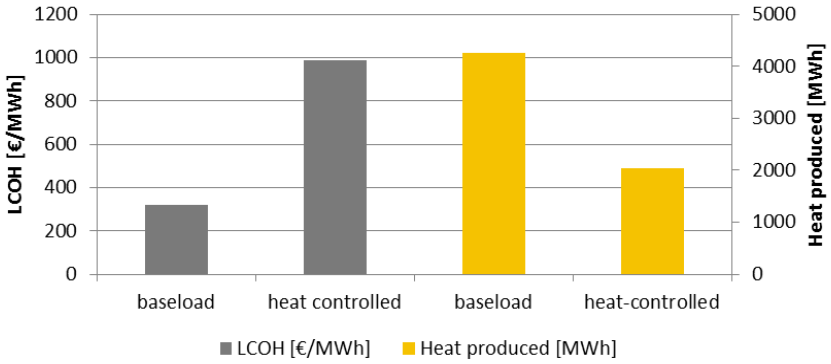


Figure 39: Comparison of baseload and heat-controlled energy provision for the Mezöberény case (Basecase; pure heat provision; ESP; $\dot{m} = 4{,}8\ kg/s$; no stimulation; no risk factors)

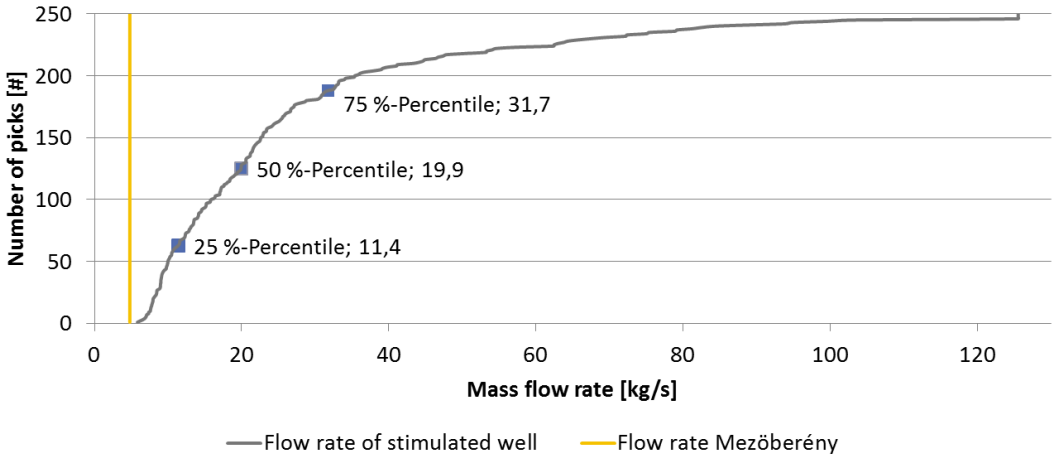


Figure 40: Effect of stimulation for the Mezöberény site (250 Monte-Carlo iterations; chemical stimulation; including risk factors; without risk mitigation measures)

As explained above, poor hydraulic properties of the Mezöberény wellbores adversely affect the economic operation of the project. The soft stimulation approach investigated in DESTRESS aims to enhance the hydraulic conditions of a site with minimum impact on the environment and people. In the example of the Mezöberény site, it shall be demonstrated which impact a stimulation could be related to the techno-economic performance of a site. The simulated cases shall picture a soft stimulation treatment. Therefore, the risk factors presented in chapter 4.3.1 are included in the simulation as well as the risk mitigation measures presented in chapter 4.3.3. All other frame conditions are kept constant with respect to the base-case presented in Table 16. Figure 40 shows the effect of stimulation, simulated for the Mezöberény site according to the literature data presented in chapter 3.1.1.5. Besides the simulated results of the soft stimulation job, the original flow rate as well as the 25 %-, 50 %- and 75 %-percentile of the distribution are plotted. As discussed in chapter 4.3.1 the effect of stimulation depends on multiple frame conditions of geological,

geophysical and chemical nature. Therefore and because of the limited data availability, the presented results should be interpreted conservative.

For the above presented effect of stimulation, the impact on the techno-economic evaluation is presented in Figure 41. The presented box plots give the median of the distribution (horizontal line in the middle of the box), the 75 %-percentile (upper limit of the box), the 25 %-percentile (lower limit of the box) and the Minimum/Maximum of the distribution shown by the whiskers. With an increase of flow rate a decrease of the LCOH can be observed. This effect is expected. Components with a high investment, e.g. wellbores, are not sensitive to the flow rate, so that the produced energy escalates quicker with the growing flow rate than the costs do. More important for the evaluation of uncertainty is that the width of the distribution is reduced with an increase of flow rate. Caused by the bigger amount of produced energy, the impact of single cost categories and the uncertainty on them is reduced. This example demonstrates, that the “economies of scale”, already investigated in (Welter, 2018), not only show their positive effect on the general techno-economic evaluation (more economic project) but also reduce the impact of uncertainty.


Figure 41: Effect of increased flow rate on techno-economic performance (Pure heat provision; baseload; ESP; 250 Monte-Carlo iterations; chemical stimulation; including risk factors; without risk mitigation measures)

Within the investigations presented in Figure 40 and Figure 41, the uncertainty on the effect of stimulation is investigated. It is possible to show that even without including risk mitigation measures (RMM) stimulation can be a valuable tool for improving the techno-economic performance of a project. The overall goal of DESTRESS is to keep/enhance the improvement of stimulation measures while reducing the impact. That is done by risk mitigation measures, which are described in detail in chapter 4.3.3. RMM cause additional costs to the project development. But, they influence the uncertainty on risk associated costs. That means, the application of RMMs is always balancing between uncertainties and invests. For the case of Mezöberény, this balancing is presented in Figure 42. It turns out, that for the chosen modelling parameters (PDFs for risk factors, costs of mitigation measures …) the RMM start to have a positive impact, with the Median. That means; in over 50 % of all cases the soft stimulation approach with RMM is the better choice only focusing on investment costs. This purely quantitative evaluation ignores qualitative effects of using risk mitigation measures. Mainly on the public acceptance side and when dealing with authorities, the qualitative effect of risk mitigation measures can’t be over emphasized. The above described effect is supported when including technical effects (change of permeability; see chapter 4.3.1) into the investigation. The box plots in Figure 43 show selected key figures of the Monte-Carlo simulation on the Mezöberény case with and without risk mitigation measures. The observations presented in Figure 42 are supported. RMM have a traceable positive effect on the techno-economic evaluation of a geothermal project.

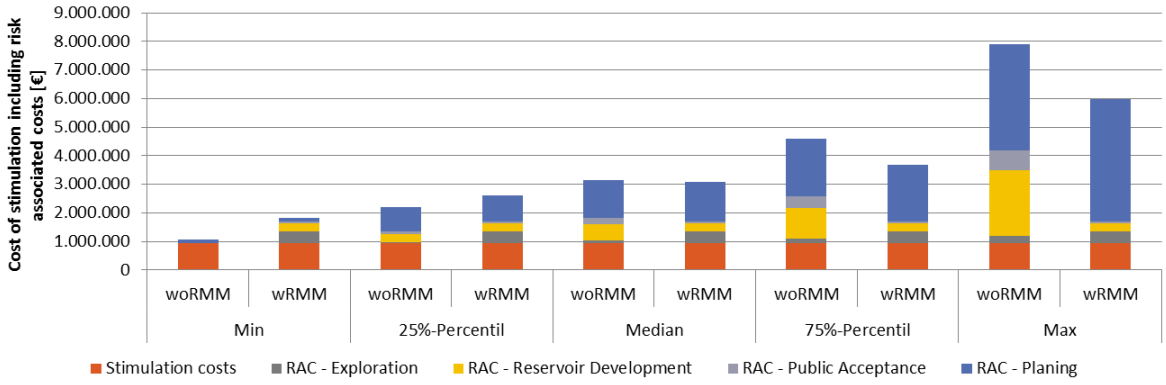


Figure 42: Stimulation costs including risk associated costs (RAC = Risk associated costs; Pure heat provision; baseload; ESP; $\dot{m} = 4{,}8\ kg/s$; 250 Monte-Carlo iterations; chemical stimulation; including risk factors; with/without risk mitigation measures)

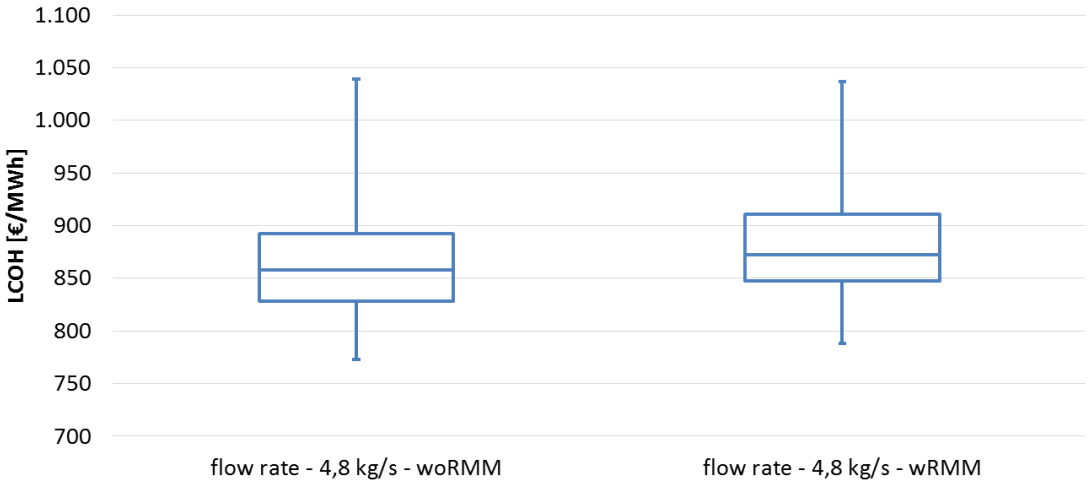


Figure 43: Effect of risk mitigation measures on the techno-economic performance (wRMM = With Risk mitigation measures; woRMM = Without Risk mitigation measures; Pure heat provision; baseload; ESP; $\dot{m} = 4{,}8\ kg/s$; 250 Monte-Carlo iterations; chemical stimulation; including risk factors; with/without risk mitigation measures)

## 5.3 Upper Rhine Graben

### 5.3.1 Presentation of site

The DESTRESS project had to undergo several changes for the demonstration. Technical, organizational and political issues forced the DESTRESS consortium to change the demonstration sites. When finalizing this study in early 2018, only the sites in Soultz-sous-Forêts and Mezöberény were in a status, being able to provide the required data. Therefore, to demonstrate the IGEM, in particular CHP, and show the effect of soft stimulation measures, a fictitious example is created. As a location the German side of the Upper Rhine Graben is chosen. The input data for the “Upper Rhine Graben” site, presented in Table 17, is fictitious, but based on expert knowledge. At the “Upper Rhine Graben” site, two deviated boreholes are assumed to explore the Buntsandstein in a depth of 3600 m. Through its favourable conditions with a reservoir temperature of 160 °C and a flow rate of 120 kg/s the site can be used for all types of heat provision. It is also assumed that a heat network with unlimited capacity can transport heat to customers. Further data on the site can be found in Table 17.

Table 17: Input parameter Upper Rhine Graben site

| | Parameter | Value/setting | Reference |
|---|---|---|---|
| **Reservoir / Thermal water circuit** | $p_{Reservoir}^{Production}$ | 33,1 MPa | Assumption |
| | $p_{Reservoir}^{Injection}$ | 33,1 MPa | Assumption |
| | $T_{Reservoir}^{Production}$ | 160 °C | Assumption |
| | $T_{Reservoir}^{Injection}$ | 160 °C | Assumption |
| | $h_{Thickness}^{Production}$ | 420 m | Assumption |
| | $h_{Thickness}^{Injection}$ | 420 m | Assumption |
| | $K^{Production}$ | 1,43*10$^{-13}$ m² | Assumption |
| | $K^{Injection}$ | 1,43*10$^{-13}$ m² | Assumption |
| | $S$ | 1*10$^{-8}$ | Assumption |
| | $\lambda_{geo}$ | 2,3 $W\ /\ mK$ | Assumption |
| | $a_{geo}$ | 9*10$^{-7}$ $m^2\ /\ s$ | Assumption |
| | $z_{Production}$ | 5000 m | Assumption |
| | $z_{Injection}$ | 5000 m | Assumption |
| | Type well | Deviated | Assumption |
| | Type pump | LSP/ESP | Assumption |
| | R | 1500 m | Assumption |
| **Power plant** | $\dot{m}_{TW}$ | 120 $kg\ /\ s$ | Assumption |
| | $\Delta T^{min}$ | 5 K | Assumption |
| | $T_{air,in}$ | 15 °C | Assumption |
| | Working medium | Isobutane | Assumption |
| | $p_{TW,in}^{Heat\ plant}$ | 2,2 MPa | Assumption |
| **CHP** | $T_{Flow}$ | 130 °C | Assumption |
| | $T_{Back\ flow}$ | 65 °C | Assumption |
| | $p_{network}$ | 8 bar | Assumption |

### 5.3.2 Results of techno-economic modelling

Heat and electricity have a different exergy level. Therefore, the techno-economic comparison of pure electricity provision and CHP is challenging from a methodological point of view. According to (IEA; NEA; OECD, 2015), heat is assessed economically with a heat price and integrated into the LCOE calculations as revenues (equation (28)). In (Welter, 2018) the sensitivity of the results to the heat price was already investigated. This shows a methodological shortcoming of the LCOE approach. Therefore, in the following different KPIs are used for the comparison of electricity provision and CHP. For the results presented in Figure 44, a heat price is derived by taking 50 % of the household gas price. In contrast to heat, renewable electricity in Germany is supported by law. The subsidiary system guaranteed by the “Erneuerbaren Energie Gesetz” (EEG) is simplified in this study to a feed-in-tariff. Following the EEG, a fixed remuneration of 252 €/MWh for 20 years is assumed (BMWi, 2018). As the period of observation in this study is 30 years (see chapter 4.2) the remaining time is evaluated with 100 €/MWh according to (Capros, et al., 2016).

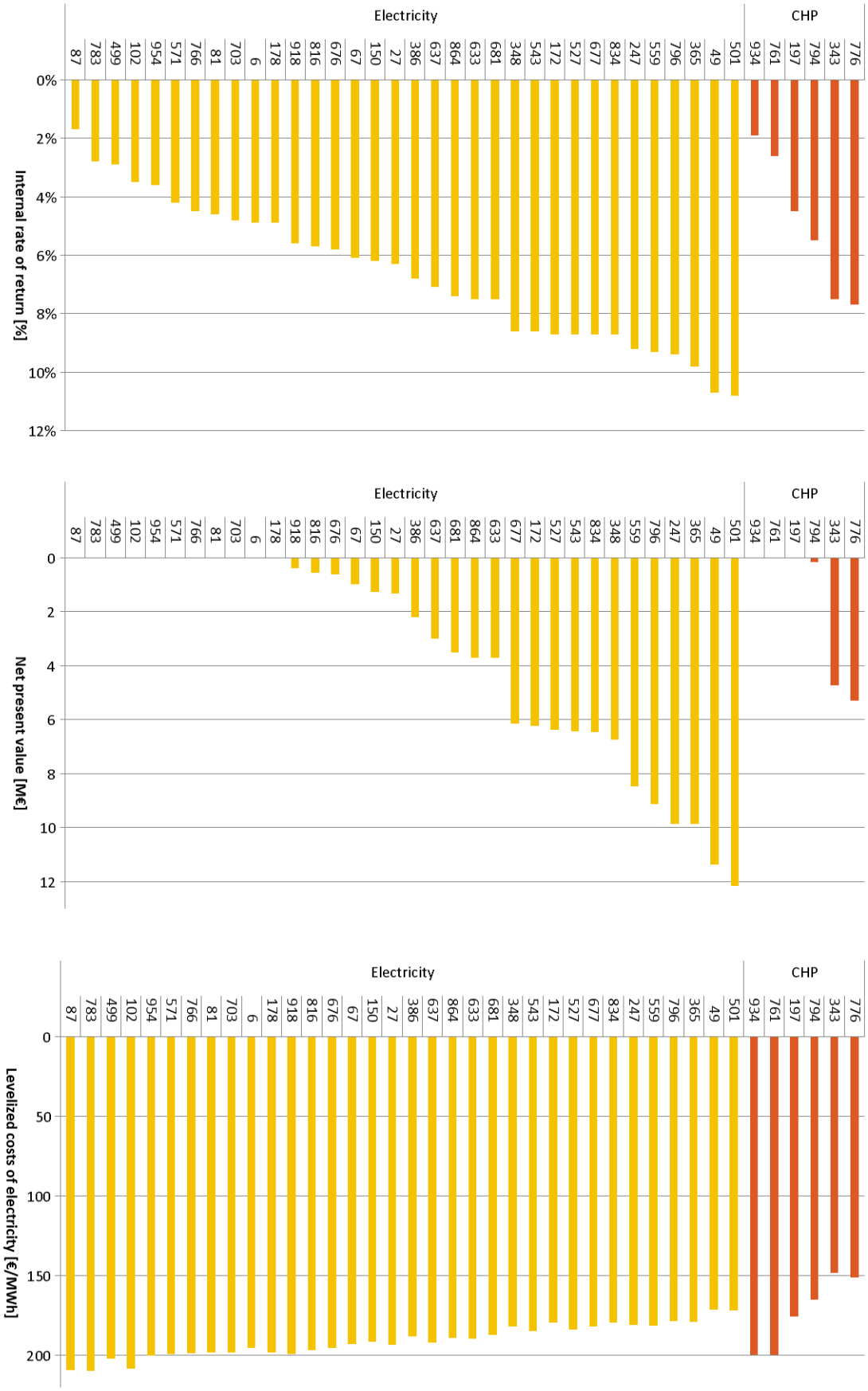


Figure 44: Comparison of pure electricity provision and CHP based on IRR, NPV and LCOE (Pure electricity/CHP provision with parallel setup; baseload; ESP; $\dot{m} = 120\ kg/s$; 150 Monte-Carlo iterations; 1000 power plant configurations; hydraulic stimulation; including risk factors; with risk mitigation measures)

Figure 44 shows the results of a comparison between pure electricity provision and CHP at the fictitious site “Upper Rhine Graben”. The Assessment is based on the internal rate of return, the net present value of the investment, as well as on the Levelized costs of electricity. These KPI are drawn on the ordinate, while on the abscissa, the investigated power plant configurations are pictured. The Monte-Carlo-Simulation of the power plant generates a defined number of randomly sampled configurations. The optimality of configurations is evaluated in the economic model. Low LCOE, a high IRR, or a high NPV can serve as selection parameters. The presented power plant configurations are selected by having an IRR > 1 % and sorted in descending order subject to their IRR.

For CHP only 6 out of 1000 power plant configurations fulfil the selection criteria, while at least 34 out of 1000 power plant configurations for pure electricity provision, have an IRR > 1 %. Fewer CHP plant configurations show a positive IRR. This would suggest that under the given assumptions on the market prices, pure electricity provision should be preferred as it is less sensitive to a non-optimal power plant configuration/operation. This finding contradicts the studies presented by (Schlagermann, 2014) and (Welter, 2018). Both studies investigated CHP and saw an advantage over pure electricity provision. (Schlagermann, 2014) as well as (Welter, 2018) used LCOE as a KPI for their investigations. Based on LCOE as KPI, the results presented in Figure 44 are consistent with other studies. Half of the presented CHP configurations show lower LCOE than the best pure electricity configuration. The apparent contradiction between LCOE and the other KPI can be explained on a methodological basis. While LCOE-calculations have the energy price as a result, IRR and NPV have it as an input parameter. Given the frame conditions of this simulation with subsidies included, apparently contradicting results can be explained. This illustrates the macro-economic character of LCOE as KPI, while NPV and IRR rather have a micro-economic focus. With methodological differences one can also explain power plant configurations with zero NPV but a positive IRR. The NPV calculations are based on an interest rate of 5,42 % as an input parameter, while for IRR calculations, the interest rate is an output. Methodological correct, power plant configurations with an IRR lower than 5,42% don’t have a positive NPV. Figure 44 also shows that none of the CHP plants is listed as an electricity plant. This suggests that the power plant configuration must be optimized on the intended purpose. The results presented in Figure 44 are based on a parallel CHP setup. For the same setup, the net power of the single power plant configurations is presented in Figure 45. On average the net power of CHP plants is 50 % below the net power of pure electricity plants. Figure 45 also points out that none of the techno-economic KPI is directly correlated with the net electrical power of the plant. Power plant configuration 783 has the third highest net power but the second lowest IRR.

It can be summarized that under the given frame conditions power plants with pure electricity provision show higher IRRs compared to CHP. Nevertheless, CHP power plants also can generate interesting IRRs with over 7%. Additionally, it was shown that a purely technical optimization is not constructive for an investor.

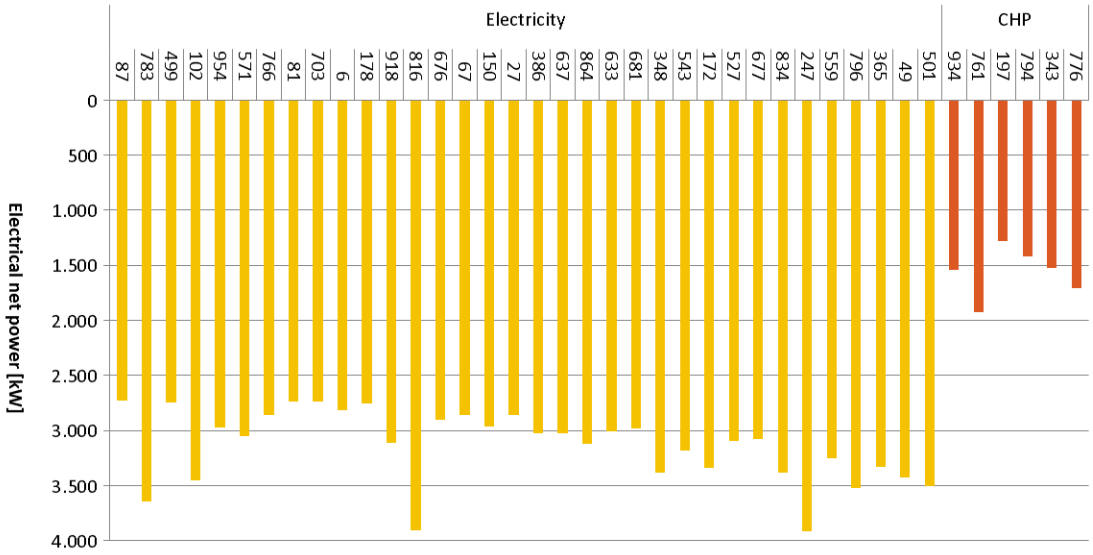


Figure 45: Net electrical power for power plant configurations selected on their IRR (Pure electricity/CHP provision with parallel setup; baseload; ESP; $\dot{m} = 120\ kg/s$; 150 Monte-Carlo iterations; 1000 power plant configurations; hydraulic stimulation; including risk factors; with risk mitigation measures)

On the example of the “Upper Rhine Graben”-site it shall be investigated, whether geothermal heat provision is competitive to other large-scale heat provision technologies. Studies on the German energy system show that for scenarios with a further increase of renewables and a decrease of CO2 emission, geothermal energy plays an important role in heat provision (Blesl M. , 2014) (Fleischer, 2019). (Blesl M. , 2014) forecasts in 2050 a renewable share in the district heating system of 68 – 88 %, which will mainly be supplied by geothermal energy. The trends shown in the mentioned forward-looking studies can be reinforced by calculations done with the IGEM. Figure 46 compares LCOH of large-scale energy provision technologies. All technologies are designed for the use in a district heating system. Besides geothermal energy, solar thermal energy, bio-methane, waste incineration and three different application of natural gas are compared. For geothermal energy flow rate of 60 kg/s, 80 kg/s, 100 kg/s and 120 kg/s including hydraulic soft stimulation with risk mitigation measures are investigated. The results show that geothermal energy is the most competitive renewable heat provision technology. Compared to bio-methane geothermal energy shows a relative reduction of heat provision costs of 96 - 128 %. And, in relation to solar thermal energy a considerable relative reduction of 33 – 76 % is calculated. Generally speaking, conventional heat provision technologies can still provide heat with lower costs. Especially subsidized natural gas-powered CHP and waste incineration plants show lower LCOH. Nevertheless, according to the results presented in Figure 46 geothermal energy is already competitive with natural gas boilers and un-subsidized CHP. Considering further technological development and economies of scale as investigated in (Janczik, 2014) and (Welter, 2018), respectively, a further decrease of LCOH of geothermal energy can be assumed.

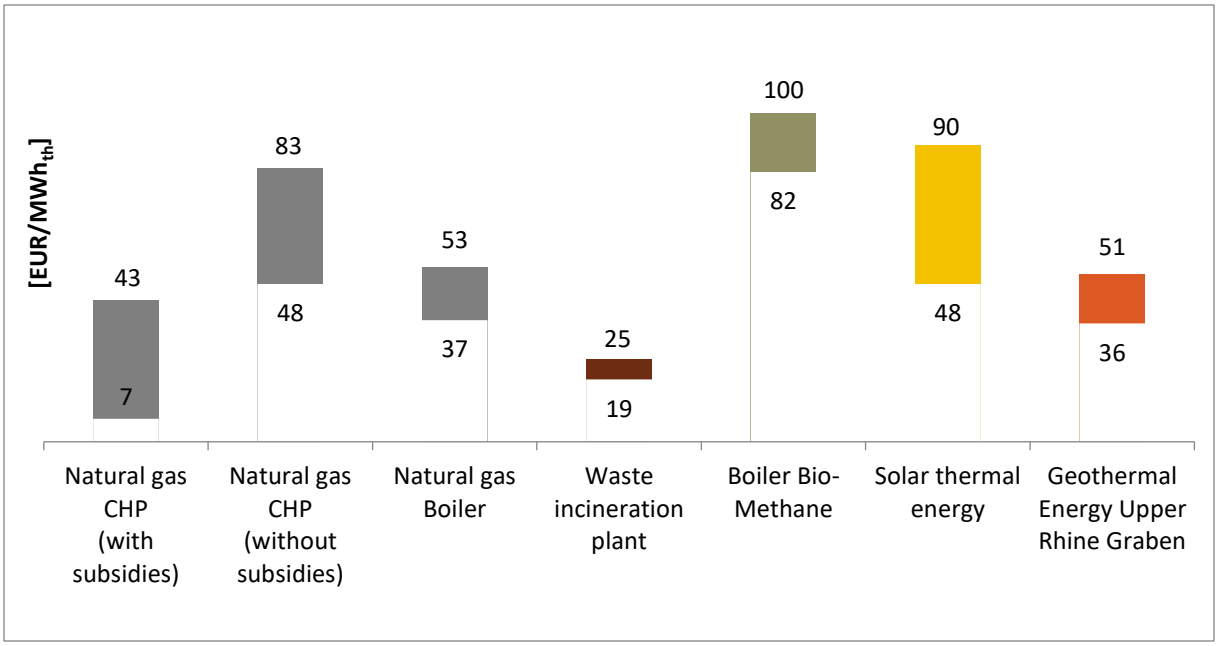


Figure 46: Comparison of LCOH of-large-scale heat provision technologies (Ertle, 2018) (Pure heat provision; baseload; 150 Monte-Carlo iterations; hydraulic stimulation; including risk factors; with risk mitigation measures; ESP; $\dot{m} = 120 \frac{kg}{s} \rightarrow 36 \frac{€}{MWh}$; $\dot{m} = 100 \frac{kg}{s} \rightarrow 39 \frac{€}{MWh}$; $\dot{m} = 80 \frac{kg}{s} \rightarrow 44 \frac{€}{MWh}$; $\dot{m} = 60 \frac{kg}{s} \rightarrow 51 \frac{€}{MWh}$)

# 6 Summary and conclusions

Deliverable 2.2 of the DESTRESS work package 2 merges the results of the DESTRESS tasks 2.1, 2.2 & 2.3. The overall goal was to improve techno-economic evaluation of geothermal energy provision. Besides pure modelling and simulation issues, improvements in techno-economic evaluation also arise from the methodological approach of evaluation. Using synergies from the oil & gas industry, the report at hand presents decision analysis. A structured approach for decision making in project development and operation. Following the single steps of the decision analysis approach, uncertainty can be integrated into techno-economic modelling. Based on this methodological structure it was possible to implement risk factors, and the uncertainty that comes with them, into a techno-economic simulation tool called Integrated geothermal energy model (IGEM).

The IGEM includes the results published in (Reith, Hehn, Mergner , & Kölbel, 2017) and presents new development steps in techno-economic modelling. It offers decisive advantages over existing models such as EURONAUT by (Heidinger, 2010), GEOPHIRES by (Beckers, Lukawski, Anderson, Moore, & Tester, 2014) or (Beckers & McCabe, 2018) and also features considerable improvements compared to the first development step of the IGEM presented in (Welter, 2018): Uncertainty accompanies the evaluation of a project over all life cycle steps. In the early phase of project development there is considerable uncertainty on frame conditions, while during the realization, risk factors can affect the project. Therefore, uncertainties regarding both technical and economic model parameters are considered and quantified using the Monte-Carl method. Ten different risk factors are currently implemented. Due to the modular structure of the model, additional risk factors can be easily incorporated. Furthermore, the present model depicts the geothermal system in more detail than the EURONAUT and GEOPHIRES models, from both a technical and an economic point of view, thus providing deeper insights into system behaviour. Another significant improvement was possible in terms of technical modelling. While in (Welter, 2018) the Organic Rankine Cycle was calculated with a heuristic optimization approach, the current version of the IGEM optimizes the power plant with the Monte Carlo method. A basis for this step is the model presented in (Collings, Yu, & Wang, 2016 ). This new approach enlarges the solution space and thereby improves the quality of optimization. In addition to this methodological improvement also the mapping of technical features is improved. The introduction of pinch analysis in all heat exchangers guarantees physically consistent power plant designs in this model. In addition, the plate heat exchangers considered by (Collings, Yu, & Wang, 2016 ) and (Welter, 2018) are replaced by shell-and-tube heat exchangers, which corresponds to the state of the art for geothermal applications. In addition, combined heat and power provision already presented in (Welter, 2018) is implemented into the Monte-Carlo simulation of the power plant and enriched with the possibility of simulating pure heat generation.

In general, the model described in chapter 3.1 is improved in its structure and has more efficient algorithms in all model parts compared to the first evolution step presented in (Welter, 2018). This enables the computation-intensive Monte Carlo simulation to quantify the influence of various risk factors while maintaining reasonable calculation times. In addition to the improvements in the technical models and the program code, the economic model part is also improved. While maintaining the general structure selected correlations are updated to map the reality more closely. Supplementary to the adaption of single parameters in existing correlations, completely new cost functions are introduced. As an example, the representation of LSP and the updated stimulation cost functions can be named. Another important step to meet the demand of DESTRESS is an adaption of the geographical focus of the cost engineering sub-models. The model according to (Welter, 2018) is restricted to a national study of the German geothermal market. With the model presented in this

report, the consideration of the of different European demonstration sites within DESTRESS becomes possible.

The development of a model is a huge task but becomes meaningless if the reality can't be mapped with good accordance, which is another major strength of the IGEM. The technical as well as the economic sub-models are validated with extraordinary detailed insight into operational and economic data of running geothermal power plants. This step lays the foundation for the significance of the IGEM.

Despite many advantages over existing technical-economic models, there are also fields of improvement that could be adapted by future research: The distribution functions for mapping the risk factors are currently implemented as semi-normal distributions. As can be seen on the implementation of the effect of stimulation, a solid data basis may reveal other distributions to map the real data more precisely. While the focus of DESTRESS was clearly on risk factors, future model developments could identify and implement uncertain model parameters for further progress in that field of research. When integrating further uncertain parameters, one should allow a positive as well as negative changes relative to a given base case. Cost engineering models as implemented in the IGEM always must be adapted to current market developments. For example, the mapping of stimulation costs could benefit from economic data of finalized stimulation measures during the DESTRESS project. To improve the technical simulation, the geometry of the air condenser in the ORC could be adapted. In the model it is currently designed as a shell-and-tube heat exchanger, in analogy to all other heat exchangers. In fact, however, air condensers have a different geometry. Furthermore, Figure 44 shows that only very few of the simulated power plant configurations are show a good techno-economic performance. By selectively narrowing the modelling space, one loses generality, but improves the significance of the results. Another interesting research question would be to investigate the sensitivities within the comparison of CHP and pure electricity provision. The same is valid for the power plant operation. Uncertainty increases the risk for possible investors. With the integration of further uncertainties into the IGEM model parameters could be identified, that could lead to a more robust techno-economic configuration of geothermal projects.

The IGEM still has room for improvement, but its value was already proven with the report at hand. From the investigations presented in this report, multiple future research question can be derived. The major task in work-package 2 was not the evaluation of single demonstration sites, but the overall improvement of techno-economic evaluation in geothermal energy provision. This goal was reached by development steps in different fields of techno-economic evaluation:

- The decision analysis approach gives the methodological framework for making structured and sound decisions in geothermal project development and operation.
- The integration of risk factors into techno-economic modelling opens new possibilities for the evaluation of projects. By the integration of uncertainty valuable additional information can be given to decision makers.
- The identification of mitigation measures can be a help for project developers and authorities.
- Power plant optimization with the Monte-Carlo approach doesn't only allow a further optimization of power plant configurations based on techno-economic results, but also investigations on the robustness of power plant configurations.
- The possibility to simulate heat, CHP and pure power provision in one model allows a consistent evaluation of different business models.
- New approaches in cost engineering give the community a sound database for early stage evaluation of geothermal power projects.

- The published data on operational power plants enable further development of other techno-economic models

Although the results of a techno-economic evaluation are always site specific, the chosen examples evaluated in chapter 5 show interesting results that can be used to derive general statements:

- Under the conditions of the Soultz-sous-Forêts site with a relatively high wellhead temperature, low flow rate and isobutane as working fluid operation conditions were deduced. While a high operational pressure in the working medium cycle and a low thermal water output temperature have a positive impact on the LCOE, the overheating doesn't show a clearly positive impact.
- The investigation of the effect of risk factors on technical model parameters on the example of the Soultz-sous-Forêts site points out, that uncertainty on technical model parameters is superimposed by economic uncertainties. Whether this suggestion is valid for real projects must be further investigated.
- On the Mezöberény case it was possible to show that with an increase of produced energy, the width of the distribution of results is reduced. Bigger projects therefore can cope with a negative realization of single uncertain parameters more easily.
- The simulations on the Mezöberény case also demonstrate, that although the costs for risk mitigation measures seem to be high, their effect is valuable. By considering the probability distribution of an uncertain techno-economic KPI, it was shown that risk mitigation measures contribute to an economic realization of a project. This statement is only receiving additional significance when taking social acceptance into account
- The comparison of CHP and pure electricity provision on the example of the fictitious Upper Rhine case, didn't only show the importance of using different KPI for the techno-economic evaluation, but also the need for a purpose tailored technical configuration of geothermal power/heat plants.
- Geothermal energy is often still blamed for being expensive. On the Upper Rhine case it was possible to show that over a wide range of flow rate geothermal energy is competitive to other large-scale renewable as well as conventional heat provision technologies.

# Literature

AACE. (2016). *Cost estimate classification system – as applied in engineering, proprocurement, and construction for the process industries.* Association for the advancement of cost engineering.

AACE. (2016). *Cost estimate classification system as applied in engineering, procurement and construction for the process industries.* Morgantown (USA): Association for the advancement of cost engineering.

Abrahamsson, M. (2002). *Uncertainty in quantitative risk analysis - chracterisation and methods of treatment.* Lund: Lund University.

Al-Ajmi, A., & Al-Harthy, M. (2010). Probabilistic wellbore collapse analysis. *Journal of Petroleum Science and Engineering*.

Ale, B., Burnap, P., & Slater, D. (2012). *Risk matrix basics.* Delft, Cardiff.

Almeida, A. T., Cavalacante, C. A., Alencar, M. H., Ferreira, R. J., de Almeida-Filho, A. T., & Garcez, T. V. (2015). *Multicriteria and multiobjective models for risk, reliability and maintenance decision analysis.* Berlin: Springer international publishing.

Andersen, L. (1998). Stochastic modelling for the analysis of blowout risk in exploration drilling. *Reliability Engineering & System Safety*, pp. 53-63.

Astolfi, M. (2014). *An Innovative Approach for the Techno-Economic Optimization of Organic Rankine Cycles.* Mailand: PhD thesis, Politecnico di Milano.

Aumayr, K. J. (2009). *Erfolgreiches Produktmanagement - Tool-Box für das professionelle Produktmanagement und Produktmarketing.* Wiesbaden: GWV Fachverlage GmbH.

Averfalk, H., & Werner, S. (2017). Essential improvements in future district heating systems. *Energy Procedia 116*, pp. 217 - 225.

Azar, J., & Samuel, G. (2007). *Drilling Engineering.* Tulsa, Oklahoma: PennWell Corp.

Bäcker, W., & Wagner, W. (2006). Reference eequations of state for the thermodynamic properties of fluid phase n-butane and isobutane. *Journal of Physical and Chemical Reference Data 35*, pp. 929-1019.

Baisch, S., Vörös, R., Rothert, E., Stang, H., Jung, R., & Schellschmidt, R. (2010). *A numerical model for fluid injection induced seismicity at Soult-sous Forêts.* International Journal of Rock Mechanics and Mining Sciences.

Balazova, M. (2004). *Mthoden zur leistungsbewertung und Leistungssteigerung der Mechatronikentwicklung.* Paderborn: Universität Paderborn.

Bauer, M., Freeden, W., Jacobi, H., & Neu, T. (2014). *Handbuch Tiefe Geothermie.* Springer-Verlag Berlin Heidelberg.

BAUJARD, C., GENTER, A., CUENOT, N., MOUCHOT, J., MAURER, V., HEHN, R., . . . VIDAL, J. (2018). EXPERIENCE LEARNT FORM A SUCCESFULL SOFT STIMULATION AND OPERATIONAL FEEDBACK AFTER 2 YEARS OF GEOTHERMAL POWER AND HEAT PRODUCTION IN RITTERSHOFEN AND SOULTZ-SOUS-FORÊTS PLANTS (ALSACE, FRANCE). *GEOTHERMAL RESOURCE COUNCIL, GRC2018*, (PP. 2241 - 2263). RENO.

BAUJARD, C., GENTER, A., DALMAIS, E., MAURER, V., HEHN, R., ROSILETTE, R., . . . SCHMITTBUHL, J. (2017). HYDROTHERMAL CHARACTERIZATION OF WELLS GRT-1 AND GRT-2 IN RITTERSHOFEN, FRANCE: IMPLICATIONS ON THE UNDERSTANDING OF NATURAL FLOW SYSTEMS IN THE RHINE GRABEN. *GEOTHERMICS*, PP. 255 - 268.

BECKERS, K. F., LUKAWSKI, M. Z., ANDERSON, B. J., MOORE, M. C., & TESTER, J. W. (2014). LEVELIZED COSTS OF ELECTRICITY AND DIRECT-USE HEAT FROM ENHANCED GEOTHERMAL SYSTEMS. *JOURNAL OF RENEWABLE AND SUSTAINABLE ENERGY 6*.

BECKERS, K. J. (2016). *LOW-TEMPERATURE GEOTHERMAL ENERGY: SYSTEMS MODELING, RESERVOIR SIMULATION, AND ECONOMIC ANALYSIS.* CORNELL: CORNELL UNIVERSITY.

BECKERS, K. J., & MCCABE, K. (2018). INTRODUCING GEOPHIRES V2.0: UPDATED GEOTHERMAL TECHNO-ECONOMIC SIMULATION TOOL. *PROCEEDINGS, 43RD WORKSHOP ON GEOTHERMAL RESERVOIR ENGINEERING.* STANFORD: STANFORD UNIVERSITY.

BILALIS, N., MARAVELAKIS, E., ANTONIADIS, A., & MOUSTAKIS, V. (2004). MAPPING PRODUCT INNOVATION PROFILE TO PRODUCT DEVELOPMENT ACTIVITIES - THE I-DSM TOOL. *ENGINEERING MANAGEMENT CONFERENCE.* SINGAPORE: IEEE.

BLESL, M. (2014). *KRAFT-WÄRME-KOPPLUNG IM WÄRMEMARKT DEUTSCHLANDS UND EUROPAS : EINE ENERGIESYSTEM- UND TECHNIKANALYSE.* STUTTGART: UNIVERSITY STUTTGART.

BLESL, M., KEMPE, S., OHL, M., FAHL, U., KÖNIG , A., JENSSEN, T., & ELTROP, L. (2009). *WÄRMEATLAS BADEN-WÜRTTEMBERG: ERSTELLUNG EINES LEITFADENS UND UMSETZUNG FÜR MODELLREGIONEN. .* STUTTGART: INSTITUT FÜR ENERGIEWIRTSCHAFT UND RATIONELLE ENERGIEANWENDUNG (IER) UNIVERSITÄT STUTTGART.

BLOY, B., DAVIS, N., SMOLEN, B., BAILEY, L., HOUWEN, O., REID, P., . . . HODDER, M. (1994). DESIGNING AND MANAGING DRILLING FLUID. *OILFIELD REVIEWS*, PP. 33-43.

BMF. (2016). *UMSATZSTEUER-UMRECHNUNGSKURSE: GESAMTÜBERSICHT FÜR DAS JAHR 2016.* BUNDESMINISTERIUM DER FINANZEN.

BMWI. (2018). ERNEUERBARE-ENERGIEN-GESETZ VOM 21. JULI 2014 (BGBL. I S. 1066), DAS ZULETZT DURCH ARTIKEL 1 DES GESETZES VOM 17. DEZEMBER 2018 (BGBL. I S. 2549) GEÄNDERT WORDEN IST.

BOMMER, J., CROWLEY, H., & PINHO, R. (2015). A RISK-MITIGATION APPROACH TO THE MANAGEMENT OF INDUCED SEISMICITY. *JOURNAL OF SEISMOLOGY*, PP. 623-646.

BOS, C. F. (2005). A FRAMEWORK FOR UNCERTAINTY QUANTIFICATION AND TECHNICAL-TO-BUSINESS INTEGRATION FOR IMPROVED DECISION-MAKING. *SPE EUROPEC/EAGE ANNUAL CONFERENCE. SPE-94109-MS.* MADRID, SPAIN: SOCIETY OF PETROLEUM ENGINEERS.

BOS, C. F. (2017). DECISION TREE ANALYSIS. TNO - NEDERLANDSE ORGANISATIE VOOR TOEGEPAST-NATUURWETENSCHAPPELIJK ONDERZOEK.

BOS, C. F., & WILSCHUT, F. (2011). *ASSESSING THE UNCERTAINTY IN THE PERFORMANCE PREDICTIONS OF NATURAL SUBSURFACE SYSTEMS THAT ARE USED FOR CO2 STORAGE.* THE HAGUE: NETHERLANDS ORGANISATION FOR APPLIED SCIENTIFIC RESEARCH.

BOUDET, H., CLARKE, C., BUDGEN, D., MAIBACH, E., ROSER-RENOUF, C., & LEISEROWITZ, A. (2014). "FRACKING" CONTROVERSY AND COMMUNICATION: USING NATIONAL SURVEY DATA TO UNDERSTAND PUBLIC PERCEPTIONS OF HYDRAULIC FRACTURING. *ENERGY POLICY*, PP. 57-67.

BOX, G. (1979). ROBUSTNESS IN THE STRATEGY OF SCIENTIFIC MODEL BUILDING. IN R. LAUNER, & G. N. WIKINSON , *ROBUSTNESS IN STATISTICS* (PP. 201 - 236). ACADEMIC PRESS.

BRACKE, R. (2014). PETROTHERMALE NUTZUNG UND STIMULATIONSOPTIONEN. IN M. BAUER, W. FREEDEN, H. JACOBI, & T. NEU, *HANDBUCH TIEFE GEOTHERMIE* (PP. 268-269). BERLIN-HEIDELBERG: SPRINGER.

BRANDT, W. (2013). TRAINING COURSE ON GEOTHERMAL ELECTRICITY, SESSION V: DRILLING. *GEOELEC TRAINING COURSE.* POTSDAM: GERMAN RESEARCH CENTER FOR GEOSCIENCE.

BRÜNGER, C. (2011). *NUTZENKONSISTENTE RISIKOPRIORISIERUNG - DIE RISK-MAP IM KONTEXT RATIONALER ENTSCHEIDUNGEN.* WIESBADEN: GABLER VERLAG.

BUDNITZ, R. J., APOSTILAKIS, G., BOORE, D. M., CLUFF, L. S., COPPERSMITH, K. J., CORNELL, C. A., & MORRIS, P. A. (1997). *RECOMMENDATIONS FOR PROBABILISTIC SEISMIC HAZARD ANALYSIS: GUIDANCE ON UNCERTAINTY AND USE OF EXPERTS.* SENIOR SEISMIC HAZARD ANALYSIS COMMITTEE.

BUNDESMINISTERIUM FÜR JUSTIZ UND VERFASSUNGSSCHUTZ. (2018). *GESETZ FÜR DEN AUSBAU ERNEUERBARER ENERGIEN - EEG 2017.* BERLIN: BUNDESMINISTERIUM FÜR JUSTIZ UND VERFASSUNGSSCHUTZ.

BUNDESVERBAND GEOTHERMIE. (2018, JUNE 20). *MONTE CARLO SIMULATION*. RETRIEVED FROM HTTP://WWW.GEOTHERMIE.DE/WISSENSWELT/LEXIKON-DER-GEOTHERMIE/M/MONTE-CARLO-SIMULATION.HTML

CAPROS, P., DE VITA, A., TASIOS, N., SISKOS, P., KANNAVOU, M., PETROPOULOS, A., . . . KESTING, M. (2016). *EU REFERENCE SCENARIO 2016 - ENERGY, TRANSPORT AND GHG EMISSIONS - TRENDS TO 2050.* BRUXELLES: EUROPEAN COMISSION.

CARR-CORNISH, S., & ROMANACH, L. (2014). DIFFERENCES IN PUBLIC PERCEPTIONS OF GEOTHERMAL ENERGY TECHNOLOGY IN AUSTRALIA. *ENERGIES*, PP. 1555-1575.

CATALLI, F., COCCO, M., CONSOLE, R., & CHIARALUCE, L. (2008). *MODELING SEISMICITY RATE CHANGES DURIGN THE 1997 UMBRIA-MAARCHE SEQUENCE (CENTRAL ITALY) THROUGH RATE- AND STATE- DEPENDETN MODEL*. JOURNAL OF GEOPHYSICAL RESEARCH.

CHABORA, E., ZEMACH, E., SPIELMANN, P., DRAKOS, P., HICKMANN, S., LUTZ, S., . . . JARPE, S. (2012). HYDRAULIC STIMULATION OF WELL 27-15, DESERT PEAK GEOTHERMAL FIELD, NEVADA, USA. *PROCEEDINGS, THIRTY-SEVENTH WORKSHOP ON GEOTHERMAL RESERVOIR ENGINEERING*, 10.

CHACARTEGUI, R., SANCHEZ, D., MUNOZ, J., & SANCHEZ, T. (2009). ALTERNATIVE ORC BOTTOMING CYCLES FOR COMBINED CYCLE POWER PLANTS. *APPLIED ENERGY 86*, PP. 2162-2170.

CHEN, M., SUN, Y., FU, P., CARRIGAN, C., LU, Z., TONG, C., & BUSCHECK, T. (2013). SURROGATE-BASED OPTIMIZATION OF HYDRAULIC FRACTURING IN PRE-EXISTING FRACTURE NETWORKS. *COMPUTERS & GEOSCIENCES*, PP. 69-79.

CHENG, M., SUN, Y., FU, P., CARRIGAN, C., & LU, Z. (2012). UNCERTAINTY ANALYSIS OF SIMULATED HYDRAULIC FRACTURING. *AMERICAN GEOPHYSICAL UNION, FALL MEETING 2012.* SAN FRANCISCO: AMERICAN GEOPHYSICAL UNION.

CICHON, M. (2013, JULI 16). *RENEWABLE ENERGY WORLD.* RETRIEVED SEPTEMBER 26, 2018, FROM HTTPS://WWW.RENEWABLEENERGYWORLD.COM/ARTICLES/PRINT/VOLUME-16/ISSUE-4/GEOTHERMAL-ENERGY/IS-FRACKING-FOR-ENHANCED-GEOTHERMAL-SYSTEMS-THE-SAME-AS-FRACKING-FOR-NATURAL-GAS.HTML

CIVAN, V. (2007). *RESERVOIR FORMATION DAMAGE.* BURLINGTON: ELSEVIER.

COLLINGS, P., YU, Z., & WANG, E. (2016 ). A DYNAMIC ORGANIC RANKINE CYCLE USTING A ZEOTROPRIC MIXTURE AS THE WORKING FLUID WITH COMPOSITION TUNING TO MATCH CHANGEING AMBIENT CONDITIONS. *APPLIED ENERGY 171*, PP. 581-591.

COMMISSION, E. (2014). MITTEILUNG DER KOMMISSION AN DEN RAT UND DAS EUROPÄISCHE PARLAMENT ÜBER DIE EXPLORATION UND FÖRDERUNG VON KOHLENWASSERSTOFFEN (Z. B. SCHIEFERGAS) DURCH HOCHVOLUMEN-HYDROFRACKING IN DER EU . *52014DC0023*.

COOPERSMITH, E., DEAN, G., MCVEAN, J., & STORAUNE, E. (2010/2011). MAKING DECISIONS IN THE OIL AND GAS INDUSTRY. *OILFIELD REVIEW*.

CUENOT, N., & GENTER, A. (2015). MICROSEISMIC ACTIVITY INDUCED DURING RECENT CIRCULATION TESTS AT THE SOULTZ-SOUS-FORÊTS EGS POWER PLANT. *PROCEEDINGS WORLD GEOTHERMAL CONGRESS.* MELBOURNE: INTERNATIONAL GEOTHERMAL ASSOCIATION.

DALLAS, L. (1998). *USA PATENT NO. US5819851A.*

DELLA VEDOVA, B., PETRONIO, L., POLETTO, F., PALMIERI, F., & MARCON, A. (2013). RESERVOIR CHARACTERIZATION FOR THE COMPLETION OF THE GEOTHERMAL DISTRICT HEATING SYSTEM IN GRADO (NE ITALY). *EUROPEAN GEOTHERMAL CONGRESS.* PISA: EUROPEAN GEOTHERMAL ENERGY COUNCIL.

DEUTSCHES INISTUT FÜR NORMUNG E.V. (2011). *RISK MANAGEMENT – PRINCIPLES AND GUIDELINES (ISO 31000:2009).* BERLIN: BEUTH VERLAG.

DIEH, T., CLINTON, J., DEICHMANN, N., CAUZZI, C., KÄSTLI, P., KRAFT, T., . . . WIEMER, S. (2017). *EARTHQUAKES IN SWITZERLAND AND SORROUNDING REGIONS DURING 2015 AND 2016.* SWISS JOURNAL OF GEOSCIENCES.

DING, Y., LUO, P., LIU, X., & LIANG, L. (2018). WELLBORE STABILITY MODEL FOR HORIZONTAL WELLS IN SHALE FORMATIONS WITH MULTIPLE PLANES OF WEAKNESS. *JOURNAL OF NATURAL GAS SCIENCE AND ENGINEERING*.

DÖVÉNYI, P., HORVÁTH, F., LIEBE , P., GÁLFI, J., & ERKI, I. (1983). GEOTHERMAL CONDITIONS OF HUNGARY. *GEOPHYSICAL TRANSACTIONS*, PP. 3-114.

DOWD, A.-M., BOUGHEN, N., ASHWORTH, P., & CARR-CORNISH, S. (2011). GEOTHERMAL TECHNOLOGY IN AUSTRALIA:. *ENERGY POLICY*, PP. 6301–6307.

DRIELS, R., & SHIN, S. Y. (2004). *DETERMINING THE NUMBER OF ITERATIONS FOR MONTE CARLO SIMULATIONS OF WEAPON EFFECTIVENESS.* NAVAL POSTGRADUATE SCHOOL.

DUDAS, G. (2012). *VIZFÖLDTANI NAPLO.* GEOLOGICAL LOG REPORT, MEZÖBERENI.

DUNN, W. L., & SHULTIS, J. K. (2011). *EXPLORING MONTE CARLO METHODS.* AMSTERDAM: ELSEVIER.

EGBERTS, P., HEEDDERIK, J.-P., VAN DER MEER, M., & VERNOUX, J. F. (1995). MODELLING OF PERMEABILITY CHANGES IN ARGILLACEOUS SANDSTONES DUE TO FLUID INJECTION. PP. 1979-1983.

ELLIS, J., & HUENGES, E. (2016). *DESTRESS: MEETING MINUTES: 1ST PROGRESS MEETING.* POTSDAM: DESTRESS.

ENBW. (2015). *COST DATA ON THE SOULTZ-SOUS-FORÊTS GEOTHERMAL POWER PLANT (CONFIDENTIAL).*

EPPELBAUM, L., KUTASOV, I., & PILCHIN, A. (2014). *APPLIED GEOTHERMICS.* BERLIN: SPRINGER VIEWEG.

ERIC VAN OORT, J. V. (1993, AUGSUST). IMPAIRMENT BY SUSPENDED SOLIDS INVASION: TESTING AND PREDICTION. *SPE PRODUCTION & FACILITIES*, PP. 178-184.

ERTLE, S. (2018). *EVALUATION OF DIFFERENT HEAT PROVISION TECHNOLOGIES BASED ON LCOH - ENBW DISTRICT HEATING DEPARTMENT - UNPUBLISHED.* KARLSRUHE: ENERGIE BADEN-WÜRTTEMBERG AG.

EU. (2009). *RICHTLINIE 2009/125EG DES EUROPÄISCHEN PARLAMENTS UND DES RATES VOM 21. OKTOBER 2009 ZUR SCHAFFUNG EINES RAHMENS FÜR DIE FESTLEGUNG VON ANFORDERUNGEN AN DIE UMWELTGERECHTE GESTALTUNG ENERGIEVERBRAUCHSRELEVANTER PRODUKTE.* AMTSBLATT DER EUROPÄISCHEN UNION.

EU COMMISSION. (2014). *EU ANTI-CORRUPTION REPORT.* BRUSSELS.

EUROSTAT. (2018, MAY 29). *EUROSTAT*. RETRIEVED FROM HTTP://EC.EUROPA.EU/EUROSTAT/WEB/PRODUCTS-DATASETS/-NRG_PC_203

EUROSTAT. (2018A, AUGUST 02). *PRODUCER PRICES IN INDUSTRY, DOMESTIC MARKET.* RETRIEVED FROM HTTP://EC.EUROPA.EU/EUROSTAT/WEB/PURCHASING-POWER-PARITIES/DATA/DATABASE

EUROSTAT. (2018B, JULY 18). *HARMONISED INDEX OF CONSUMER PRICES (HICP).* RETRIEVED FROM HTTP://EC.EUROPA.EU/EUROSTAT/WEB/PRODUCTS-DATASETS/-/NRG_PC_205

EUROSTAT. (2018C, APRIL 13). *PURCHASING POWER PARITIES, PRICE LEVEL INDICES AND REAL EXPENDITURES FOR ESA 2010 AGGREGATES.* RETRIEVED FROM HTTP://EC.EUROPA.EU/EUROSTAT/WEB/PURCHASING-POWER-PARITIES/DATA/DATABASE

EUROSTAT. (2018D, MAY 25). *GAS PRICES FOR NON-HOUSEHOLD CONSUMERS.* RETRIEVED FROM HTTP://EC.EUROPA.EU/EUROSTAT/WEB/PRODUCTS-DATASETS/-/NRG_PC_203

EVANS, K. F., ZAPPONE, A., KRAFT, T., DEICHMANN, N., & MOIA, F. (2012). *A SURVEY OF THE INDUCED SEISMIC RESPONSES TO FLUID INJECTION IN GEOTHERMAL AND CO2 RESERVOIRS IN EUROPE.* GEOTHERMICS.

EYERER, S. (2018). VERIFICATION OF THE SIMULATION OF THE OBERHACHING GEOTHERMAL POWER PLANT. (S. WELTER, & C. BORMANN, INTERVIEWERS)

EYERER, S., SCHIFFLECHNER, C., HOFBAUER, S., WIELAND, C., ZOSSEDER, K., BAUER, W., . . . SPLIETHOFF, H. (2017). *POTENTIAL DER HYDROTHERMALEN GEOTHERMIE ZUR STROMERZEUGUNG IN DEUTSCHLAND.* GEOTHERMIE-ALLIANZ BAYER.

FABER, M., MAES, M. A., BAKER, J. W., VROUWENVELDER, T., & TAKADA, T. (2007). PRINCIPLES OF RISK ASSESSMENT OF ENGINEERED SYSTEMS. *APPLICATIONS OF STATISTICS AND PROBABILITY IN CIVIL ENGINEERING*.

FISCHER, T. (2010). *HYDRAULISCHE VERSUCHE UNTER GEOTHERMALEN BEDINGUNGEN AM BEISPIEL DER GEOTHERMIEANLAGE BRUCHSAL IM RAHMEN DES LOGRO-PROJEKTES.* KARLSRUHE: KARLSRUHE INSTITUTE OF TECHNOLOGY.

FLEISCHER, B. (2019). *SYSTEMEFFEKTE VON BIOENERGIE IN DER ELEKTRIZITÄTS- UND FERNWÄRMEWIRTSCHAFT.* STUTTGART: UNIVERSITÄT STUTTGART.

FÖRDERER, A., SEYFARTH, R., WELTER, S., KAYMAKCI, E., & KÖLBEL , T. (2018). *QUANTIFICATION OF RISK FACTORS IN SOFT STIMULATION ACTIVITIES.* KARLSRUHE: ENBW ENERGIE BADEN-WÜRTTEMBERG AG.

FRANCKE, H. (2014). *THERMO-HYDRAULIC MODEL OF THE TWO-PHASE FLOW IN THE BRINE CIRCUIT OF A GEOTHERMAL POWER PLANT.* BERLIN: TECHNISCHE UNIVERSITÄT BERLIN.

FREDRIKSSON, P., & SVENSSON, J. (2003). POLITICAL INSTABILITY, CORRUPTION AND POLICY FORMATION: THE CASE OF ENVIRONMENTAL POLICY. *JOURNAL OF PUBLIC ECONOMICS*, PP. 1383-1405.

FRICK, S., KALTSCHMITT, M., & SCHRÖDER, G. (2010). LIFE CYCLE ASSESSMENT OF GEOTHERMAL BINARY POWER PLANTS USING ENHANCED LOW-TEMPERATURE RESERVOIRS. *ENERGY 35*, PP. 2281 - 2294.

FROST, J. (2010). INTRODUCTION OF THE LINESHAFT DOWNHOLE GEOTHERMAL PUMP TO THE EUROPEAN INDUSTRY. *PROCEEDINGS, 2ND EUROPEAN GEOTHERMAL REVIEW.* MAINZ.

FROST, J. (2013). CASE HISTORY OF THE LINESHAFT DOWNHOLE GEOTHERMAL PUMP IN LADAU. *3RD EUROPEAN GEOTHERMAL REVIEW.* MAINZ.

FUKUMI, A. (2012). THE EFFECT OF POLITICAL INSTABILITY ON POWER SUBSIDIES: AN ANALYSIS OF INDIAN STATES. IN T. SATO, *THE BRICS AS REGIONAL ECONOMIC POWERS IN THE GLOBAL ECONOMY* (PP. 15-26).

GAUSMEIER, J., PFÄNDER, T., & LEHNER, A.-C. (2016). *STRATEGISCHE UNTERNEHMENSFÜHRUNG MIT SZENARIO-MANAGEMENT* (VOL. HANDBUCH UNTERNEHMENSORGANISATION). (D. SPATH, & E. WESTKÄMPER, EDS.) WIESBADEN: SPRINGER VERLAG.

GENTER, A. (2019, FEBRUARY 19). QUANTIFICATION OF THE EFFECT OF STIMULATIONS THROUGH MODELLING. (S. WELTER, INTERVIEWER)

GEO-LOG KFT. (2012). *HYDROGEOLOGICAL LOG-BOOK K-116.*

GEO-LOG KFT. (2012). *HYDROGEOLOGICAL LOG-BOOK K-116 MEZÖBERÉNY.*

GEO-LOG KFT. (2012). *WELL LOG INJECTION MEZÖBERÉNY.*

GEOTHERMIA EXPRESSZ KFT. (2016). *CONCEPTION PLAN MEZÖBERÉNY.*

GIARDINI, D. (2009). *GEOTHERMAL QUAKE RISK MUST BE FACED.* NATURE.

GIBOWICZ, S. J., & LASOCKI, S. (2001). *SEISMICITY INDUCED BY MINING: THEN YEARS LATER.* ADVANCES IN GEOPHYSICS.

GISCHIG, V. S., & WIEMER, S. (2013). *A STOCHASTIC MODEL FOR INDUCED SEISMICITY BASED ON NOLINEAR PRESSURE DIFFUSION AND IRREVERSIBLE PERMEABILITY ENHANCEMENT. .* GEOPHYSICAL JOURNAL INTERNATIONAL.

GLEIßNER, W. (2015). „SZENARIO-ANALYSE UND SIMULATION: EIN FALLBEISPIEL MIT EXCEL UND CRYSTAL BALL". IN R. GLEICH, S. GÄNßLEN, & H. LOSBICHLER, *CHALLENGE CONTROLLING 2015* (PP. 241-264).

GOOD ENERGY ALLIANCE IRELAND. (2018). *FRACKING IN FRANCE*. RETRIEVED 09 14, 2018, FROM HTTPS://GOODENERGIESALLIANCE.COM/FRACKING-IN-FRANCE/

GRANT, M. A., & BIXLEY, P. F. (2011). *GEOTHERMAL RESERVOIR ENGINEERING* (VOL. 2ND EDITION). AMSTERDAM: ELSEVIER.

GRAY, D., & REX, R. (1966). FORMATION DAMAGE IN SANDSTONES CAUSED BY CLAY DISPERSION AND MIGRATION. *CLAYS AND CLAY MINERALS*, PP. 355-366.

GUINOT, F. (2019, FEBRUARY 19). QUANTIFICATION OF THE EFFECT OF STIMULATIONS THROUGH MODELLING. (S. WELTER, INTERVIEWER)

GUTH, A. (2011). *MONTE-CARLO-SIMULATION DER STROMGESTEHUNGSKOSTEN IM OBERRHEINGRABEN.* KARLSRUHE: ENERGIE BADEN-WÜRRTEMBERG AG; KARLSRUHER INSTITUTE OF TECHNOLOGY.

HAAGORT, J. (2004). RAMEY'S WELLBORE HEAT TRANSMISSION REVISITED. *SPE JOURNAL*, PP. 465 - 474.

HEBERLE, F. (2013). *UNTERSUCHUNGEN ZUM EINSATZ VON ZEOTROPEN FLUIDGEMISCHEN IM ORGANIC RANKINE CYCLE FÜR DIE GEOTHERMISCHE STROMERZEUGUNG.* BAYREUTH: UNIVERSITÄT BAYREUTH.

HEBERLE, F., & BRÜGGEMANN, D. (2016). THERMO-ECONOMIC ANALYSIS OF ZEOTROPIC MIXTURES AND PURE WORKING FLUIDS IN ORGANIC RANKINE CYCLES FOR WASTE HEAT RECOVERY. *ENERGIES 9*, PP. 226-241.

HEHN, R. (2018, AUGUST 20). OPERATING DATA OF THE SOULTZ-SOUS-FORÊTS GEOTHERMAL POWER PLANT. (S. WELTER, INTERVIEWER)

HEIDINGER, P. (2010). INTEGRAL MODELING AND FINANCIAL IMPACT OF THE GEOTHERMAL SITUATION AND POWER PLANT AT SOULTZ-SOUS-FORÊTS. *COMPTES RENDUS GEOSCIENCE 342*, PP. 626 - 635.

HELD, S., GENTER, A., KOHL, T., KÖLBEL, T., SAUSSE, J., & SCHOENBALL, M. (2014). ECONOMIC EVALUATION OF GEOTHERMAL RESERVOIR PERFORMANCE THROUGH MODELING THE COMPLEXITY OF THE OPERATING EGS IN SOULTZ-SOUS-FORÊTS. *GEOTHERMICS 51*, PP. 270 – 280.

HERFELD, U. (2007). *MATRIX-BASIERTE VERKNÜPFUNG VON KOMPONENTEN UND FUNKTIONEN ZUR INTEGRATION VON KONSTRUKTION UND NUMLERISCHER SIMULATION.* MÜNCHEN: UNIVERSITÄT MÜNCHEN.

HICKMAN, S., & DAVATZES, N. (2010). IN-SITU STRESS AND FRACTURE CHARACTERIZATION FOR PLANNING OF AN EGS STIMULATION IN THE DESERT PEAK GEOTHERMAL FIELD, NEVADA. *THIRTY-FIFTH WORKSHOP ON GEOTHERMAL RESERVOIR ENGINEERING.* STANFORD, CA: USGS.

HOFFMANN, H. (2019, FEBRUARY 19). QUANTIFICATION OF THE EFFECT OF STIMULATIONS THROUGH MODELLING. (S. WELTER, INTERVIEWER)

HOLTHAUS, U. (2007). *ÖKONOMISCHES MODELL MIT RISIKOBETRACHTUNG FÜR DIE PROJEKTENTWICKLUNG.* DORTMUND: UNIVERSITÄT DORTMUND.

HONDO, H. (2005). LIFE CYCLE GHG EMISSION ANALYSIS OF POWER GENERATION SYSTEMS: JAPANESE CASE. *ENERGY 30*, PP. 2042 - 2056.

HORVÁTH, F., MUSITZ, B., BALÁZS, A., VÉGH, A., UHRIN, A., NÁDOR, A., . . . WÓRUM, G. (2015, JANUARY). EVOLUTION OF THE PANNONIAN BASIN AND ITS GEOTHERMAL RESOURCES. *GEOTHERMICS*, PP. 328-352.

HOTH, P., SEIBT, A., KELLNER, T., & HUENGES, E. (1997). *GEOWISSENSCHAFTLICHE BEWERTUNGSGRUNDLAGEN ZUR NUTZUNG HYDROGEOTHERMALER RESSOURCEN IN NORDDEUTSCHLAND.* POTSDAM: GERMAN RESEARCH CENTER FOR GEOSCIENCE.

HOWARD, R. A., & ABBAS, A. E. (2016). *FOUNDATIONS OF DECISION ANALYSIS.* BOSTON: PEARSON.

HUBER, M. L., PERKINS, R. A., FRIEND, D. G., SENGERS, J. V., ASSAEL, M. J., METAXA, I. N., . . . VOGEL, E. (2012). NEW INTERNATIONAL FORMULATION FOR THE THERMAL CONDUCTIVITY OF H2O. *JOURNAL OF PHYSICAL AND CHEMICAL REFERENCE DATA*.

HUENGES, E., & ELLIS, J. (2016, 11 01). *DESTRESS PROJECT WEBSITE.* RETRIEVED FROM ABOUT: HTTP://WWW.DESTRESS-H2020.EU/EN/WHO-WE-ARE/ABOUT/

HUIJTS, N., MOLIN, E., & STEG, L. (2012). PSYCHOLOGICAL FACTORS INFLUENCING SUSTAINABLE ENERGY TECHNOLOGY ACCEPTANCE: A REVIEW-BASED COMPREHENSIVE FRAMEWORK. *RENEWABLE & SUSTAINABLE ENERGY REVIEWS*, PP. 525–531.

HUSEN, S., BACHMANN, C., & GIARDINI, D. (2007). *LOCALLY TRIGGERED SEISMICITY IN THE CENTRAL SWISS ALPS FOLLOWING THE LARGE RAINFALL EVEN OF AUGUST 2005.* GEOPHYSICAL JOURNAL INTERNATIONAL.

IEA; NEA; OECD. (2015). *INTERNATIONAL ENERGY AGENCY, NUCLEAR ENERGY AGENCY AND ORGANISATION FOR ECONOMIC CO-OPERATION AND DEVELOPMENT: PROJECTED COSTS OF GENERATING ELECTRICITY.*

IZGEC, O., DEMIRAL, B., BERTIN, H., & AKIN, S. (2006). EXPERIMENTAL AND NUMERICAL MODELING OF DIRECT INJECTION OF CO2 INTO CARBONATE FORMATIONS. *SOCIETY OF PETROLEUM ENGINEERS*, PP. 1-16.

JAKOBY, W. (2013). *PROJEKTMANAGEMENT FÜR INGENIEURE.* WIESBADEN: SPRINGER VERLAG.

JANCZIK, S. (2014). *TIEFE GEOTHERMIE IN DEUTSCHLAND - EINE ENERGIEWIRTSCHAFTLICHE ANALYSE DES STANDES UND MÖGLICHER ENTWICKLUNGEN.* HAMBURG: VERLAG DR. KOVAC.

JONES JR., F. (1964). INFLUENCE OF CHEMICAL COMPOSITION OF WATER ON CLAY BLOCKING OF PERMEABILITY. *JOURNAL OF PETROLEUM TECHNOLOGY*, PP. 441-446.

JONES, T., & DETWILER, R. (2016). FRACTURE SEALING BY MINERAL PRECIPITATION: THE ROLE OF SMALL-SCALE MINERAL HETEROGENEITY. *GEOPHYSICAL RESEARCH LETTERS*, PP. 7564–7571.

JONKMAN, R., BOS, C. F., BREUNESE, J. N., MORGAN, D. T., & SPENCER, J. A. (2000). BEST PRACTICES AND METHODS IN HYDROCARBON RESOURCE ESTIMATION, PRODUCTION AND EMISSIONS FORECASTING, UNCERTAINTY EVALUATION AND DECISION MAKING. *SOCIETY OF PETROLEUM ENGINEERS*.

JUNG, R., RÖHLING, S., OCHMANN, N., ROGGE, S., SCHELLSCHMIDT, R., SCHULZ, R., & THIELEMANN, T. (2002). *ABSCHÄTZUNG DES TECHNISCHEN POTENZIALS DER GETHERMISCHEN STROMERZEUGUNG UND DER GEOTHERMISCHEN KRAFT-WÄRMEKOPPLUNG (KWK) IN DEUTSCHLAND.* HANNOVER: BUNDESANSTALT FÜR GEOWISSENSCHAFTEN UND ROHSTOFFE.

KEMP, I. C. (2007). *PINCH ANALYSIS AND PROCESS INTEGRATION (SECOND EDITION).* OXFORD: BUTTERWORTH-HEINEMANN.

KERN, D. Q. (1950). *PROCESS HEAT TRANSFER.* MCGRAW HILL.

KFT., GEO-LOG. (2012). *HYDROGEOLOGICAL LOG-BOOK K-116 MEZÖBERÉNY.*

KHILAR, K., & FOGLER, H. (1984). THE EXISTENCE OF A CRITICAL SALT CONCENTRATION FOR PARTICLE RELEASE. *JOURNAL OF COLLOID AND INTERFACE SCIENCE*, PP. 214-224.

KHILAR, K., VAIDYA, R., & FOGLER, H. (1990). COLLOIDALLY-INDUCED FINES RELEASE IN POROUS MEDIA. *JOURNAL OF PETROLEUM SCIENCE AND ENGINEERING*, PP. 213-221.

KIND, M., & SAITO, Y. (2013). *STRÖMUNGSSIEDEN VON GEMISCHEN, VDI WÄRMEATLAS.* VDI-GESELLSCHAFT FÜR VERFAHRENSTECHNIK UND CHEMIEINGENIEURWESEN.

KONSTANTIN, P. (2013). *PRAXISBUCH ENERGIEWIRTSCHAFT – ENERGIEUMWANDLUNG, -TRANSPORT UND -BESCHAFFUNG IM LIBERALISIERTEN MARKT.* HEIDELBERG: SPRINGER-VERLAG.

KONSTANTIN, P. (2017). *PRAXISBUCH ENERGIEWIRTSCHAFT.* SPRINGER VERLAG.

KROON, I. B., & MAES, M. A. (2008). *BACKGROUND DOCUMENTS ON RISK ASSESSMENT IN ENGINEERING . THEORETICAL FRAMEWORK FOR RISK ASSESSMENT AND EVALUATION.* CALGARY: JOINT COMMITEE OF STRUCTURAL SAFETY.

KRUSEMANN, G. P., & DE RIDDER, N. A. (2000). *ANALYSIS AND EVALUATION OF PUMPING TEST DATA .* INTERNATIONAL INSTITUTE FOR LAND RECLAMATION AND IMPROVEMENT.

LAUX, H., SCHENK-MATHES, H. Y., & GILLENKIRCH, R. M. (2012). *ENTSCHEIDUNGSTHEORIE.* BERLIN: SPRINGER VERLAG.

LEGARTH, B. A. (2003). *ERSCHLIEßUNG SEDIMENTÄRER SPEICHERGESTEINE FÜR EINE GEOTHERMISCHE STROMERZEUGUNG.* BERLIN: TECHNISCHE UNIVERSITÄT BERLIN.

LEMMENS, S. (2015). A PERSPECTIVE ON COSTS AND COST ESTIMATION TECHNIQUES FOR ORGANIC RANKINE. *3RD INTERNATIONAL SEMINAR ON ORC POWER SYSTEMS.* BRUSSELS.

LEMMON, E. W., & JACOBSEN, R. T. (2004). VISCOSITY AND THERMAL CONDUCTIVITY EQUATIONS FOR NITROGEN, OXYGEN, ARGON, AND AIR. *INTERNATIONAL JOURNAL OF THERMOPHYSICS 25*, PP. 21-69.

LEMMON, E. W., HUBER, M. L., & MCLINDEN, M. O. (2013). NIST STANDARD REFERENCE DATABASE 23: REFERENCE FLUID THERMODYNAMIC AND TRANSPORT PROPERTIES REFPROP, VERSION 9.1. *NATIONAL INSTITUE OF STANDARDS AND TECHNOLOGY*.

LEMMON, E. W., JACOBSEN, R. T., PENONCELLO, S. G., & FRIEND, D. G. (2000). THERMODYNAMIC PROPERTIES OF AIR AND MIXTURES OF NITROGEN, ARGON, OXYGEN FROM 60 TO 2000K AT PRESSURES TO 2000MPA. *JOURNAL OF PHYSICAL AND CHEMICAL REFERENCE DATA 29*, PP. 331-385.

LEWITZ, O. (2010). WARUM PROJEKTE EINEN BUSINESS CASE BRAUCHEN. IN K.-P. FÄHNRICH, & B. FRANCZYK, *INFORMATIK 2010. SERVICE SCIENCE - NEUE PERSPEKTIVEN FÜR DIE INFORMATIK. BAND 2* (P. 1005). BONN: GESELLSCHAFT FÜR INFORMATIK.

LI, L., AL-MUNTASHERI, G., & LIANG, F. (2016). A REVIEW OF CROSSLINKED FRACTURING FLUIDS PREPARED WITH PRODUCED WATER. *PETROLEUM*, PP. 313-323.

LI, W., DONG, Z., & WANG, C. (2017). *RISK ASSESSMENT FOR GROUNDWATER CONTAMINATION FROM HYDRAULIC FRACTURED SHALE TO AQUIFERS.* ABU DHABI: SOCIETY OF PETROLEUM ENGINEERS.

LINDI, O. (2017). ANALYSIS OF KICK DETECTION METHODS IN THE LIGHT OF ACTUAL BLOWOUT DISASTERS. *M.SC. THESIS*. NORWEGIAN UNIVERSITY OF SCIENCE AND TECHNOLOGY.

LIU, R., MENTZER, R., MANNAN, S., & HASAN, R. (2014). CONSEQUENCE ANALYSIS OF UNCONTROLLED FLUID FLOW IN WELLBORE. *SYMPOSIUM SERIES NO. 159 HAZARDS 24*. INSTITUTION OF CHEMICAL ENGINEERS.

LOBIANCO, L. F., & WARDANI, W. (2010). ELECTRICAL SUBMERSIBLE PUMPS FOR GEOTHERMAL APPLICATIONS,. *PROCEEDINGS, 2ND EUROPEAN GEOTHERMAL REVIEW*. MAINZ.

LUKYANOW, A., & CHUGUNOV, N. (2015). UNCERTAINTY ANALYSIS FOR HYDRAULIC FRACTURING MODELING IN CONTAINING OIL AND GAS. *AIP CONFERENCE PROCEEDINGS.* AMERICAN INSTITUTE OF PHYSICS.

MACKAY, E. (2003). PWRI: SCALE FORMATION RISK ASSESSMENT AND MANAGEMENT. *SPE 5TH INTERNATIONAL SYMPOSIUM ON OILFIELD SCALE.* ABERDEEN: SOCIETY OF PETROLEUM ENGINEERS.

MACMILLAN, F. (2000). *RISK, UNCERTAINTY AND INVESTMENT DECISION-MAKING IN THE UPSTREAM OIL AND GAS INDUSTRY.* ABERDEEN: UNIVERSITY OF ABERDEEN.

MAJER, E. L., NELSON, J., ROBERTSON-TAIT, A., SAVY, J., & WONG, I. (2013). *BEST PRACTICES FOR ADRESSING INDUCED SEISMICITY ASSOCIATED WITH ENHANCED GEOTHERMAL SYSTEMS (EGS).* LAWRENCE BERKELEY NATIONAL LABORATORY.

MAJER, E., BARIA, R., STARK, M., OATES, S., BOMMER, J., & SMITH, B. H. (2007). *INDUCED SEISMICITY ASSOCIATED WITH ENHANCED GEOTHERMAL SYSTEMS.* SCIENCE DIRECT.

MARTÍNEZ-GARZÓN , P., KWIATEK, G., SONE, H., BOHNHOFF, H., DRESEN, G., & HARTLINE, C. (2014). *SPATIOTEMPORAL CHANGES, FAULTING REGIMES, AND SOURCE PARAMETERS OF INDUCED SEISMICITY: A CASE STUDY FROM THE GEYSERS GEOTHERMAL FIELD.* JOURNAL OF GEOPHYSICAL RESEARCH: SOLID EARTH.

MEGIES, T., & WASSERMANN, J. (2014). MICROSEISMICITY OBSERVED AT A NON-PRESSURE-STIMULATED GEOTHERMAL POWER PLANT. *GEOTHERMICS*, PP. 36-49.

MOUCHOT, J., RAVIER, G., SEIBEL, O., & PRATIWI, A. (2019). DEEP GEOTHERMAL PLANTS OPERATION IN UPPER RHINE GRABEN: LESSONS LEARNED. *EUROPEAN GEOTHERMAL CONGRESS 2019.* DEN HAAG: EUROPEAN GEOTHERMAL ENERGY COUNCIL.

MOUCHOT, J., GENTER, A., CUENOT, N., SCHEIBER, J., SEIBEL, O., BOSIER, C., & RAVIER, G. (2018). FIRST YEAR OF OPERATION FROM EGS GEOTHERMAL PLANTS IN ALSACE, FRANCE: SCALING ISSUES. *PROCEEDINGS, 43RD WORKSHOP ON GEOTHERMAL RESERVOIR ENGINEERING.* STANFORD: STANFORD UNIVERSITY.

MUNTENDAM-BOS, A. G., ROEST, J. P., & DE WAAL, J. A. (2015). *A GUIDELINE FOR ASSESSING SEISMIC RISK INDICED BY GAS EXTRACTION IN THE NETHERLANDS.* THE LEADING EDGE.

NAMI, P., SCHELLSCHMIDT, R., SCHINDLER, M., & TISCHNER, T. (2008). CHEMICAL STIMULATION OPERATIONS FOR RESERVOIR DEVELOPMENT OF THE DEEP CRYSTALINE HDR/EGS SYSTEM AT SOULTZ-SOUS-FORÊTS. *PROCEEDINGS OF THE THIRTY-THIRD WORKSHOP ON GEOTHERMAL RESERVOIR ENGINEERING STANFORD UNIVERSITY* (PP. 296 - 306). STANFORD: STANFORD UNIVERSITY.

NATURAL RESOURCE DEFENSE COUNCIL (NRDC). (2012, JULI). *HYDRAULIC FRACTURING CAN POTENTIALLY CONTAMINATE DRINKING WATER SOURCES.* RETRIEVED SEPTEMBER 25, 2018, FROM HTTPS://WWW.NRDC.ORG/SITES/DEFAULT/FILES/FRACKING-DRINKING-WATER-FS.PDF

NGUGI, P. K. (2002). *TECHNICAL, ECONOMIC AND INSTITUTIONAL EVALUATION OF ADOPTING DIRECTIONAL DRILLING BY KENGEN.* REYKJAVÍK: UNITED NATIONS UNIVERSITY – GEOTHERMAL TRAINING PROGRAMM.

OCEAN DRILLING PROGRAMME. (2004). ODP LOGGING MANUAL.

OCHI, J., & VERNOUX, J. (1996). ORIGIN OF PERMEABILITY REDUCTION UNDER HIGH-FLOW-RATE INJECTION CONDITIONS. *BRGM*, PP. 637-650.

OERTEL, H., & REVIOL, M. B. (2015). *STRÖMUNGSMECHANIK FÜR INGENIEURE UND NATURWISSENSCHAFTLER.* WIESBADEN: SPRINGER VIEWEG.

OSBORN, S. G., VENGOSH, A., WARNER, N. R., & JACKSON, R. B. (2011). *METHANE CONTAMINATION OF DRINKING WATER ACCMOPANYSING GAS-WELL DRILLING AND HYDRAULIC FRACTURING.* PROCEEDINGS OF THE NATIONAL ACADEMY OF SCIENCES OF THE UNITED STATES OF AMERICA.

PAYERA, S. (2018). UNDERSTANDING SOCIAL ACCEPTANCE OF GEOTHERMAL ENERGY: CASE STUDY FOR ARAUCANIA REGION, CHILE. *GEOTHERMICS*, PP. 138-144.

PERKINS, R. A. (2002). MEASUREMENT AND CORRELATION OF THE THERMAL CONDUCTIVITY OF ISOBUTANE FROM 114K TO 600K AT PRESSUERS TO 70MPA. *JOURNAL OF CHEMICAL & ENGINEERING DATA 47*, PP. 1272-1279.

PERRIN, J., & COOK, T. (2016). *US ENERGY INFORMATION ADMINISTRATION*. RETRIEVED FROM HYDRAULICALLY FRACTURED WELLS PROVIDE TWO-THIRDS OF U.S. NATURAL GAS PRODUCTION: HTTPS://WWW.EIA.GOV/TODAYINENERGY/DETAIL.PHP?ID=26112

PORTIER, S., VUATAZ, F., NAMI, P., SANJUAN, B., & GÉRARD, A. (2009, JULI 30). CHEMICAL STIMULATION TECHNIQUES FOR GEOTHERMAL WELLS: EXPERIMENTS ON THE THREE-WELL EGS SYSTEM AT SOULTZ-SOUS-FORÊTS, FRANCE. *GEOTHERMICS 38*, PP. 349-359.

QUIRK, J., & SCHOFIELD, R. (1955). THE EFFECT OF ELECTROLYTE CONCENTRATION ON SOIL PERMEABILITY. *JOURNAL OF SOIL SCIENCE*, P. 163.

R. DRIELS, M., & S. SHIN, Y. (2004). *DETERMINING THE NUMBER OF ITERATIONS FOR MONTE CARLO SIMULATIONS OF WEAPON EFFECTIVENESS.* NAVAL POSTGRADUATE SCHOOL .

RAMEY, H. J. (1962). WELLBORE HEAT TRANSMISSION. *JOURNAL OF PETROLEUM TECHNOLOGY, 14*, PP. 427 - 435.

RAVIER, G. (2019). SUPPORT SCHEME FOR GEOTHERMAL ENERGY IN FRANCE. (S. WELTER, INTERVIEWER)

RAVIER, G., GRAF, J. J., & VILLADANGOS, G. (2015). OPERATING A LINESHAFT PRODUCTION PUMP IN A SMALL PUMP CHAMBER UNDER HIGHLY AGGRESSIVE GEOTHERMAL FLUID CONDITIONS: RESULTS FROM THE SOULTZ EGS SITE. *PROCEEDINGS OF THE WORLD GEOTHERMAL CONGRESS.* MELBOURNE.

REITH, S. (2015). TECHNO-ECONOMIC ANALYSIS OF DIFFERENT DRILLING CONCEPTS IN A HOLISTIC MODEL OF A GEOTHERMAL POWER PLANT. *DER GEOTHERMIEKONGRESS.* ESSEN: BUNDESVERBAND GEOTHERMIE GERMANY.

REITH, S. (2018A). *TECHNISCH-ÖKONOMISCHE ANALYSE DER ENERGIEGEWINNUNG AUS TIEFENGEOTHERMIE IN DEUTSCHLAND.* STUTTGART: UNIVERSITÄT STUTTGART.

REITH, S., HEHN, R., MERGNER , H., & KÖLBEL, T. (2017). *SYSTEMATIC PREPARATION OF THE TECHNO-ECONOMIC EVALUATION OF SOFT STIMULATION.* POTSDAM: DESTRESS CONSORTIUM.

REITH, S., KÖLBEL, T., SCHLAGERMANN, P., PELLIZZONE, A., & ALLANSDOTTIR, A. (2013). *PUBLIC ACCEPTANCE OF GEOTHERMAL.* GEOELEC.

REITH, S., SIEFERT, D., MERGNER, H., KÖLBEL , T., & MÜNCH, W. (2018). RISK FACTORS WITHIN TECHNO-ECONOMIC EVALUATION OF SOFT-STIMULATION MEASURES. *PROCEEDINGS OF THE 43RD WORKSHOP ON GEOTHERMAL RESERVOIR ENGINEERING.* STANFORD: STANFORD UNIVERSITY.

ROYDEN, L. H., HORVATH, F., & BUCHFIEL, B. (1982, AUGUST). TRANSFORM FAULTING, ENTENSION AND SUBDUCTION IN THE CARPATHIAN PANNONIAN REGION. *GEOLOGICAL SOCIETY OF AMERICA*, PP. 717-725.

RÜKHAAK, W., LIANG, P., BARTELS, J., HELDMANN, C.-D., HOMUTH, S., & SASS, I. (2015, APRIL). THERMO-HYDRO-MECHANICAL-CHEMICAL COUPLED MODELING OF GEOTHERMAL DOUBLET SYSTEMS IN LIMESTONES. PP. 1-11.

SALMAN, H. (2015). HYDRAULIC FRACTURING DESIGN: BEST PRACTICES FOR A FIELD DEVELOPMENT PLAN. LISBOA.

SANJUAN, B., MILLOT, R., INNOCENT, C., DEZAYES, C., SCHEIBER, J., & BRACH, M. (2016). MAJOR GEOCHEMICAL CHARACTERISTICS OF GEOTHERMAL BRINES FROM THE UPPER RHINE GRABEN GRANITIV BASEMENT WIRH CONSTRAINTS ON TEMPERATURE AND CIRCULATION. *CHEMICAL GEOLGY 428*, PP. 27-47.

SCHAWEL, C., & BILLING, F. (2014). *TOP 100 MANAGEMENT TOOLS.* WIESBADEN: SPRINGER VERLAG.

SCHEIBER, J. (2018). OPERATION PARAMETERS FOR THE SOUTLZ-SOUS-FORÊTS PLANT. (S. WELTER, & C. BORMANN, INTERVIEWERS)

SCHEIBER, J., NITSCHKE, F., SEIBT, A., & GENTER, A. (2012). GEOCHEMICAL AND MINERALOGICAL MONITORING OF THE GEOTHERMAL POWER PLANT IN SOULTZ SOUS FORETS (FRANCE). *PROCEEDINGS, THIRTY-SEVENTH WORKSHOP ON GEOTHERMAL RESERVOIR ENGINEERING.* STANFORD, CA.

SCHIEFER, H., & SCHIEFER, F. (2018). *STATISTICS FOR ENGINEERS.* SPRINGER VIEWEG.

SCHILL, E., CUENOT, M., & KOHL, T. (2015). REVIEW OF THE HYDRAULIC DEVELOPMENT IN THE MULTI-RESERVOIR / MULTI-WELL EGS-PROJECT OF SOULTZ-SOUS-FORÊTS. *PROCEEDING OF THE WORLD GEOTHERMAL CONGRESS.* MELBOURNE: INTERNATIONAL GEOTHERMAL ASSOCIATION.

SCHILL, E., GENTER, A., CUENOT, N., & KOHL, T. (2017). HYDRAULIC PERFORMANCE HISTORY AT THE SOULTZ EGS RESERVOIRS FROM STIMULATION AND LONG-TERM CIRCULATION TESTS. *GEOTHERMICS 70*, PP. 110 - 124.

SCHLAGERMANN, P. (2014). *EXERGOÖKONOMISCHE ANALYSE GEOTHERMISCHER STROMBEREITSTELLUNG AM BEISPIEL DES OBERRHEINGRABENS.* MÜNCHEN: TECHNISCHE UNIVERSITÄT MÜNCHEN.

SCHMIDT, R., BUCHER, K. M., & STOBER, I. (2017B). REACTIVITY OF GEOTHERMAL RESERVOIR ROCKS UNDER TEMPERATURE CONDITIONS FOUND IN THE UPPER RHINE GRABEN (GERMANY). *PROCEDIA EARTH AND PLANETARY SCIENCE*, PP. 881-884.

SCHMIDT, R., BUCHER, K., DRÜPPEL, K., MUNDHENK, & STOBER, I. (2017A). EXPERIMENTAL INTERACTION OF HYDROTHERMAL NA-CL SOLUTION WITH FRACTURE SURFACES OF GEOTHERMAL RESERVOIR SANDSTONE OF THE UPPER RHINE GRABEN. *APPLIED GEOCHEMISTRY*, PP. 36-52.

SCHRÖDER, H., & SCHNEIDER, J. (2014). TIEFPUMPEN ZUR STEIGERUNG DER WIRTSCHAFTLICHKEIT IN DER TIEFEN GEOTHERMIE. *UMWELTTECHNOLOGIE UND ENERGIE IN BAYERN*.

SCHULZ, R., & JOBMANN, M. (1989). *HYDROGEOTHERMISCHE ENERGIEBILANZ UND GRUNDWASSERHAUSHALT DES MALMKARSTES IM SÜDDEUTSCHEN MOLASSEBECKEN - TEILGEBIET: HYDROGEOTHERMIK.* HANNOVER: BUNDESMINISTERIUM FÜR FORSCHUNG UND TECHNOLOGIE.

SEIBEL, O. (2018). OPERATION DATA SOULTZ-SOUS-FORÊTS. (S. WELTER, & C. BORMANN, INTERVIEWERS)

SEITZ, J. (2015). *ERARBEITUNG EINES INVESTITIONSKOSTENMODELLS MIT FALLSPEZIFISCHEN EINGANGSVARIABLEN FÜR TIEFENGEOTHERMISCHE STROM- UND WÄRMEERZEUGUNG IN NIEDERENTHALPIEGEBIETEN.* STUTTGART: MASTER'S THESIS, UNIVERSITÄT STUTTGART.

SHAH, M. (1979). A GENERAL CORRELATION FOR HEAT TRANSFER DURING FILM CONDENSATION. *INTERNATIONAL JOURNAL OF HEAT AND MASS TRANSFER 22*, PP. 547 – 556.

SHALE GAS INFORMATION PLATFORM, & GFZ POTSDAM. (2018). *FRACTURING-FLÜSSIGKEITEN: ZUSAMMENSETZUNG UND NUTZUNG*. RETRIEVED FROM SHIP - SHALE GAS INFORMATION PLATFORM: HTTP://WWW.SHALE-GAS-INFORMATION-PLATFORM.ORG/DE/CATEGORIES/GRUNDWASSERSCHUTZ/GRUNDLAGEN/FRACTURING-FLUIDE/

SHUTONG, P. (1997, SEPTEMBER). A MODEL FOR PREDICTING INJECTIVITY DECLINE IN WATER-INJECTION WELLS. *SPE FOMATION EVALUATION*, PP. 194-201.

SIEDER, E. N., & TATE, G. E. (1936). HEAT TRANSFER AND PRESSURE DROP OF LIQUIDS IN TUBES. *INDUSTRIAL & ENGINEERING CHEMISTRY 28*, PP. 1429-1435.

SIKLÓSI. (2017). *INTERNAL REPORT.*

SOTTILOTTA, C. (2013). CONCEPT AND MEASUREMENT OF POLITICAL RISK: FROM THEORY TO PRACTICE. ROME, ITALY: LIBERA UNIVERSITA INTERNAZIONALE DEGLI STUDI SOCIALI.

SPETZLER , C., WINTER, H., & MEYER, J. (2016). *DECISION QUALITY - VALUE CREATION FROM BETTER BUSINESS DECISSIONS.* HOBOKEN: WILEY PUBLISHER.

STOBER, I., & BUCHER, K. (2014). *GEOTHERMIE.* FREIBURG: SPRINGER SPEKTRUM.

SYSTEMAIR. (2018, 06 19). *VENTILATOREN UND ZUBEHÖR (KATALOG)*. RETRIEVED FROM HTTPS://WWW.SYSTEMAIR.COM/DE/DEUTSCHLAND/SUPPORT/

SZANYI, J., KOVÁCS, B., MEDGYES, T., KÓBOR, T., KURUNCZI, M., & VASS, I. (2010). INJECTION OF THERMAL WATER INTO POROUS RESERVOIRS. *PROCEEDINGS WORLD GEOTHERMAL CONGRESS*, (PP. 51-58). BALI.

THE DUTCH STATE SUPERVISION OF MINES (SSM). (2015). *HAZARD AND RISK ASSESSMENT FOR INDUCED SEISMICITY GRONINGEN -UPDATE 1ST MAY 2015.*

TOFFOLO, A., LAZZARETTO, A., MANENTE, G., & PACI, M. (2014). A MULTI-CRITERIA APPROACH FOR THE OPTIMAL SELECTION OF WORKING FLUID AND DESIGN PARAMETERS IN ORGANIC RANKINE CYCLE SYSTEMS. *APPLIED ENERGY 121*, PP. 219-232.

TOTH, A. (2010). STEAM BLOWOUT FROM AN OVER PRESSURE GEOTHERMAL RESERVOIR IN HUNGARY. *THIRTY-FIFTH WORKSHOP ON GEOTHERMAL RESERVOIR ENGINEERING.* STANFORD, CA.

TÓTH, A. (2012). GEOTHERMAL ENERGY PRODUCTION AND UTILIZATION IN HUNGARY. *GEOSCIENCE AND ENGINEERING*, PP. 315-319.

TÓTH, A. N. (2016). GEOTHERMAL ENERGY IN HUNGARY.

TOWLER, G., & SINNOTT, R. (2013). *CHAPTER 19 - HEAT TRANSFER EQUIPMENT, CHEMICAL ENGINEERING DESIGN.* BOSTON: BUTTERWORTH-HEINEMANN.

TURBODEM. (2015). DESIGN DATA ORC SOULTZ-SOUS-FORETS (CONFIDENTIAL).

TURTON ET AL. . (2013). *ANALYSIS, SYNTHESIS, AND DESIGN OF CHEMICAL PROCESSES.* PEARSON EDUCATION INC.

TURTON, R., BAILIE, R. C., WHITING, W. B., SHAEIWITZ, J. A., & BHATTACHARYYA, D. (2013). *ANALYSIS, SYNTHESIS, AND DESIGN OF CHEMICAL PROCESSES.* PEARSON EDUCATION INC.

UNGEMACH, P. (2003, MAY). REINJECTION OF COOLED GEOTHERMAL BRINES INTO SANDSTONE RESERVOIRS. *GEOTHERMICS*, PP. 743–761.

UNGEMACH, P., & ROQUE, C. (1988, AUGUST). CORROSION AND SCALING OF GEOTHERMAL WELLS INF THE PARIS BASIN. DAMAGE, DIAGONISIS, REMOVAL AND INHIBITION.

US CENSUS BUREAU. (2013). *DATA*. RETRIEVED 09 03, 2018, FROM HTTPS://WWW.CENSUS.GOV/DATA.HTML

VAN EIJS, R. M., MULDERS, F. M., NEPVEU, M., KENTER, C. J., & SCHEFFERS, B. C. (2006). *CORRELAITON BETWEEN HYDROCARBON RESERVOIR PROPERTIES AND INDUCED SEISMICITY IN THE NETHERLANDS.* ENGINEERING GEOLOGY.

VETTER, O., KANDARPA, V., STATTOM, M., & VEITH, E. (1987, FEBRUARY). PARTICLE INVASION INTO POROUS MEDIUM AND RELEATED INJECTIVITY PROBLEMS. *SPE PAPERS*, PP. 101-120.

VLCEK, J., EISNER, L., STABILE, T., & TELESCA, L. (2017). *TEMPORAL RELATIONSHIP BETWEEN INJECTION RATES AND INDUCED SEISMICITY.* SPRINGER INTERNATIONAL PUBLISHING AG.

VOGEL, E., KÜCHENMEISTER, C., & BICH, E. (2000). VISCOSITY CORRELATIONS FOR ISOBUTANE OVER WIDE RANGES OF THE FLUID REGION. *INTERNATIONAL JOURNAL OF THERMOPHYSICS 21*, PP. 343-356.

WAGNER, W. (2004). *WÄRMEÜBETRAGUNG.* VOGEL BUCHVERLAG.

WANG, X.-Q., LI, X.-P., LI, Y.-R., & WU, C.-M. (2015). PAYBACK PERIOD ESTIMATION AND PARAMETER OPTIMIZATION OF SUBCRITICAL ORGANIC RANKINE CYCLE SYSTEM FOR WASTE HEAT RECOVERY. *ENERGY 88*, PP. 734-745.

WELTER, S. (2018). *TECHNISCH-ÖKONOMISCHE ANALYSE DER ENERGIEGEWINNUNG AUS TIEFENGEOTHERMIE IN DEUTSCHLAND.* STUTTGART: UNIVERSITÄT STUTTGART.

WELTER, S., BREHME, M., NOWAK, K., KAYMAKCI, E., & KÖLBEL, T. (2019). *IDENTIFICATION AND QUANTIFICATION OF RISK MITIGATION MEASURES WITH RESPECT TO SOFT SIMULATION TECHNIQUE BASED ON RELEVANT TECHNICAL NON-TECHNICAL FACTORS.* POTSDAM: DESTRESS RESEARCH PROJECT.

WHITE, C. (2012). THE CONTEXT OF PUBLIC ACCEPTANCE OF HYDRAULIC FRACTURING: IS LOUISIANA UNIQUE? LOUISIANA STATE UNIVERSITY.

WIEMER, S., KRAFT, T., TRUTNEVYTE , E., & ROTH, P. (2017). *"GOOD PRACTICE" GUIDE FOR MANAGING INDUCED SEISMICITY IN DEEP GEOTHERMAL ENERGY PROJECTS IN SWITZERLAND.* SWISS SEISMOLOGICAL SERVICE (SED).

WOLF, P., & KIRCHNER, G. (2013). *VDI-WÄRMEATLAS, KONSTRUKTIVE HINWEISE FÜR DEN BAU VON WÄRMEÜBERTRAGERN.* VDI-GESELLSCHAFT VERFAHRENSTECHNIK UND CHEMIEINGENIEURWESEN.

YOU, Z., YANG, Y., BADALYAN, A., BEDRIKOVETSKY, P., & HAND, M. (2016). MATHEMATICAL MODELLING OF FINES MIGRATION IN GEOTHERMAL RESERVOIRS. *GEOTHERMICS*, PP. 123-133.

ZIMEMRMANN, G. (2019, FEBRUARY 19). QUANTIFICATION OF THE EFFECT OF STIMULATIONS THROUGH MODELLING. (S. WELTER, INTERVIEWER)

ZIMMERMANN, G., BLÖCHER, G., & HUENGES, E. (2012). ENHANCED GEOTHERMAL SYSTEMS (EGS) - POTENTIAL AND STIMULATION TREATMENTS. *VORTRÄGE AUF DER DPG-FRÜHJAHRSTAGUNG - ARBEITSKREIS ENERGIE IN DER DEUTSCHEN PHYSIKALISCHEN GESELLSCHAFT*, (P. 12). BERLIN.

# A. Decision gate review process

As introduced in section 1.2.1 and in Table 1 above, a project's maturity evolves along so-called Decision Gates (DGs). When reaching Decision Gate, a so-called Decision Gate Review (DGR) is performed, with the goal to evaluate the maturation of the project. If the decision gate review has been fulfilled according to the requirements of management, then the projects gets further funding and can proceed. In the following examples for decision gate reviews are presented.

## A.1. DECISION GATE REVIEW # 1: Approval of Project Initiation

Table 18: DECISION GATE REVIEW # 1: Approval of Project Initiation (Jonkman, Bos, Breunese, Morgan, & Spencer, 2000)

| **Objectives of the Review** | **Key Issues to be Demonstrated** | **Outcome of the Review** |
|---|---|---|
| Validate the basis to pursue the business opportunity<br><br>Initiate the project | – Information has been gathered in a manner that ensures the opportunity being initiated is understood<br>– The correct conclusions have been drawn from the information gathered<br>– Key risks and costs associated with initiation have been identified and can be appropriately managed<br>– The opportunity has a reasonable chance of success and is worth pursuing<br>– Value drivers and Stakeholder aspirations are identified and understood<br>– Alignment with key Stakeholders and a strategy for managing the Stakeholders relationships<br>– Project definition is unambiguous and realistic, with agreed and shared objectives<br>– The plans for the next stages are realistic and fit for purpose and have identified the required Skills and Resources<br>– Key organizational and support requirements have been identified<br>– Clarity on future decision points and commitments and the data needs to support these<br>– Basis for any immediate commitments i.e. seismic, exploration drilling, is sound (i.e. exploration well proposal)<br>– Key risks and uncertainties have been bracketed on a fully integrated basis, and work programmes and<br>– processes designed to address them | Support for project initiation (Objectives / activities / resources / timing / costs / technology applications)<br><br>Agreement on terms of reference and specific items to be resolved for Decision Gate Review # 2. |

## A.2. DECISION GATE REVIEW # 2: Approval of Concept Short List

Table 19: DECISION GATE REVIEW # 2: Approval of Concept Short List (Jonkman, Bos, Breunese, Morgan, & Spencer, 2000)

| **Objectives of the Review** | **Key Issues to be Demonstrated** | **Outcome of the Review** |
|---|---|---|
| To confirm that resolution of uncertainties supports continuation of definition and move to Concept selection.<br><br>Has the project been effectively framed and is there enough knowledge to start the process of selecting the concept and defining the plan ? | – The business environment is understood, and the project has been framed within its context. All risks/opportunities have been identified, prioritised and analysed to define the key appraisal strategies.<br>– The economics (incl. Costs), are modelled to an appropriate level and justify continuation.<br>– Scenarios have been developed to cover the full range of risks/uncertainties: surface, subsurface, operational, infrastructure and business environment.<br>– Potential options are aligned with the objectives, value drivers and key stakeholders' aspirations.<br>– Subsurface uncertainty quantification is robust over the entire range of possible outcomes.<br>– Uncertainties related to schedule, commercial environment, competition, government and partnering aspects have been identified.<br>– All available data has been used in subsurface outcome definition, i.e. static and dynamic modelling integrates as good as possible all observations.<br>– Support requirements have been identified and accounted for, to the appropriate level of detail, in the decision making.<br>– The necessary organization and resource/skills have been identified and staff continuity has been planned through the remaining phase(s).<br>– There is clarity on future decision points and commitments and the data requirements to support these.<br>– The plans for the next stages are realistic and fit for purpose. | Support for subsurface uncertainty range and outcomes<br><br>Support for ranges of in-place HC resource volumes and technical reserves.<br><br>Support for range of integrated field devt concepts.<br><br>Support for continuation into Concept Selection.<br><br>Agreement on ToR and specific items to be resolved for Decision Gate Review # 3 |

## A.3. DECISION GATE REVIEW # 3: Project Concept Selection and Definition

Table 20: DECISION GATE REVIEW # 3: Project Concept Selection and Definition (Jonkman, Bos, Breunese, Morgan, & Spencer, 2000)

| Objectives of the Review | Key Issues to be Demonstrated | Outcome of the Review |
|---|---|---|
| To confirm approval of the Concept Selection. | The selected development concept and plan for project definition and the PDO / PIO[7] preparation phase:<br>– Is realistic and realisable<br>– Is founded on key value drivers and consideration of critical issues and success factors being aligned.<br>– Is compatible with the business environment and key stakeholder aspirations.<br>– Maximises the opportunity value in alignment with objectives.<br>– Takes account of the full life-cycle of the project and maximises the life-cycle value.<br>– Incorporates Operations/Maintenance requirements.<br>– Has been framed with quality cost and production data and is linked to a strategy to further reduce costs/increase value.<br>– The business case remains clear and is supported by economics<br>– Project execution, contracting and procurement strategies have been identified and fully considered in the proposed concept and plan.<br>– Key stakeholders are aligned with plans for the concept selection and project definition stage: plans cover their ongoing engagement/management.<br>– The plans for managing risks and opportunities are robust and they include an assessment of compound risks and appraisal strategy revision tied to the value of information.<br>– The plan to reach and support PDO / PIO[7] is realistic and addresses all of the project attributes (subsurface evaluation, project execution, production facilities evaluation and project execution,<br>– Operations, stakeholder management), and identifies the resources needed to deliver.<br>– Project management systems and process, including Project Execution Plan, SHE / Quality Management / Project control and | Support for the concept selection process.<br><br>Support for the selected concept.<br><br>Support for the plan and cost estimates to prepare the basis for design, project specifications and update of the Project Execution Plan (PEP).<br><br>Agreement on terms of reference and specific items to be resolved for Decision Gate Review. #4 |

[7] PDO = Plan for Development and Operation, PIO = Plan for Installation and Operation

| | | |
|---|---|---|
| | Procurement, Risk / opportunity management etc., have been identified and plans are in place for their preparation.<br>– Operational items detailed in Decision Gate Review #6 to be addressed.<br>– The necessary organisation, resource skills and planned staff continuity through the remaining phase(s) have been identified. | |

## A.4. DECISION GATE REVIEW # 4: Approval to issue PDO / PIO[7]

Table 21: DECISION GATE REVIEW # 4: Approval to issue PDO / PIO1 (Jonkman, Bos, Breunese, Morgan, & Spencer, 2000)

| **Objectives of the Review** | **Key Issues to be Demonstrated** | **Outcome of the Review** |
|---|---|---|
| Project considered sound and ready to execute, prior to and conditional on PDO / PIO approval. | – Project objectives are clearly defined and plans for execution are in place, aligned with those objectives.<br>– Key stakeholders are aligned with plans for execution: plans cover their ongoing engagement/management.<br>– Full project scope is expressed in tangible cost, time and resources with sufficient accuracy, and a strategy is in place to further optimize costs/increase value.<br>– Economics screening has been appropriately updated and maximum value has been achieved.<br>– The risk and opportunity management plan is maintained and robust.<br>– Project execution plans and contracting strategies and plans are appropriate for the level of definition, residual risk and uncertainty and aligned with the business environment and market conditions. Planned contracting tactics are optimum and cover both the major and minor contracts.<br>– The required management systems, processes and procedures including Project Execution Plan,<br>– Procurement Strategy, SHE program, Quality Management, Project Controls, Procurement and other support functions are defined and in place to support the project during the execution phase.<br>– Appropriate review and audit plans are in place for the execution phase and Operations hand over.<br>– The project completion and hand over strategy has been developed.<br>– The plans to mobilize operations and maintenance resources, systems, processes and procedures are in place. | Support for the PDO / PIO<br><br>Agreement on terms of reference and specific items to be resolved for Decision Gate # 5 Review<br><br>Support for the Project Execution and Procurement Strategy |

| | | |
|---|---|---|
| | – The key project team personnel are in place to initiate execution according to the plan.<br>– Operational items detailed in Decision Gate Review #6 (DGR #6) to be addressed.<br>– The project resource plan and organization is optimum and can be mobilized in accordance with the schedule. | |

## A.5. DECISION GATE REVIEW # 5: Approval to Start Execution

Table 22: DECISION GATE REVIEW # 5: Approval to Start Execution (Jonkman, Bos, Breunese, Morgan, & Spencer, 2000)

| Objectives of the Review | Key Issues to be Demonstrated | Outcome of the Review |
|---|---|---|
| To confirm that the conditions as at Decision Gate Review # 4 are still valid. | – No substantial changes<br>– Any changes do not impact situation at DGR #4<br>– Any changes which do impact the situation at DGR #4 have been identified and properly addressed through incorporation in forward work plans or re-working previous work to an appropriate degree. | Support that conditions at DGR #4 are still valid<br><br>Support that changes to the conditions at DGR #4 have been properly incorporated, and that plans for any re-work are appropriate<br><br>Agreements of terms of reference and specific items to be resolved for Decision Gate Review #6. |

## A.6. DECISION GATE REVIEW # 6: Approval to Start Operation

Table 23: DECISION GATE REVIEW # 6: Approval to Start Operation (Jonkman, Bos, Breunese, Morgan, & Spencer, 2000)

| Objectives of the Review | Key Issues to be Demonstrated | Outcome of the Review |
|---|---|---|
| To confirm ready to start operation and hand over of Operator ship | – Objectives for operation and hand over of Operator ship are clearly defined and plans for execution are in place, aligned with those objectives<br>– Key stakeholders are aligned with plans for execution: plans cover their ongoing engagement / management<br>– Production operations scope is expressed in tangible cost, time and resources with sufficient accuracy, and a strategy is in place to further reduce costs / increase value<br>– Economics screening has been appropriately updated and maximum value has been achieved<br>– The risk and opportunity management plan is maintained and robust<br>– The required management systems, processes and procedures including | Support for start of production<br><br>Support hand over of Operator ship<br><br>Agreement of terms of reference and specific items to be resolved for Decision Gate Review # 7 |

| | | |
|---|---|---|
| | Operations Reference Plan, SHE, Quality Management, Financial controls and other support functions are defined and in place to support hand over of Operator ship and production operations<br>– Appropriate review and audit plans are in place for the operation phase and hand over of Operator ship<br>– The detailed plans to mobilize operations and maintenance resources, systems, processes and procedures are in place<br>– The key operation personnel are in place to initiate start-up / handover according to the plan<br>– The operation resource plan and organization is optimum and can be mobilized in accordance with the schedule<br>– A detailed technical pre-start up audit has been satisfactorily completed | |

## A.7. DECISION GATE REVIEW # 7: Post Implementation Assessment

Table 24: DECISION GATE REVIEW # 7: Post Implementation Assessment (Jonkman, Bos, Breunese, Morgan, & Spencer, 2000)

| **Objectives of the Review** | **Key Issues to be Demonstrated** | **Outcome of the Review** |
|---|---|---|
| To assess to what degree the objectives of the development project has been fulfilled<br><br>To assess whether Operations are being undertaken in accordance with requirements<br><br>To provide experience feedback for future projects | – Has the project delivered to expectations, is it on targets to meet its social, environmental and economic promise ?<br>– Are the operations and maintenance resources, systems, processes and procedures performing in accordance with the requirements ?<br>– What are the key life cycle learning's arising from the execution process ?<br>– What are the remaining opportunities and risks, and how are they being managed ?<br>– What actions can be taken at this stage to further optimize the opportunity value ?<br>– What were keynote best practices and can any additional best practices be identified ? | Support for the Operations Reference Plan<br><br>Support for the Asset Reference Plan |

# B. Quantification of risk factors in soft stimulation activities Calculation of interest rates including taxes

## B.1. Introduction

The EU initiated DESTRESS (Demonstration of soft stimulation treatments of geothermal reservoirs) project investigates the effects, effectiveness and efficiency of soft hydraulic stimulation in geothermal reservoirs. Soft stimulation techniques aim to improve reservoir performance while minimizing environmental impacts such as induced seismicity. Applied techniques include cyclic/fatigue, multi-stage, chemical and thermal stimulation (Huenges & Ellis, 2016). Hydraulic stimulation in the context of geothermal reservoirs differs from hydraulic fracturing, which is also known as fracking and broadly applied in the production of unconventional gas reservoirs. Fracturing, as the name implies, aims to create new fractures in low-permeability rock formations while the goal in hydraulic stimulation is the widening, cleaning and activation of present natural fractures. The creation of new fractures inherently bears a greater risk for induced seismic activity. Other notable differences include the reservoir depth, which is often in approximately 4 km depth for geothermal reservoirs. Unconventional gas reservoirs mostly lie in depths of 1-2 km or less. The stimulation of geothermal reservoirs therefore takes place in greater distances from aquifers that are used for drinking water supply than fracking in gas reservoirs. The fluids used in stimulation, furthermore, usually contain less to no environmentally harmful substances compared to fracturing fluids (Bracke, 2014).

The following report investigates the risks involved with stimulation practices. The mechanisms behind these risks are explained and the causes behind them are described in the most quantitative manner possible. The following phenomena are investigated:

- Public acceptance of the technology
- Subsurface interactions between stimulation fluid and geological formations
- Political instability
- Downhole loss of tools
- Blowout
- Induced seismicity
- Unwanted subsurface hydraulic connections
- Lack of information in planning and from the view of the authorities

This report is based on existing research. The engineering of geothermal reservoirs is a relatively young approach with only 15 projects realized worldwide since 1972 (Bracke, 2014). Fracking in oil and gas has meanwhile been employed in at least 300.000 wells in the USA alone (Perrin & Cook, 2016) and been a subject of international controversy. The available resources on the topic are therefore focused on the oil and gas industry. Since, as described above, the practices for reservoir engineering differ significantly between hydrocarbon and geothermal exploration, research results relevant for this report are evaluated critically and put into the context of geothermal reservoirs.

## B.2. Risk evaluation

### B.2.1. Public acceptance

Public acceptance is a critical factor in the development of geothermal energy projects and related stimulation activities. Quantification of this issue proves difficult, because it is tied to several socio-economic factors. Public acceptance is furthermore influenced by the values, experiences and priorities of individual citizens, which emphasizes the inherently subjective nature of this issue. Depending on the locality, further cultural factors may influence the reaction of the population towards new developments. In Chile, for example, the spiritual relationship between the population and volcanoes has been found to be an obstacle that inhibits public acceptance (Payera, 2018). As such, the culture and customs in the development area must be considered. The following study data focuses on hydraulic fracturing but, because of the similarities between the technologies, it should be an approximation of the public opinion towards soft stimulation.

The causes of social resistance are manifold. An analysis of German media reports identified four key sources thereof (Reith, Kölbel, Schlagermann, Pellizzone, & Allansdottir, 2013) (Carr-Cornish & Romanach, 2014):

- Environmental issues
- Lack of involvement of the public
- Not in my backyard (NIMBY)-attitude
- Financial issues

The most easily controllable factor of those is arguably the involvement of the public, which might also help to mitigate anxiety about environmental and financial issues.

The involvement and information of the public has been shown to have a drastic influence on the public perception and acceptance (Reith, Kölbel, Schlagermann, Pellizzone, & Allansdottir, 2013). This involves the provision of information to the public. (Carr-Cornish & Romanach, 2014) found, that 42 % of participants were initially unsure of their acceptance towards geothermal energy. After the provision of informational material, which highlighted both advantages and risks of the technology, only 19 % of the participants felt unsure while the percentage of participants who were in agreement with the technology rose from 50 % to 74 %. Information of the public therefore has the potential to reduce the part of the population who feels unsure by 45 % while almost 80 % of the “converted” participants chose to support the technology afterwards.

This is in accordance with previous findings that higher subjective knowledge of citizens leads to higher acceptance rates (Huijts, Molin, & Steg, 2012). Identifying geothermal energy as a renewable energy source also helps to increase the acceptance rate (Dowd, Boughen, Ashworth, & Carr-Cornish, 2011). Direct mention of the term “fracking”, on the other hand, decreases the public support that is received: When asked about the technology, 42,5 % of the subjects that did not hear the term “fracking” in the provided information material judged it as safe, as opposed to 34,5 % of the subject that heard the word. Likewise, when asked if the state should apply the technology, 51,6 % of the former group said yes as opposed to 36,6 % of the control group. Highlighting the differences between fracking and soft stimulation in information campaigns could therefore prove useful in increasing public acceptance.

Implementing these aspects in a well-designed information campaign can potentially increase the amount of acceptance in a given community. Increasing the acceptance by 24 % is possible, as is shown

by (Carr-Cornish & Romanach, 2014). Transferring this quantification to other projects and communities would prove difficult, however. Subject of that study were citizens in Western Australia and different results might have been obtained with different target populations. Furthermore, to estimate the effect of an information campaign on public acceptance the pre-existing mindset of the local population must be known which cannot be expected for most projects.

Other studies have identified demographic factors that might have an influence on the public acceptance of geothermal projects and hydraulic stimulation efforts. Gender appears to be a demographic variable that influences acceptance. Several studies show, that men are more likely to support emerging technologies, which also applies to geothermal energy and hydraulic stimulation and fracturing (Boudet, et al., 2014) (White, 2012). White (2012) identified other factors that influence the public acceptance of hydraulic fracturing that might show more spatial variation than gender distribution. Demographics in the three US states Pennsylvania, Texas and Louisiana were surveyed and linked to the public opinion towards the technology. Exact quantification of the public resistance in these states is not given, but a clear difference between the states can be seen with Louisiana showing the highest level of public acceptance, Pennsylvania showing the lowest level and Texas taking the middle ground. For the sake of semi-quantification, the states are here assigned the acceptance levels of low (Pennsylvania), medium (Texas) and high (Louisiana).

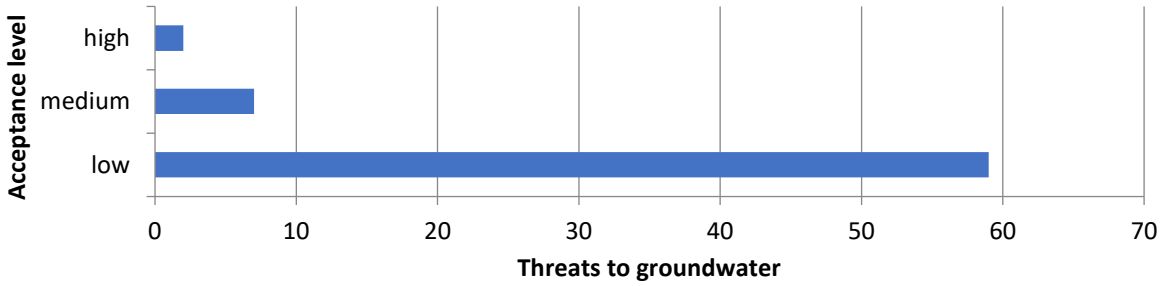


Figure 47: Occurrences of threats to groundwater versus the acceptance level towards hydraulic fracturing More incidents of groundwater-threats correlate with lower acceptance levels. Data from (White, 2012)

Figure 47 shows the total occurrences of groundwater threats as a result of hydraulic fracturing in the three US states. The least acceptance is observed in the state with the most groundwater threatening accidents. Investigating the previously recorded number of incidents in a region that is of interest for hydraulic reservoir stimulation can give a good indication as to how much resistance can be expected.

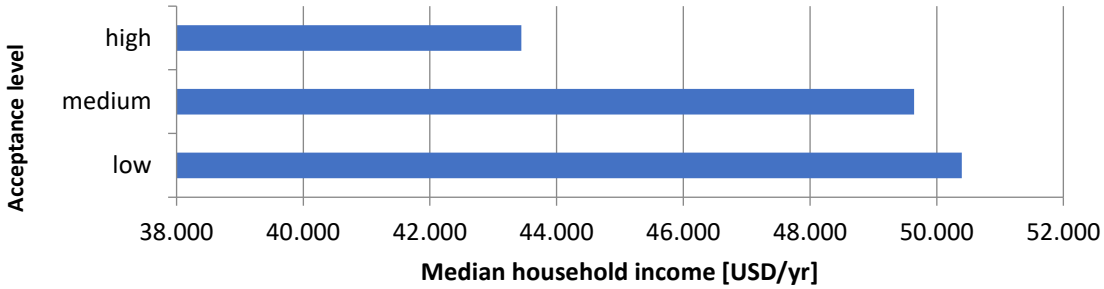


Figure 48: Median household income versus the acceptance level towards hydraulic fracturing. A lower income appears to correlate with higher acceptance levels. Data from (White, 2012)

The median income (Figure 3) appears to correlate negatively with the acceptance levels, which is in line with the phenomenon that socially weaker communities appear to be less critical towards new technologies (White, 2012). The median household income in 2012 in the USA was $51,017 (US Census

Bureau, 2013), which puts the most acceptant state Louisiana more than $6,000 below the US-national average while the other two states are similar to the median. These findings might have implications for the public resistance in newly developed areas, and a significant negative difference from the national median income could be an indicator for stronger public acceptance. The density of wells through which hydraulic fracturing has been conducted, appears to have an impact on the public acceptance of the technology (Figure 49). The least public acceptance is found where more than 0.04 wells/km$^2$ have been fractured (White, 2012).

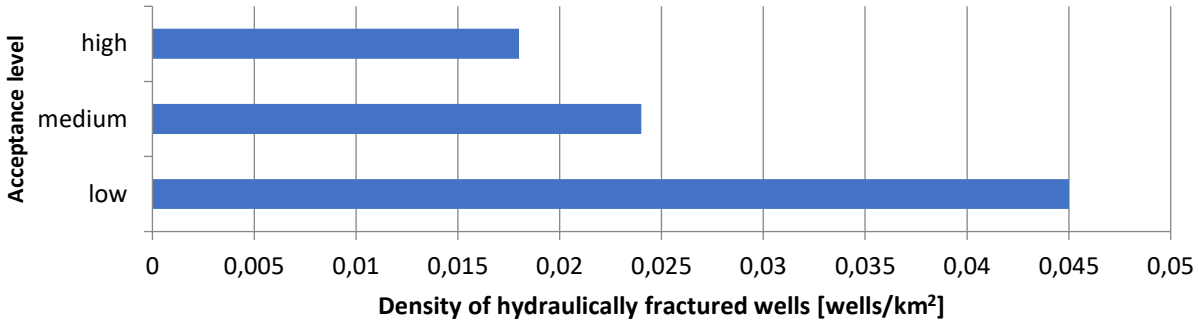


Figure 49: Density of hydraulically fractured wells versus the acceptance level. A lower well density correlates with higher public acceptance. Data from (White, 2012)

Multiple regression analysis of a national survey furthermore identified the political and ideological beliefs of the population to be a strong influence on the support of fracking. Egalitarian worldviews of the population were found to negatively impact the public acceptance while conservative political views positively influenced public acceptance. The magnitude of the influence is very similar for both with beta values of 0.284 for the former and 0.28 for the latter (Boudet, et al., 2014). It is unclear, however, if extrapolation of this data to specific projects is useful, because of the unique aspects of different countries' political systems.

The NIMBY-phenomenon raises the question of the distance between the development site and the next population centre. An Australian study on the public perception of geothermal energy showed, that a large portion of people who are not generally opposed to the technology want the distance from their homes to be greater than 100 km (Carr-Cornish & Romanach, 2014). Meanwhile public acceptance appears to be higher in regions with a high natural seismic activity, since concerns of induced or triggered seismicity are of low concern for the local population (Bommer, Crowley, & Pinho, 2015).The abovementioned data give an insight into quantifiable parameters that can have an impact on the public acceptance. It needs to be emphasized that the resistance of the public against hydraulic fracturing is subject to several socio-cultural, economic, ecologic and political factors and therefore inherently unpredictable. The potential public acceptance can therefore only be estimated roughly according to the criteria listed in Table 25.

Table 25: Location characteristics and their influence on the public acceptance of geothermal projects and soft stimulation

| **Low public acceptance** | **Medium public acceptance** | **High public acceptance** |
|---|---|---|
| -Density of stimulated wells is higher than average | -Density of stimulated wells is around average | -Density of stimulated wells is lower than average |
| -Median household income is above or around the national average | -Median household income is slightly national average | -Median household income is far below national average |

| | | |
|---|---|---|
| -The political orientation of the population is largely liberal | -The political orientation of the population is ambivalent | -The political orientation of the population is largely conservative |
| -The population consists of significantly more than 50% women | -The population consists of approximately 50% women and 50% men | -The population consists of significantly more than 50% men |
| -Over twenty groundwater threatening incidents related to hydraulic stimulation have occurred in the area | -Over five groundwater threatening incidents related to hydraulic stimulation have occurred in the area | -Less than five groundwater threatening incidents related to hydraulic stimulation have occurred in the area |
| -No public information campaigns were conducted | -A public information campaign was conducted | -A public information campaign was conducted including workshops for citizen participation |
| -Project site is next to a population centre | -Project site is 50 km away from the next population centre | -Project site is over 100 km away from the next population centre |
| Virtually no natural seismicity in the area | Low-medium natural seismicity in the area | High natural seismicity in the area |

### B.2.2. Fluid-rock and fluid-fluid interactions

Interactions between drilling and stimulation fluid and the formation rocks can potentially negatively alter the reservoir properties. This is called “formation damage” (FD). Since hydraulic stimulation is most prominently applied in the hydrocarbon industry, specifically in the production of shale gas, most existing literature on fluid-rock interactions refers to shale formations. These shale formations are unsuited as aquifers and therefore geothermal fluid reservoirs (Jung, et al., 2002) which leads to a scarcity of publications on fluid-rock interactions regarding hydraulic stimulation that are relevant for geothermal energy production. Shale formations are still problematic for geothermal exploitation because the swelling of reactive clays like smectite is a general issue in drilling (Bloy, et al., 1994).

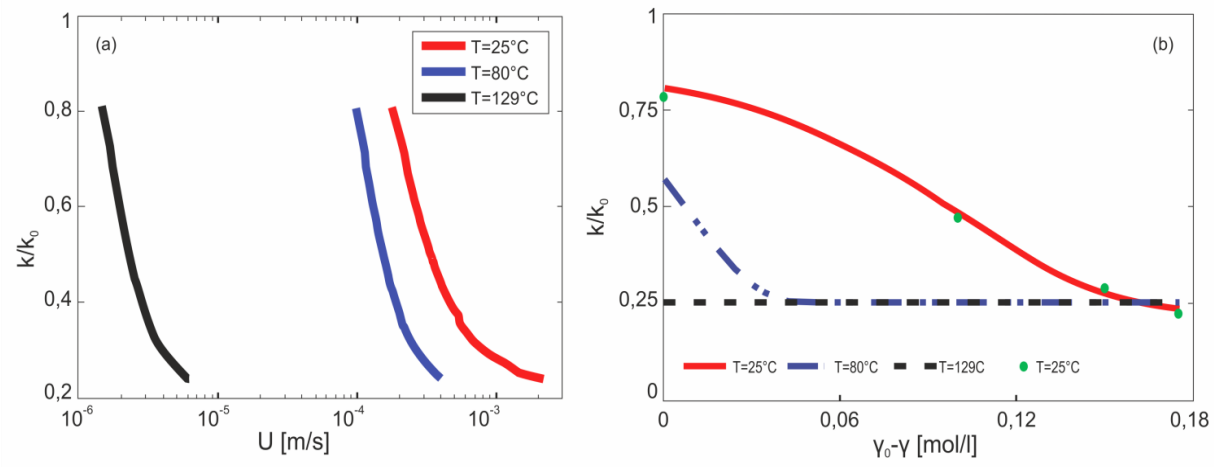


Figure 50: Influence of temperature on the permeability reduction by fines migration. A significant permeability drop occurs for much lower flow velocities U at 129°C than at lower temperatures (a). The reduction in salt concentration γ (NaCl) that is needed to mobilize the fines is also significantly lower at higher temperatures (b) (You, Yang, Badalyan, Bedrikovetsky, & Hand, 2016)

A greater issue than clay swelling is the migration of fines, the effects of which have often been attributed to the former. The problem is especially relevant for sandstone reservoirs. Fines migration is the mobilization of fine particles in the pores which subsequently clog pore throats and reduce reservoir permeability. It is triggered by high pore flow velocities and by low salt concentrations (Gray & Rex, 1966). High velocities mobilize particles by increasing the kinetic energy exerted onto them. Lower salt concentrations lead to the destabilization of the electrostatic bond to the matrix that

immobilizes the particle. High ionic strengths counterbalance repellent forces and stabilize the particle. A loss in ionic strength causes the repellent forces between particle and matrix to dominate, which leads to the mobilization of the particle. These two mobilization processes are also temperature dependent. Higher temperatures lead to fines migration commencing sooner than at lower temperatures, which is shown in Figure 50 (You, Yang, Badalyan, Bedrikovetsky, & Hand, 2016). The permeability drop at a given concentration of NaCl doubles with a T increase from 25 °C to 80 °C and it triples with an increase from 25 °C to 129 °C. Most investigations regarding electrolyte concentration and fines migration focus on single salt-systems (Quirk & Schofield, 1955) (Khilar & Fogler, 1984). The applicability on natural systems suffers from this simplification, since there are almost always numerous ionic species present in natural groundwaters. Total ionic strength is a simple measure for the sum of the electrolytes in solution and therefore a suitable quantification of mixed salt-systems. Ionic strength does influence the mobilization of fines, which has been shown in elaborate mathematical models which are, however, based on single salt NaCl systems (You, Yang, Badalyan, Bedrikovetsky, & Hand, 2016). The presence of bivalent ions, in natural systems predominantly calcium, can significantly reduce the critical ionic strength for fines migration occurs (Khilar & Fogler, 1984). A study of the two-salt system NaCl-$CaCl_2$ quantifies this influence of Ca on the mobilization threshold by observing the molar fraction of sodium and calcium in core injection experiments on a sandstone. The results are displayed in Table 26.

Table 26: Critical ionic strengths for fines migration. Particle mobilization occurs significantly below these thresholds. The ionic strengths in dependency of the Ca/Na percentages were determined experimentally (Khilar, Vaidya, & Fogler, 1990).

| %Ca | %Na | Critical ionic strength (M) |
|---|---|---|
| 0 | 100 | 0,071 ± 5x10-4M |
| 5 | 95 | 0,025 ± 5x10-4M |
| 10 | 90 | 0,005 ± 5x10-4M |
| 15 | 85 | <<0,001 |

Small amounts of calcium in solution mitigate the release of fines by significantly lowering the ionic strength threshold for mobilization (Khilar & Fogler, 1984). These results are not directly applicable to geothermal applications because of the temperature dependency, however. This increases the risk of fines migration even if the critical ionic strength is surpassed in a given reservoir.

Critical ionic strengths for fines migration. Particle mobilization occurs significantly below these thresholds. The ionic strengths in dependency of the Ca/Na percentages were determined experimentally (Khilar, Vaidya, & Fogler, 1990).

At the same time there are various other bivalent ions present in natural systems, which might stabilize the particles and further decrease the critical ion strength, preventing fines migration. Considering the thermal water at the Mezöberény site in Hungary, which shows an ionic strength of 84 mM and a Ca/(Ca+Mg) ratio of 0,554 % (data from the geological log report 116; 318/2012 (Dudas, 2012)), fines migration is not expected to become an issue there if thermal effects are neglected. The ionic strength of the thermal waters at the Soultz-sous-Forêts site in France is approximately 1,825 M with a Ca/(Ca+Mg) ratio of 12,9 % (data from (Scheiber, Nitschke, Seibt, & Genter, 2012)). Here, the mobilization of fines also cannot be expected if thermal effects are neglected. Neglecting the thermal influence potentially leads to an underestimation of the fines migration risk. Applying the critical ionic

strengths from Table 26 to the geothermal fluids should therefore be done with a generous margin of error. In Soultz the ionic strength and Ca concentrations are above the critical value by a great margin. The reservoir is, furthermore, located in the crystalline basement (Scheiber, Nitschke, Seibt, & Genter, 2012), which furthermore reduces the risk of fines migration. The siltstone reservoir in Mezöberény can be expected to contain a portion of fines that may be significant enough to reduce the permeability. The ionic strength of the Mezöberény water is furthermore greater than the threshold given in Table 26 but not by as great of a margin as in Soultz. If the temperature effect on the mobilization of fines is as great as the model by You et al suggests then fines migration is to be expected at the Mezöberény site, which is likely to lead to a reduction in permeability. The considerations explained above also apply to the drilling and stimulation fluids that are applied in the exploitation process.

Besides the overall salinity of the water the rate in salinity drop has an influence on fines mobilization: Fast drops in ionic strength are more likely to mobilize fine particles than a slow, gradual decrease (Jones Jr., 1964). An abrupt decrease may happen if the main reservoir is depleted during production and hydraulically connected to a low-salinity aquifer or if a fluid is introduced that has a lower ionic strength than the formation water.

The risk for permeability reductions due to fines migration, which may be as great as 75 % (You, Yang, Badalyan, Bedrikovetsky, & Hand, 2016) can, in conclusion, be assessed by the following criteria:

The risk for permeability reduction up to 75 % by fines migration increases significantly if

- The reservoir is located in sandstone or comparable porous media
- No fines-migration inhibitors are present in the system
- The ionic strength is lower than the critical values given in Table 26
    - The ionic strength should surpass the given thresholds with a large safety margin to compensate the mobilizing effect of higher temperatures (see Table 26)
- The flow velocity is above a critical threshold: $<10^{-4}$ m/s for T < 80 °C and $<2x10^{-}$ m/s for T > 129 °C
- The reservoir is connected to a low-salinity aquifer

An exact quantification of the risk of permeability reduction is not possible because of the temperature dependence of the mobilization and a lack of empirical data in the available literature.

Ultimately permeability losses need to be counteracted by the operating fluid's chemistry. Inhibitors such as cations or polymers can mitigate clay swelling and fines migration. Clay swelling ultimately leads to the clogging of pore throats by the mobilization of fine particles, similar to fines migration. Reactive clays like those of the smectite group are principally at risk for swelling and subsequent dispersion and mobilization. The presence of these clays therefore principally increases the risk of formation damage by fluid-rock interaction (Civan, 2007). Identifying these clays before reservoir stimulation and adjusting the fluid accordingly is therefore crucial for a successful operation. The success of the operation is thus directly linked to the drilling and/or stimulation operator's experience and expertise, which is not possible to quantify beforehand.

The chemistry of injected fluids shows broad variations depending on the application, and so do the interactions with formation fluids. In the context of hydraulic stimulation, the source water is important. In the oil and gas industry the use of produced formation water as a base fluid is a common practice, which, however, introduces several complications (Li, Al-Muntasheri, & Liang, 2016). Produced waters often show high total dissolved solids (TDS) contents. Divalent cations such as calcium

and magnesium will precipitate as hydroxides in significant amounts at room temperature at a pH above 9,2. The use of highly saline base fluids to stimulate a reservoir with very alkaline formation water could thus lead to the clogging of pores by hydroxide precipitates (Li, Al-Muntasheri, & Liang, 2016). Other authors highlight the risk of the precipitation of scaling by mixing two incompatible brines (Mackay, 2003), in the case of geothermal reservoirs the formation and stimulation fluids. The precipitation patterns and rates are dependent on the chemistry of the injected fluid, the formation fluid, the formation minerals and the pore- and fracture geometries (Jones & Detwiler, 2016). Small reservoir heterogeneities have a significant impact on the precipitation behaviour of solids. While the mineralogy and fluid chemistry of the underground reservoir are often known reasonably well, information about fracture surface roughness and small-scale mineral heterogeneities at reservoir depth is hardly possible to obtain. Numerical information about observed permeability drops caused by stimulation operations in geothermally relevant reservoirs is rare. A realistic quantification of the risk that fluid-rock and fluid-fluid interactions bear is therefore not possible.

### B.2.3. Political instability

The stability of the political establishment can potentially severely disrupt an entire nation's energy sector. India, for examples, has been struggling to provide a stable energy network to the population for decades. This struggle is partly caused by a political system that is characterized by partisanship and corruption, leading to unstable flow of federal subsidies and permits (Fukumi, 2012). Regarding hydraulic stimulation and fracturing the biggest impact of politics is arguably legislation. With several environmental concerns that are linked to the technology, mostly in respect to the production of shale gas reservoirs, hydraulic fracturing is a subject of controversy and has even been banned completely for gas production in France (Good Energy Alliance Ireland, 2018). The ban does not apply to geothermal energy. This principally shows that differentiation between the different applications of hydraulic stimulation is possible in policy making.

If the permit for hydraulic stimulation is legally permitted for a geothermal project, the greatest risk through political instability would be the repeal of that permission. The risk is therefore dependent on stringency and reliability in policy making. This stringency negatively correlates with political stability in countries with relatively low levels of corruption (Fredriksson & Svensson, 2003). Albeit corruption exists and continues to be a problem in Europe (EU Commission, 2014), the corruption in relation to many developing countries is low. Instability could thus disrupt policies that are in place regarding hydraulic stimulation. While indexes for political stability can estimate the risk of sudden policy changes in a country, the exact changes or even the directions thereof are subject to a broad variety of factors. A change in legislation could lead to a fatal complete ban of hydraulic stimulation activities. It could also, however, lead to the deregulation of hydraulic stimulation for economic reasons. There is, therefore, an inherent uncertainty that comes with political destabilization and subsequent changes in legislation. Even if these uncertainties could be quantitatively accounted for, current models that predict political change often fail to do so accurately (Sottilotta, 2013). An accurate quantification of the risk that political instability poses to hydraulic stimulation is thus not viable.

### B.2.4. Lost in hole

The loss of drilling materials such as drilling tools, fluids and logging instruments accounts for roughly $3 billion in annual drilling expenses for the oil and gas industry. These costs are caused by both the material's value and resulting non-productive time.

The scenario in which hydraulic stimulation would lead to a loss of tools is in subsequent logs. According to the legacy of the ocean drilling program there are four main causes that may cause a tool to become stuck (Ocean Drilling Programme, 2004):

- The tool is stuck in a bride or by cavings
- The tool is not stuck, but cannot be pulled up past a bridge
- The tool is stuck in the base of the pipe
- The tool is not stuck but cannot be pulled past the pipe

Since the occurrence of bridges in the well appears to be a major cause of stuck tools the probability of tool loss appears to be linked to borehole stability. Models for wellbore stability exist (Al-Ajmi & Al-Harthy, 2010) (Ding, Luo, Liu, & Liang, 2018) but not to the accuracy in which they could predict bridges that could cause tools to become stuck. Quantification of the risk for stuck tools could be conducted by an empirical approach which comprehends existing data about stuck tool occurrences. Such datasets or quantifications following this approach are, however, not present in the available English literature. A quantification of the “lost in hole” risk is therefore not feasible.

### B.2.5. Blowout

A blowout is the rapid and uncontrolled release of a fluid (gas or liquid) from the borehole, which may lead to the loss of the borehole, economic and ecologic damage and even the loss of human life (Lindi, 2017). The precursor to such an event is a so called “kick”, which describes the entering of a formation fluid into the well. This occurs when the pressure of the formation fluid exceeds the pressure of the circulating fluid. The main controlling factor is therefore the injection pressure and mud weight density (Azar & Samuel, 2007). Even though detection systems for kicks exist, they are often faulty and lead to false alarms, which harshly decrease their reliability (Lindi, 2017).

A primary cause for blowouts is human error. Linked to this is bad communication between actors, which was partly responsible for the catastrophe in 2010 at the “Deepwater Horizon” drilling platform. Human error is a risk in a variety of ways such as bad casing installation, violation of planning or ignorance towards bad test results (Lindi, 2017). This ignorance is promoted by the tendency of warning systems to give false alarms. Cost cutting in general increases the blowout risk. Even if the necessary systems are provided and maintained, cost cutting leads to time pressure and long shifts, which increase the risk of human error in monitoring. Cost cutting can also lead to faulty cementing, which is a known cause of blowouts (Lindi, 2017).

Failure of technical systems such as the blowout preventer (BOP) or the downhole safety valve (DHSV) furthermore lead to accidents. These systems’ failure can be largely avoided by regular maintenance. A challenge for hydraulic stimulation is that most kick detection systems are designed for drilling operation. The chances of a blowout occurrence increase in the completion phase, which includes stimulation (Lindi, 2017).

Since an increase in permeability increases migration rates and therefore the potential formation pressure (Liu, Mentzer, Mannan, & Hasan, 2014), hydraulic stimulation inherently bears a risk for blowout. A sudden rise in formation pressure can occur if a secondary, high pressure reservoir is connected to the borehole during well completion or drilling (Toth, 2010). Detailed knowledge of the geology surrounding the target reservoir, especially regarding further, high pressure reservoirs, is therefore a strong indicator for an increased risk of a blowout. Such detailed knowledge is, however, lacking in most cases.

There exist stochastic approaches to estimate the blowout risk (Andersen, 1998) and blow out preventers are developed specifically for hydraulic stimulation (USA Patentnr. US5819851A, 1998). The issue is, that these approaches are centred around hydrocarbon production. A solid stochastic approach regarding the blowout risk of hydraulic stimulation of geothermal reservoirs is currently not feasible due to the underwhelming amount of data that is available on the topic. Most available data are either specific to oil and gas production or restricted to drilling operations. To summarize the results from above, the following factors can be determined that increase the likelihood of a blowout:

- Cost reduction
    - Decrease of equipment maintenance and testing
    - Overworked staff
- Unreliability of kick detection systems
- Presence of secondary high-pressure reservoirs in the vicinity of the target reservoir

### B.2.6. Induced Seismicity

To estimate the risk of induced seismicity, it's necessary to identify the parameters that influence the occurrence of such events. Several studies (Wiemer, Kraft, Trutnevyte , & Roth, 2017), (Majer, et al., 2007), (Vlcek, Eisner, Stabile, & Telesca, 2017), (Muntendam-Bos, Roest, & de Waal, 2015), (Van Eijs, Mulders, Nepveu, Kenter, & Scheffers, 2006) tried to investigate these parameters in order to control seismicity in both gas and geothermal fields and to prevent larger events with critical consequences.

The Swiss Seismological Service (SED) represented by Wiemer published a "'Good Practice' Guide for Managing Induced Seismicity in Deep Geothermal Energy Projects in Switzerland", where they did some detailed research on the topic of induced seismic. They distinguished the seismic risk of different geothermal systems. According to Wiemer, shallow geothermal systems are not known to cause earthquakes. In case of EGS, induced earthquakes are required for creating a reservoir. In deep hydrothermal projects, target zones are often major fault zones due to their highly increased permeability. This includes the chance that the fault zones turn out to be more seismogenic than expected (Dieh, et al., 2017).

Induced earthquakes are caused by a range of physical mechanisms, which act together to a varying degree (Wiemer, Kraft, Trutnevyte , & Roth, 2017). The primary physical mechanisms are:

- **Pore pressure change:** Increasing pore pressure on pre-stressed faults may eventually cause these faults to rupture, releasing generally small fractions. The higher and the more rapid the pore pressure changes are, the more likely is the occurrence of seismic events (Muntendam-Bos, Roest, & de Waal, 2015). A natural example of seismic events due to increased pore pressure are rain-triggered earthquakes (Husen, Bachmann, & Giardini, 2007),
- **Earthquake-earthquake interactions:** Static and dynamic stress changes of induced earthquakes may act as a trigger for additional earthquakes themselves (Catalli, Cocco, Console, & Chiaraluce, 2008).
- **Deformation related changes:** Volume changes through injection or extraction of fluids changes the strain/stress conditions on nearby faults that may be tectonically prestressed (Gibowicz & Lasocki, 2001).
- **Temperature changes:** Cooling or heating of the reservoir rock by injecting fluids causes local thermal contraction or expansion, which can lead to the release of stress. According to (Martínez-Garzón , et al., 2014), thermoelastic stress induced by the injection of cool water in

the high temperature rock is the dominant reason for induced seismicity in EGS, especially near the injection well.

- **Chemical alterations:** Chemical alteration due to the injection of non-native fluids can cause changes in the coefficient of friction on the fracture surfaces. If the friction is reduced, smaller seismic events are more likely to occur. Events with a magnitude M > 3.0 are more likely to happen if the friction is increased (Majer, et al., 2007).

Even though a lot of influencing parameters are known, the interaction between and the influence of each is not yet fully understood. Further, the modelling and risk assessment of induced seismicity is problematic due to some other uncertainties. The earth crust is critically stressed in most places and crisscrossed with faults of all sizes, where both location and current loading status are rarely known and cannot be imaged using geophysical techniques (Wiemer, Kraft, Trutnevyte , & Roth, 2017). Furthermore, the stress distribution and material properties on the reservoir scale can be highly heterogeneous and are often largely unknown. Also, the consequences of infrequent and rare large events, that often dominate public discussions, are difficult to estimate, since there are only few or no observation data exist, and models are extrapolated well beyond their calibrated range (Wiemer, Kraft, Trutnevyte , & Roth, 2017).

Still, some general statements can be made: The larger the injected volume, the larger the volume of rock affected by stressing changes and the more events are likely to happen. Whether or not the maximum possible magnitude is also scaling with the injected volume is currently a debated issue (Baisch, et al., 2010). Deeper systems are generally believed to be producing more induced earthquakes as a consequence of the strength profile, as shown in Figure 51. Furthermore, the seismic risk seems to depend on the reservoir rock type. Crystalline basement rocks are typically believed to be more seismogenic than sedimentary rocks (Evans, Zappone, Kraft, Deichmann, & Moia, 2012).

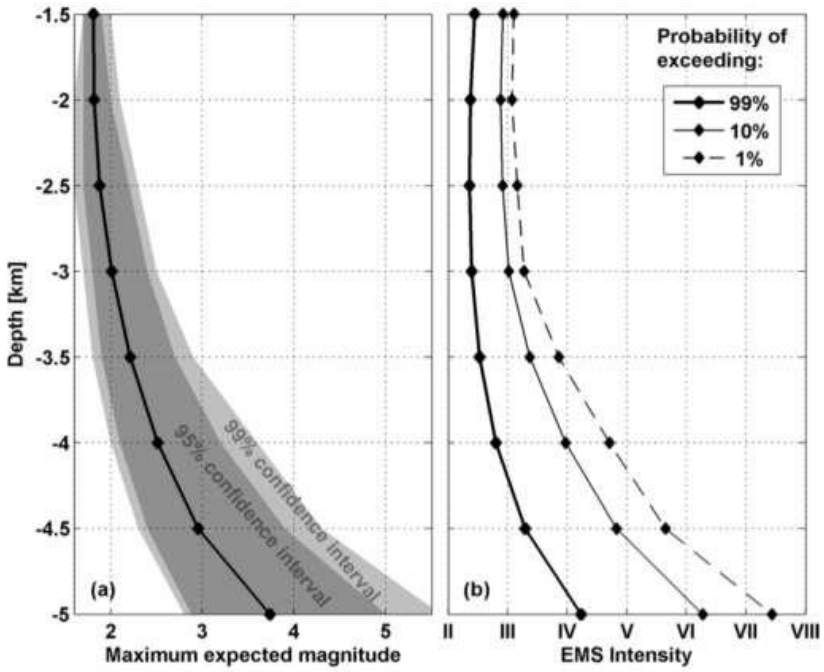


Figure 51: Depth dependence of the maximum expected magnitude derived from 1000 model realizations (Gischig & Wiemer, 2013). EMS - European Macroseismic Scale

(Muntendam-Bos, Roest, & de Waal, 2015) describes a guideline for assessing and managing seismic risk induced by gas production in the Netherlands. Depending on the probability of seismic events and

the estimated maximum magnitude, Dutch gas fields are subdivided into three levels of assessment. For low probability fields (level 1), the risk is classified based on three key parameters, which partially match with the ones (Wiemer, Kraft, Trutnevyte , & Roth, 2017) published: 1. the ratio between the pore pressure drop and the initial pore pressure; 2. the fault density of the reservoir and 3. The stiffness ratio between the seal and the reservoir rock, which indicates, whether fluid production causes subsidence of the surface or stress on the reservoir rock. Level 2 and 3 assessments include parameters like public sensitivity, construction standards of buildings and the risk of fatality for persons in the exposed area. In the past, the calculation of the hazard factor by a probabilistic seismic hazard analysis (PSHA) has been the standard method to estimate the hazards. A PSHA estimates the likelihood that various levels of earthquake-caused ground motion will be exceeded at a given location in a given future time period (Budnitz, et al., 1997).

The Dutch State Supervision of Mines (Staatstoezicht op de Mijnen (SodM)) published several data about seismic-risk in Gas fields in the Netherlands (The Dutch State Supervision of Mines (SSM), 2015). They estimate the risk resulting from induced seismicity for each building in a specific area by computing the local annual individual fatality risk (LAIFR):

$$P_{LAIFR}(F) = \int_0^\infty f_{haz}(pga)\Sigma_a F_{dam}(pga, S_a)F_{fat}(pga, S_a)\, dgpa$$

Where *pga* is the Peak Ground Acceleration, $f_{haz}(pga)$ is the probability density distribution of the hazard, $F_{dam}(pga,S_a)$ is the cumulative distribution function for building damage (fragility curve) and $F_{fat}(pga,S_a)$ is the cumulative distribution function for fatal injuries (fatality curve).

The Peak Ground Acceleration is a common way to estimate the hazard of seismic events. It can be simply read from an Acceleration record for an earthquake (Figure 52).

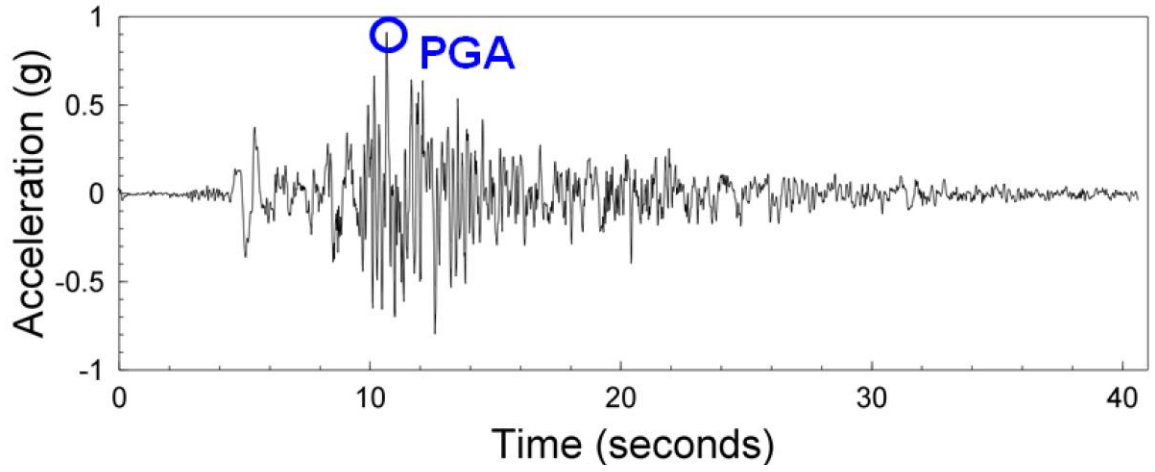


Figure 52: Acceleration record for a typical strong tectonic earthquake, with the PGA indicated (The Dutch State Supervision of Mines (SSM), 2015).

Figure 53 shows the societal-risk (fatality curve) for seismic events of different strength for the Gronning gas field. According to (Muntendam-Bos, Roest, & de Waal, 2015), this kind of guideline refers to the Dutch policy for industrial risk, because a specific seismic-risk policy is non-existent. Since a techno-economic risk assessment doesn't include an estimation of the societal risk, techniques like fatality curves are usually not involved.

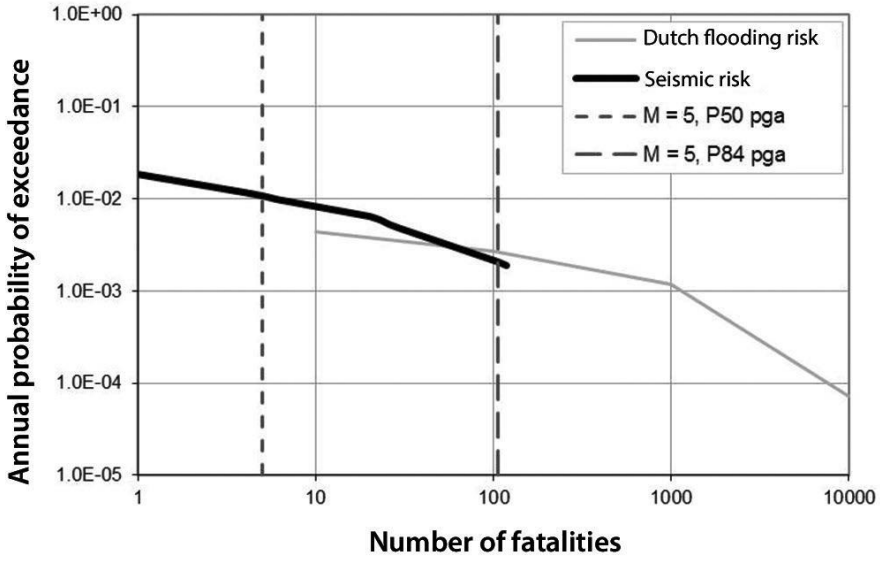


Figure 53: Societal-risk f-N curve for the central area of the Groningen gas field. For reference, the f-N curve for Dutch flooding risk is also shown (Muntendam-Bos, Roest, & de Waal, 2015).

Precondition is, of course, that seismic events occurred in these fields in the past. Since this is not the case for most hydrocarbon and geothermal fields, it's important to estimate the risk before seismic events occur.

In conclusion, there seem to be several parameters that induce seismicity, which influence each other more or less. The change of the pore pressure and the decrease of temperature caused by the injected fluid were mentioned in several studies as the most important factors. These can be directly related to the injection rates of the fluid by hydrofracking. Furthermore, the regional geology, the depth of the wellbore, properties and density of the fault regime, chemical alteration of the fracture surface and a change in the volume of the reservoir also have an impact of the occurrence and the magnitude of seismic events. Induced seismicity risk management is currently a substantial scientific challenge because not enough reliable and validated methodologies and tools to assess and monitor the risk exist (Giardini, 2009), (Majer, Nelson, Robertson-Tait, Savy, & Wong, 2013) (Wiemer, Kraft, Trutnevyte , & Roth, 2017). If seismic events occurred in the investigated fields in the past, the peak ground acceleration appears to be a good way to estimate the seismic-risk.

### B.2.7. Lack of information

The lack of information about a stimulation project increases the risk for the abovementioned issues to occur. This is discussed above for the various issues. The chances for a blowout, for example, increase if the formation gas pressure is unknown. The risk for induced seismicity is likewise greater if the local stress field is unknown and the fracturing flow rates are too high. A lack of information about the hydrogeological conditions can lead to communication between geothermal- and drinking water reservoirs. Any of these scenarios has great potential to negatively influence public acceptance. The mitigation of these issues is, furthermore, more challenging if critical information is missing. Risks that arise through missing information and are related to the other risk factors presented in this report are discussed more thoroughly in the respective sections. This section focuses on a lack of information that is mostly unrelated to the issues mentioned above. Missing information poses a risk to hydraulic stimulation in two ways:

- Data is lacking to properly plan the stimulation

- The authorities require more information about the project

In hydraulic fracturing for shale gas operations several factors play into the operation planning: Pump rate; proppant size and concentration; fracture density, spacing, geometry and conductivity; flow back; reservoir depth and thickness; seismic events; faults; rock and formation fluid properties. These factors vary widely from location to location and knowledge thereof is essential for a successful operation (Salman, 2015). While some of these factors like flowback are less relevant for geothermal reservoirs, the variety of factors is similar.

Incomplete reservoir characterization and complex hydraulic and mechanical conditions introduce uncertainty regarding the factors mentioned above. This limits the optimization of the technical planning (Cheng, Sun, Fu, Carrigan, & Lu, 2012) and the prediction of reservoir performance (Lukyanow & Chugunov, 2015). Optimal planning of a stimulation depends strongly on formation properties like the rock strength, which requires core samples for laboratory testing, and information about the local stress field. The latter is relevant to predict the propagation of opened fractures and therefore the orientation of preferential flow paths (Hickman & Davatzes, 2010). Information about stress field and natural fracture orientation can be acquired through acoustic and electrical logs (Hickman & Davatzes, 2010). A lack of this information introduces significant uncertainty regarding the fracture network that is created by hydraulic stimulation. This translates into an uncertainty regarding the productivity of an enhanced geothermal system (EGS).

Due to the low number of EGS projects worldwide comprehensive data about the factor mentioned above is not available. The lack of engineering information bears some inherent unpredictability because of the multitude of factors that influence the success of hydraulic stimulation. Uncertainties can be avoided by thorough logging and reservoir characterization beforehand, however (Hickman & Davatzes, 2010). Empirical quantification of this risk is therefore not feasible.

A 2012 study modelled the influence of 11 parameters on fracture density, opened fracture length, area density and others. These parameters characterize the “natural fracture topology, in situ stress, geomechanical behavior of the rock matrix and joint interfaces, and pumping operation” (Cheng, Sun, Fu, Carrigan, & Lu, 2012) and were fed into fracture simulators. The results of the simulation indicate that information about the pre-existing fracture network is the most sensitive parameter for well optimization (Chen, et al., 2013), but no quantification of the topic is given. A quantification of the risk based on analytical methods is therefore not possible.

The information about hydraulic stimulation that is required by the authorities depends on the country and its jurisdiction. The EU has issued some guidelines for hydraulic fracturing which are, however, not legally binding for the member states (Commission, 2014). In general, the failure to provide the necessary information that are required by the local authorities bears the risk of the withdrawal of the operation license. Based off this assumption, knowledge of the required information and adequate communication with the authorities is essential. Proceeding a stimulation without providing the authorities with the required information results in a very high risk of the termination of the project. This risk cannot be quantified due to a lack of empirical data on the topic, but it is essential to avoid it by acquiring and providing the necessary information to the local authorities.

### B.2.8. Unwanted subsurface hydraulic connections

Unwanted hydraulic effects include subsurface hydraulic connections, hydraulic shortcut and ground water contamination, all caused by too effective stimulation, wrong doublet design and/or highly conductive fault planes.

Geothermal doublets or triplets require hydraulic connectivity in the far field on one hand but no hydraulic shortcut on the other (Della Vedova, Petronio, Poletto, Palmieri, & Marcon, 2013). A hydraulic shortcut occurs if the hydraulic connectivity between the production and the injection well is so good, that the cold, injected fluid flows too fast towards the production well and doesn't warm up enough before being produced. For geothermal doublets, the two wells are usually about 1-2 km apart (Stober & Bucher, 2014). Detailed information of the reservoir is required, especially of the major fault orientation. According to (Della Vedova, Petronio, Poletto, Palmieri, & Marcon, 2013), there are 3 ways to produce a hydraulic shortcut:

1. Fault plane: The production and the injection well are in the orientation of a fault plane with much better permeability than the reservoir. The permeability of a 0.05 m thick fracture is 500 to 1000 times higher than of the reservoir.
    a. Therefore, knowledge of thrust and fault systems, which favour the fluid circulation, is important to evaluate the position of the 2nd well
2. Too short distance: If the two wells are too close to each other, the injected fluid can't warm up fast enough before being produced
3. Too much fracking: Due to too much fracking, the permeability of the reservoir is too good, which causes a hydraulic shortcut

At this point, it's important to distinguish between hydraulic fracturing to produce shale gas and geothermal hydraulic fracturing. Even though acids like HCl and HF are sometimes used in geothermal fracture fluids, hydraulic fracturing only relies on the pressure of the injected fluid, which is mainly water (Cichon, 2013). Gas fracture fluids can contain components like biocides, aromatic hydrocarbons or surfactant to win the gas from the shale. Further information about the chemical addition in gas fracture fluids can be found in numerous online platforms (Shale Gas Information Platform & GFZ Potsdam, 2018).

In 2011, Osborn et al. investigated methane contamination of drinking water accompanying gas-well drilling and hydraulic fracturing in Pennsylvania and upstate New York. They documented an increase of the average methane concentration by nearly factor 20 from 1.1 mg $CH_4$ $L^{-1}$ to 19.2 mg $CH_4$ $L^{-1}$ in active gas extraction areas (Osborn, Vengosh, Warner, & Jackson, 2011) (Li, Dong, & Wang, 2017). They indicate that fluid flow and discharge to shallow aquifers is caused by the high-pressure injection of fracturing fluids. According to the Water Authority of Great Neck North, geothermal wells pose many threats to the public drinking water. Drilled Boreholes increase the potential for contamination of the groundwater exponentially, since, especially if improperly constructed, they act as a connection between two aquifers/a zone of contamination and an aquifer (Natural Resource Defense Council (NRDC), 2012). Out-of-zone fracture growth can occur while performing hydraulic fracturing. That means fractures grow into other geologic formations, potentially including groundwater aquifers. Also, connections that already exist due to extensive natural faults and fractures can be more delicate to hydraulic fracturing. Neighbouring wells can act as a vertical pathway for the fracturing fluid into groundwater aquifers. Therefore, detailed information about existing wells is as important as geologic and hydrologic mapping to identify pre-existing natural pathways and groundwater flow. An estimation of the freshwater use and the resulting wastewater volume is recommended, too. To avoid contamination of the through-drilled layers, proper well construction is important. Therefore, it's necessary to ensure that the casing is properly cemented and that it will be set at least 100 feet below the deepest groundwater aquifer that needs to be protected (Natural Resource Defense Council (NRDC), 2012). If the well isn't built properly, failure of the casing can occur during the hydraulic fracturing due to the high pressure, too, which potentially leads to groundwater contamination as well (Li, Dong, & Wang, 2017). A continuous monitoring of key performance indicators like pressure and

injection rates can indicate a transition of fracturing fluid into unwanted layers (Natural Resource Defense Council (NRDC), 2012).

Even though ground water contamination is the biggest threat, there could be other unwanted subsurface hydraulic connections. For example, if the fracturing fluid is mixed with the formation water of an unknown layer, solid matter could be precipitated out of the fluid (Li, Al-Muntasheri, & Liang, 2016)That could potentially decrease the permeability. For further information the reader is referred to the chapter on fluid-rock and fluid-fluid interactions.

# C. Literature review - effect of stimulation

| | Country | Location | Type of stimulation | Acid | pre II [l/(s*bar)] | post II [l/(s*bar)] | pre PI [l/(s*bar)] | post PI [l/(s*bar)] | Improvement ratio I1 | Improvement ratio I2 | Improvement [%] | Year | Reference |
|---|---|---|---|---|---|---|---|---|---|---|---|---|---|
| 1 | Iceland | MG-11 | Hydraulic | | | | | | 62,5 | 2,2 | 2741% | 1971 | 1975_Tomasson Thorsteinsson_Use of injection packer for hydrothermal drillhole stimulation in iceland |
| 2 | Turkey | Aydın Kuyucak - KS1 | Chemical | HCl | 0,53 | 14,34 | | | | | 2616% | 2017 | 2017_Eker et al_Enhancement of geothermal reservoir through varying acidizing operation procedures in Aydin Kuyucak geothermal field |
| 3 | Iceland | MG-14 | Hydraulic | | | | | | 73,7 | 2,9 | 2441% | 1972 | 1975_Tomasson Thorsteinsson_Use of injection packer for hydrothermal drillhole stimulation in iceland |
| 4 | Iceland | SN-12 | Hydraulic | | | | 0,1 | 2,2 | | | 2100% | 1994 | 1996_Tulinius et al_Stimulation of well SN-12 in the seltjarnarnes low-temperature field in SW-Iceland.pdf |
| 5 | Germany | Groß-Schönebeck | Hydraulic | | | | 0,004 | 0,0849 | | | 2023% | 2010 | 2010_Zimmermann et al_Cyclic waterfrad stimulation to develop an EGS - conceptual design and experimental results |
| 6 | France | Soultz-sous-Forêts - GPK4 | Hydraulic | | 0,01 | 0,2 | | | | | 1900% | 2004 | 2008_Nami et al_Chemical stimulation Soultz-sous-forets |
| 7 | USA | RRGP-4 | Hydraulic | | | | 0,03 | 0,56 | | | 1900% | 1979 | 2004_Combs et al_Geothermal well stimulation technology - a preliminary review.pdf |
| 8 | USA | 55-29 | Hydraulic | | 3,7 | 47 | | | | | 1170% | 2012 | 2013_Petty et al_Improving geothermal project economics with multi-zone stimulation.pdf |
| 9 | Italy | L-14 | Chemical | HCl | | | | | | | 1150% | 1984 | 1985_Barelli et al_Well stimulation in Latera field |
| 10 | Iceland | MG-28 | Hydraulic | | | | | | 26,5 | 2,2 | 1105% | 1974 | 1975_Tomasson Thorsteinsson_Use of injection packer for hydrothermal drillhole stimulation in iceland |
| 11 | Italy | Lardarello - 3 | Chemical | HCl-HF | 1,5 | 18 | | | | | 1100% | 2006 | 2009_Protier et al_chemical stimulation EGS system at soultz-sous-forets |
| 12 | Iceland | MG-5 | Hydraulic | | | | | | 7,1 | 0,6 | 1083% | 1970 | 1975_Tomasson Thorsteinsson_Use of injection packer for hydrothermal drillhole stimulation in iceland |
| 13 | Turkey | Aydın Kuyucak - KS2 | Chemical | HCl | 0,25 | 2,75 | | | | | 1012% | 2017 | 2017_Eker et al_Enhancement of geothermal reservoir through varying acidizing operation procedures in Aydin Kuyucak geothermal field |
| 14 | Iceland | MG-3 | Hydraulic | | | | | | 3,2 | 0,31 | 932% | 1970 | 1975_Tomasson Thorsteinsson_Use of injection packer for hydrothermal drillhole stimulation in iceland |
| 15 | El Salvador | Berlin - 3 | Chemical | HCl-HF | 0,2 | 1,98 | | | | | 890% | 2002 | 2009_Protier et al_chemical stimulation EGS system at soultz-sous-forets |
| 16 | Iceland | MG-18 | Hydraulic | | | | | | 15,8 | 1,7 | 829% | 1973 | 1975_Tomasson Thorsteinsson_Use of injection packer for hydrothermal drillhole stimulation in iceland |
| 17 | Phillipines | MG7RD | Chemical | HCl, HF, sandstone acid | 15,4 | 114 | | | | | 640% | 2005 | 2012_Alcala_Acid stimulation of geothermal wells in Mexico, el salvador and the philipines.pdf |
| 18 | Philippines | Leyte - 3 | Chemical | HCl-HF | 1,52 | 10,8 | | | | | 611% | 1998 | 2009_Protier et al_chemical stimulation EGS system at soultz-sous-forets |
| 19 | France | Soultz-sous-Forêts - GPK2 | Hydraulic | | 0,05 | 0,35 | | | | | 600% | 2000 | 2008_Nami et al_Chemical stimulation Soultz-sous-forets |
| 20 | Mexico | AZ-68D | Chemical | HCl/HF | | | | | | | 540% | 2008 | 2012_Alcala_Acid stimulation of geothermal wells in Mexico, el salvador and the philipines.pdf |
| 21 | Italy | Lardarello - 2 | Chemical | HCl-HF | 4 | 25 | | | | | 525% | 2006 | 2009_Protier et al_chemical stimulation EGS system at soultz-sous-forets |
| 22 | El Salvador | Berlin - 2 | Chemical | HCl-HF | 1,4 | 8,6 | | | | | 514% | 2002 | 2009_Protier et al_chemical stimulation EGS system at soultz-sous-forets |
| 23 | Iceland | MG-27 | Hydraulic | | | | | | 6,84 | 1,13 | 505% | 1974 | 2016_Covell_Hydraulic well stimulation in low temperature geothermal areas for direct use.pdf |

Figure 54: Literature review on effect of stimulation

| | Country | Location | Type of stimulation | Acid | pre II [l/[s*bar]] | post II [l/[s*bar]] | pre PI [l/[s*bar]] | post PI [l/[s*bar]] | Improvement ratio I1 | Improvement ratio I2 | Improvement [%] | Year | Reference |
|---|---|---|---|---|---|---|---|---|---|---|---|---|---|
| 24 | Iceland | MG-4 | Hydraulic | | | | | | 8,5 | 1,6 | 431% | 1970 | 1975_Tomasson Thorsteinsson_Use of injection packer for hydrothermal drillhole stimulation in iceland |
| 25 | Turkey | Alaşehir - DP-1 | Chemical | HCl | | | | | | | 421% | 2015 | 2015_Akin et al_Coiled Tubing acid stimulation Alasehir geothermal field, turkey |
| 26 | Germany | Bad Urach | Hydraulic | | 0,00204 | 0,01 | | | | | 420% | 2002 | 2003_Schanz et al_Hot dry rock project Bad Urach - general overview |
| 27 | Germany | Groß-Schönebeck | Hydraulic | | | | 0,028 | 0,142 | | | 407% | 2010 | 2010_Zimmermann et al_Cyclic waterfrad stimulation to develop an EGS - conceptual design and experrimental results |
| 28 | Switzerland | Basel | Hydraulic | | | | | | | | 400% | 2006 | 2008_Häring_Characterisation of the Basel 1 enhanced geothermal system |
| 29 | Italy | Lardarello - 1 | Chemical | HCl-HF | 11 | 54 | | | | | 391% | 2006 | 2009_Protier et al_chemical stimulation EGS system at soultz-sous-forets |
| 30 | Italy | Lardarello - 5 | Chemical | HCl-HF | 11 | 54 | | | | | 391% | 2006 | 2009_Protier et al_chemical stimulation EGS system at soultz-sous-forets |
| 31 | Iceland | MG-39 | Hydraulic | | | | | | | | 390% | 1977 | 2016_Covell_Hydraulic well stimulatiom in low temperature geothermal areas for direct use.pdf |
| 32 | El Salvador | Berlin - 1 | Chemical | HCl-HF | 1,6 | 7,6 | | | | | 375% | 2002 | 2009_Protier et al_chemical stimulation EGS system at soultz-sous-forets |
| 33 | Mexico | AZ-56R | Chemical | HCl/HF | | | | | | | 367% | 2006 | 2012_Alcala_Acid stimulation of geothermal wells in Mexico, el salvador and the philipines.pdf |
| 34 | USA | Desert peak 27-17 | Hydraulic | | 0,064106 | 0,293056 | | | | | 357% | 2010 | 2012_Hydraulic Stimulation of Well 27-15, dessert peak geothermal field Nevada, USA.pdf |
| 35 | Phlippines | Tiwi | Chemical | HCl-HF | 2,52 | 11,34 | | | | | 350% | 1995 | 2009_Protier et al_chemical stimulation EGS system at soultz-sous-forets |
| 36 | Phlippines | Bacman - 1 | Chemical | HCl-HF | 0,68 | 3,01 | | | | | 343% | 1995 | 2009_Protier et al_chemical stimulation EGS system at soultz-sous-forets |
| 37 | Iceland | HE-8 | Hydraulic, Thermal | | 1,5 | 6,5 | | | | | 333% | 2003 | 2006_Axeksson et al_Stimulation of geothermal wells in basaltic rock in iceland.pdf |
| 38 | Germany | Groß-Schönebeck | Hydraulic | | | | 0,066 | 0,281 | | | 326% | 2010 | 2010_Zimmermann et al_Cyclic waterfrad stimulation to develop an EGS - conceptual design and experrimental results |
| 39 | Indonesia | Awi 3 | Hydraulic | | 0,74 | 2,95 | | | | | 300% | 2012 | 2016_Covell_Hydraulic well stimulatiom in low temperature geothermal areas for direct use.pdf |
| 40 | USA | Desert peak 27-15 | Hydraulic | | 0,009158 | 0,036632 | | | | | 300% | 2010 | 2012_Hydraulic Stimulation of Well 27-15, dessert peak geothermal field Nevada, USA.pdf |
| 41 | USA | Cosco - 34A-9 | Hydraulic | | 8,07 | 31,5 | | | | | 290% | 2004 | 2006_Rose et al_ A comparison of hydraulic stimulation experiments at the Soultz, France and Cosco, California EGS |
| 42 | El Salvador | Berlin - 4 | Chemical | HCl-HF | 0,9 | 3,4 | | | | | 278% | 2002 | 2009_Protier et al_chemical stimulation EGS system at soultz-sous-forets |
| 43 | Iceland | Hlídardalur | Hydraulic | | | | | | | | 250% | 1970 | 2016_Covell_Hydraulic well stimulatiom in low temperature geothermal areas for direct use.pdf |
| 44 | Iceland | MG-9 | Hydraulic | | | | | | 6,2 | 1,8 | 244% | 1971 | 1975_Tomasson Thorsteinsson_Use of injection packer for hydrothermal drillhole stimulation in iceland |
| 45 | Iceland | MG-8 | Hydraulic | | | | | | 2,7 | 0,84 | 221% | 1971 | 1975_Tomasson Thorsteinsson_Use of injection packer for hydrothermal drillhole stimulation in iceland |
| 46 | Germany | Gt N 4 | Chemical | HCl | | | | | | | 218% | 2010 | GTN_intern |
| 47 | Australia | Habanero-3 | Hydraulic | | | | 0,16 | 0,5 | | | 213% | 2008 | 2016_Covell_Hydraulic well stimulatiom in low temperature geothermal areas for direct use.pdf |

Figure 55: Literature review on effect of stimulation

Figure 56: Literature review on effect of stimulation

| | Country | Location | Type of stimulation | Acid | pre II [l/[s*bar]] | post II [l/[s*bar]] | pre PI [l/[s*bar]] | post PI [l/[s*bar]] | Improvement ratio I1 | Improvement ratio I2 | Improvement [%] | Year | Reference |
|---|---|---|---|---|---|---|---|---|---|---|---|---|---|
| 48 | Mexico | AZ-9AD | Chemical | HCl/HF | | | | | | | 209% | 2005 | 2012_Alcala_Acid stimulation of geothermal wells in Mexico, el salvador and the philipines.pdf |
| 49 | Mexico | Las Tres Virgines - 2 | Chemical | HCl-HF | 1,2 | 3,7 | | | | | 208% | 2003 | 2009_Protier et al_chemical stimulation EGS system at soultz-sous-forets |
| 50 | Germany | Landau | Hydraulic | | | | 0,2 | 0,6 | | | 200% | 2006 | 2010_Schindler et al_Successful Hydraulic Stimulation Techniques for Electric Power Production in the ORG |
| 51 | El Salvador | TR-7 | Chemical | HCl, phosphonic, HF, boric acid | 0,549 | 1,561 | | | | | 184% | 2002 | 2012_Alcala_Acid stimulation of geothermal wells in Mexico, el salvador and the philipines.pdf |
| 52 | El Salvador | Berlin - 5 | Chemical | HCl-HF | 1,65 | 4,67 | | | | | 183% | 2002 | 2009_Protier et al_chemical stimulation EGS system at soultz-sous-forets |
| 53 | Mexico | Los Azufres | Chemical | HCl-HF | 3,3 | 9,1 | | | | | 176% | 2006 | 2009_Protier et al_chemical stimulation EGS system at soultz-sous-forets |
| 54 | Phillipines | OP-5DA | Chemical | HCl, sandstone acid | | | | | | | 173% | 2005 | 2012_Alcala_Acid stimulation of geothermal wells in Mexico, el salvador and the philipines.pdf |
| 55 | Mexico | AZ-9A | Chemical | HCl/HF | | | | | | | 168% | 2006 | 2012_Alcala_Acid stimulation of geothermal wells in Mexico, el salvador and the philipines.pdf |
| 56 | Phillipines | 4R7D | Chemical | HCl, HF, sandstone acid | 6,8 | 17,7 | | | | | 160% | 2005 | 2012_Alcala_Acid stimulation of geothermal wells in Mexico, el salvador and the philipines.pdf |
| 57 | Phlippines | Leyte - 2 | Chemical | HCl-HF | 0,68 | 1,77 | | | | | 160% | 1998 | 2009_Protier et al_chemical stimulation EGS system at soultz-sous-forets |
| 58 | USA | Rossi 21-19 | Chemical | HCl, HF | | | 0,92 | 2,33 | | | 155% | 1984 | 2004_Combs et al_Geothermal well stimulation technology - a preliminary review.pdf |
| 59 | Mexico | Las Tres Virgines - 1 | Chemical | HCl-HF | 0,8 | 2 | | | | | 150% | 2003 | 2009_Protier et al_chemical stimulation EGS system at soultz-sous-forets |
| 60 | Mexico | AZ-51 | Chemical | HCl/HF | | | | | | | 147% | 2010 | 2012_Alcala_Acid stimulation of geothermal wells in Mexico, el salvador and the philipines.pdf |
| 61 | Mexico | AZ-52 | Chemical | HCl/HF | | | | | | | 143% | 1987 | 2012_Alcala_Acid stimulation of geothermal wells in Mexico, el salvador and the philipines.pdf |
| 62 | Mexico | AZ-36 | Chemical | HCl/HF | | | | | | | 133% | 2010 | 2012_Alcala_Acid stimulation of geothermal wells in Mexico, el salvador and the philipines.pdf |
| 63 | Mexico | AZ-8 | Chemical | HCl/HF | | | | | | | 128% | 1988 | 2012_Alcala_Acid stimulation of geothermal wells in Mexico, el salvador and the philipines.pdf |
| 64 | Iceland | SN-12 | Hydraulic | | | | 2,2 | 5 | | | 127% | 1994 | 1996_Tulinius et al_Stimulation of well SN-12 in the seltjarnarnes low-temperature field in SW-Iceland.pdf |
| 65 | France | GRT-1 | Thermal | | 0,6 | 1,3 | | | | | 117% | 2017 | 2017_Baujard et al_Hydrothermal characterization of wells GR 1 and GRT-2 in Rittershofen |
| 66 | Iceland | RN-21 | Hydraulic | | 6 | 13 | | | | | 117% | 2006 | 2009_Axelsson Thorhallson_Review of well stimulation operations in iceland.pdf |
| 67 | USA | 58-30 | Hydraulic | | | | | | | | 112% | 1980 | 2004_Combs et al_Geothermal well stimulation technology - a preliminary review.pdf |
| 68 | Phillipines | OP-3D | Chemical | HCl, sandstone acid | | | | | | | 104% | 2005 | 2012_Alcala_Acid stimulation of geothermal wells in Mexico, el salvador and the philipines.pdf |
| 69 | Indonesia | Awi 18-1 | Hydraulic | | 1,11 | 2,25 | | | | | 104% | 2010 | 2015_Yoshioka_Zonal Hydraulic Stimulation in the Salak geothermal field.pdf |
| 70 | France | Soultz-sous-Forêts - GPK4 | Chemical | NTA | | | 0,2 | 0,4 | | | 100% | 2006 | 2008_Nami et al_Chemical stimulation Soultz-sous-forets |
| 71 | Turkey | Alaşehir - BY-6 | Chemical | HCl | | | | | | | 100% | 2015 | 2015_Akin et al_Coiled Tubing acid stimulation Alasehir geothermal field, turkey |

| | Country | Location | Type of stimulation | Acid | pre II [l/[s*bar]] | post II [l/[s*bar]] | pre PI [l/[s*bar]] | post PI [l/[s*bar]] | Improvement ratio I1 | Improvement ratio I2 | Improvement [%] | Year | Reference |
|---|---|---|---|---|---|---|---|---|---|---|---|---|---|
| 72 | Phlippines | Leyte - 1 | Chemical | HCl-HF | 3,01 | 5,84 | | | | | 94% | 1997 | 2009_Protier et al_chemical stimulation EGS system at soultz-sous-forets |
| 73 | Phillipines | 4R12D | Chemical | HCl, HF, sandstone acid | 30,1 | 58,4 | | | | | 94% | 2005 | 2012_Alcala_Acid stimulation of geothermal wells in Mexico, el salvador and the philipines.pdf |
| 74 | Australia | Habanero-1 | Hydraulic | | | | | | | | 93% | 2003 | 2016_Covell_Hydraulic well stimulatiom in low temperature geothermal areas for direct use.pdf |
| 75 | Mexico | AZ-25 | Chemical | HCl/HF | | | | | | | 88% | 2008 | 2012_Alcala_Acid stimulation of geothermal wells in Mexico, el salvador and the philipines.pdf |
| 76 | France | GRT-1 | Hydraulic - Chemical | C6H8O7 | 1,3 | 2,4 | | | | | 85% | 2017 | 2017_Baujard et al_Hydrothermal characterization of wells GR 1 and GRT-2 in Rittershofen |
| 77 | El Salvador | TR-10 | Chemical | HCl, phosphonic, HF, boric acid | 0,684 | 1,223 | | | | | 79% | 2002 | 2012_Alcala_Acid stimulation of geothermal wells in Mexico, el salvador and the philipines.pdf |
| 78 | Lithuania | Klaipeda KDGP-1I | Hydraulic | backflush | 0,28 | 0,5 | | | | | 79% | 2012 | Geotherma_ operational data |
| 79 | Guadeloupe | BO-4 | Thermal | | | | | | | | 75% | 1998 | 2004_Combs et al_Geothermal well stimulation technology - a preliminary review.pdf |
| 80 | Phillipines | LG4D | Chemical | HCl, HF | | | | | | | 72% | 2005 | 2012_Alcala_Acid stimulation of geothermal wells in Mexico, el salvador and the philipines.pdf |
| 81 | Switzerland | X | Chemical | HCL | <0,5 | 0,5-1,2 | | | | | 70% | | GTN_intern |
| 82 | Turkey | Alaşehir - BY-2 | Chemical | HCl | | | | | | | 68% | 2015 | 2015_Akin et al_Coiled Tubing acid stimulation Alasehir geothermal field, turkey |
| 83 | Germany | Groß-Schönebeck | Hydraulic | | | | 0,034 | 0,057 | | | 68% | 2010 | 2010_Zimmermann et al_Cyclic waterfrad stimulation to develop an EGS - conceptual design and experrimental results |
| 84 | Germany | Landau | Hydraulic | | | | 0,6 | 1 | | | 67% | 2006 | 2010_Schindler et al_Successful Hydraulic Stimulation Techniques for Electric Power Production in the ORG |
| 85 | Iceland | RN-18 | Hydraulic | | 1,2 | 2 | | | | | 67% | 2006 | 2009_Axelsson Thorhallson_Review of well stimulation operations in iceland.pdf |
| 86 | France | Soultz-sous-Forêts - GPK4 | Chemical | HCl | 0,2 | 0,33 | | | | | 65% | 2005 | 2008_Nami et al_Chemical stimulation Soultz-sous-forets |
| 87 | USA | Desert peak 27-17 | Hydraulic | | 0,293056 | 0,476216 | | | | | 63% | 2010 | 2012_Hydraulic Stimulation of Well 27-15, dessert peak geothermal field Nevada, USA.pdf |
| 88 | Lithuania | Klaipeda KDGP-1I | Chemical | HCl | 0,53 | 0,86 | | | | | 62% | 2010 | Geotherma_ operational data |
| 89 | Lithuania | Klaipeda KDGP-4I | Chemical | HCl | 0,53 | 0,85 | | | | | 60% | 2010 | Geotherma_ operational data |
| 90 | Germany | Gt NG 2 | Chemical | HCl | | | | | | | 50% | 2012 | GTN_intern |
| 91 | Iceland | Leirá (SW-Iceland) | Hydraulic | | | | | | | | 50% | 1970 | 2016_Covell_Hydraulic well stimulatiom in low temperature geothermal areas for direct use.pdf |
| 92 | Turkey | Alaşehir - BY-5 | Chemical | HCl | | | | | | | 47% | 2015 | 2015_Akin et al_Coiled Tubing acid stimulation Alasehir geothermal field, turkey |
| 93 | Phlippines | Bacman - 2 | Chemical | HCl-HF | 0,99 | 1,4 | | | | | 41% | 1995 | 2009_Protier et al_chemical stimulation EGS system at soultz-sous-forets |
| 94 | USA | Desert peak 27-16 | Chemical | | 0,04579 | 0,064106 | | | | | 40% | 2010 | 2012_Hydraulic Stimulation of Well 27-15, dessert peak geothermal field Nevada, USA.pdf |
| 95 | Phillipines | PN31D | Chemical | HCl, HF | | | | | | | 38% | 2005 | 2012_Alcala_Acid stimulation of geothermal wells in Mexico, el salvador and the philipines.pdf |

Figure 57: Literature review on effect of stimulation

| | Country | Location | Type of stimulation | Acid | pre II [l/(s*bar)] | post II [l/(s*bar)] | pre PI [l/(s*bar)] | post PI [l/(s*bar)] | Improvement ratio I1 | Improvement ratio I2 | Improvement [%] | Year | Reference |
|---|---|---|---|---|---|---|---|---|---|---|---|---|---|
| 96 | Mexico | AZ-57 | Chemical | HCl/HF | | | | | | | 33% | 2010 | 2012_Alcala_Acid stimulation of geothermal wells in Mexico, el salvador and the philipines.pdf |
| 97 | Mexico | AZ-15 | Chemical | HCl/HF | | | | | | | 32% | 1980 | 2012_Alcala_Acid stimulation of geothermal wells in Mexico, el salvador and the philipines.pdf |
| 98 | Phillipines | | Hydraulic | | 1,13 | 1,43 | | | | | 27% | 2013 | 2016_Covell_Hydraulic well stimulatiom in low temperature geothermal areas for direct use.pdf |
| 99 | USA | Desert peak 27-16 | Chemical | | 0,036632 | 0,04579 | | | | | 25% | 2010 | 2012_Hydraulic Stimulation of Well 27-15, dessert peak geothermal field Nevada, USA.pdf |
| 100 | France | Soultz-sous-Forêts - GPK4 | Chemical | OCA | | | 0,4 | 0,5 | | | 25% | 2007 | 2008_Nami et al_Chemical stimulation Soultz-sous-forets |
| 101 | France | Paris Basin | Chemical | HCl | 8,2 | 10,2 | | | | | 24% | 1998 | 1998_Ventre_Soft acidizing of damaged geothermal injection wells.pdf |
| 102 | Iceland | MG-6 | Hydraulic | | | | | | 1,6 | 1,3 | 23% | 1970 | 1975_Tomasson Thorsteinsson_Use of injection packer for hydrothermal drillhole stimulation in iceland |
| 103 | France | Paris Basin | Chemical | HCl | 7,5 | 9,2 | | | | | 23% | 1998 | 1998_Ventre_Soft acidizing of damaged geothermal injection wells.pdf |
| 104 | France | Soultz-sous-Forêts - GPK4 | Chemical | RMA | 0,33 | 0,4 | | | | | 21% | 2006 | 2008_Nami et al_Chemical stimulation Soultz-sous-forets |
| 105 | USA | Desert peak 27-17 | Hydraulic | | 0,476216 | 0,5769544 | | | | | 21% | 2010 | 2012_Hydraulic Stimulation of Well 27-15, dessert peak geothermal field Nevada, USA.pdf |
| 106 | Iceland | SN-12 | Hydraulic | | | | 5 | 6 | | | 20% | 1994 | 1996_Tulinius et al_Stimulation of well SN-12 in the seltjarnarnes low-temperature field in SW-Iceland.pdf |
| 107 | Iceland | RN-15 | Hydraulic | | 6 | 7 | | | | | 17% | 2006 | 2009_Axelsson Thorhallson_Review of well stimulation operations in iceland.pdf |
| 108 | France | Soultz-sous-Forêts - GPK3 | Chemical | OCA | 0,35 | 0,4 | | | | | 14% | 2007 | 2008_Nami et al_Chemical stimulation Soultz-sous-forets |
| 109 | Iceland | RN-16 | Hydraulic | | 3,5 | 4 | | | | | 14% | 2006 | 2009_Axelsson Thorhallson_Review of well stimulation operations in iceland.pdf |
| 110 | Mexico | AZ-7 | Chemical | HCl/HF | | | | | | | 13% | 2000 | 2012_Alcala_Acid stimulation of geothermal wells in Mexico, el salvador and the philipines.pdf |
| 111 | France | Soultz-sous-Forêts - GPK2 | Chemical | HCl | 0,4 | 0,45 | | | | | 13% | 2003 | 2008_Nami et al_Chemical stimulation Soultz-sous-forets |
| 112 | Lithuania | Klaipeda KDGP-11 | Chemical | HCl+HF | 0,33 | 0,36 | | | | | 9% | 2015 | Geotherma_ operational data |
| 113 | Iceland | RN-19 | Hydraulic | | 5 | 5,4 | | | | | 8% | 2006 | 2009_Axelsson Thorhallson_Review of well stimulation operations in iceland.pdf |
| 114 | France | Paris Basin | Chemical | HCl | 6,3 | 6,8 | | | | | 8% | 1998 | 1998_Ventre_Soft acidizing of damaged geothermal injection wells.pdf |
| 115 | France | Soultz-sous-Forêts - GPK3 | Chemical | HCl | 0,35 | 0,35 | | | | | 0% | 2003 | 2008_Nami et al_Chemical stimulation Soultz-sous-forets |
| 116 | France | Soultz-sous-Forêts - GPK4 | Hydraulic | | 0,2 | 0,2 | | | | | 0% | 2005 | 2008_Nami et al_Chemical stimulation Soultz-sous-forets |
| 117 | USA | The Geysers | Chemical | HCl-HF | 1 | 1 | | | | | 0% | 2006 | 2009_Protier et al_chemical stimulation EGS system at soultz-sous-forets |
| 118 | USA | Fenton Hill | Chemical | Na2CO3 | 1 | 1 | | | | | 0% | 1977 | 2009_Protier et al_chemical stimulation EGS system at soultz-sous-forets |
| 119 | Germany | Landau | Chemical | HCl | | | 1 | 1 | | | 0% | 2006 | 2010_Schindler et al_Successful Hydraulic Stimulation Techniques for Electric Power Production in the ORG |

Figure 58: Literature review on effect of stimulation

| | Country | Location | Type of stimulation | Acid | pre II [l/s*bar]] | post II [l/s*bar]] | pre PI [l/s*bar]] | post PI [l/s*bar]] | Improvement ratio I1 | Improvement ratio I2 | Improvement [%] | Year | Reference |
|---|---|---|---|---|---|---|---|---|---|---|---|---|---|
| 120 | Phillipines | PN13D | Chemical | HCl, HF | | | | | | | 0% | 2005 | 2012_Alcala_Acid stimulation of geothermal wells in Mexico, el salvador and the philipines.pdf |
| 121 | Iceland | RN-20 | Hydraulic | | 5 | 5 | | | | | 0% | 2006 | 2009_Axelsson Thorhallson_Review of well stimulation operations in iceland.pdf |
| 122 | Iceland | RN-22 | Hydraulic | | 10 | 10 | | | | | 0% | 2006 | 2009_Axelsson Thorhallson_Review of well stimulation operations in iceland.pdf |
| 123 | Lithuania | Klaipeda KDGP-11 | Mechanical | Radial Jetting Drilling | 0,31 | 0,31 | | | | | 0% | 2017 | Geotherma_ operational data |
| 124 | Germany | Gen-1St-A1 | Chemical | SSB-007+HCL | | 0,02 | 0,032 | | | | 0% | 2017 | 2018 Wolfgramm et al_Erschließung, Test und Analyse des ersten kluftdominierten Dolomitaquifers im tiefen Malm des Molassebeckens FK 0324004D |
| 125 | Iceland | LJ-6 | Hydraulic | | | | | | | | 0% | 1970 | 2016_Covell_Hydraulic well stimulatiom in low temperature geothermal areas for direct use.pdf |
| 126 | Iceland | LGJ-8 | Hydraulic | | | | | | | | 0% | 1970 | 2016_Covell_Hydraulic well stimulatiom in low temperature geothermal areas for direct use.pdf |
| 127 | USA | RRGP-5 | Hydraulic | | | | | | | | 0% | 1979 | 2004_Combs et al_Geothermal well stimulation technology - a preliminary review.pdf |
| 128 | Italy | L-1 | Hydraulic, Chemical | | | | | | | | 0% | 1982 | 2004_Combs et al_Geothermal well stimulation technology - a preliminary review.pdf |
| 129 | Italy | L-6 | Hydraulic, Chemical | | | | | | | | 0% | 1982 | 2004_Combs et al_Geothermal well stimulation technology - a preliminary review.pdf |
| 130 | Indonesia | Awi 20-1 | Hydraulic | | | | | | | | 0% | 2012 | 2016_Covell_Hydraulic well stimulatiom in low temperature geothermal areas for direct use.pdf |
| 131 | Phillipines | K6 | Hydraulic | | | | | | | | 0% | 2013 | 2016_Covell_Hydraulic well stimulatiom in low temperature geothermal areas for direct use.pdf |
| 132 | Südkorea | Pohang | Hydraulic | | | | | | | | 0% | 2018 | Personal contact Hannes Hoffmann GFZ Potsdam |
| 133 | Phillipines | PN27D | Chemical | HCl, HF | | | | | | | -12% | 2005 | 2012_Alcala_Acid stimulation of geothermal wells in Mexico, el salvador and the philipines.pdf |
| 134 | El Salvador | TR-1B | Chemical | HCl, phosphonic, HF, boric acid | 0,659 | 0,557 | | | | | -15% | 2006 | 2012_Alcala_Acid stimulation of geothermal wells in Mexico, el salvador and the philipines.pdf |
| 135 | USA | LF-30 | Explosive | | | | | | | | -36% | 1981 | 2004_Combs et al_Geothermal well stimulation technology - a preliminary review.pdf |
| 136 | USA | Baca-23 | Hydraulic | | | | | | | | -58% | 1981 | 2004_Combs et al_Geothermal well stimulation technology - a preliminary review.pdf |

Figure 59: Literature review on effect of stimulation

# D. Program flow charts

## D.1. Overall model

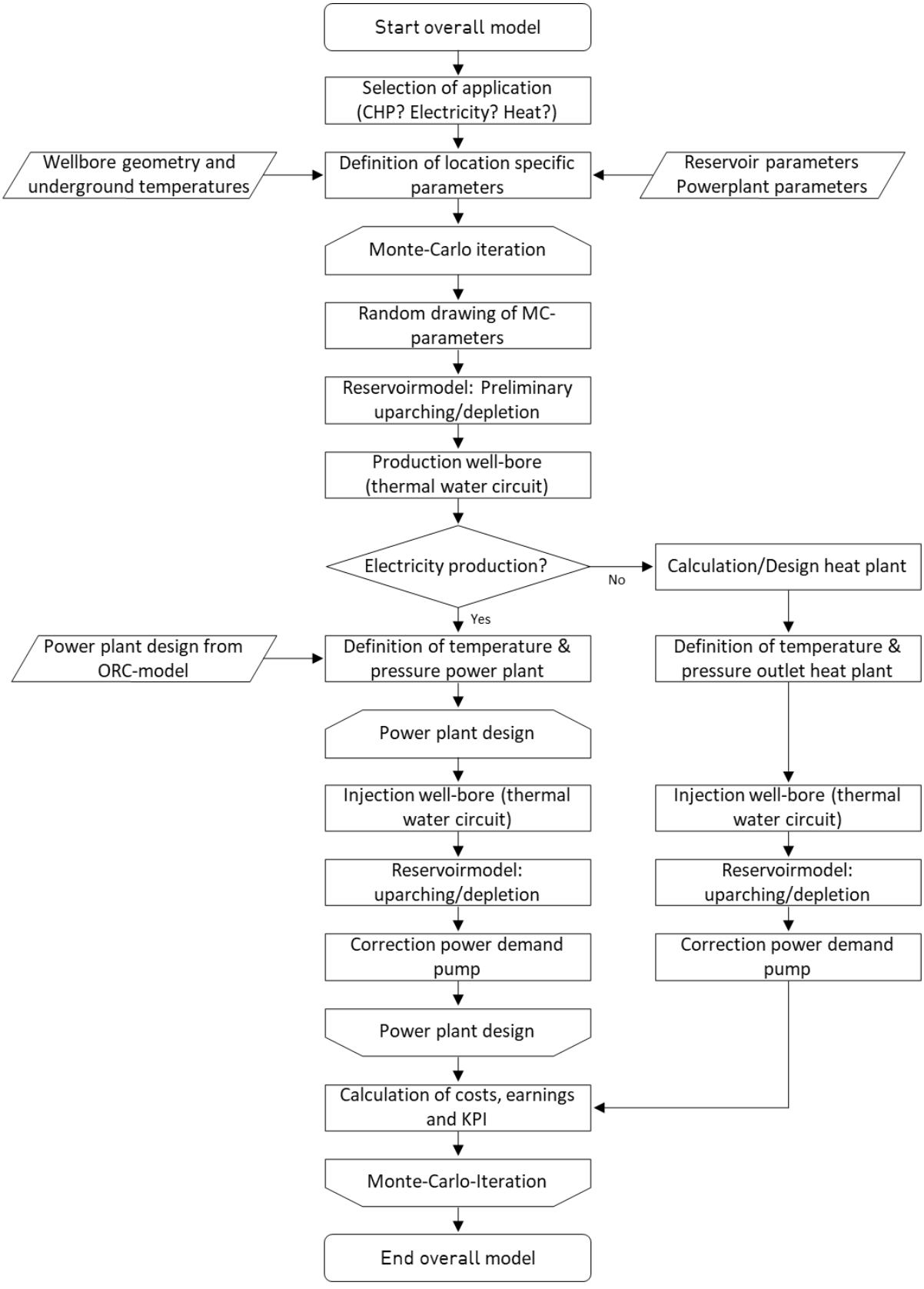


Figure 60: Program flow chart overall model

## D.2. Power plant

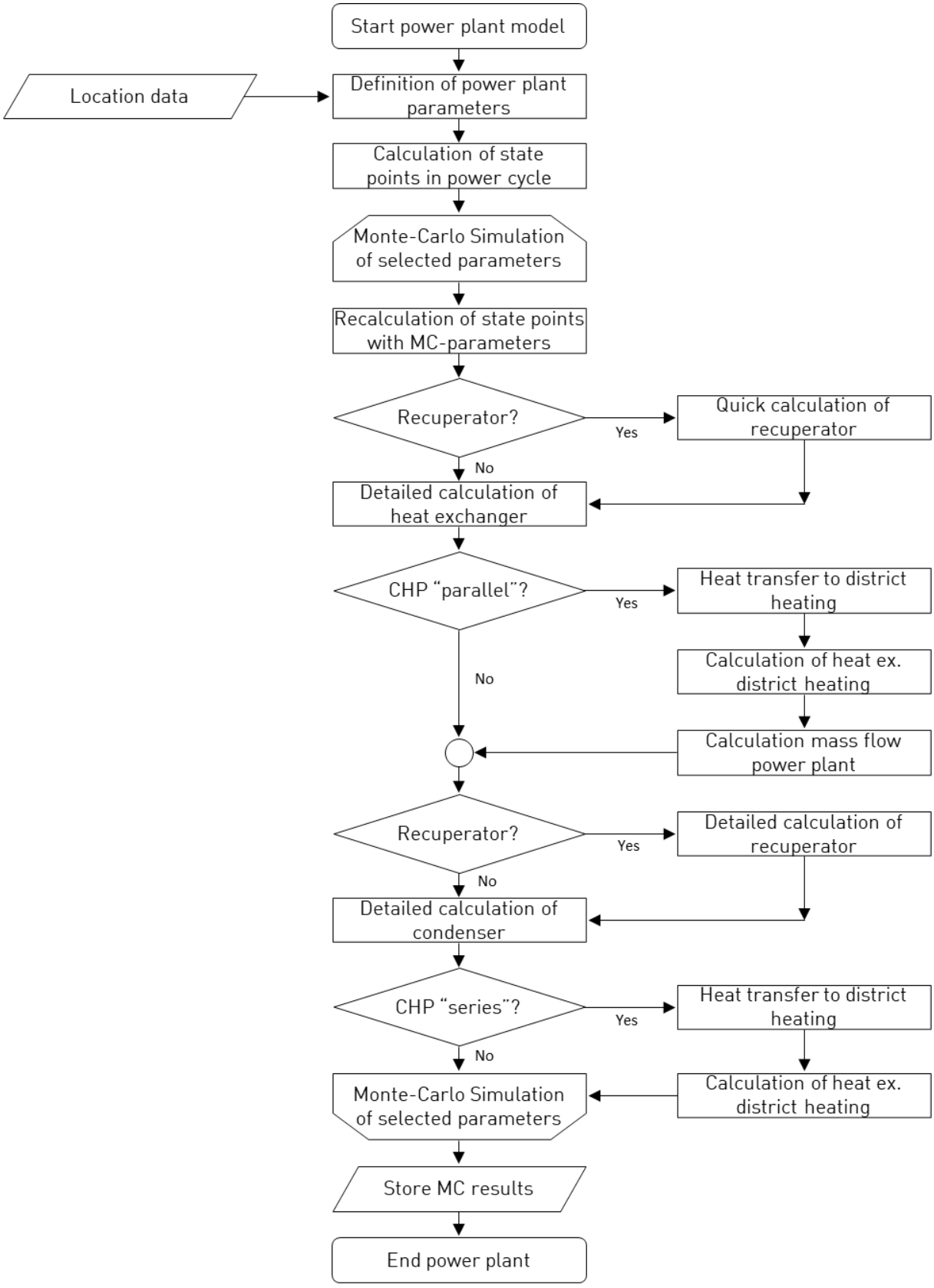


Figure 61: Program flow chart power plant model

## D.3. Wellbore

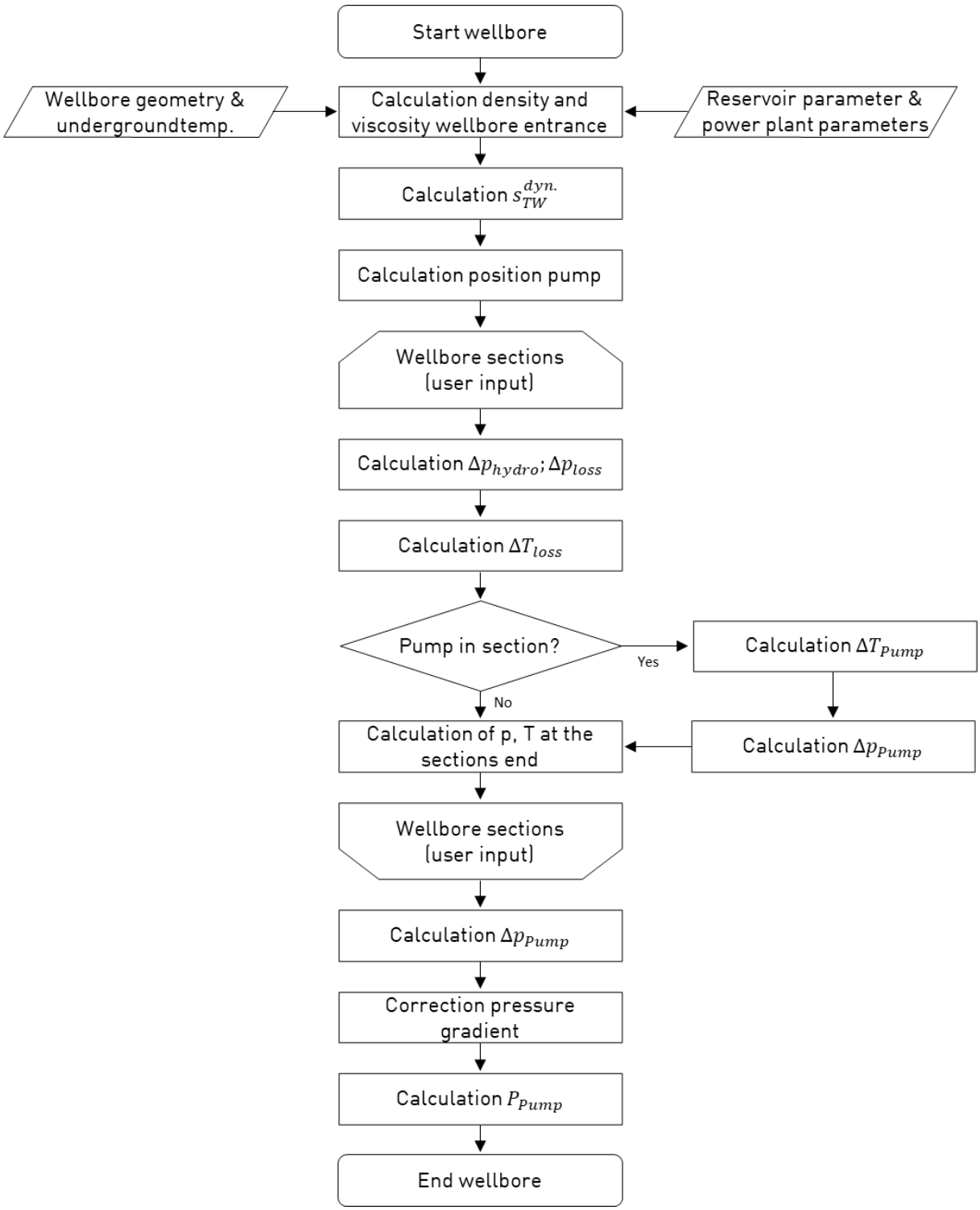


Figure 62: Program flow chart wellbore model

## E. Calculation of overall heat transfer coefficient

The procedure for determining the heat transfer coefficient in each section of the heat exchanger is explained below. Knowing this coefficient, the required heat exchanger areas can be determined as described in section 3.1.3.1. The index i is neglected for better clarity. All quantities except diameters and mass flows refer to a sub-section i. First the equations for the evaporator are introduced and then deviations in the calculation of the heat transfer coefficient in the condenser are presented. The procedure for recuperators and heat exchangers for heat extraction corresponds in principle to the calculation steps for the evaporator.

**Evaporator**: For hot geothermal fluid in the pipes and working medium in the jacket, the overall heat transfer coefficient is calculated according to equation (57).

$$k = \left( \frac{1}{\alpha_{WM}} + \frac{r_{out} * ln\left(\frac{r_{out}}{r_{in}}\right)}{\lambda_{pipe}} + \frac{r_{out}}{r_{in}} * \frac{1}{\alpha_{TW}} \right)^{-1} \quad (57)$$

The inner and outer diameter of the pipes can be derived from data in Table 3, where also the heat conductivity of the pipe $\lambda_{pipe}$ can be found. To calculate the overall heat transfer coefficient, the heat transfer coefficients of thermal water ($\alpha_{TW}$) and the working medium ($\alpha_{WM}$) are necessary. These can be calculated with the Nusselt-number according to equations (58) and (59).

$$\alpha_{WM} = \frac{Nu_{WM} * \lambda_{WM}}{d_h^{jacket}} \; and \; \alpha_{TW} = \frac{Nu_{TW} * \lambda_{TW}}{d_h^{pipe}} \quad (58)$$

$$With \; d_h^{jacket} = \frac{4 * (p_t^2 - \pi * r_{out}^2)}{2 * \pi r_{out}} \; and \; d_h^{pipe} = 2 * r_{in} \quad (59)$$

Here, $d_h$ stands for the hydraulic diameter. There are several empirical correlations for the Nusselt-number (Nu), depending on the application. Analogous to (Heberle & Brüggemann, 2016) and (Welter, Technisch-ökonomische Analyse der Energiegewinnung aus Tiefengeothermie in Deutschland, 2018), there is a distinction between the Nusselt-number for the jacket and the pipes. For the heat transfer in pipes, equations (60) (Sieder & Tate, 1936) and (61) (Kern, 1950) for the jacket are used.

$$Pipe \; (thermal \; water) \; Nu_{TW} = 0{,}27 * (Re_{TW})^{0{,}8} * (Pr_{TW})^{0{,}33} \quad (60)$$

$$Jacket \; (working \; medium) \; Nu_{WM} = 0{,}36 * (Re_{WM})^{0{,}55} * (Pr_{WM})^{0{,}33} \quad (61)$$

The Prandtl-number (Pr) is defined according to equation (62), where $c_p$stands for the heat capacity, $\eta$ for the dynamic viscosity, and $\lambda$ for the heat conductivity.

$$Pr = \frac{c_p * \eta}{\lambda} \quad (62)$$

In order to calculate the Reynolds (Re) number, equation (64) is used, in which $\rho$ stands for the density and $u$ for the velocity of the investigated fluid (thermal water/working medium).

$$Re = \frac{\rho * u * d_h}{\eta} \quad (63)$$

The last unknown parameter is the velocity of the fluid in the respective section. To determine the velocity in each section, first the number of pipes n in the heat exchanger is determined taking into account the maximum fluid velocity according to equation (64) (Wolf & Kirchner, 2013) (see also Table 3).

$$n = \frac{4 * \dot{m}_{TW}}{\pi * \left(d_{in}^{pipe}\right)^2 * \rho_{TW}^{min} * u_{TW}^{max}} \quad (64)$$

For this purpose, the point of lowest density ($\rho_{TW}^{min}$) of the thermal water flowing in the pipe is considered. In the evaporator, the density of the thermal water at point IV, the evaporator inlet, is used. The number of pipelines n is then determined for the given inner diameter of the pipes, so that the maximum velocities at the critical points are just undershot.

The velocity of the thermal water within the pipelines is calculated as follows:

$$u_{TW} = \frac{4 * \dot{m}_{TW}}{\pi * n * \left(d_h^{pipe}\right)^2 * \rho_{TW}} \quad (65)$$

For the jacket, further considerations are necessary: Using the known number of tubes n and the tube spacing defined in Table 3, the tube bundle diameter is estimated according to (Towler & Sinnott, 2013) and modified with the jacket clearance to approximate the jacket diameter on its inner side (Equation (66)). The relationship applies to aligned tube bundles with a tube spacing of 1.25*$d_{out}$ and a passage (Towler & Sinnott, 2013). A value of 100mm is assumed for the jacket clearance (Towler & Sinnott, 2013).

$$d_{in}^{jacket} = d_{out}^{pipe} * \left(\frac{n}{0{,}215}\right)^{\frac{1}{2{,}207}} + jacket\ clearance \quad (66)$$

Using this information, the diameter $d^*$ effective for the flow velocity in the jacket can be calculated according to expression (67) (Wagner, 2004) and finally the fluid velocity in the jacket with equation (68) can be calculated:

$$d^* = \frac{{d_{in}^{jacket}}^2 - n + d_{out}^2}{d_{in}^{jacket} + n + d_a} \quad (67)$$

$$u_{WM} = \frac{4 * \dot{m}_{wm}}{\pi * \left(d_h^*\right)^2 * \rho_{WM}} \quad (68)$$

In principle, the procedure shown applies to all main sections of the evaporator. If there is a phase change of the working medium in the actual evaporating part, the heat transfer coefficient of the working medium is replaced by the relationship (69).

$$\alpha_{WM} = \alpha_{WM}^{liquid} * \left\{(1-X)^{0{,}01} * \left[(1-X) + 1{,}2 * X^{0{,}4} * \left(\frac{\rho_{WM}^{liquid}}{\rho_{WM}^{gas}}\right)^{0{,}37}\right]^{-0{,}22} + X^{0{,}01} * \left[\frac{\alpha_{WM}^{liquid}}{\alpha_{WM}^{gas}} * (1 + 8 * (1-X)^{0{,}7} * \frac{\rho_{WM}^{liquid\ 0{,}67}}{\rho_{WM}^{gas}}\right]^{-2}\right\}^{-0{,}5} \quad (69)$$

X stands for the vapour content and the quantities marked "liquid" and "gas" are determined using the procedure described above provided that the working medium is completely liquid or completely gaseous. The density $\rho_{WM}^{liquid}$ or $\rho_{WM}^{gas}$ is determined by evaluating the NIST database according to (Lemmon, Huber, & McLinden, 2013) for the boundary of each subsection during evaporation and then averaging the boundary values obtained. The heat transfer coefficients $\alpha_{WM}^{liquid}$ or $\alpha_{WM}^{gas}$ are determined by the equations (57) to (68). Equation (69) thus represents an interpolation between the liquid and gaseous state of the working medium at a given temperature and pressure. All equations presented apply in the same form to mixtures of working mediums, whereby the material values of the mixture must be used (Kind & Saito, 2013).

**Condensator**: In contrast to the evaporator, the working medium in the condenser flows in the tubes of the heat exchanger. Air flows through the jacket. Accordingly, the indices in equations (57) to (69) change from "WM" to "Air" and from "TW" to "WM". To illustrate the influence of the fins, equation (61) is replaced by correlation (70) from (Wagner, 2004)

$$Nu_{air} = 0{,}38 * Re^{0{,}6} * Pr_{air}^{0{,}33} * \left(\frac{A(with\ fins)}{A(without\ fins)}\right)^{-0{,}15} \quad (70)$$

The influence of the fins is quantified through the proportion of the outer surface area of the pipe with and without fins. This ratio can be calculated with the geometrical data of the fins given in Table 3. Furthermore, for the determination of the heat transfer during the phase change of the working medium in the tubes of the condenser, correlation (71) (Shah, 1979) applies instead of (69).

$$Nu_{WM} = 0{,}023 * \left(Re_{WM}^{liquid}\right)^{0{,}8} * \left(Pr_{WM}^{liquid}\right)^{0{,}4} * \left[(1-X)^{0{,}8} + \frac{(3{,}8 * X^{0{,}76} * (1-X)^{0{,}04})}{p_{reduced}^{0{,}38}}\right] \quad (71)$$

The pressure $p_{reduced}$ is a measure for the ratio of boiling pressure and critical pressure and is determined using expression (72).

$$p_{reduced} = \frac{p(X=0,T_i)}{p_{crit}} \quad (72)$$

The heat transfer coefficient can be derived for working medium in a pipe using equation (57).

# Imprint


| | |
|---|---|
| Project Lead | GFZ German Research Centre for Geosciences<br>Telegrafenberg<br>14473 Potsdam (Germany)<br>www.gfz-potsdam.de/en/home/ |
| Project Coordinator | Prof. Ernst Huenges<br>huenges@gfz-potsdam.de<br>+49 (0)331/288-1440 |
| Project Manager | Dr. Justyna Ellis<br>ellis@gfz-potsdam.de<br>+49 (0)331/288-1526 |
| Project Website | www.destress-h2020.ch |




## Liability claim



## DESTRESS is co-funded by


National Research Foundation of Korea (NRF)
Korea Institute for Advancement of Technology (KIAT)
Swiss State Secretariat for Education, Research and Innovation (SERI)